Thermally Activated Concrete Fines as Supplementary Cementitious Materials

Zur Erlangung des akademischen Grades eines

DOKTOR-INGENIEURS

von der Fakultät für

Bauingenieur-, Geo- und Umweltwissenschaften

des Karlsruher Instituts für Technologie (KIT)

genehmigte

DISSERTATION

von

Jan P. Höffgen, M.Sc.

aus Bonn

Tag der mündlichen

Prüfung: 22.05.2026

Referent: Prof. Dr.-Ing. Frank Dehn

Korreferent: Prof. Dr.ir. Eddie Koenders

Karlsruhe (2026)

Abstract

Recycling fine concrete waste (or recycled concrete fines) is a significant obstacle to circular construction. The concentration of hardened cement paste (HCP) with decreasing particle size effectively hinders its use as recycled aggregates, as HCP is porous and has lower strength than natural aggregate. This impairs the workability of fresh concrete and results in insufficient performance of hardened concrete. So far, advanced processing methods have failed to provide a definitive solution to this issue. Different approaches have been successful in separating natural aggregates from HCP. However, while this produces recycled aggregates of improved quality, the second waste stream, consisting of enriched HCP, lacks applicability.

In this context, recycling as a binder with the goal to substitute cement offers a valuable alternative. Here, different methods exist. Fine concrete waste can replace a portion of the Portland cement clinker raw meal, which is subject to constraints imposed by the chemical composition. Alternatively, the dilution effect limits the use of (inert) ground concrete fines as a supplementary cementitious material. In contrast, thermal activation has proven to be a promising compromise, in which dehydrated HCP exhibits hydraulic reactivity, and the aggregate fraction in concrete waste serves as an inert filler.

Although a literature review indicates high research activity in this field, this thesis addresses significant gaps. While published results primarily focus on activation procedures for (practically non-existent) hydrated cement paste or on a single type of industrial concrete waste, the comprehensive research program of this work assesses the behavior of 12 laboratory-made artificial concrete fines with deliberately altered aggregate content, binder composition, or aggregate mineralogy, as well as 25 different industrial concrete fines.

The first part of the experimental program assesses the behavior of these fines after processing at temperatures between 100 °C and 800 °C, focusing on their hydration behavior and their contribution to compressive strength. Regardless of their composition, thermally activated concrete fines exhibit rapid rehydration, as evidenced by accelerated heat evolution during hydration. The total heat release, however, depends on the aggregate content. Extensive mortar compressive strength tests indicate a correlation between mass loss during thermal activation and the contribution to compressive strength, regardless of fines composition and origin. The chemical and mineralogical composition of the artificial fines also has a major impact on compressive strength, which is not mirrored by industrial fines. From these results, a model based on the k-value approach specified in EN 206:2013 is derived.

In the second part of the experimental work, a subset of both artificial and industrial fines is used for concrete production. In contrast to the literature, the effect of cement substitution on compressive strength is compensated for by applying the aforementioned model. The subsequent

analysis of mechanical properties shows a good agreement with reference supplementary cementitious materials and existing concrete design proposals. However, the substitution of cement with thermally activated concrete fines adversely affects the resistance to carbonation and chloride ingress due to a reduced binding capacity. Furthermore, the elution of harmful substances shows the need for additional research regarding the binding capacity for heavy metals.

Overall, the results in this thesis extend previous findings by providing a new method for predicting compressive strength based on concrete fines properties, highlighting individual consistencies and discrepancies with existing design provisions. Facilitating the recycling of concrete fines as a substitute for cement also enables the implementation of new procedures to separate HCP and natural aggregates as distinct materials, thereby advancing fully circular concrete construction.

Kurzfassung

Die Kreislaufführung von feinem Betonabbruch (sog. Betonbrechsanden) stellt eine große Herausforderung dar. Die Anreicherung von erhärtetem Zementstein (HCP) mit abnehmender Partikelgröße behindert die Anwendung als rezyklierte Gesteinskörnung erheblich: HCP ist porös und weist eine geringere Festigkeit im Vergleich zu natürlichen Gesteinskörnungen auf. Dies beeinträchtigt die Verarbeitbarkeit des Frischbetons und führt zu unzureichenden Festbetoneigenschaften. Bisherige Aufbereitungsverfahren liefern bislang keine eindeutige Lösung für dieses Problem. In der Forschung und Praxis werden verschiedene Ansätze entwickelt, um natürliche Gesteinskörnungen von HCP zu trennen. Dies führt zwar zu rezyklierten Gesteinskörnungen mit verbesserter Qualität. Der zweite Abfallstrom aus angereichertem HCP lässt sich jedoch bislang nicht sinnvoll verwerten.

Für diesen Zweck stellt die Verwendung von Betonbrechsanden als Zementersatz eine vielversprechende Alternative dar. Feiner Betonabbruch kann einen Teil des Rohmehls in der Portlandzementklinkerherstellung ersetzen. Dies ist jedoch durch dessen chemische Zusammensetzung begrenzt. Der Einsatz von (inerten) gemahlenen Betonbrechsanden als Zementhauptbestandteil wird durch den Verdünnungseffekt eingeschränkt. Eine thermische Aktivierung hat sich als vielversprechender Kompromiss erwiesen, wonach dehydratierter HCP hydraulische Reaktivität aufweist. Die in den Betonbrechsanden enthaltene natürliche Gesteinskörnung wirkt als inerter Füller.

Obwohl eine Literaturrecherche eine hohe Forschungsaktivität auf diesem Gebiet zeigt, deckt diese Arbeit bedeutende Forschungslücken ab. Während veröffentlichte Ergebnisse sich hauptsächlich auf Aktivierungsverfahren von (in der Praxis nicht vorhandenem) hydratisiertem Zementstein oder jeweils eine einzelne Art industrieller Betonbrechsande konzentrieren, werden in einem umfassenden Forschungsprogramm das Verhalten von 12 im Labor hergestellten, künstlichen Betonbrechsanden mit gezielt variierter Zusammensetzung der Bindemittel und der Gesteinskörnung sowie des Gehalts letzterer untersucht. Ergänzt wird dies durch 25 verschiedene industriell hergestellte Betonbrechsande.

Der erste Teil des experimentellen Programms bewertet das Verhalten dieser Betonbrechsande nach einer thermischen Behandlung bei Temperaturen zwischen 100 °C und 800 °C im Hinblick auf ihr Hydrationsverhalten und ihren Druckfestigkeitsbeitrag. Unabhängig von ihrer Zusammensetzung zeigen thermisch aktivierte Betonbrechsande eine schnelle Rehydration, was sich durch eine beschleunigte Hydrationswärmeentwicklung bemerkbar macht. Die Wärmeabgabe hängt jedoch vom Gesteinskörnungsgehalt ab. Umfangreiche Mörteldruckfestigkeitsprüfungen zeigen eine gute Korrelation zwischen dem Massenverlust während der thermischen Aktivierung und dem Druckfestigkeitsbeitrag – unabhängig von der Zusammensetzung und

Herkunft der Betonbrechsande. Die chemische und mineralogische Zusammensetzung der im Labor hergestellten Betonbrechsande beeinflusst die Druckfestigkeit stark. Industrielle Betonbrechsande weisen hier eine weniger stark ausgeprägte Beeinflussung auf. Aus diesen Ergebnissen wird ein Modell auf Basis des k-Wert-Ansatzes nach EN 206:2013 abgeleitet.

Im zweiten Teil der experimentellen Arbeit wird eine Auswahl sowohl künstlicher als auch industrieller Betonbrechsande zur Betonherstellung verwendet. Im Gegensatz zur Literatur wird der Einfluss der Zementsubstitution auf die Druckfestigkeit durch Anwendung des oben genannten Modells kompensiert. Die anschließende Analyse der mechanischen Eigenschaften zeigt eine gute Übereinstimmung mit etablierten Betonzusatzstoffen und bestehenden Bemessungskonzepten. Die Substitution von Zement durch thermisch aktivierte Betonbrechsande beeinträchtigt jedoch den Widerstand gegen Carbonatisierung und Chlorideindringung aufgrund eines verminderten Bindungsvermögens. Darüber hinaus zeigt die Elution umweltgefährdender Stoffe die Notwendigkeit weiterer Forschung zur Bindung von Schwermetallen auf.

Die Ergebnisse dieser Arbeit erweitern die bisherigen Erkenntnisse maßgeblich, indem sie eine neue Methode zur Vorhersage der Druckfestigkeit auf Basis der Eigenschaften von Betonbrechsanden bieten und individuelle Übereinstimmungen sowie Abweichungen mit bestehenden Bemessungsvorgaben aufzeigen. Die Wiederverwertung von Betonbrechsanden als Zementersatz ermöglicht zudem die Umsetzung neuer Verfahren zur Trennung von natürlicher Gesteinskörnung und Zementstein (HCP) als zwei separate Materialströme, um so einem vollständig kreislauffähigen Betonbau näherzukommen.

Acknowledgements

One of the most important aspects of scientific research is collaboration, and my thesis would not have been possible without the support of many individuals. Foremost, I would like to thank Prof. Dr.-Ing. Frank Dehn for his continuous guidance, patience, and unwavering trust in my work. The freedom he gave me to explore and refine my ideas laid the foundation for this thesis.

I am deeply grateful to my co-supervisor, Prof. Dr.ir. Eddie Koenders (TU Darmstadt), and to the members of my thesis committee – Prof. Dr.-Ing. Thomas Matschei (RWTH Aachen), Prof. Dr. Frank Schilling, and Prof. Dr.-Ing. Hans H. Stutz – for their feedback and encouragement throughout the process.

This work also stems from a strong educational foundation. I extend my sincere thanks to Prof. Dr.-Ing. Harald S. Müller and Prof. Dr.-Ing. Michael Haist, whose teaching inspired my interest in concrete research. Special thanks are due to Prof. Will Hanson, Ph.D. and Prof. Zhichao Liu, Ph.D. (formerly of the University of Michigan) for providing my first opportunity for international collaboration – an experience that broadened my perspective immeasurably.

I am profoundly grateful to my colleagues at KIT, past and present, for their invaluable scientific input and stimulating discussions – particularly Dr.-Ing. Andreas Wiedmann, Dr.-Ing. Engin Kotan, Dr.-Ing. Viktória Malárics-Pfaff, Dr.-Ing. Michael Vogel, Martin Umminger, Dr.-Ing. David Alós Shepherd, Dr.-Ing. Richard Caron, Sarah Lamparter, Vanessa Mercedes Kind, Carla Neuhaus, Matthias Mohs, Maureen Denu, Sophia Markus, Judith Herrmann, Attila Ibuk, Sebastian Rauscher, Simon Schafroth, Prof. Dr.-Ing. Lukas Knittel, and Dr.-Ing. Lukas Windeck. My thanks extend to all my colleagues for their support and the meaningful discussions we had. I especially appreciate the out-of-the-box thinking that arose from discussions with Dr. Andreas Bogner, Astrid Hirsch, and Prof. Dr. Katja Emmerich, whose expertise in chemistry and mineralogy provided fresh perspectives on my research challenges.

The success of this thesis hinged on the dedication of our laboratory team, who made experimental work feasible: Marcel Lakrar, Patrick Wehres, Andrea Ochs, Ute Kiefer, and Stephan Gehlsen. Thank you for your insight and for your patience with me! I am equally grateful to the students who contributed through their Bachelor's and Master's theses – their curiosity and hard work expanded the experimental scope of this work far beyond what I could have achieved alone.

Finally, I owe my deepest gratitude to my wife, Sabrina, my children Jakob and Julian, my parents, and my grandparents for their unwavering support – and for continuously reminding me that there are more important aspects to life than working on a doctoral thesis.

Karlsruhe, January 2026

The experimental work for this thesis was funded within the research project "Experimentelle Untersuchung der Möglichkeit einer thermisch-mechanischen Aufbereitung von Betonbrechsand zur Herstellung eines reaktiven Betonzusatzstoffs (THEMA Betonbrechsand)" by the Dres. Edith und Klaus Dyckerhoff-Stiftung, grant no. T0218/36374.

Für Hanne.

Contents

List of Figures

List of Tables

Chapter 1

Introduction

Concrete is – quite literally – one of the foundations of modern societies. Concrete is required for providing infrastructure and housing. In recent decades, worldwide concrete production has increased many times over, thereby creating a unique set of problems. Figure 1.1 illustrates the global cement production and CO_2 emissions over the past century.

Concrete is a composite of different raw materials – mainly aggregates, cement, and water. Firstly, the sourcing of aggregates is a local process that faces various challenges, including shortages. Secondly, cement production contributes to up to 8 % of global CO_2 emissions, which are hard to abate due to chemical processes and processing requirements [183]. Thirdly, concrete is also one of the most prevalent types of waste [231]. Modern concrete structures are rarely built for eternity, and an increasing number of those are being demolished. Recycling of these wastes may mitigate all three problems. Waste processing reduces the need for landfill disposal. The production of recycled aggregates reduces the demand for natural aggregates, and the substitution of cement lowers CO_2 emissions of concrete production.

While recycled aggregates are increasingly common and well researched, cement recycling is an emerging, albeit highly active, research field with few industrial applications. Therefore, this thesis aims to provide new insights into the thermal activation of concrete waste as a method for cement recycling.

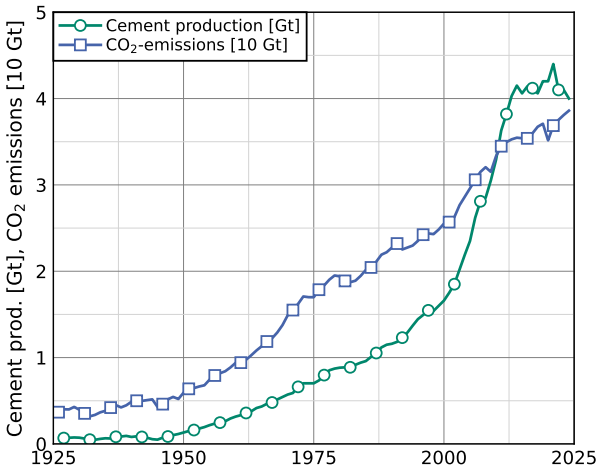

Fig. 1.1: Worldwide production of cement and CO_2 emissions. Data from [8, 168].

The main body of this thesis is subdivided into three parts. The first part gives an overview of standard procedures for concrete recycling. The second part presents experimental results on the development of compressive strength in mortar containing thermally activated concrete waste as a supplementary cementitious material. The long-term performance of concrete following cement substitution with these processed waste materials is analyzed in the third part.

This thesis is a cumulation of six individual research publications. Strength development (P1 and P2) and long-term behavior (P3 and P4) are each covered in distinctive works. While P1 and P4 use different types of industrially processed concrete waste as precursors, P2 and P3 assess waste composition through laboratory-made artificial precursors. The appendix includes reprints of these publications with additional supplementary data. Two additional publications detail preliminary work, which lays the groundwork for the present thesis (A1), and gives an outlook into applying the findings beyond concrete production (A2)*.

*For licensing reasons, publications A1 and A2 are not reprinted within this thesis. Therefore, and owing to the preliminary nature of these works, the detailed analysis within this thesis concentrates on P1–P4.

Chapter 2

Context

The recycling of concrete waste poses a significant obstacle for circular concrete construction. The following sections outline the advantages of activating concrete waste within the broader context of concrete production and recycling. The first section describes the production of concrete and its raw materials, followed by a depiction of mineral construction and building waste and its application as recycled aggregates. The chapter concludes with a presentation of different recycling pathways for concrete binders.

The contents of this chapter have previously been published in a report [91], which was altered and updated to meet the requirements for this thesis.

2.1 Cement and Concrete Technology

Concrete is a multi-component material that consists of coarse and fine aggregates, cement, water, supplementary cementitious materials, and admixtures. While aggregates comprise the bulk of the material, the cement paste composition, with the water-cement ratio (w/c) as the key parameter, defines the predominant properties of concrete. Supplementary cementitious materials (SCMs) may partially replace cement, and relatively small quantities of admixtures affect individual concrete properties, such as workability and air content.

2.1.1 Cement

Cement denotes a diverse group of finely ground hydraulic binders, which react with water to form a solid matrix, the so-called hardened cement paste (HCP). Cement, which is standardized in several parts of EN 197*, consists of main constituents and minor additional constituents. The former comprise cement clinker and optional supplementary cementitious materials. Minor additional constituents, which are limited to a content of 5 wt% of the total cement weight, cover a wide range of materials used for improving the physical properties of cement. Most importantly, calcium sulfate is used for regulating the setting behavior [141].

*This thesis uses the European and German standardization. Regionally, other standards with differing content may apply. Furthermore, other types of cement, such as very low heat special cements, use different standards, which are not relevant to the scope of this thesis.

Clinker

The most important constituent of Portland cement is Portland cement clinker (short: clinker), which is produced by burning clinker raw meal – a mixture of limestone, clay, marl, quartz sand, and iron ore – at 1450°C. The required compositional ratios of the raw meal depend on the chemical profile of the individual components [248]. Table 2.1 presents the typical compositional ranges for the raw meal mixture.

Tab. 2.1: Mineral oxide composition of clinker raw meal. CCN: Cement chemist notation. [56, 252]

Oxide notation	CCN	Proportion [wt%]
CaO	C	60 – 69
SiO_2	S	20 – 25
Al_2O_3	A	4 – 7
Fe_2O_3	F	0.2 – 5

Due to the burning of fossile fuels, which are required for achieving high processing temperatures, and the release of chemically bound CO_2 from raw meal components, the production of 1 t clinker is associated with the emission of ca. 800 kg–900 kg CO_2 [192]. Less than half of these can be abated through the switch to renewable fuels, while the remainder would require a switch to alternative raw materials, which do not contain chemically bound CO_2 [10, 59, 248].

Through the incineration process, the key clinker phases form [20, 252]:

- Tricalcium silicate ($3\,CaO \cdot SiO_2$; C_3S, Alite), 45 wt%–80 wt%,
- Dicalcium silicate ($2\,CaO \cdot SiO_2$; C_2S, Belite), 0 wt%–32 wt%.
- Tricalcium aluminate ($3\,CaO \cdot Al_2O_3$; C_3A), 7 wt%–15 wt%, and
- Calcium aluminferrite ($4\,CaO \cdot Al_2O_3 \cdot Fe_2O_3$; C_4AF), 4 wt%–14 wt%.

The raw meal composition requires careful adjustment to achieve the desired uniform clinker properties.

The hydration of clinker phases produces distinct hydraulic phases that serve different functions in fresh and hardened paste. In short, alite reacts to calcium silicate hydrates (C-S-H), which form an interconnected matrix for strength bearing, and calcium hydroxide ($Ca(OH)_2$, CH, also: portlandite), which provides carbonation resistance in reinforced concrete. The belite reaction is slower than the alite reaction and yields similar hydration products, but with a lower share of $Ca(OH)_2$. Aluminous and ferrous clinker phases serve as flux in the clinkering process, and hydration products provide a resistance against chloride or sulfate ingress. Furthermore, in the presence of calcium sulfate ($CaSO_4$), calcium aluminate forms calcium aluminosulfate hydrates (AFm and AFt), which give cement paste a thixotropic behavior for a limited time and therefore allow workability [20, 141].

Supplementary Cementitious Materials

Supplementary cementitious materials (SCMs) may be used either as cement main constituents, or as concrete additives [17, 47, 73, 115, 208]. The definitions distinguish between SCMs added

during cement batching and those added during concrete mixing. Individualized standardized requirements apply, affecting the concrete design process. However, for the more relevant concrete parameters, this differentiation is insignificant.

SCMs are classified by their reactivity. Inert SCMs exhibit no chemical reactivity with other concrete components. Aside from a mere dilution of the reactive phases, inert SCM particles may act as nuclei for the hydration of cement clinker [176, 202]. The dilution effect can be partially negated through a higher fineness of the cement clinker, but ultimately limits the applicability of inert SCMs. Pozzolanic SCMs contain high amounts of amorphous siliceous or aluminous phases, which react with calcium hydroxide to form strength-developing hydrates [119, 224, 260]. Because concrete durability requires high alkalinity in the pore solution, the consumption of calcium hydroxide effectively limits the technically feasible substitution rates [80]. Higher substitution rates are possible for SCMs with elevated calcium content, where calcium hydroxide is increasingly required as reaction catalyst rather than as reactant [82, 173, 175]. These so-called latent-hydraulic SCMs generally exhibit calcium oxide (C) to silicon dioxide (S) molar ratios $C/S > 0.5$. For $C/S > 1.5$, binders may show hydraulic behavior, with cement clinker ranging between $2.0 \leq C/S \leq 3.0$ [17, 90]. Subsequently, reaction products from SCMs exhibit a significant bandwidth, depending on their chemical compositions.

The impact of SCMs on concrete performance is either considered implicitly through the categorization of blended cements or explicitly when used as an additive in the concrete mixing process. The latter often relies on the k-value concept described in CEN/TR 16639:2014. Here, the contribution of SCMs to concrete parameters – usually, compressive strength – is considered through an equivalent water-cement ratio w/c_{eq}, at which the concrete performance is identical to a concrete of the same water-cement ratio without additives.

$$\frac{w}{c_{\mathrm{eq}}} = \frac{w}{c + k \cdot a} \qquad \text{with } w\text{: water content, } c\text{: cement content, } a\text{: additive content} \tag{2.1}$$

Standardized k-values may reach as high as $k = 2.0$ for silica fume, but are generally smaller than 1.0, which indicates a degradation of concrete strength and durability following the substitution of cement. EN 206:2013 and DIN 1045-2:2023-08 define $k = 0.4$ for pozzolanic fly ash and latent-hydraulic ground granulated blast-furnace slag (and, for limited applications, $k = 0.6$ for the latter). For inert SCMs, $k = 0.0$ applies. However, researchers have found less conservative k-values, such as $k = 0.6$ for fly ash or $k = 0.15$ for inert limestone powder [88, 89, 290]. In EN 206:2013, equivalent water-cement ratios are also used to assess durability requirements through exposure classes. Additionally, additives may partially contribute to fulfilling requirements for the minimum cement content.

The use of SCMs predates the invention of Portland cement, and various pozzolans, primarily derived from volcanic ash, have been used extensively [156, 191]. In recent years, the demand for SCMs has increased, as exemplified through fig. 2.1. However, due to a decreasing use of coal for producing electricity or raw iron, the availability of fly ash or blast-furnace slag is locally constricted, with a bleak perspective [161, 248, 249, 252]. Ongoing research seeks to identify and establish additional types of SCMs, such as calcined clays and various types of incineration ashes [17, 70, 101, 224, 249].

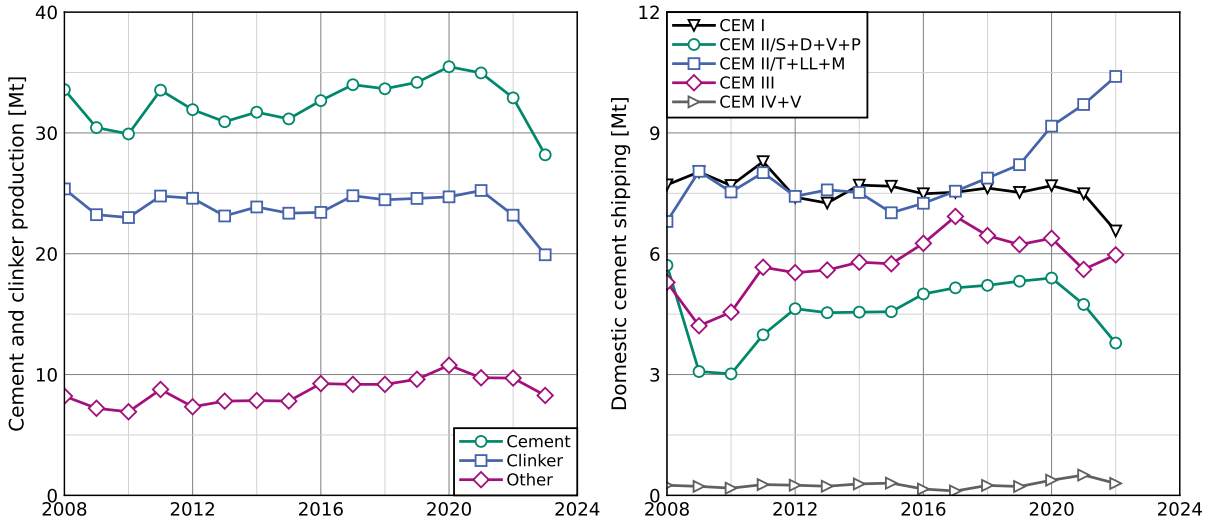

Fig. 2.1: Production of cement and clinker (left) and domestic shipping of different types of blended cements (right) in Germany [250, 251, 253–256]. Cement types according to EN 197-1:2011 and EN 197-5:2021.

2.1.2 Aggregates

Aggregates constitute the largest share of a unit volume of concrete and serve as the granular base material, which is surrounded by the hardening cement paste matrix. As long as they are chemically stable and do not interact with the cement paste, requirements, i.e., in EN 12620:2008, focus on physical and geometrical properties, such as water absorption, density, hardness, grain shape, and particle size distribution [230].

Aggregates are usually locally sourced and processed. Therefore, the chemical and mineralogical composition exhibits regional variations, which subsequently affect the chemical composition of concrete.

The overall consumption of sand and gravel surpasses the demand for concrete aggregates. Civil engineering and building construction require approximately half of these resources (see fig. 2.2). However, the former uses mainly loose aggregates, and only approximately 26 wt% serve as aggregates in concrete. Building construction requires approximately 77 wt% of sand and gravel as concrete aggregates. In sum, approximately 50 wt% of sand and gravel are used in concrete production[†].

[†]Data from [32]. The detailed timeline illustrated in fig. 2.2 ends with the year 2020. More recent iterations are limited to the total production of sand and gravel.

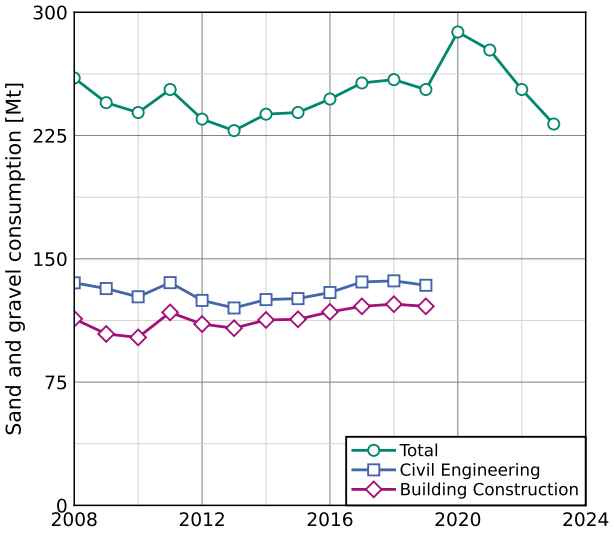

Fig. 2.2: Total consumption of sand and gravel in Germany [18, 19, 25, 30–32, 54].

2.2 Mineral Construction and Demolition Waste

At the end of its service life, a concrete structure can be demolished, and its components may serve as recycled building materials. Figure 2.3 details the recorded construction and demolition (C+D) waste in Germany, which amounts to roughly half of all waste streams (by weight) in Germany. The largest share constitutes soil, stones, and dredging soils, which can often be reused or recycled without further processing [231]. Mineral waste (concrete, bricks, tiles, ceramics) generally requires processing before further application [164].

Processing comprises the separation of different material components – steel, concrete, bricks, timber, insulation etc. – and, as a second step, fragmentation. The extent of the latter depends on the aspired recycling use case. Most commonly, processed concrete waste substitutes crushed natural aggregates in unbound layers in road construction [162, 164]. The application as recycled concrete aggregates poses stricter requirements for physical and mechanical material parameters.

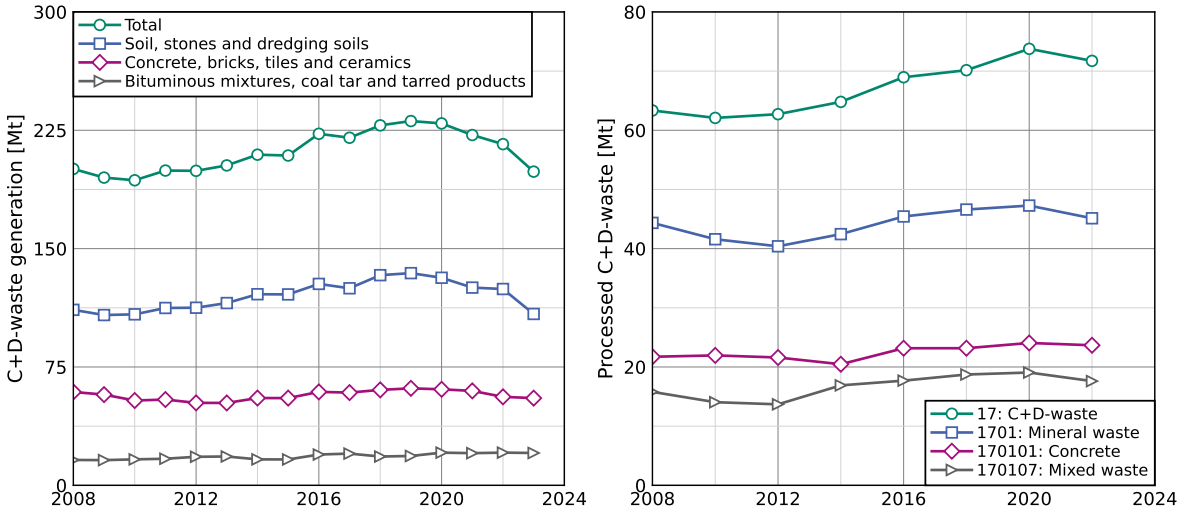

Fig. 2.3: Construction and Demolition (C+D) waste generated (left) and processed (right) in Germany [231].

2.3 Recycled Concrete Aggregates

Recycled aggregates obtained from concrete waste processing consist of hardened cement paste and natural aggregates used for the production of the parent concrete. Compared with natural aggregates, hardened cement paste may adversely affect the physical properties of recycled aggregates and, subsequently, the performance of concrete.

2.3.1 Properties of Recycled Concrete Aggregates

Recycled concrete aggregate properties exhibit high variations. This is due to several overlapping influences, such as the composition of the parent concrete, defined through the types of aggregates and cement and the water-binder ratio, and processing techniques. Furthermore, because hardened cement paste has a lower crushing value than natural aggregates, processing may yield coarse aggregates with low cement paste content, whereas the latter concentrates with increasing particle fineness [57, 121, 125]. Concrete waste usually consists of 70 wt%–80 wt% aggregates. The aggregate content in fine recycled aggregates mostly ranges between 40 wt%–60 wt% and may even go as low as 20 wt% [104]. This requires expensive crushing, fractioning, and sorting procedures [39, 67]. Subsequently, variations in cement paste content also affect the chemical, physical, and mechanical properties of recycled aggregates, and the impact is greater for finer recycled aggregate fractions.

For concrete production, the most important physical aggregate properties are their density and water absorption. Compared with natural aggregates, the increased hardened cement paste content results in a lower particle density and a higher water absorption. A review of fine recycled aggregates and their natural counterparts in [169] yielded a decreasing particle density[‡] from $\rho_{SSD} = 2.63(4)\,\mathrm{kg/dm^3}$ to $\rho_{SSD} = 2.28(18)\,\mathrm{kg/dm^3}$. For the same aggregates, water absorption[§] increased from $WA_{24\,\mathrm{h}} = 1.1(9)\,\mathrm{wt\%}$ to $WA_{24\,\mathrm{h}} = 8.5(22)\,\mathrm{wt\%}$. In a different review in [218], fine recycled aggregates exhibited $\rho_{SSD} = 2.30(10)\,\mathrm{kg/dm^3}$ and $WA_{24\,\mathrm{h}} = 9.5(26)\,\mathrm{wt\%}$. For coarse aggregates, the lower hardened cement paste content has a less pronounced effect on physical aggregate properties. Results in [218] yielded $\rho_{SSD} = 2.44(8)\,\mathrm{kg/dm^3}$ and $WA_{24\,\mathrm{h}} = 4.9(17)\,\mathrm{wt\%}$. Figure 2.4 presents different empirical relationships between the two codependent material parameters[¶].

2.3.2 Impact of Recycled Aggregates on Concrete Properties

The replacement of natural dense aggregates with recycled aggregates generally has an adverse effect on the performance of the resulting concretes.

In fresh concrete, the high proportion of crushed aggregate surfaces reduces workability due to increased specific surface area and lower packing density [45, 53, 122, 240]. In addition, adhering mortar absorbs mixing water from the fresh concrete, causing a further, time-dependent loss of workability [104]. In construction practice, two principal approaches are applied to

[‡] ρ_{SSD}: particle density at saturated surface dry condition

[§] $WA_{24\,\mathrm{h}}$: Water absoption during submersion for 24 h

[¶] Silva.2014 [218] and Omary.2016 [172] specify density in oven dry condition, while Verian.2018 [257] does not indicate the moisture state. The empirical parameters specified in [218] contain a rounding error. The corresponding author kindly provided the correct data.

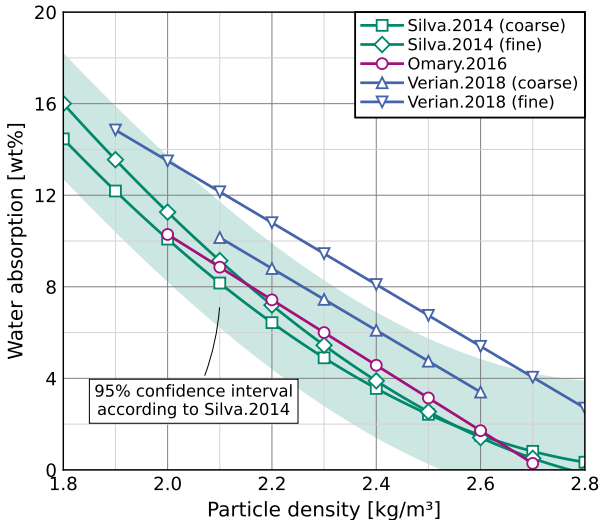

Fig. 2.4: Empirical relationship between water absorption (24 h) and particle density (oven dry) of recycled concrete aggregates from different reviews [172, 218, 257].

compensate for the increased water absorption of recycled aggregates [216]. The use of specially tailored retarding superplasticizers improves workability and enhances retention of consistency over time. However, a more economical solution is to add additional water, either by pre-wetting the recycled aggregates or by increasing the mixing water content to compensate for aggregate water absorption. In practice, the required amount is commonly estimated based on the water absorption of the aggregates within 10 min [164, 196]. The applicability of this approach is limited by the maximum permissible water-cement ratios specified for the exposure classes in accordance with EN 206:2013.

In hardened concrete, replacing natural dense aggregates with recycled aggregates generally reduces compressive strength. This behavior can be attributed to the fracture mechanics of concrete: cracks typically initiate in the interfacial transition zones (ITZs) between the cement paste matrix and the aggregates [201]. In these regions, stress concentrations arise due to differences in material stiffness. Moreover, the ITZs are characterized by a locally increased water-cement ratio, resulting in higher porosity and reduced cohesion caused by one-sided growth of hydration products. With progressive cracking, microcracks within the ITZs coalesce into macrocracks that propagate through the cement paste matrix. In normal-strength concrete, dense natural aggregates impede crack propagation. By contrast, concretes incorporating recycled aggregates exhibit an increased volume-related ITZ area. This increase results from both the higher specific surface area of the crushed aggregates and from the presence of ITZs within the recycled aggregate particles originating from the parent concrete [64, 148, 279]. In addition, recycled aggregates are pre-damaged by microcracks induced during the crushing process of concrete demolition waste [148].

The properties of the ITZs between cement paste and recycled aggregates are affected by the moisture condition of the aggregates. Water-absorbing aggregates generally promote denser ITZs, whereas fully water-saturated aggregates may locally increase the water-cement ratio in the ITZs by releasing water into the cement paste [132, 309]. Because of their cement paste content, recycled aggregates are also less effective at inhibiting crack propagation than natural

aggregates and may even promote cracking when concrete with a strength higher than that of the parent concrete is produced [148].

In addition to reduced compressive strength, concretes with recycled aggregates generally exhibit inferior deformation-related and durability-related properties. Table 2.2 summarizes the effects of a complete replacement (100 %) of coarse and fine aggregates by recycled aggregates on selected hardened concrete properties. The specified ranges indicate the 95 % and 5 % confidence intervals and assume a linear relationship between concrete properties and the substitution rate. The higher porosity of recycled aggregates facilitates the ingress of aggressive media into the concrete, particularly when the quality of the recycled parent concrete is poor, or when the water absorption of the aggregates is compensated for by an increased mixing water dosage [159, 261, 272, 305]. In contrast, the higher cement paste content in recycled aggregates may increase the binding capacity of harmful substances, such as chlorides [247]. However, the increased cement paste content associated with recycled aggregates generally results in a reduced modulus of elasticity, an increased creep coefficient, and increased shrinkage [63, 272, 284].

Tab. 2.2: Relative hardened concrete properties at 100 % aggregate replacement by recycled aggregates (RA). Reported values of the 95 % and 5 % confidence intervals, i.e., a complete substitution of coarse aggregates yields a compressive strength range, where 95 % of the results exceed 56 % of the reference strength, and 5 % exceed 117 % of the reference strength.

		coarse RA			fine RA		
Compressive strength	[220]	56	–	117	55	–	107
Splitting tensile strength	[219]	40	–	114	54	–	87
Modulus of elasticity	[222]	44	–	96	55	–	98
Creep coefficient	[215]	100	–	180			
Shrinkage	[217]		<	180			
Carbonation depth	[221]	82	–	247	148	–	870
Chloride diffusion	[223]	90	–	165	40	–	295

Table 2.2 exemplifies that coarse and fine recycled aggregates have a similar impact on mechanical concrete properties. The ingress of chlorides and CO_2, however, may be significantly increased when fine recycled aggregates are used. This is due to the concentration of hardened cement paste in these fines, in addition to an increased specific surface area [29, 62].

As shown in table 2.2, it is feasible to produce concrete with an unaltered compressive strength even when coarse and fine recycled aggregates replace the entire aggregate fraction. However, it must be emphasized that the empirical relationships between hardened concrete properties that underlie structural design standards (e.g., EN 1992) may no longer be valid under such conditions. This limitation arises from the differing effects of aggregate replacement on compressive strength and on other hardened concrete properties. Therefore, concrete design standards, such as EN 206:2013, restrict the substitution of natural with recycled aggregates.

2.3.3 Advanced Processing of Recycled Concrete Aggregates

To eliminate discrepancies between natural and recycled aggregates and the concrete produced from them, advanced processing methods focus on improving the performance of recycled aggregates. These can be divided into two categories. On the one hand, predominantly mechanical,

thermal, and chemical methods focus on optimizing the separation of cement paste from natural aggregates. On the other hand, chemical or physical treatments can be used to strengthen and densify the hardened cement paste adhering to the natural aggregate particles.

Methods for removing the hardened cement paste from the original aggregates aim at achieving a complete recovery of natural coarse and fine aggregates that can be used for the production of new concretes without or with only minor restrictions.

The fundamental process for this purpose is the optimized crushing or grinding of the recycled aggregates. After demolition, concrete waste is generally not available in a usable particle size distribution. In a subsequent comminution step, useful particle size gradations are generated. By applying optimized processes, the particle shape can be improved toward more cubic or spherical grains. This is associated with increased abrasion of the cement paste. Predominantly, rotating mills are used for this purpose, whereas conventional crushers do not lead to improved particle shapes. These processes exploit the different strengths of the cement paste and the natural aggregates and are therefore particularly effective for low-strength concrete precursors [164].

Due to the different thermal behavior of hardened cement paste and aggregates, thermal processing can be used for enhancing the separation of paste and aggregates [74, 195]. In addition, differences in thermal expansion coefficients generate internal stresses between cement paste and aggregate, resulting in cracking within the interfacial transition zones. Temperatures in the range of 250 °C–500 °C have proven sufficient. Optimum processing temperatures for reclaiming aggregates with low paste content range from 500 °C to 1000 °C [74, 83, 180]. However, high temperatures may trigger chemical processes within the natural aggregates, but increase the decomposition of the cement paste. Heat treatment can be carried out in conventional furnaces. Microwave treatment has also proven effective, as it exploits the increased porosity of the interfacial transition zones to generate temperature gradients and internal stresses at these locations [158].

Alternatively, the cement paste matrix can be weakened by acid treatment. Both inorganic acids (hydrochloric acid, HCl; sulfuric acid, H_2SO_4; nitric acid, HNO_3; phosphoric acid, H_3PO_4; carbonic acid, H_2CO_3) and organic acids (acetic acid, $C_2H_4O_2$; tannic acid, $C_{76}H_{52}O_{46}$) are suitable for this purpose. In this process, the hydrate phases of the cement paste are dissolved in order to achieve separation. Care must be taken to ensure compatibility between the acid used and the natural aggregates of the concrete waste being processed, in order to avoid dissolution of the latter [55, 99, 107, 109, 211].

Following the weakening of the cement paste, it must be separated from the primary natural aggregates. Due to the reduced cohesion, crushing or grinding is generally not required for this step. Instead, sieving or air classification is often sufficient [39, 74].

Methods aimed at strengthening and densifying the cement paste fraction of recycled concrete aggregates focus on sealing the pore structure and closing microcracks. Research in this area is predominantly directed toward optimizing recycled aggregates across the entire range of commonly used particle sizes.

One option for the pretreatment is mixing recycled aggregates with a binder suspension upstream of the actual concrete production process. In this approach, the individual particles

are first coated with an additional binder layer, thereby improving particle shape and the bond between the treated aggregate particle and the subsequently formed cement paste. If sufficiently fine binders are used, they can penetrate pores and microcracks and thus seal them. Suitable materials include high-strength cements or supplementary cementitious materials such as ground granulated blast-furnace slag, fly ash, or silica fume. In particular, the latter has shown to yield additional benefits for the strength development of the resulting concrete. However, coating individual particles is time-, energy-, and especially material-intensive. The demand for suspension increases with the specific surface area of the material to be treated [96, 116, 212, 266].

Instead of binder suspensions, recycled aggregates can be treated with aqueous solutions, containing, for example, sodium silicate or organic polymers – often in combination. These substances can deposit within the pores or render the surface of the recycled aggregates hydrophobic. However, the performance of these materials varies. While improving workability, individual polymer solutions may have adverse effects on concrete strength or durability [118, 211, 229].

Such negative interactions can be avoided if the deposited materials are already established constituents of concrete, which is the case for calcium carbonate. Two fundamental approaches can be distinguished in this context: bioprecipitation and carbonation.

The precipitation of calcium carbonate exploits the metabolism of various microorganisms that, among other things, emit carbon dioxide. In a calcium-rich environment, this carbon dioxide reacts to form calcium carbonate. By locally confining this reaction to the pores and microcracks of a recycled aggregate particle, these can be sealed and closed within a few days [262, 301]. In addition, carbonation products can bind fine particles to larger aggregate particles [315].

Alternatively, during carbonation, phases of the cement paste react with carbon dioxide from the surrounding air to form calcium carbonate. The most important reaction is the carbonation of calcium hydroxide, although other cement paste phases may also carbonate to a lesser extent. Since calcium hydroxide is predominantly located in the pores and interfacial transition zones of the cement paste, these regions are densified and strengthened by carbonation. The effectiveness of carbonation depends on several parameters. Natural carbonation – which represents an undesirable reaction in concrete structures due to the depassivation of reinforcing steel – requires several years at a CO_2 concentration of 0.4 ‰ in atmospheric air to reach relevant concrete depths in the millimeter range. Analogous to laboratory tests used to determine the carbonation resistance of concretes, chemical reactions can be accelerated. Increasing the CO_2 concentration leads, on the one hand, to faster carbonation of calcium hydroxide. In addition, the reactivity of calcium silicate hydrate increases with CO_2 concentration, thereby enabling further beneficial effects. On the other hand, negative effects on the physical properties of treated aggregates have been observed at very high CO_2 concentrations. Effective concentrations are reported to lie in the range of 20 %–50 % [182] or 40 %–60 % [134]. Furthermore, the carbonation rate can be increased by a moderate rise in gas pressure in the range of 10 kPa–500 kPa. Typical climatic boundary conditions (20 °C–30 °C and 40 %–70 % r.h.) have also proven to be effective. Because carbonation progresses continuously with increasing exposure time, longer durations improve

treatment efficiency. However, the carbonation rate decreases as carbonation progresses because the calcium carbonate formed in the pores increasingly impedes CO_2 penetration. The majority of CO_2 uptake occurs within the first hour after exposure. After one day, the reaction enters a stable phase with very slow increases in carbonation [126, 134, 182, 239].

While all presented processing techniques have proven effective, the economic feasibility requires additional research. A detailed comparison and assessment of the methods described is provided in [66, 163, 171, 186, 207, 211, 267]. Ultimately, strengthening the adhering cement paste through carbonation stands as the most promising procedure, as it uses CO_2, a cost-negative resource. Methods that improve the separation of natural aggregates and hardened cement paste are effective but increase processing costs and produce a residual waste stream containing concentrated cement paste or its derivatives, which cannot be used as aggregates in concrete and require alternative recycling applications.

2.4 Recycled Concrete Binders

While concrete waste with high contents of hardened cement paste is increasingly difficult to recycle as aggregates, especially the fines fraction has shown promising behavior as a recycled binder. Cement recycling can be classified into three groups, where waste containing materials are either used as a clinker raw meal component or serve as a finely ground filler. An intermediate approach aims to activate the hardened cement paste while leaving the inert aggregates unaltered.

2.4.1 Concrete Waste in Clinker Production

The production of cement clinker requires a narrowly tailored raw meal composition for achieving a sufficient amount of reactive phases (see section 2.1.1). Pure hardened cement paste can be used almost entirely as raw meal in cement production, with at most minor additions [317]. After thermal treatment at the conventional clinker burning temperature of 1450 °C, the relevant clinker phases form from the melt. In some cases, lower temperatures have also been identified as effective [130, 139].

However, since concrete waste contains significant amounts of supplementary cementitious materials or natural aggregates, the required calcium-to-silicon (C/S) ratio is unfavorably altered. As a result, the melt derived from crushed concrete does not form sufficiently reactive phases. The proportion of concrete waste in the raw meal must therefore be selected such that the resulting chemical composition meets the requirements described in section 2.1.1 [48]. In this context, the calcium content of the concrete waste is of particular relevance, as calcium carbonates are used to offset deviating raw meal compositions caused by concrete waste [2, 48]. For quartzitic natural aggregates, the separation of hardened cement paste from aggregates is therefore important to reduce the required calcium carbonate content in the raw meal [200]. With increasing quartz contents in concrete waste, it has also been observed that even with optimized raw meal composition, only incomplete formation of tricalcium silicate from the melt occurs – in favor of increased amounts of free lime and quartz. Consequently, cement strength and the flowability of cement pastes decrease [123]. Concrete waste with calcitic natural ag-

gregates can be used to a larger extent even without optimized separation processes. However, irrespective of the type of primary aggregates, separation is desirable to obtain the highest possible ratio of calcium silicate hydrates to calcium carbonates in the raw meal for achieving the most significant possible reduction in CO_2 emissions in the clinker burning process [123]. In laboratory investigations, up to 25 wt% of the raw meal has been successfully replaced with concrete waste, whereas in pilot-scale production, a substitution of up to 15 wt% has proven feasible [100]. While most concrete waste samples exhibit compositions that allow for a substitution of 10 wt%–20 wt% of the raw meal, lower substitution rates around 5 wt% have proven to be more stable and easier to control [120, 121].

Because the raw meal composition must be monitored and adapted to the concrete waste composition, this method favors batch processes over continuous clinker production. This, in turn, allows for novel conceptualizations. One alternative is to replace the flux material in electric arc furnaces for steel production through clinker raw meal [58]. A different option reduces the processing temperature through combining a raw meal with a slightly reduced calcium-to-silicon ratio and a carbon melt in a high-pressure reactor to produce so-called belite clinker [117, 232–234, 316]. Both procedures have been shown to allow for the partial adoption of concrete waste.

The concept of recycling concrete waste as clinker raw meal has ultimately culminated in the concept of "Completely Recyclable Concrete" (CRC), in which the composition of all mineral concrete constituents is selected during production to correspond to a raw meal composition. This uses a mixture of calcitic and quartzitic aggregates, such that, after demolition, the entire concrete can be repurposed as raw meal [140, 197, 198].

2.4.2 Ground Concrete Waste

Finely ground concrete waste can be applied as a (mostly) inert supplementary cementitious material (SCM). The simplified interpretation as a two-phase material consisting of natural aggregates and hardened cement paste explains individual contributions exceeding a mere filler effect.

Natural aggregates in concrete waste may be chemically inert, such as limestone, or contain reactive phases, which allow their use as pozzolanic supplementary cementitious materials [135]. Additionally, a high-energy grinding can mechanochemically activate siliceous mineral phases through amorphisation [7, 69, 185, 225].

The hardened cement paste fraction in concrete waste may contain unreacted clinker or SCMs. Upon grinding, these particles outcrop, and retain their reactivity when used as abinder in fresh concrete [26, 67, 181, 192]. Hydrated cement phases may serve as nuclei for the reaction of anhydrous cement clinker, as long as the particles exhibit a sufficient fineness [57]. Additionally, silicon and aluminium ions may dissolve and enhance the pozzolanic reactivity when used in blended cements [57, 69].

While the high specific surface area and porosity of ground concrete waste are beneficial for the nucleation effect, which accelerates hydration and strength development, the subsequent water adsorption is detrimental to fresh concrete workability [108, 110, 127–129, 138, 155, 241, 285]. The strength contribution of ground concrete waste strongly depends on phase composi-

tions and fineness, and ranges between no negative impact and complete dilution [36, 94, 95, 125, 127, 133, 146, 155, 272, 287].

Other mechanical concrete properties are likewise affected. Concrete containing ground concrete waste as SCM tends to exhibit lower tensile strength [35, 51, 52, 310] and elastic moduli [11, 147]. Correspondingly, shrinkage deformations are increased [36, 113, 127].

As ground concrete particles are porous, concrete porosity increases with the incorporation of the former as SCM [36, 81, 113, 125, 146, 272]. Conversely, sufficiently fine particles may reduce porosity due to the nucleation effect [34, 57, 84, 125, 160]. Increasing porosity negatively affects concrete durability, namely carbonation, chloride ingress, and freeze-thaw-resistance [36, 52, 81, 95, 145, 146, 155, 278, 287].

In conclusion, the substitution of up to 30 wt% of cement through ground concrete waste has proven economically feasible when considering mechanical concrete properties. For durability, a generalization is difficult, as the combination of precursor material and processing may yield a great bandwidth of performance properties. Furthermore, the recycling of concrete waste as supplementary cementitious material must assess the potential impact of harmful substances, such as heavy metals or organic compounds, which may negatively affect the handling or the environment [61, 72, 106, 177].

2.4.3 Carbonation Activated Concrete Waste

Carbonation activation of hardened cement paste extends the procedure described in section 2.3.3. At high CO_2 concentrations, not only portlandite, but also calcium silicate (aluminate) hydrates react to form $CaCO_3$ [4, 107, 210, 297]. The latter leaves a silica-alumina gel, which exhibits a pozzolanic reactivity [74, 178, 210]

The activation processes distinguish three different moisture states. Wet carbonation, where CO_2 is dissolved in water (as carbonic acid, H_2CO_3), provides the highest degrees of carbonation [209, 242, 271, 294]. In contrast, dry carbonation requires a less sophisticated setup, but yields reduced carbonation rates [174, 271]. Moist (or semi-dry) carbonation can be regarded as a compromise between the former approaches [71, 294]. Increasing the processing temperature from 20 °C up to 80 °C has a positive effect on the velocity of the reaction [151, 296]. Accordingly, carbonation efficiency increases with reducing particle size [4, 65, 157].

After the indispensable comminution process, carbonation activated concrete waste may be employed as a reactive supplementary cementitious material. Aggregates are not affected by this procedure and may only exhibit reactivity after mechanical activation (section 2.4.2). $CaCO_3$ formed from the carbonation process serves as a finely distributed filler and hydration nuclei [41, 131, 210]. Due to the high specific surface area of activated cement paste, workability is impaired, and hydration is accelerated [55, 97, 102, 152]. However, the negative impact on fresh concrete consistency is less pronounced than for uncarbonated ground concrete waste [41, 237]. The enhanced reaction of alite in the blended cement requires the dosage of a setting regulator [294]. In contrast to established pozzolans, such as fly ash, carbonation-activated cement paste exhibits a fast compressive strength development [293, 295, 298]. The silica-alumina gel reacts with portlandite from the clinker hydration and forms calcium (aluminate) silicate hydrates (C-(A)-S-H) with a low ratio of calcium to silicon [131, 293, 298, 311, 312].

Compared to ground concrete waste or limestone filler, concrete strength increases following the partial cement substitution through carbonation-activated cement paste [46, 97, 131, 237, 295]. This effect is supported by a reduction of cement paste porosity [153, 237]. The decline of compressive strength amplifies with increasing substitution rate. A substitution up to 40 wt% of cement has proven feasible without overly compromising concrete performance [293].

Concrete durability following the partial cement substitution through carbonated concrete waste has not yet been thoroughly investigated. A reduction of the binding capacity of CO_2 is to be expected for the pozzolanic reaction of the carbonated cement paste. Furthermore, a reduction of the binding capacity of chlorides has been experimentally observed [150].

2.4.4 Thermally Activated Concrete Waste

Thermal activation relies on the decomposition of cement hydrates at elevated temperatures. The de- and rehydration of hardened cement paste has been intensively investigated. The subsequent paragraphs detail the impact of cement substitution through thermally activated cement paste on various concrete properties.

Thermal Decomposition of Hardened Cement Paste

With increasing processing temperature, the different mineral phases in hardened cement paste disintegrate. The individual decomposition temperature ranges are still subject to various research activities.

Ettringite (AFt) decomposes at temperatures below 115 °C, depending on partial water vapour pressure in the ambient air [16, 313, 314]. Monosulfate (AFm) loses chemically bound water in a temperature range up to 250 °C [15, 263]. Tricalcium aluminate hexahydrate (C_3AH_6) dehydrates between 260 °C and 400 °C [93]. At around 110 °C, calcium silicate hydrates (C-S-H) start to decompose [13]. Due to the dissimilarity of C-S-H, the dehydration temperature ranges up to 300 °C [15], 400 °C [13], or 500 °C [9]. Portlandite (CH) decomposes in the temperature range of 400 °C–550 °C [13, 15, 300]. Between 650 °C and 900 °C, $CaCO_3$ decomposes [114, 199]. Depending on the cristallinity of $CaCO_3$, the calcination range may extend to 550 °C–1000 °C [13].

While the decomposition of $CaCO_3$ is associated with the emission of carbon dioxide (CO_2), the disintegration of hydrates releases water [5]. The mineral residue of the decomposition of portlandite and calcium carbonate is free lime (CaO), which exhibits a uniform distribution among the processed cement paste [15, 105, 170, 203, 204, 235]. Conversely, the mineral composition of dehydrated C-S-H depends on the processing temperature. At 650 °C, where C-S-H is effectively depolymerized, dehydrated particles have a high porosity in combination with a reduced density [187, 282]. With increasing temperature, particle morphology changes, resulting in increased density and smaller particles [170, 187, 235]. The chemical composition of dehydrated C-S-H is similar to belite (C_2S), with C/S-ratios ranging between 1.7–1.9 [5, 24, 75, 170, 190], which is sufficient for the formation of $\alpha'_L C_2S$ [38, 170, 187, 238]. Alternatively, the dehydration of C-S-H can yield $\alpha'_H C_2S$ [1, 24, 206, 288]. Generally, both variants of $\alpha' C_2S$ are reactive [204, 235, 274]. However, increasing processing temperature promotes the formation of βC_2S with low reactivity [1, 170, 187, 204, 281]. For temperatures exceeding 800 °C, microstruc-

ture continues to disintegrate [147], allowing for the formation of alite (C_3S) from C_2S and lime as well as tricalcium aluminate (C_3A) [317] and the subsequent melt when exceeding 1250 °C [114, 199].

Rehydration and Setting Behavior

Dehydrated cement paste generally shows a high potential for rehydration at contact with water. The hydration mechanisms and, subsequently, the workability and strength development of dehydrated cement paste differ from those of Portland cement.

Dehydrated cement paste – both as a standalone material or as partial cement substitution – exhibits an increased water demand for achieving standard consistency, and reduced setting times [15, 277]. Water demand increases and setting times decrease with higher processing temperatures [187, 213, 246, 281]. This can be attributed to two mechanisms: water ad- and absorption in porous particles as well as rehydration of free lime.

As hydrated cement paste is porous, porosity remains after thermal processing, exemplified through increased specific surface areas [15, 21, 38, 110]. Mixing water is rapidly absorbed into these loose particles and is adsorbed at the intraparticle surface [292].

The lime stemming from the decomposition of portlandite or, at higher processing temperature, from the calcination of calcium carbonates forms small particles, which are uniformly distributed among the dehydrated cement paste. This results in a high reactivity, exemplified through observations, where lime starts to rehydrate with ambient moisture during cooling. Portlandite from this reaction exhibits a lower decomposition temperature than portlandite from the hydration of Portland cement, which supports the hypothesis of small particles [9, 79, 203]. Lime quickly reacts with mixing water, thus increasing water demand [21, 204].

As both water absorption in porous particles and portlandite formation are fast, but still time-dependent effects, findings suggest an interdependence of water demand and setting times, as the determination of the latter uses a binder paste based on the former. When both effects are fully compensated for through a high water demand, the effect on setting times is negated. However, when dehydrated cement paste consumes additional water not accounted for in the determination of the water demand, setting times are reduced. Conversely, excessive water may result in increased setting times [92, 187].

These effects generally result in a reduced workability of fresh concrete or mortar [21, 50, 147, 264]. The influence can be countered by adding chemical admixtures, such as retarders or superplasticizers [22, 98, 270, 299]. Alternatively, dehydrated cement paste can be doped with mineral setting regulators. While the ettringite decomposition is reversible [16, 313], the presence or further addition of gypsum is beneficial for reducing water demand and increasing setting times [243]. Alternative setting regulators, such as sodium citrate or sodium gluconate, are likewise effective, with borax showing the highest potential for reducing water demand and increasing setting times [306, 308]. Prolonged grinding after thermal processing also has a positive effect on workability, as it reduces intraparticle porosity and thus water absorption potential [21].

These observations for water demand and setting times are mirrored through hydration heat measurements. Upon contact with water, calorimetry measurements show an immediate heat

release, which is several times higher than the corresponding heat release from Portland cement [9, 270, 292]. The hydration heat can only partially be explained by lime reaction [9, 15, 170, 214], but also by the formation of C-S-H from the accelerated rehydration of $\alpha'C_2S$ [9, 15, 24, 170, 214], monosulfoaluminate (AFm) [9, 15, 23, 24, 170], and ettringite (AFt) [15, 170, 214]. The following induction period is shortened, and the start of the acceleration period is advanced [9, 23, 203, 270, 292]. The total heat release of dehydrated cement paste is therefore higher compared to Portland cement until up to 3 d [15, 187]. Afterwards, hydration decelerates, resulting in a lower total heat compared to Portland cement [203, 246]. Hydration heat increases with higher processing temperatures [203, 243].

Similar to Portland cement clinker particles, dehydrated cement paste forms internal and external hydration products. Internal hydration products are mainly C-S-H from the rehydration of $\alpha'C_2S$, similar to C-S-H from Portland cement [187, 277], while external hydration products consist of AFm [277]. This induces differences in the microstructure of hydrated Portland cement and rehydrated cement paste. The microstructure of rehydrated cement paste is loose and porous, especially for processing temperatures below 500 °C [38, 187, 214, 277]. For higher processing temperatures, the formation of hydration products results in a densification of the microstructure [187, 277]. After rehydration, the microstructure resembles that of the original hydrated cement paste, which, in turn, is affected by the original water-cement ratio [277]. The alkalinity of the pore solution from rehydrated cement paste is lower than that of the pore solution from Portland cement or blended cements [193].

Porosity

Porosity of paste, including thermally processed cement paste, depends on processing parameters such as temperature and grinding, as well as the substitution rate.

Thermal processing at 400 °C and below tends to increase cement paste porosity when used as partial Portland cement substitution [203, 270]. Samples containing activated cement paste processed at 600 °C–700 °C exhibit the lowest porosity. Overall, at a fixed water-binder ratio, the Portland cement substitution through processed cement paste does not significantly affect total porosity [23, 203, 246, 274, 281]. The quick absorption of mixing water into porous hardened cement paste particles reduces the effective water-binder ratio, and subsequently, the porosity, in the surrounding paste, while intraparticle porosity is increased in comparison to Portland cement [23]. With ongoing rehydration, porosity and critical pore diameter generally decline, as the microstructure becomes more refined [23, 246, 270, 277]. However, this effect is smaller than in pure Portland cement paste [246]. For processing temperatures exceeding 700 °C, porosity gradually increases with the higher water demand [203, 258].

For small substitution rates, porosity is not affected, but increases with higher incorporation of processed cement paste [274]. Finely ground thermally processed cement paste particles have a densifying effect on the microstructure, which is mitigated at high substitution rates [184].

Compressive Strength Development

The accelerated hydration of dehydrated cement paste affects the compressive strength development through the fast formation of hydration products from lime and $\alpha'C_2S$, which reduces

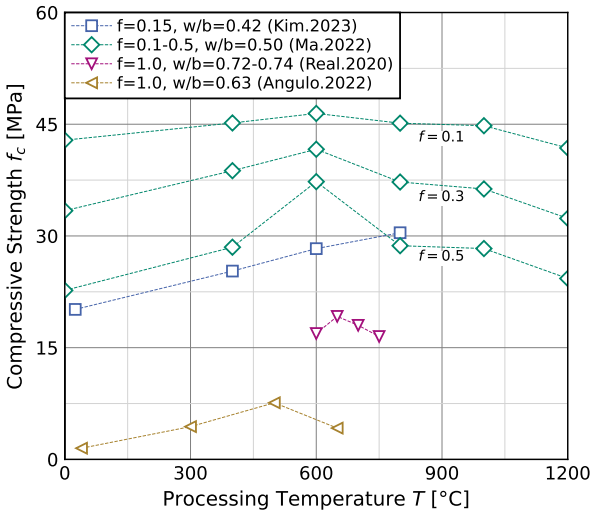

Fig. 2.5: Influence of processing temperature and substitution rate of hardened cement paste on compressive strength (w/b: water-binder ratio, f: cement substitution rate) [9, 111, 147, 187]

the water-cement ratio in the surrounding paste [15, 23, 204]. Mortar specimens obtain similar strength as Portland cement references at an age up to 3 d [23, 187].

At an age of 28 d and later, compressive strength of rehydrated thermally processed cement paste is reduced, compared to reference Portland cement samples [23, 111, 187, 203]. The underlying mechanism is the impeded interparticle connectivity through the less extensive development of external hydration products [184, 213].

As a partial Portland cement substitution, in addition to the filler effect, the water uptake in dehydrated cement paste reduces the effective water-cement ratio in the remaining paste, which in turn results in a denser microstructure [184, 243, 270]. This counteracts the aforementioned microstructural distortion. For substitution rates of Portland cement up to 25 wt%–40 wt%, the effect of dehydrated cement paste on compressive strength remains negligible [22, 38, 124, 147, 184, 243, 246, 274]. At higher substitution rates, the loosening effect prevails, and compressive strength declines [38, 203]. Additionally, the impaired workability of dehydrated cement paste can result in poor densification [184, 203]. The use of superplasticizer instead of adjusting water content for achieving standard consistency has a positive effect on compressive strength at high substitution rates up to 100 wt% [37, 292].

The influence of the thermal processing temperature on compressive strength has been widely researched, without reaching a consensus. While agreeing with the strength increase through thermal processing compared to ground concrete waste or hardened cement paste, findings for the processing temperature yielding the highest compressive strength range between 350 °C and 800 °C [42, 68, 86, 111, 112, 147, 170, 203, 235, 264, 274, 277, 281, 304]. Figure 2.5 demonstrates these findings for cement paste processed at different temperatures, where the water-binder ratio for strength testing was held constant throughout the individual series. The presented results also show the decline of compressive strength with an increase in substitution rate f.

Tensile Strength

As concrete or mortar tensile strength is rarely measured directly due to its elaborate and expensive test setup, the assessment of tensile strength relies on indirect procedures, such as flexural or splitting strength [149].

Overall, the flexural strength of mortar containing processed cement paste follows the same dependences as compressive strength, including processing temperature and cement substitution rate [23, 112, 147]. Pores from insufficient compacting, as a consequence of poor workability, have a reduced effect on flexural strength, in comparison to compressive strength. However, flexural strength is negatively impacted by an increased amount of cracks in the specimen [203].

Similar observations are made for the splitting strength [111]. In general, the empirical relationship between tensile strength obtained from the splitting test and compressive strength agrees with the provisions in EN 1992-1-1:2004 [189].

Elastic Modulus

Cement substitution through thermally processed concrete waste has a negative impact on the modulus of elasticity, which can be determined either as static or dynamic modulus [60, 154].

The dynamic modulus of elasticity is reduced as a consequence of cement substitution through thermally processed cement paste, as these particles exhibit a lower density. Increasing processing temperatures result in higher dynamic moduli [21]. Overall, the dynamic modulus and compressive strength follow similar influencing factors, such as pore refinement through reactive phases, and therefore exhibit a good interdependency [78].

Overall, the modulus of elasticity decreases with lower compressive strength. Yet, in contrast to compressive strength, a decreasing static modulus of elasticity can be observed for low substitution rates, due to the reduced particle stiffness [189].

Shrinkage

As the microstructural resistance to shrinkage deformation follows the same mechanisms as the modulus of elasticity, shrinkage increases with reduced elastic moduli, i.e., through reduced particle density and stiffness, as well as reduced compressive strength [40]. However, for low substitution rates, this effect is mitigated by the densification effect of processed cement paste [85, 189, 244]. Processed cement paste with high particle stiffness, through cement paste with low water-cement ratio, or increasing processing temperatures, results in reduced shrinkage [40, 112]. Drying shrinkage is significantly affected by the amount of evaporating water [112]. Mortar or concrete, where the increased water demand of processed cement paste is countered through additional mixing water, exhibits increased shrinkage deformations, which are only partially explained by decreasing compressive strength [40]. Processed cement paste has been found to reduce early basic shrinkage up to a concrete age of 1 d [184].

Capillary Absorption

Capillary absorption is linked to the development of porosity and follows the same influencing factors. Generally, water absorption increases with increasing Portland cement substitution

through processed cement paste, especially when the increased water demand is compensated for by additional mixing water [40]. At a constant water-binder ratio, the mixing water uptake in processed cement paste particles reduces the water-binder ratio of the surrounding paste, which mitigates overall capillary absorption [22, 37, 40, 78].

The thermal processing has a reducing effect on capillary absorption [112, 147, 244, 273, 274]. Increasing the processing temperature up to 1000 °C leads to gradually declining capillary absorption coefficients [147]. However, for 1200 °C, capillary absorption increases again [273].

Carbonation

The partial Portland cement substitution through thermally activated cement paste has a positive effect on carbonation resistance. This is caused by the densification of the microstructure following the water consumption by processed cement paste particles, which overcompensates for the reduction of carbonatable phases [22, 37]. A complete substitution of Portland cement through activated cement paste results in decreased carbonation resistance alongside a reduced compressive strength [282].

Chloride Diffusion

Chloride ingress is affected by the open porosity and subsequently increases with increasing Portland cement substitution through thermally processed cement paste [22, 37]. Therefore, increasing processing temperature between 20 °C and 1200 °C gradually reduces chloride transport [86, 111]. Higher substitution rates increase chloride ingress due to their higher porosity [184]. A reduction in particle size has a mitigating effect on chloride transport [86].

Freeze-Thaw Action

Apart from the overall strength reduction, mortar or concrete including thermally processed concrete waste shows a similar response to freeze-thaw action compared to reference systems with Portland cement, due to their pore size distribution [3, 269]. Consequently, the relative change in dynamic modulus of elasticity and tensile strength for mortar containing thermally processed concrete waste is increased due to the lower base values [3, 244]. Accordingly, pore diameters and mass loss increase for higher substitution rates [3, 269]. Thermal processing has a mitigating effect on damage evolution, as upon rehydration, a higher amount of hydration products is formed [269].

Other mortar or concrete properties

Thermally activated concrete waste can be used for the immobilization of radioactive waste, as heavy metals are absorbed into the structure of the hydration products [110].

The thermal conductivity of lightweight concrete containing thermally processed fine concrete waste is lower than a Portland cement reference [193].

Impact of Processing Parameters

Aside from the aforementioned effect of processing temperature on the rehydration behavior of activated cement paste, other thermal processing parameters, such as heating or cooling rates or annealing time, may also affect the outcome. Table 2.3 provides an overview of the statistical analysis of different processing parameters.

Tab. 2.3: Statistical analysis of processing parameters in literature
R+: heating ramp, PT: processing temperature, PD: time at processing temperature, PSD: maximum particle size, R-: cooling ramp

	Fixed selection				Varying selection			
Parameter	R+	PT	PD	PSD	PT	PD	R-	PSD
Unit	K/min	°C	min	µm	°C	min	K/min	µm
Arith. mean	9	632	174	143	680	94	260	133
Standard dev.	4	90	162	72	252	73	518	87
No. of papers	48	30	59	47	46	4	2	6

Among the reviewed publications, the influence of processing temperature has been investigated the most. The influence of different processing temperatures is discussed among the aforementioned paragraphs for the individual material properties.

While many publications report the duration of the thermal processing, there is a great variation between individual works. However, the direct influence of processing duration has been examined in only three publications. While C-S-H dehydrates within 60 min after reaching the target temperature, increasing the holding time has no beneficial effect [79, 259]. However, increasing the duration of thermal processing can lead to greater mass loss at a fixed temperature and, subsequently, result in higher mortar strength [75].

Reducing the heating rate promotes the decomposition of mineral phases, e.g., portlandite, at lower temperatures [300]. However, the influence of the heating rate on rehydration has not been investigated. The cooling rate is most often left undefined, and published results are inconclusive [56, 206].

Grinding has a beneficial overall effect on the performance of thermally processed cement paste and concrete waste. Finer particles result in a better rehydration due to a more uniform distribution, in addition to a filler and nucleation effect. Subsequently, compressive strength increases with smaller particle sizes [13, 21, 23, 124, 205, 277, 303, 304]. Similar to Portland cement, a higher fineness results in a higher water demand due to the increased specific surface area [40]. However, when grinding follows thermal processing, two advantageous effects can be observed: first, grinding is facilitated [79]. Secondly, extended grinding may result in decreased specific surface area, despite a smaller particle size [13].

In contrast to the general thermal processing procedure, other options have proven efficient: instead of a furnace setup, hardened concrete paste can be activated through microwave power, where similar dehydration products form [286]. Through autoclaving combined with calcium hydroxide addition, the amount of C-S-H in recycled concrete waste can be increased, which allows for a higher dehydration potential [143, 225].

Influence of Concrete Waste Composition

The thermal activation of concrete waste primarily affects the hardened cement paste, leaving the aggregates unaltered. Calcination of calcitic aggregates begins at ca. 700 °C [114, 199], quartzitic aggregates exhibit a reversible microstructure change at 573 °C and are otherwise stable until 1150 °C [74, 114, 199], and granite decomposes at a processing temperature higher than 1215 °C [74]. Research on thermal activation largely focuses on laboratory-made artificial hardened cement paste as a precursor. Alternatively, when investigating more practically applicable concrete waste, research uses the fine fraction. This is due to the concentration of hardened cement paste with a smaller particle size. These so-called (recycled) concrete fines (RCF), however, differ from hardened cement paste in several aspects:

- Most research projects use a single laboratory-made cement paste with a fixed water-cement ratio, most commonly between 0.40 and 0.55. Recycled concrete fines have an undetermined water-cement ratio, which may vary if fines originate from more than one building element. Besides, w/c in concrete waste often exceeds 0.55, as many requirements for durability and strength are met with higher water-cement ratios.
- Cement paste in recycled concrete fines typically consists of a Portland cement and water mixture but may include alternative, secondary binders, such as granulated blast-furnace slag or pozzolans (see section 2.1.1).
- Through interactions with the environment during the lifespan of a building, the cement paste in concrete waste may be altered, i.e., through chemical processes such as carbonation or by the ingress of diverse substances like chlorides.
- The presence of fine aggregates in recycled concrete fines is inevitable. The ratio of aggregate to hardened cement paste in recycled concrete fines varies with the parent concrete and mechanical processing parameters.
- While aggregates are generally stable for the most-used thermal activation temperature range, aggregates with different mineral composition are known to influence hardened concrete properties [135].

The water-cement ratio in hardened cement paste affects the performance as a binder following thermal activation. The porosity and microstructure of thermally processed cement paste strongly depend on the microstructure before activation, and thus, on its water-cement ratio [23]. Subsequently, a lower water-cement ratio (w/c) in the precursor results in lower water demand and prolonged setting times [40, 283]. However, strength development and capillary absorption are not affected, in contrast to shrinkage, where the higher particle stiffness results in reduced deformations [40].

Thermally activated cement paste containing supplementary cementitious materials (SCMs) performs similarly to that of Portland cement paste. However, across different types of SCM, individual behavior can be observed. Hydration products in binary cement pastes differ in their chemical and mineralogical compositions. Due to the reduction of Portland cement, the amount of portlandite decreases. In the case of latent-hydraulic or pozzolanic SCMs, additional C-S-H

is formed. Alternatively, granulated blast-furnace slag or fly ash may contribute aluminium, which may react to calcium aluminate silicate hydrates (C-A-S-H) [280]. These phases lead to a higher rehydration potential. This can be followed in heat flow measurements: slag-cement-paste exhibits an increased release of hydration heat upon rehydration for all processing temperatures, while hydration heat development of thermally processed fly ash-cement paste is reduced [280, 281]. Compressive strength development of pure activated binary cement paste mirrors hydration heat development, with slag-cement paste achieving the highest and fly ash-cement paste the lowest strength [280]. Cement paste containing pozzolanic silica fume has a positive effect on compressive strength, while inert limestone powder reduces strength development [205, 280]. However, when the processing temperature of limestone-cement paste exceeds the limestone calcination temperature, excessive free lime is formed and adds to the rehydration potential [280]. Overall, for all binary cement pastes, compressive strength exhibits a negative correlation with total porosity [280].

Atmospheric carbonation may have a significant impact on the reactivation potential of thermally processed concrete fines. Through carbonation, portlandite and ettringite are transformed, and the thermal processing below the calcination temperature leaves these phases inert. Subsequently, the rehydration reactivity of carbonated concrete fines is reduced [24, 243, 317]. In contrast, an enforced carbonation before thermal activation may increase the compressive strength contribution [265].

Fine natural aggregates mixed with hardened cement paste have a diluting effect on rehydration following thermal activation, due to their inert state [21, 37, 39]. The reduced reactivity results in decreased compressive strength at similar processing temperatures and mix designs [39]. Overall, the comparison of fig. 2.5 and fig. 2.6 shows a similar trend for the effect of processing temperature on compressive strength, albeit at a much smaller magnitude, which can be explained by the lower amount of reactivated paste. Figure 2.6 (right) shows a steeper decline of compressive strength with increasing substitution rate when comparing processed concrete fines to activated cement paste. Additionally, when processed concrete fines are used instead of activated cement paste, water absorption and carbonation rate increase [22, 112, 193]. Conversely, the higher content of inert particles in recycled concrete fines has a mitigating effect on water demand and concrete shrinkage [40, 189].

Interaction of thermally activated cement paste and secondary binders

Overall, binary binder systems consisting of thermally activated cement paste and slag or fly ash, or ternary systems additionally incorporating Portland cement, exhibit an improved performance.

Grinding dehydrated cement paste together with slag improves grinding efficiency by reducing particle agglomerations triggered through agglomeration induced by the ball-mill effect of slag [307]. The combined thermal activation of blended concrete fines and clay increases reactivity and enhances compressive strength [136].

As fly ash and slag positively affect water demand and workability when substituting Portland cement, a similar influence can be observed in mixes incorporating activated cement paste instead of Portland cement [142, 204, 264, 302]. The utilization of silica fume, fly ash, or slag also

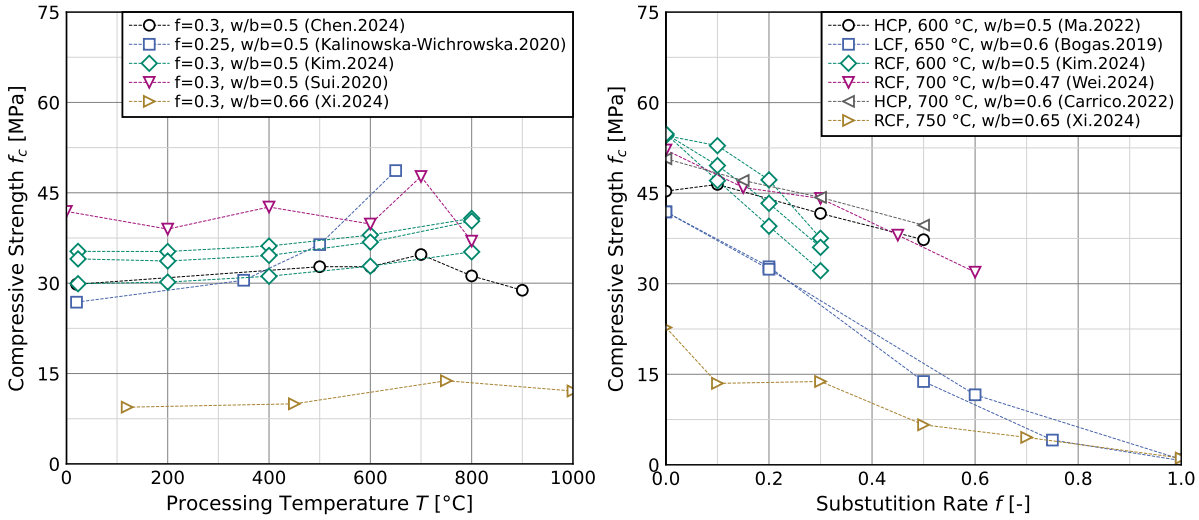

Fig. 2.6: Influence of processing temperature (left) and substitution rate (right) of recycled concrete fines on compressive strength, for fixed water-binder ratios [21, 40, 42, 105, 112, 147, 235, 269, 277]. HCP: Hydrated cement paste, LCF: Laboratory concrete fines, RCF: Recycled concrete fines.

yields higher compressive strength, as free lime (CaO) in dehydrated cement paste – resulting from the decomposition of portlandite or, at higher processing temperatures, the disintegration of calcium carbonates – reacts with these latent-hydraulic or pozzolanic materials [142, 204, 214, 264, 289, 291]. The combination of activated cement paste and slag proves particularly effective, as the relatively weak external hydration products of rehydrated cement paste are compensated by reaction products from slag [307]. In a limestone calcined clay cement, dehydrated cement paste can replace up to 20 wt% of clinker without adversely affecting compressive strength [103].

Alternatively, as with slag or fly ash, thermally activated cement paste can serve as a precursor in Portland-cement-free alkali-activated binders. Adding alkali activators to dehydrated cement paste modifies the hydration product composition while decreasing quartz and gypsum content, promoting the formation of C-S-H and C-A-S-H from lime and C_2S [275, 276]. Alkali-activated dehydrated cement paste exhibits reduced porosity and enhanced chloride diffusion resistance [137, 166, 167, 275].

Ecological impact

The processing and subsequent use of thermally activated concrete fines have ecological impacts across several areas.

Thermal activation of concrete fines requires energy for material preparation (separation and drying), for maintaining processing temperatures, and for grinding. Grinding requires less electrical energy compared to clinker [226]. Processing temperatures are significantly reduced, thereby requiring less energy. The removal of moisture from concrete fines accounts for the highest relative energy demand in the entire processing procedure [226–228, 243]. In total, the energy demand for wet concrete fines activation can be up to 60 % higher than that of Portland cement production [226]. The activation of dry concrete fines requires less thermal energy compared to Portland cement [226, 265].

When using a similar fuel mix to provide thermal energy for concrete fines drying and activation, CO_2 emissions from concrete fines activation are between 22 % and 39 % lower than those from Portland cement production [226, 227]. These reductions stem from the avoidance of the calcination process in clinker production [226]. Additionally, because processing temperatures are lower than the clinker burning temperature and drying occurs at significantly lower temperatures, the entire process can rely solely on electrical energy, eliminating the need for fossil fuels [228]. Assuming a future renewable energy system, CO_2 emissions from electrical energy use will drastically decrease [188], so that the activation of concrete fines at 450 °C emits up to 94 % less CO_2, and at 800 °C, up to 76 % less, compared to Portland cement clinker production [87].

Finally, recycling concrete waste reduces the need to consume primary resources. Through substituting Portland cement, this comprises mainly clinker raw meal components. When thermal processing combines the production of an alternative concrete binder with the manufacturing of improved fine recycled aggregates, this also impacts mining for concrete aggregates [228].

A comprehensive life-cycle analysis of thermally activated concrete fines as a Portland cement substitution requires the consideration of the entire concrete production process, including the need for admixtures such as superplasticizers for offsetting the negative impact of incorporating concrete fines on concrete performance and to produce equally durable concrete structures [188, 299].

Chapter 3

Research Scope

Hardened cement paste (HCP), which adheres to natural aggregates to form concrete, is a major obstacle to recycling concrete waste. This challenge is most prevalent when considering the fine fraction of crushed concrete, where HCP concentration is increased. This results in higher porosity and, consequently, lower strength and hardness compared to natural aggregates.

The application of these waste materials as fine recycled aggregates in concrete production is hindered by their high content of hardened cement paste, which adversely affects both fresh and hardened concrete properties. Processing methods for optimizing the properties of fine recycled aggregates can only mitigate this issue – especially procedures that improve the separation of HCP and aggregates and thereby produce an even finer HCP-rich fraction.

The recycling of fine concrete waste as cement (or, more generally, as binder) may not only offer an alleviation to the issue of material circularity, but also address the need for substituting cement clinker to reduce CO_2 emissions. Due to the lack of alternative high-quality recycling options for concrete fines, they provide an abundantly available waste material. There are no official statistical data regarding the amounts of fine concrete waste. A survey conducted for [91] allowed for estimating an annual output of 5 Mt–10 Mt of fine concrete waste in Germany. This amount is within the range of the annual consumption of supplementary cementitious materials and therefore may serve as an alternative or addition to them.

For cement recycling, the chemical and mineralogical composition of concrete waste provides a key challenge. Figure 3.1 illustrates the chemical composition of various batches of fine concrete waste found in literature. For the application as a clinker raw meal component, increasing deviations from the optimum raw meal composition signify lower substitution rates and thus a limitation on this recycling option. Furthermore, variations of waste compositions require extensive monitoring and adjustments to the relative compositions of individual raw meal fractions, besides concrete waste.

For the application as supplementary cementitious material, the chemical composition is of reduced importance. However, the mineralogical composition may significantly affect concrete performance. This includes variations in aggregate composition at individual contents and in the hydration products of different supplementary cementitious materials within the hardened cement paste.

Previous research on hardened cement paste has shown that thermal activation provides a promising processing method. Regardless, despite a high publication activity in this field, various

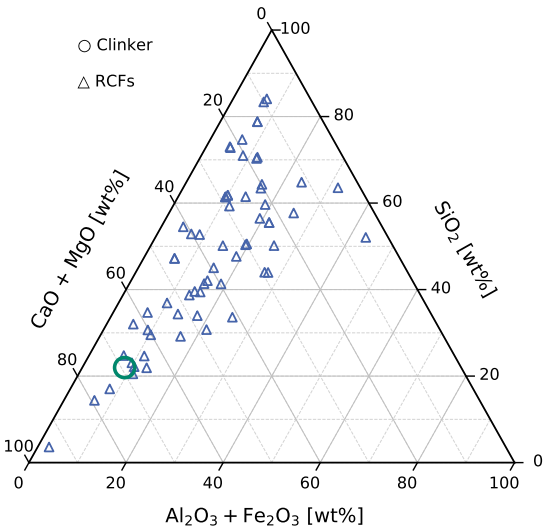

Fig. 3.1: Ternary illustration of the chemical composition of fine concrete waste found in literature [2, 13, 27, 41, 43, 48, 49, 51, 67, 69, 76, 81, 84, 100, 108, 112, 125, 127, 129, 130, 133, 138, 145, 155, 165, 192, 194, 210, 225, 235, 236, 241, 243, 246, 268–270, 275, 287, 289, 304, 316], and cement clinker (table 2.1).

issues remain unclear. This thesis aims to address several key aspects of thermal activation of concrete waste for the application as supplementary cementitious material.

The overall feasibility of this undertaking is highlighted in the first publication (A1) of this thesis. The results show the positive effects of thermal activation on compressive strength and durability, and demonstrate the need to compensate for strength loss as a prerequisite for further analyses. This publication lays the groundwork for the subsequent experimental program.

A1 Jan P. Höffgen, Michael Vogel, Oliver Blask, and Frank Dehn. „Entwicklung thermisch-mechanisch aktivierter Betonbrechsande als Betonzusatzstoff – Projektvorstellung und erste Ergebnisse“. Beton- und Stahlbetonbau 118, No. 4 (2023): 239–246. https://doi.org/10.1002/best.202200127.

While thermal activation of pure hardened cement paste may ultimately result in almost unaltered concrete compressive strength, the application of fine concrete waste from industrial sources reduces compressive strength. Numerous publications assess the effect of hardened cement paste, and a similar number address industrial concrete waste. However, the impact of varying concrete compositions has yet to be systematically investigated. The literature review has identified a limited number of publications focusing on artificial hardened cement paste containing supplementary cementitious materials. Still, the influence of the content and composition of natural aggregates in concrete waste remains unclear. Addressing this issue directly translates into quantifying the impact of concrete waste heterogeneity. Therefore, the first experimental and analytical part of this thesis aims to develop a model to predict the compressive strength of thermally activated concrete waste used as a supplementary cementitious material. For this, a set of 12 different laboratory-made artificial concrete fines and 25 different industrial fines obtained from concrete recycling plants are used as precursors for thermal activation. Table 3.1 contains the composition of the artificial fines. Here, seven mortars vary the amount and type of

aggregates. Based on pure CEM I-paste (CEM), siliceous river sand (RS), limestone sand (LS), and greywacke (GW) are used to produce mortars with a cement paste content ranging between 50 v% and 75 v%. The naming scheme combines both parameters, i.e., RS50 for a mortar with river sand and 50 v% paste. For the assessment of binder composition, ground granulated blast-furnace slag (S) and fly ash (FA) substitute 30 wt% of CEM I in CEM (named S0 and FA0) and RS50 (named S50 and FA50). Industrial fines are named after the processing plant (A–H) and the precursor particle size, i.e., particles ranging from 0 mm to 2 mm obtained from plant A1 are named A1-0/2. "F" denotes filter cake from wet processing plants. For the indication of processing parameters, a suffix including the processing temperature is added to the name of the precursor.

Tab. 3.1: Composition of artificial fines used as precursors for thermal activation. w/b: water-binder ratio; v_p: paste volume; A: aggregates; FA: fly ash; S: blast-furnace slag; RS: river sand; LS: limestone sand; GW: greywacke (from P2, table 2).

	Binder	w/b	v_p [v%]	A
CEM	100 wt% CEM I	0.5	100	–
RS75	100 wt% CEM I	0.5	75	RS
RS62			62.5	
RS50			50	
LS75	100 wt% CEM I	0.5	75	LS
LS50			50	
GW75	100 wt% CEM I	0.5	75	GW
GW50			50	
FA0	70 wt% CEM I + 30 wt% FA	0.5	100	–
FA50			50	RS
S0	70 wt% CEM I + 30 wt% S	0.5	100	–
S50			50	RS

While concrete compressive strength is the key property for structural design, other mechanical and durability properties are equally important but are usually derived from compressive strength via empirical relationships. Previous literature has shown the impact of cement substitution using thermally activated concrete waste, but this is often superimposed by reduced compressive strength. The second experimental and analytical part of this thesis, therefore, has the goal to assess mechanical and durability properties with a full compensation of compressive strength alterations due to varying concrete waste compositions. Here, a subset of both artificial fines and industrial fines is selected for the detailed analyses, including a comparison with established SCMs. Furthermore, this part aims at validating the aforementioned compressive strength prediction model.

Figure 3.2 gives an overview of the experimental and analytical approach used for this thesis.

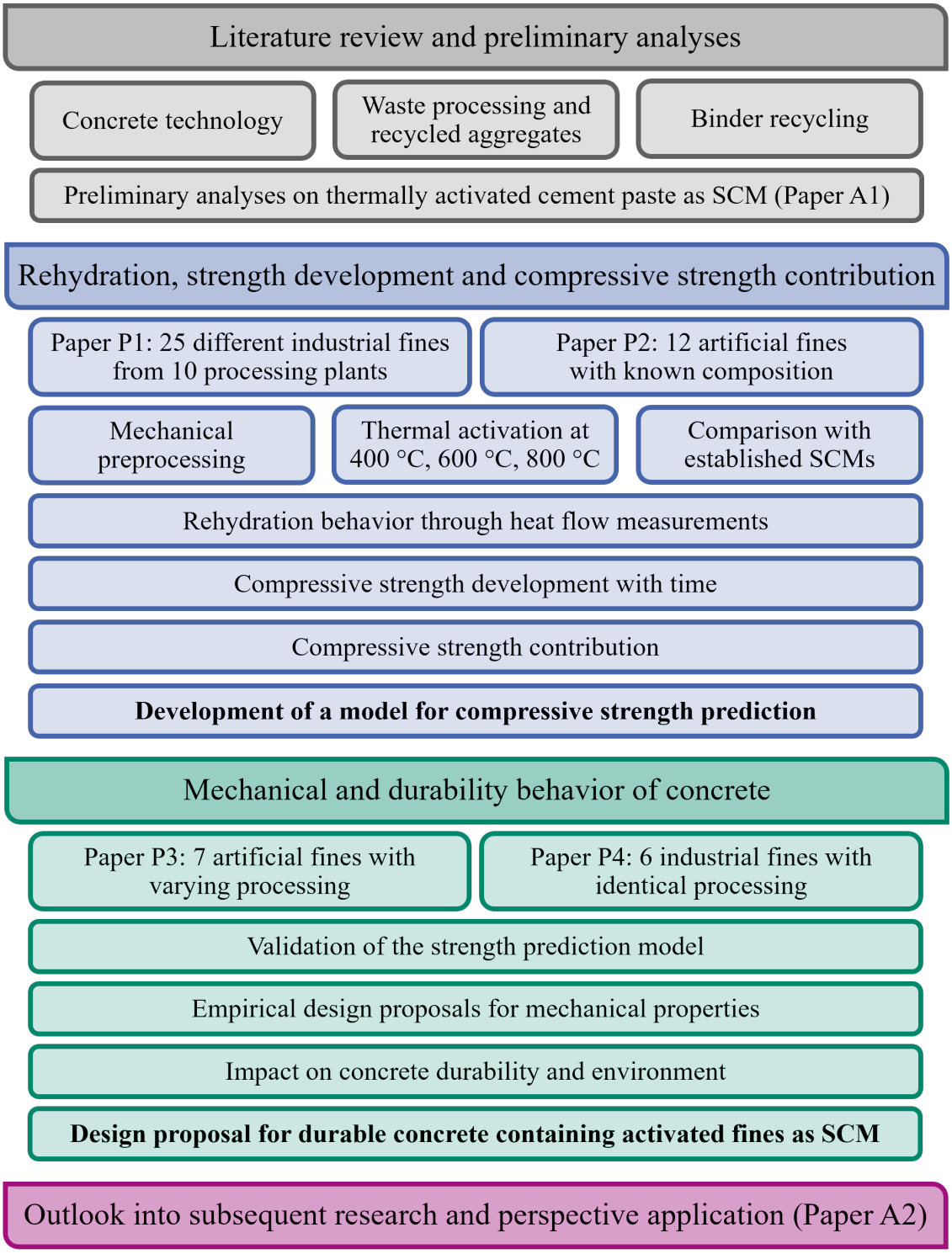

Fig. 3.2: Overview of the approach used for this thesis.

Chapter 4

Influence of Thermally Activated Concrete Fines on Mortar Compressive Strength

The compressive strength at the age of 28 d is the most important material parameter for designing concrete structures. Specifications such as Eurocode 2 (EN 1992, with numerous subdivisions) rely on compressive strength as a decisive input for subsequent structural design. Therefore, concrete production requires a method for predicting compressive strength before or during mixing. In addition to experienced personnel, this knowledge usually derives from empirical relationships among raw materials, mix design, and compressive strength development. Thus, the use of thermally activated concrete fines as a novel cementitious material requires a new approach to predicting compressive strength.

This chapter discusses two publications that address this issue from different starting points.

P1 Jan P. Höffgen, Sebastian Bruckschlögl, Bernhard Wetz, and Frank Dehn. „Influence of Thermally Activated Industrial Concrete Fines of Different Origin on Mortar Strength Development“. Case Studies in Construction Materials 23, October 2025: e05427. https://doi.org/10.1016/j.cscm.2025.e05427.

P2 Jan P. Höffgen and Frank Dehn. „Influence of Thermally Activated Artificial Concrete Fines Composition on Mortar Strength Development“. Developments in the Built Environment 24, December 2025: 100775. https://doi.org/10.1016/j.dibe.2025.100775.

While both publications share the same foundation in reference materials, mix design, and experimental procedures, the main difference lies in the types of concrete fines used in the analysis.

The first publication is based on 25 different concrete fines, obtained from 10 processing plants. Further variations include the type of precursor, temporal aspects, and different preprocessing. The second publication uses 12 laboratory-made artificial concrete fines, whose compositions were deliberately altered to represent a wide range of possible concrete fines.

The following sections provide recaps of key findings from both publications, including a unifying discussion of the results and additional analyses.

4.1 Key Findings in P1 and P2

Thermal Activation Procedure

P1 presents an experimental analysis of different processing parameters for thermal activation. As a precursor, artificial hardened cement paste (the later CEM in P2) is used, since all relevant chemical processes are confined to the cement paste fraction in concrete fines. One notable exception is the disintegration of carbonatic minerals, especially in calcitic aggregates. However, as this process is mostly averted in order to avoid CO_2 emissions, the possible implications of calcitic aggregate decomposition for the thermal activation procedure were deemed less important.

The results show that the effect of the activation at 600 °C is not affected by other processing parameters, such as holding time, heating, or cooling rates. While holding time exhibits an insignificant effect for activation at 800 °C, the dehydroxilation of $Ca(OH)_2$ appears to be time dependant. Although the activation at 400 °C is below the decomposition range determined on the precursor (see P1, fig. 2), a holding time of 2 h reduces the amount of $Ca(OH)_2$ in the processed paste. Another temporal effect is caused by heat propagation. While small sample sizes, such as cricibles in the thermogravimetric setup, exhibit a virtually homogeneous temperature field, increasing sample sizes signify a longer duration until the entire sample reaches the target temperature. Conversely, increasing sample sizes requires longer processing durations for achieving reproducible results. Ultimately, thermal activation parameters were selected to suit all precursors, and identical parameters were used in both publications.

The application of concrete fines as supplementary cementitious material requires grinding. For organisational reasons, grinding of artificial and industrial concrete fines was different for both kinds of precursors. In practice, thermal activation of coarser materials is easier to realize in existing setups, and grinding of thermally activated, and thus weakened particles requires less energy. Therefore, this procedure is applied to industrial fines. For artificial fines, the two steps are reversed. Instead of grinding individual batches in a laboratory mill after thermal activation, processing relies on an industrial mill, where the entirety of the different kinds of artificial fines is milled prior to thermal activation. This allows for an increased number of parameter combinations, as grinding in the laboratory mill has proven to be very time-consuming. Furthermore, it is ensured that all precursors have similar particle size distributions. Conversely, ground industrial fines exhibit a coarser particle size distribution compared to artificial fines, which may negatively affect hardened concrete properties (compare P1, table 2; P2, fig. 3).

Concrete Fines Composition

The composition of artificial fines aims to represent typical concrete fines compositions. While P2, fig. 1 shows a good agreement between the artificial fines oxide phase composition and the fine concrete waste compositions detailed in the literature, the chemical composition of the industrial fines exemplified in P1, fig. 5 is less diverse. Compared with the referenced fines composition, these industrial fines exhibit a similar, low content of Al_2O_3 and Fe_2O_3. Apparently, none of the fines contain calcitic aggregates, indicated by the rather low ratio of CaO to SiO_2. The chemical composition lies in the range of the artificial types RS50, RS62, and RS75, which denote fines

with 25 v%–50 v% siliceous river sand as fine aggregates. Preprocessing fines with a smaller mesh size generally increases the ratio of CaO to SiO_2, suggesting the hypothesized concentration of hardened cement paste in precursors with smaller particle size.

However, the chemical composition cannot be used as an indicator for the cement paste content, as both SiO_2 and CaO may be present in hardened cement paste as well as aggregates. The results of the thermogravimetric analyses in P1, fig. 6 provide an additional insight into the thermal decomposition of selected concrete fines. When selecting 600 °C as decisive temperature for dehydration, mass loss ranges between 3.6 wt% (A1-0/2) and 12.6 wt% (D-F). The increasing mass loss with reducing precursor particle size substantiates the hypothesis of hardened cement paste concentration. Nevertheless, none of the industrial fines with a precursor size of 2 mm surpass the mass loss of RS50 (6.1 wt%), and only the filter cake D-F exceeds RS75 (10.5 wt%), despite the similar chemical composition (P2, fig. 6). However, when comparing the total mass loss of industrial fines to RS50 and RS75, the former exhibit a lower, almost undeterminable mass loss around 500 °C, and a higher mass loss around 800 °C. This indicates that in industrial fines, $Ca(OH)_2$ originating from Portland cement hydration has been converted to $CaCO_3$ by natural carbonation.

Hydration Heat Development

The investigation of the hydration heat of blended cement containing processed artificial concrete fines indicates the effects of the substitution rate, activation temperature, and binder composition. The substitution rate of 30 wt% results in similar hydration heat flow for the four activated paste samples in P2, fig. 7. Increasing the substitution up to 100 wt% results in deviating behavior, with S0-600 behaving most similarly to the CEM I reference, but with an increased hydration heat flow in the first 6 h of the test. For CEM-600, this behavior yields an overall accelerated behavior. Since FA0-600, where the thermogravimetric analysis shows almost no $Ca(OH)_2$, which would have been converted to CaO during activation, and CEM-400, where $Ca(OH)_2$ is still present as hydroxide, exhibits a strongly deviating behavior, the influence of CaO on the hydraulic behavior of thermally activated cement paste is evident.

For artificial fines containing aggregates of different types and contents, these effects become less apparent. The hydration heat development in P2, fig. 5 and 6 varies slightly, but ultimately exhibits a similar total hydration heat as the reference blend of CEM I and slag in P1, fig. 7. The blends of CEM I and industrial fines exhibit very similar hydration heat developments, which exceed the reference blends containing fly ash or limestone powder, and agree with results for artificial fines containing aggregates. The only exception is the fresh concrete recycling filter cake D-F, which exhibits increased total hydration heat, particularly within the first 6 h.

Compressive Strength Development

The increased early hydration heat flow of CEM I blended with processed concrete fines is mirrored by the temporal compressive strength development. The ratio of compressive strength after 2 d and 28 d is similar to the CEM I reference at corresponding strength for all types of fines, while slag and fly ash yield a retarded strength development (P1, fig. 8; P2, fig. 8–10).

Compressive Strength Contribution

The substitution of 30 wt% CEM I through supplementary cementitious materials results in a reduction of compressive strength. The only exceptions are pure paste artificial fines. CEM I paste activated at 600 °C exhibits no measurable effect on compressive strength. A higher activation temperature, as well as pastes containing fly ash or slag, yield an increase in strength. For artificial concrete fines containing aggregates, compressive strength declines, matching the behavior of industrial concrete fines. Reducing processing temperature to 400 °C, or even 100 °C, has a similar effect on compressive strength.

These observations lead to a model for compressive strength contribution, which gives a linear relationship between the loss of chemically bound water and k-values (established in EN 206 and CEN/TR:16639) as a measure for reactivity. Equation (4.1) and eq. (4.4) illustrate the models from P1 and P2, respectively. Both approaches use the same relationship between the water-cement ratio and compressive strength derived from 14 mortar series with CEM I. P1 used 137 mixes with industrial concrete fines, and P2 used 171 mixes with artificial concrete fines as individual data sets.

Industrial concrete fines (P1)

$$k = k'_m \cdot \Delta m_{TG} + k_0 \tag{4.1}$$

$$k'_m = 5.30 \tag{4.2}$$

$$k_0 = 0.10 \tag{4.3}$$

Artificial concrete fines (P2)

$$k = k_h \cdot \Delta m + k_a + k_b \tag{4.4}$$

$$k_h = 5.70 \tag{4.5}$$

$$k_a = \begin{cases} 0.00 & \text{for LS} \\ 0.10 & \text{for RS} \\ 0.30 & \text{for GW} \end{cases} \tag{4.6}$$

$$k_b = \begin{cases} 0.15 & \text{for CEM I} \\ 0.30 & \text{for CEM I + S} \\ 0.45 & \text{for CEM I + FA} \end{cases} \tag{4.7}$$

Both models show a good agreement of the relationship between k and mass loss Δ_m up to a processing temperature of 600 °C. When transforming the inclination into the chemically bound water content of one unit-weight of CEM I, the results (0.21 g/g for artificial fines and 0.23 g/g for industrial fines) show an excellent agreement with established benchmarks [28, 144, 179]. However, the analysis of the results underscored that the mass loss of industrial fines must be determined in a non-oxidizing atmosphere, as the mass loss is distorted by organic carbon. Due to their origin, artificial fines have experienced no such contamination.

The two model approaches show a discordance of k-values for ground concrete fines without thermal activation (k_0 for industrial fines and $k_a + k_b$ for artificial fines). The cause for these diverging results could not be conclusively determined with the present data. Three complemen-

tary hypotheses may serve as starting points for future investigations. In addition to differences in particle size distributions, high-energy milling of artificial fines may have further altered the microstructure. This effect is commonly described as mechano-chemical activation, and usually requires prolonged grinding [6, 7, 14, 44, 245, 311, 312]. However, a marginal activation cannot be ruled out, which affects k_0 and k_a. Furthermore, drying the precursor fines at 105 °C was a necessary compromise to enable grinding of artificial fines in an industrial mill, but may have induced a different error: as decomposition of cement paste phases begins at lower temperatures (compare section 2.4.4), these dehydration mass changes do not appear in Δ_m, but increase k_0 and k_b. This becomes more relevant as paste content increases. Finally, despite the prolonged storage duration of bulk artificial fines, some residual unhydrated cement particles may be present, and increase reactivity.

4.2 Additional Analyses to P1 and P2

4.2.1 Impact of the Thermal Activation Procedure

P1 describes the analysis of different activation parameters on the dehydration of hardened cement paste (artificial fines type "CEM"). The procedure followed a two-step approach, where first, CEM is activated in a thermogravimetric setup at different heating and cooling rates, as well as activation temperatures and holding times. Secondly, for the activation temperature of 600 °C, combinations of holding times and sample sizes are assessed. For spatial reasons, the evaluation in P1 has been limited to thermogravimetric measurements. Hereinafter, additional results for mineralogical, calorimetric, and mortar strength measurements are presented.

In addition to the thermogravimetric analyses on the artificial fines CEM presented in P1, fig. 3, the samples obtained from the processing in the thermogravimetric setup were characterized through X-ray diffraction (XRD) measurements. While the results presented in P1 only exhibit a significant effect of the holding time at the target temperature of 400 °C, the results presented in fig. 4.1 and fig. 4.2 give a more detailed view.

The XRD measurements underscore the partial decomposition of portlandite with increasing holding time at 400 °C through a reduced intensity of the portlandite peaks and an increased intensity of the lime peaks. A similar, albeit less pronounced trend can be observed for the target temperatures 600 °C and 800 °C, which was not apparent in the thermogravimetric results. Here, the calcite peaks exhibit a decreasing intensity, while lime marginally increases.

This behavior also becomes apparent when assessing the heating rate at a target temperature of 600 °C. For 1 K/min, where the overall duration is significantly increased, the lime peak shows an increasing intensity in favor of the calcite peak. Furthermore, at 1 K/min, the cristallinity of the belite (C_2S) peak is altered. The cooling rate, however, shows no impact.

The batch size of 5 g in the thermogravimetric setup allowed for hydration heat measurements within the experimental framework of P1 (duplicate determination, 1.75 g CEM I, 0.75 g activated CEM-100, 1.5 g water, 20 °C). The key results of the heat flow calorimetry measurements are shown in table 4.1.

The results correspond to the findings from the thermogravimetric evaluation, where neither the heating nor the cooling rate has a measurable influence on the activation outcome (P1,

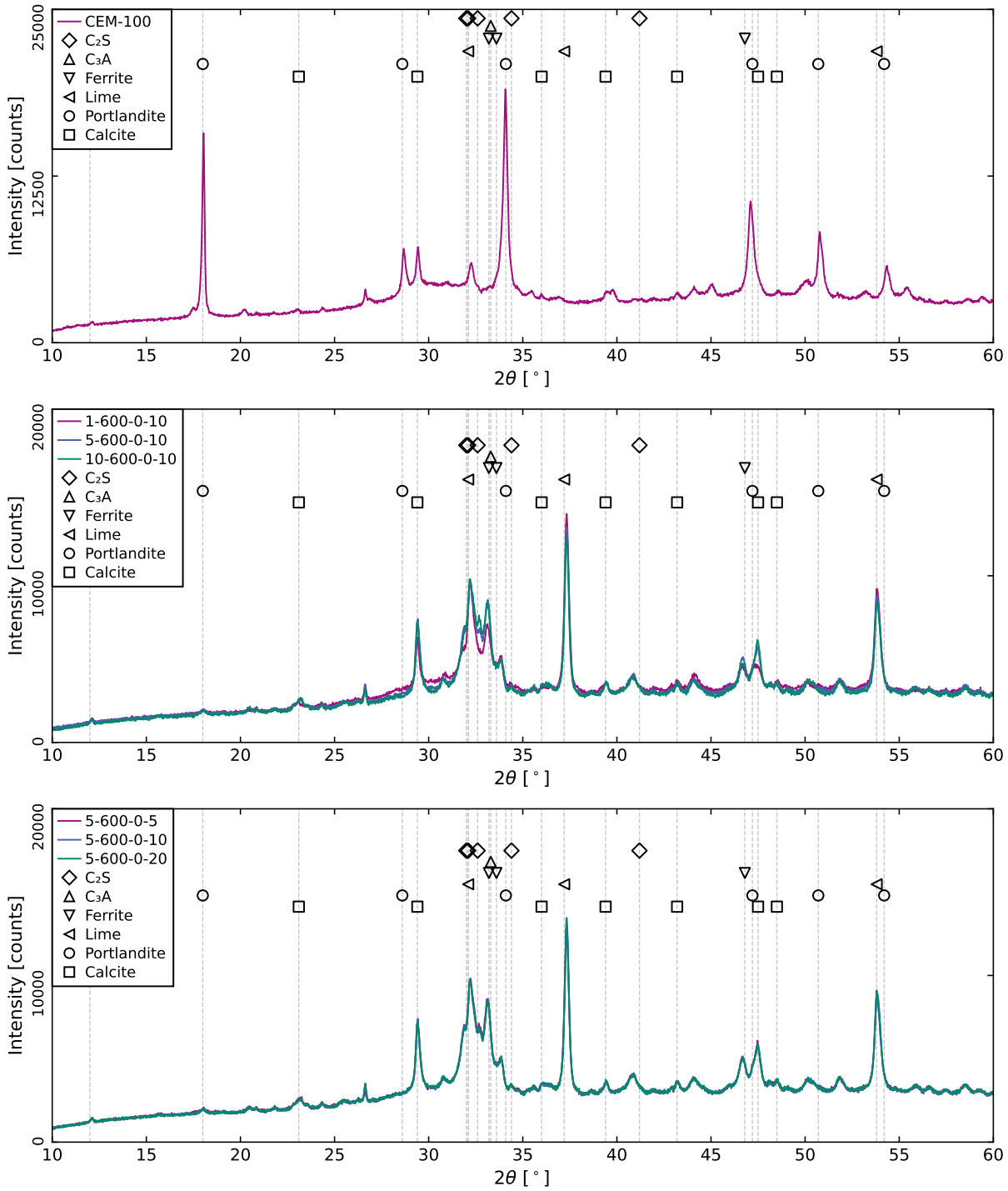

Fig. 4.1: XRD analysis of CEM-100 before thermal processing (top) and after activation in the thermogravimetric setup with different heating rates (mid) and cooling rates (bottom). Notation: heating rate [K/min]–target temperature [°C]–holding time [h]–cooling rate [K/min] (P1, fig. 3).

fig. 3). Due to the small sample size, it is also apparent that dehydration is already complete upon reaching the target temperature (except for the processing temperature of 400 °C, which is only limitedly reflected in the heat flow calorimetry measurements). An additional holding time has no effect. An accelerated heat of hydration development is observed with increasing processing temperature. While the heat development of the samples prepared at 400 °C most closely resembles the reference measurement with pure CEM I, the heat release in the first 30 min

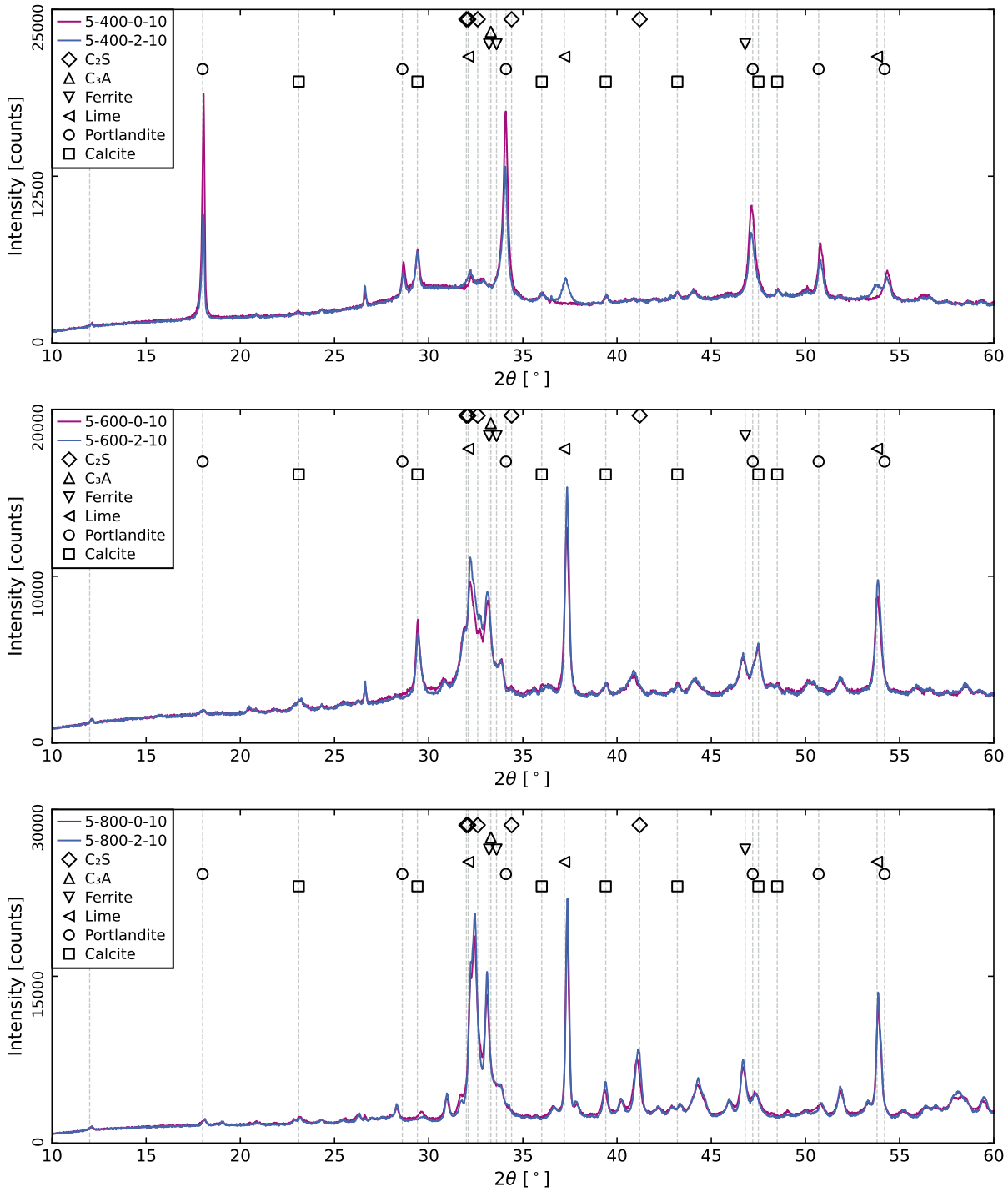

Fig. 4.2: XRD analysis of CEM at different target temperatures. Notation: heating rate [K/min]–target temperature [°C]–holding time [h]–cooling rate [K/min] (P1, fig. 3).

after contact with water increases significantly for the samples treated at 600 °C and 800 °C. These results mirror the increased amount of lime indicated in the XRD measurements in fig. 4.2. At 800 °C, a shift of the local heat flow maximum to earlier times is also apparent. This behavior mirrors the results for activated CEM, as illustrated in P2, fig. 5. The only difference is the higher initial heat flow during the first hours of measurement, which increases the overall hydration heat for thermogravimetrically activated CEM relative to the larger samples.

Tab. 4.1: Hydration heat of blended cements consisting of 70 wt% CEM I and 30 wt% artificial fines "CEM" following activation in a thermogravimetric setup with different parameters.
Notation: CEM-heating rate [K/min]–target temperature [°C]–holding time [min]–cooling rate [K/min]
Q_t: cumulative heat at duration t, W_t: heat flow at duration t, t_b: duration at local heat flow minimum, t_p: duration at local heat flow maximum.

	$Q_{0.5\,\mathrm{h}}$ J/g	t_b h	W_{t_b} mW/g	Q_{t_b} J/g	t_p h	W_{t_p} mW/g	Q_{t_p} J/g	$Q_{5\,\mathrm{d}}$ J/g
CEM I	18.8	2.4	0.4	23.2	11.4	2.8	72.5	296.8
CEM-5K-400C-0h-10K	19.5	2.3	0.7	26.0	11.1	2.0	74.5	280.6
CEM-5K-400C-2h-10K	25.0	2.4	0.7	31.8	11.5	2.1	82.9	289.8
CEM-1K-600C-0h-10K	46.2	2.9	0.7	56.2	12.0	2.5	109.5	312.8
CEM-5K-600C-0h-5K	51.7	3.0	0.6	60.9	12.0	2.4	111.2	310.4
CEM-5K-600C-0h-10K	51.0	3.0	0.6	60.3	11.9	2.4	110.7	313.8
CEM-5K-600C-0h-20K	50.9	3.1	0.5	59.6	12.2	2.4	109.7	311.5
CEM-5K-600C-2h-10K	52.1	3.0	0.6	62.0	12.0	2.3	111.8	305.0
CEM-10K-600C-0h-10K	43.1	2.6	0.6	51.1	11.8	2.3	99.8	293.1
CEM-10K-600C-2h-10K	40.3	2.8	0.8	52.6	11.4	2.2	100.6	287.8
CEM-5K-800C-0h-10K	79.5	2.3	0.8	86.8	9.5	1.7	120.1	295.8
CEM-5K-800C-2h-10K	82.1	2.0	0.7	88.0	9.0	1.5	117.1	276.7

Tab. 4.2: Mortar compressive strength f_c at 2 d and 28 d and corresponding mass loss Δm for artificial fines "CEM" activated at 600 °C with different durations and sample sizes.

	Parameters	f –	w/b –	w/b_{FM} –	Δm –	$f_{c,2\,\mathrm{d}}$ MPa	$f_{c,28\,\mathrm{d}}$ MPa
CEM-600	3 h - 150 g	0.3	0.5	0.51	0.161	28.4(5)	47.5(11)
CEM-600	3 h - 750 g	0.3	0.5	0.51	0.149	29.0(6)	51.0(15)
CEM-600	3 h - 1 kg	0.3	0.5	0.51	0.143	32.1(6)	48.4(8)
CEM-600	6 h - 150 g	0.3	0.5	0.51	0.165	31.1(7)	51.4(23)
CEM-600	6 h - 750 g	0.3	0.5	0.51	0.163	28.7(8)	49.3(19)
CEM-600	6 h - 1 kg	0.3	0.5	0.51	0.161	30.3(6)	49.8(27)
CEM-600	6 h - 1.5 kg	0.3	0.5	0.51	0.157	26.8(5)	49.4(14)
CEM-600	0 h - RF	0.3	0.5	0.51	0.139	28.0(7)	48.3(12)
CEM-600	1 h - RF	0.3	0.5	0.50	0.131	25.4(5)	44.0(26)

The activated fines from larger samples have been used for the production and subsequent testing of mortar bars with 30 wt% substitution of CEM I at a water-binder ratio of $w/b = 0.5$. Production and test execution were performed according to the descriptions in P1. Results are given in table 4.2. The description of the parameter combinations corresponds to P1, fig. 4.

Ultimately, the results show that with the increased mass loss in P1, fig. 4, strength increases. The discrepancies, however, are minor and within the standard deviations of the individual tests. The results for the rotary furnace indicate reduced strength, which may be attributed to the altered processing. Postprocessing of samples from the rotary furnace could not replicate the crucible handling in the stationary furnace, owing to a slower cooling protocol. This exemplifies reduced mass loss, which did not align with the results from subsequent thermogravimetric

measurements in P1. However, mortar strength is significantly reduced for the sample with an activation duration of 1 h. The thermogravimetric analysis of this sample shows increased mass loss at low temperatures, indicating unintended exposure to moisture.

4.2.2 Alternative Model Approaches

P1 and P2 use a linear model for the prediction of k-values, as reiterated in section 4.1. P2 also mentions two additional, and ultimately discarded, models, which are presented hereinafter. Computation follows the same boundaries as described in P2.

The first alternative model approach, according to eq. (4.8), neglects effects from the type of binder or the type of aggregate. k-values are calculated as the product of the mass loss from thermal activation (Δm) with a parameter k_{h0}. The least-squares method yields $k_{h0} = 8.80$. The sum of the squared errors is $\Delta^2 = 20.4$.

$$k = k_{h0} \cdot \Delta m \tag{4.8}$$

Figure 4.3 shows both the results of the computation for k according to eq. (4.8) (modeled k versus measured k) and the corresponding calculated mortar compressive strengths f_c versus the measured $f_{c,28\,\mathrm{d}}$. For this purpose, in addition to the 98 results used for the regression analysis of k_{modeled}, all series with different binder contents are evaluated (coefficient of determination $R^2 = 0.40$). It is noteworthy that low k-values for artificial fines that have not been thermally activated are underestimated by this model approach.

The second alternative model investigates a more detailed consideration of the artificial fines composition. For this purpose, it is assumed that the additive contributions of the aggregate and the binder type are proportional to the content of aggregate, or hydrated binder, in the processed artificial fines. To achieve this, in addition to the proportion of dehydrated cement paste (m_{pdh} according to eq. (4.13)), the proportion of aggregate m_a and the proportion of hydrated binder m_{ph} in the (partially) dehydrated artificial fines must be calculated. The mass fraction of the binder m_{pr} in the solids during artificial fine production serves as the input quantity.

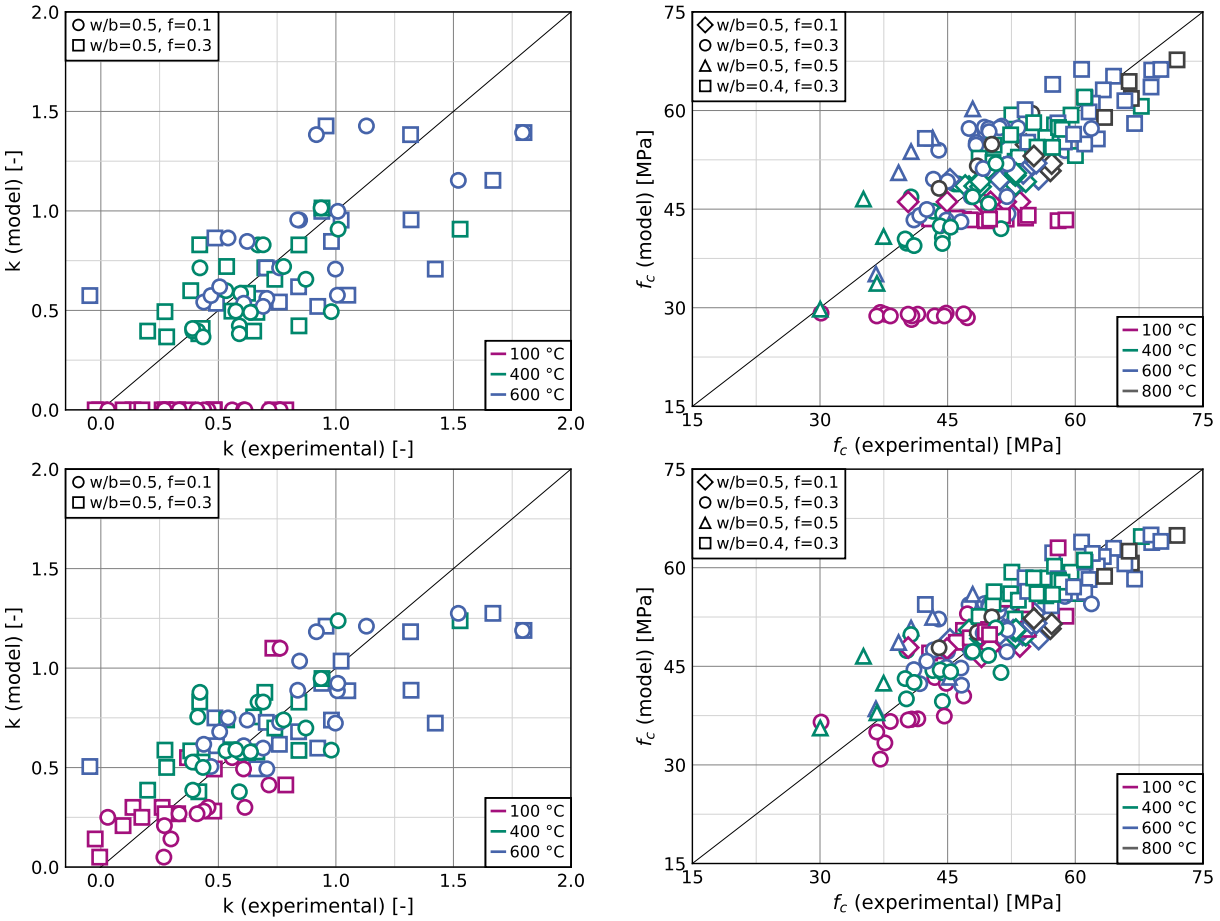

Fig. 4.3: Modeled k-values for a CEM I substitution rate through processed RCFs of $f = 0.3$ over k-values obtained from measurements (left), and modeled compressive strength over measured compressive strength (right). Top row: Model according to eq. (4.8), bottom row: model according to eq. (4.9). Marker shape indicates mix design, and color indicates activation temperature.

$$k = k_{h0} \cdot m_{pdh} + k_{a0} \cdot m_a + k_{b0} \cdot m_{ph} \tag{4.9}$$

$$m_a = \frac{1 - m_{p100}}{1 - \Delta m} \tag{4.10}$$

$$m_{ph} = (m_{p100} - m_{pdh} \cdot (1 - \Delta m) - \Delta m) \cdot \frac{1}{1 - \Delta m} \leq 1 \tag{4.11}$$

$$m_{p100} = \frac{m_{pr} \cdot (1 + m_{h0})}{m_{pr} \cdot (1 + m_{h0}) + 1 - m_{pr}} \tag{4.12}$$

$$m_{pdh} = \Delta m \cdot \left(1 + \frac{1}{m_{h0}}\right) \tag{4.13}$$

$$m_{h0} = 0.23 \tag{4.14}$$

$$k_{h0} = 1.35 \tag{4.15}$$

$$k_{a0} = \begin{cases} 0.05 & \text{for LS} \\ 0.25 & \text{for RS} \\ 0.60 & \text{for GW} \end{cases} \tag{4.16}$$

$$k_{b0} = \begin{cases} 0.30 & \text{for CEM I} \\ 0.30 & \text{for CEM I + S} \\ 1.10 & \text{for CEM I + FA} \end{cases} \tag{4.17}$$

Despite the significantly more complex structure, the model adaptation only slightly increases the sum of the squared errors to $\Delta^2 = 14.9$. The coefficient of determination for the compressive strength decreases insignificantly ($R^2 = 0.73$). The results are illustrated in fig. 4.3 (bottom row).

4.2.3 Impact of the Substitution Rate

While the models in P1 and P2 have been calibrated with a CEM I substitution rate of $f = 0.3$, the results indicate an impact of f on the obtained results: P1 discusses the superposition of material scatter and deviations of the reference series from the idealized relationship between the water-cement ratio and compressive strength. P2 extends the model for strength prediction by factoring in the substitution rate f.

P1, eq. (9) illustrates that the proportion of supplementary cementitious materials in the binder (f) enters the calculation of k in a hyperbolic manner. However, the experimental data, which the water-binder ratio to strength relationship is based on, exhibit scatter – both within each series and, to a greater extent, between different series produced on different occasions (see P1, fig. 10). Deviations of the results for the individual results from the linear trend range between -3.7 MPa and 4.0 MPa. The procedure for calculating k of an individual mortar mix assumes that the computational relationship represents the concrete behavior perfectly. Ultimately, due to the calculation, all scatter – whether from the supplementary material or the other base concrete components – is projected onto the resulting k-values.

For CEM I, by definition, $k = 1.0$ applies. This can be verified through back-calculation using P1, eq. (9) by setting $f = 1.0$. The individual k-values are then calculated as the ratio of w/b to w/c_{eq}, yielding values in the range of 0.93 to 1.09, with a mean value of 1.00.

The influence of the substitution rate can then be illustrated by interpreting P1, eq. (9) as a function of f. The CEM I used is virtually split into a binder with a known k-value (1.0) at a proportion of $(1 - f)$, and a binder at proportion f whose k-value is to be determined. This effect is illustrated in fig. 4.4. For $f = 0.5$, the resulting range of k is $0.86 \leq k(f = 0.5) \leq 1.18$, while maintaining a mean value of $k = 1.00$. As the substitution rate decreases, this range widens to $0.77 \leq k(f = 0.3) \leq 1.30$ and $0.30 \leq k(f = 0.1) \leq 1.89$. These effects are inherent to the model and must be accounted for when interpreting subsequent experimental results for mortar containing thermally activated concrete fines.

When CEM I is partially substituted through a different material with primarly unknown behavior, scatter of k is expected to increase. To assess model accuracy, the analysis requires eliminating the aforementioned deviations. The scatter reduces when comparing compressive strength, as the influence of SCMs is mitigated by the substitution rate. P1, table 4 presents a rudimentary statistical analysis of the model residuals $\Delta f_c = f_{c,measured} - f_{c,modeled}$ for the mortar mixes with pure CEM I, established SCMs, and processed industrial fines. The cumulative distributions of residuals Δf_c for selected parameter combinations are visualized in fig. 4.5.

All results for the CEM I base mixes lie within a range of ± 4 MPa, which agrees with the conformity criterion in EN 206:2013. Overall, the substitution of 30 wt% of CEM I through established SCMs (slag, S, fly ash, FA, or limestone powder, L) results in an underestimation of compressive strength by the application of k-values prescribed in EN 206:2013, which un-

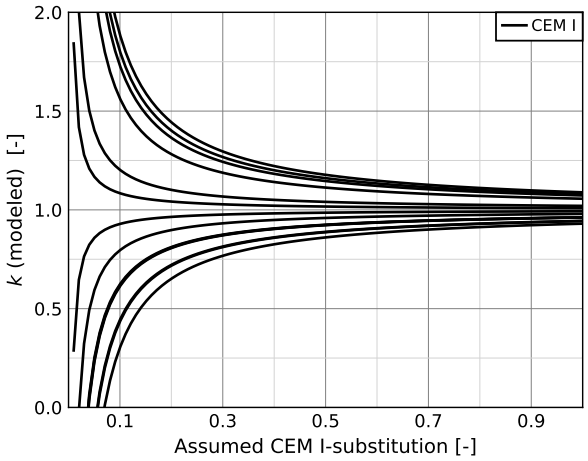

Fig. 4.4: Theoretical translation of deviations of CEM I-compressive strength to k-values for different assumptions of the substitution rate f.

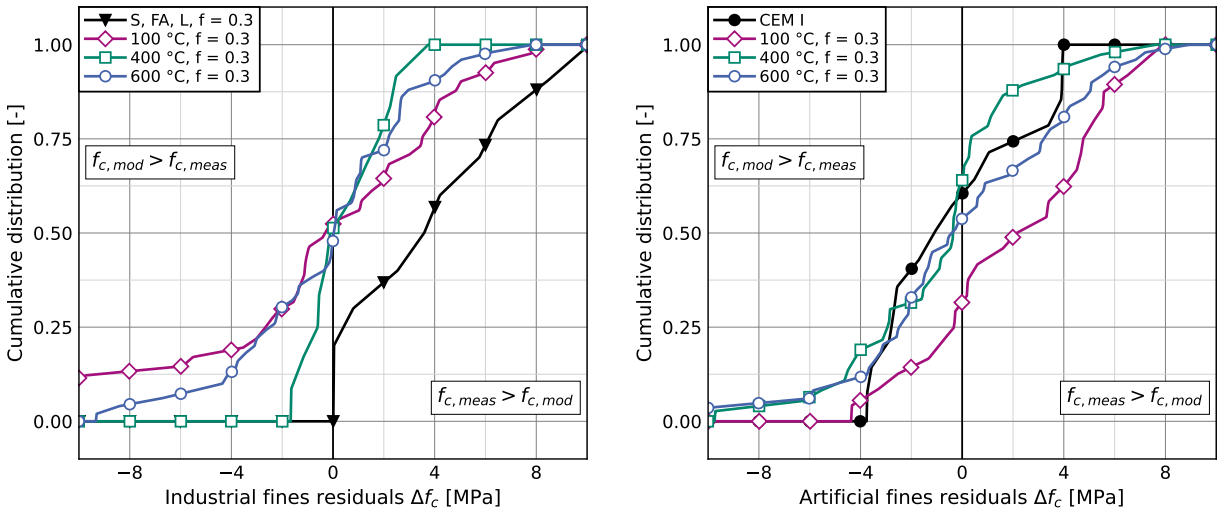

Fig. 4.5: Cumulative distribution of measured and modeled compressive strength for reference mixes and mortar with concrete fines processed at different temperatures for a substitution rate of $f = 0.3$ (left: industrial fines, right: artificial fines).

derlines the conservative approach in standardization. However, the present results also imply the additional potential of a performance-based concept, including the determination of individual material parameters for established SCMs. In addition to underestimating compressive strength, the CEM I substitution with S, FA, and L also marginally increases the scatter of measured compressive strength, expressed through an increased standard deviation.

Figure 4.5 also provides a visualization of the cumulative distribution of residuals Δf_c for different processing temperatures of industrial and artificial concrete fines. The increased scatter of mortar containing processed industrial fines is mostly caused by mixes with fines processed at 100 °C, where only 63 % of residuals are within the range of ±4 MPa. The deviation reduces for fines activated at higher temperatures. At 600 °C, 78 % of compressive strength results deviate less than ±4 MPa from the modeled values, and at 400 °C, no residuals exceed ±4 MPa, albeit at a small sample size. The evaluation of residuals for processed artificial fines shows a different behavior. For 600 °C, 69 % of the residuals are within the range of ±4 MPa, and for 400 °C, this value increases to 73 %. For 100 °C, the distribution of the residuals exhibits a pronounced

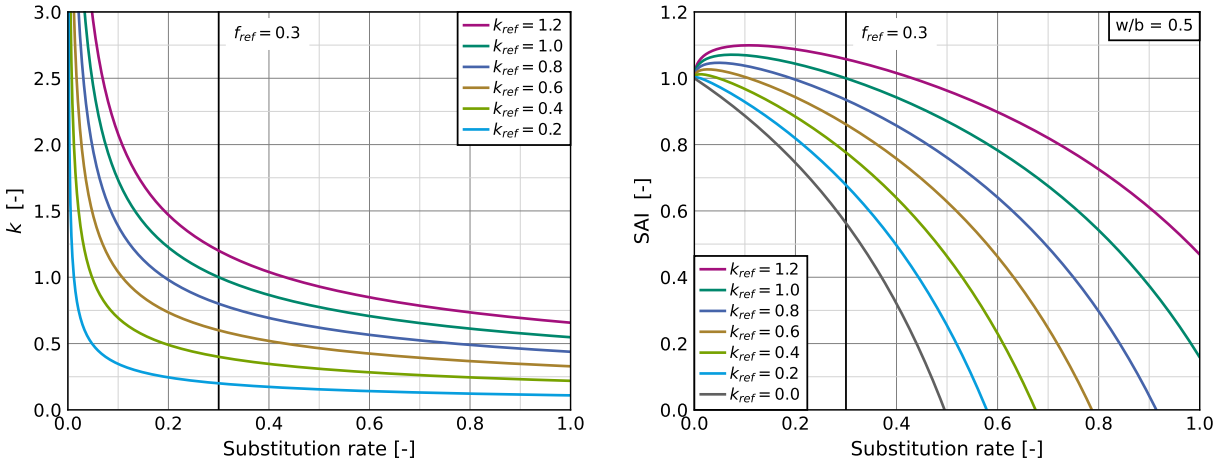

Fig. 4.6: Visualization of the impact of the substitution rate on k-values (left) and strength activity indices (SAI, right) based on P2.

shift, which indicates an underestimation of measured strength by the model. Still, 58 % of the results lie within the desired range.

P2, eq. (14) entails a model adaptation, where the impact of the substitution rate on the k-values is considered through an additional factor (see eq. (4.18)). In P2, k_{ref} corresponds to k-values determined for the substitution rate $f_{ref} = 0.3$.

$$k = k_{ref} \cdot \left(\frac{f_{ref}}{f} \right)^{0.5} \tag{4.18}$$

Figure 4.6 plots eq. (4.18) for different k_{ref}. For $f \to 0$, k increases infinetely. However, when calculating strength, this effect is countered by the multiplication with f, so that the resulting strength is always finite. This is exemplified in fig. 4.6 for the present relationship between w/b and f_c at a set $w/b = 0.5$. For simplification, the diagram uses the reference strength of $f_{c,ref} = 52\,\text{MPa}$ to obtain strength activity indices (SAI). Especially for high k-values, the increase at low substitution rates results in a slight increase in compressive strength. For increasing f, the model predicts an accelerating decline in strength regardless of k_{ref}.

While this model adaptation has been calibrated for a small dataset in P2, these findings also match results for industrial fines in P1: here, the overall average results for $f = 0.3$ and $w/b = 0.5$ are $k = 0.30$. From this, eq. (4.18) predicts $k = 0.52$ for $f = 0.1$. Measured results yield $k = 0.51$ on average. In literature, a negligible impact of cement substitution up to 25 wt%–40 wt% with activated cement paste has been reported [22, 38, 124, 147, 184, 243, 246, 274]. This matches the area in fig. 4.6 (right), where SAI exceeds 1.0 for $k_{ref} > 0.9$. For processed industrial concrete fines, the literature reports a nonlinear decrease in strength, similar to fig. 4.6 [12, 37, 77, 112, 270, 302].

Chapter 5

Influence of Thermally Activated Concrete Fines on Concrete Long-Term Behavior

During their service life, concrete structures are exposed to individual mechanical loads as well as varying moisture and temperature conditions, or contamination by harmful substances. These types of exposure result in alterations of the structural behavior and may ultimately lead to structural failure. To prevent this, design specifications like Eurocode 2 and EN 206 require concrete compositions whose mechanical and durability behavior is empirically ensured, i.e., through lower thresholds for compressive strength and cement content, and upper limits for the water-cement ratio. Empirical relationships for the mechanical behavior are generally derived from compressive strength.

For novel binders, which substitute Portland cement, the applicability of existing provisions must be verified in order to ensure concrete material behavior within the service life of a structure. For this purpose, the model for compressive strength prediction described in chapter 4 is applied to produce concrete with different types of concrete fines with different target compressive strengths. This enables the assessment of the effect of activated concrete fines as a supplementary cementitious material on various concrete properties, both with and without strength compensation.

The following sections elaborate on two manuscripts, one which have been submitted for publication, and the other awaits the acceptance of the former.

P3 Jan P. Höffgen, Marius Schmitt, and Frank Dehn. „Influence of Thermally Activated Artificial Concrete Fines Composition on Concrete Long-Term Behavior“. Journal of Building Engineering 122, March 2026: 115767. https://doi.org/10.1016/j.jobe.2026.115767.

P4 Jan P. Höffgen, Lukas Reichert, Bernd Susset, Annegret Walz, Peter Grathwohl, and Frank Dehn. „Influence of Thermally Activated Industrial Concrete Fines of Different Origin on Concrete Long-Term Behavior“. Developments in the Built Environment 26, April 2026: 100948. https://doi.org/10.1016/j.dibe.2026.100948.

Tab. 5.1: Identification of industrial fines labels in P4 with abbreviations used in P1.

P4	R1	R2	R3	R4	R5	R6
P1	A2-0/2	F-0/2	A2-0/0.25	B1-0/0.25	D-F	G-F

Analogous to P1 and P2 in chapter 4, P3 and P4 employ a similar setup, but use distinct precursor materials. The binders used in these analyses constitute a subset of the fines used for building the strength prediction model. P3 combines seven different artificial fines, three processing temperatures, and three substitution rates. P4 compares six different industrial fines at a single activation temperature to three established supplementary cementitious materials. Table 5.1 lists the corresponding fines abbreviations used in P1 and P4.

The following sections comprise a comparison of the key findings of both publications and selected additional analyses.

5.1 Key Findings in P3 and P4

Chemical Composition

Processed concrete fines contain reactive calcium oxide (CaO) and silicon dioxide (SiO_2). P3 shows that in hydrated cement paste, the amounts of both phases are reduced due to the higher water content. (Partially) dehydrated cement paste exhibits increasing amounts of reactive phases, although reactive CaO is reduced compared to the precursor CEM I. This can be attributed to partial carbonation, which shows in an increased carbon content. A significant share of CaO is present as "free" calcium oxide, which denotes lime (CaO) or calcium hydroxide ($Ca(OH)_2$) from the hydration of CEM I. The partial substitution of CEM I through fly ash or slag at the production of artificial concrete fines reduces both free and reactive CaO in favor of SiO_2. Aggregates reduce the amount of reactive phases, depending on their mineralogical composition. Siliceous aggregates, especially greywacke with a high amorphous content, increase the amount of reactive SiO_2. Noteworthy is also the complete reduction of free CaO following the thermal activation of RS50 at 600 °C, which suggests a phase transformation in conjunction with SiO_2 (P3, table 2).

Despite the overall similar chemical composition in terms of total CaO and SiO_2 content, industrial fines exhibit a reduced amount of reactive phases, compared to artificial fines. Especially, free CaO exists only in marginal quantities, possibly due to carbonation. The findings also show an increase in reactive phases with reduced precursor particle size. This corroborates the hypothesis of a hardened cement paste concentration in these fines (P4, table 1, compare section 2.3)).

Porosity

As hardened cement paste is porous, so are processed concrete fines. Based on the results for CEM I, nitrogen adsorption yields increased specific surface areas through the BET-method (Brunauer, Emmett and Teller), and increased porosity through the BJH-method (Barrett,

Joyner and Halenda). When using established supplementary cementitious materials as a benchmark, porosity still increases. However, specific surface areas, particularly for industrial fines with a high proportion of inert phases, are comparable to those of fly ash or limestone powder (P4, table 1). Artificial fines containing aggregates yield similar results as industrial fines, while porosity and specific surface areas increase with a reduction of the aggregate content (P3, table 1).

The partial substitution of CEM I through processed concrete fines has no conclusive effect on total porosity through mercury intrusion, as the introduction of porous dehydrated cement paste and dense aggregate particles counteract each other (P3, fig. 8; P4, fig. 1, fig. 3). However, when assessing the cumulative volume of (harmful) pores with a radius $r_p > 25\,\text{nm}$, the substitution in all cases increases, especially for fines with low paste contents or low processing temperatures (P3, fig. 9).

Strength Development

The concrete design in P3 and P4 uses two different concrete compositions for each supplementary cementitious material. The first approach substitutes CEM I without compensating for strength alteration (suffix "-1"). The second approach uses the model defined in P1 and P2 to adjust the water-binder ratio to produce concrete with similar compressive strength (suffix "-2"). Thus, P3 and P4 serve as validation for the model with different concrete compositions. By applying the model developed in P1, the results show a good agreement for industrial concrete fines. In contrast, artificial fines yield lower-than-expected compressive strength (P3, fig. 2; P4, fig. 4). This – ultimately unresolved issue – could be caused by ageing of the precursors during their multi-year storage. However, the discrepancies are sufficiently small to permit further analysis of the data.

The assessment of the individual mix designs of concrete containing processed concrete fines yields a high demand for superplasticizer for achieving the target workability (P3, table A.5; P4, table A.2). The demand increases for fines with a high content of dehydrated phases, as exemplified by the "-1"-series with a constant water-binder ratio. However, when targeting a compressive strength ("-2"-series), superplasticizer dosage converges since these fines exhibit a higher compressive strength contribution and, therefore, only require a moderate reduction of the water-binder ratio.

The partial substitution of CEM I through processed concrete fines has an accelerating effect on compressive strength development. Conversely, the use of fly ash or slag results in lower early strength. This is consistent with the slightly slower strength development of concrete containing fines with greywacke. However, especially concrete with fines processed at 100 °C, or increasing substitution rates, exhibit relatively high early strength (P3, fig. 2; P4, fig. 4).

Beyond alterations of compressive strength, the flexural strength at 28 d is not affected by CEM I substitution. Concrete containing slag, fly ash, or limestone powder follows the same relationship between these material parameters as concrete with artificial or industrial fines.

In conclusion, these findings suggest a good applicability of established design specifications.

Deformation Behavior

P3 and P4 analyze the deformation behavior through the dynamic modulus of elasticity and shrinkage.

Almost all concrete mixes containing supplementary cementitious materials, including artificial and industrial concrete fines, follow the relationship between compressive strength and dynamic modulus, established by CEM I reference mixes. The only unresolved deviation from this behavior is the two series with the filter cake R5, in which the dynamic moduli are lower than those of other concrete mixes with comparable strength (see P3, fig. 3; P4, fig. 6).

Shrinkage of concrete containing processed fines correlates better with the dynamic modulus of elasticity in comparison with compressive strength. Shrinkage deformations of concrete mixes with blended cements, however, are increased compared to CEM I reference mixes. Only artificial fines processed at 100 °C exhibit a deviating behavior, where the shrinkage deformations are delayed. This may be attributed to these fines having undergone microstructural shrinkage deformations prior to their use as supplementary cementitious materials (see P3, fig. 6; P4, fig. 8).

Durability

The durability analyses in P3 and P4 cover capillary absorption, chloride penetration, carbonation, and freeze-thaw resistance.

The capillary water absorption coefficient of concrete containing processed concrete fines or limestone powder increases following the substitution. This effect, however, can be compensated for by adjusting the water-binder ratio (P3, fig. 7; P4, fig. 9). A similar relationship can be observed between water absorption and pore volume (P3, fig. 9). The resistance to freeze-thaw-cycles, which was investigated for a reduced set of concrete mixes, shows a good agreement with the capillary water absorption coefficient (P3, fig. 13).

Chloride penetration depth of concrete containing processed fines is increased compared to mixes with pure CEM I, slag, or fly ash (P3, fig. 7; P4, fig. 9). Artificial fines appear to exhibit a higher chloride penetration. The reason for this remains unresolved, but since the double determinations of the reference mixes with pure CEM I (and fly ash) show a similar offset, a variation in the raw materials cannot be ruled out. The first production of the CEM I reference and the mixes with fly ash took place alongside the casting of the series with industrial fines, and the repetition was produced alongside the series with artificial fines. Nonetheless, the results show that processed concrete fines cannot compete with slag or fly ash, which are known for their chloride-binding hydration products, but exhibit a performance similar to that of limestone powder.

The partial substitution of CEM I results in a reduction of the carbonation resistance (P3, fig. 7; P4, fig. 9). Porosity and CO_2 binding are key parameters for affecting carbonation depth. The use of fines, which leads to low pore volume within the cement paste, result in reduced carbonation depths. CO_2 binding is affected by the content of $Ca(OH)_2$. For processed concrete fines, this can be directly determined from the content of free CaO. However, for fines containing an increased amount of reactive SiO_2, higher carbonation depths are prevalent. This is caused

by the pozzolanic reaction of these compounds with $Ca(OH)_2$, reducing the amount of SiO_2 that is available for carbonation (P3, fig. 11).

In conclusion, the results show that all investigated durability parameters can be adjusted by adapting the water-binder ratio. However, compensation for compressive strength alone is often insufficient, as additional factors, such as increased pore volume or reduced binding capacity, further affect durability. In conclusion, the durability of concrete containing processed concrete fines ranges between that of concrete with pure CEM I and that of concrete with limestone powder as an established supplementary cementitious material.

Leaching

Concrete fines may contain harmful substances, such as heavy metals or organic carbohydrates. In contact with water, these may be eluted and thus pose an environmental threat. In addition to quantifying solid phase fractions, elution tests on dried and thermally activated industrial fines, as well as concrete containing the latter as supplementary cementitious materials, exhibit a diverse behavior (P4, fig. 10, table 2–5). The thermal activation at 600 °C effectively reduces the total organic content (TOC) and especially polycyclic aromatic hydrocarbons (PAH). The effect of activation on different anions is inconclusive, but concentrations are generally at levels that do not raise concern. Heavy metals, which may be chemically or physically bound within cement hydrate phases, are individually affected by thermal activation and may limit specific applications. The copper concentration decreases after thermal activation and remains low in the concrete eluate. Conversely, the elution of chromium increases after thermal activation but decreases again in concrete.

5.2 Additional Analyses to P3 and P4

5.2.1 Chemical Composition

The model presented in chapter 4 uses the temperature-dependent mass loss as a major material property for predicting the strength contribution of processed concrete fines. The approaches for industrial and artificial fines, however, differ in their constant parameters, reflecting different contributions from binder and aggregate compositions. The determination of reactive CaO and SiO_2 gives better insight into these observations. Figure 5.1 illustrates the relationship between the total content of both reactive components in the blended binders and compressive strength of concrete mixtures with a constant water-binder ratio of $w/b = 0.5$. For both types of fines, compressive strength increases with a higher amount of reactive phases. The reduced k-values, and, accordingly, compressive strength of concrete containing activated industrial fines correspond to a reduced amount of reactive phases. Similarly, increasing amounts of reactive SiO_2 in artificial fines containing greywacke or reaction products from slag or fly ash result in high compressive strength.

While fig. 5.1 details the influence of both reactive CaO and SiO_2, the effect cannot be assessed with an isolated approach. Calcium silicate hydrate, as the most important cement hydration product for matrix strength, exhibits a CaO/SiO_2 molar ratio between 1.7 and 1.90

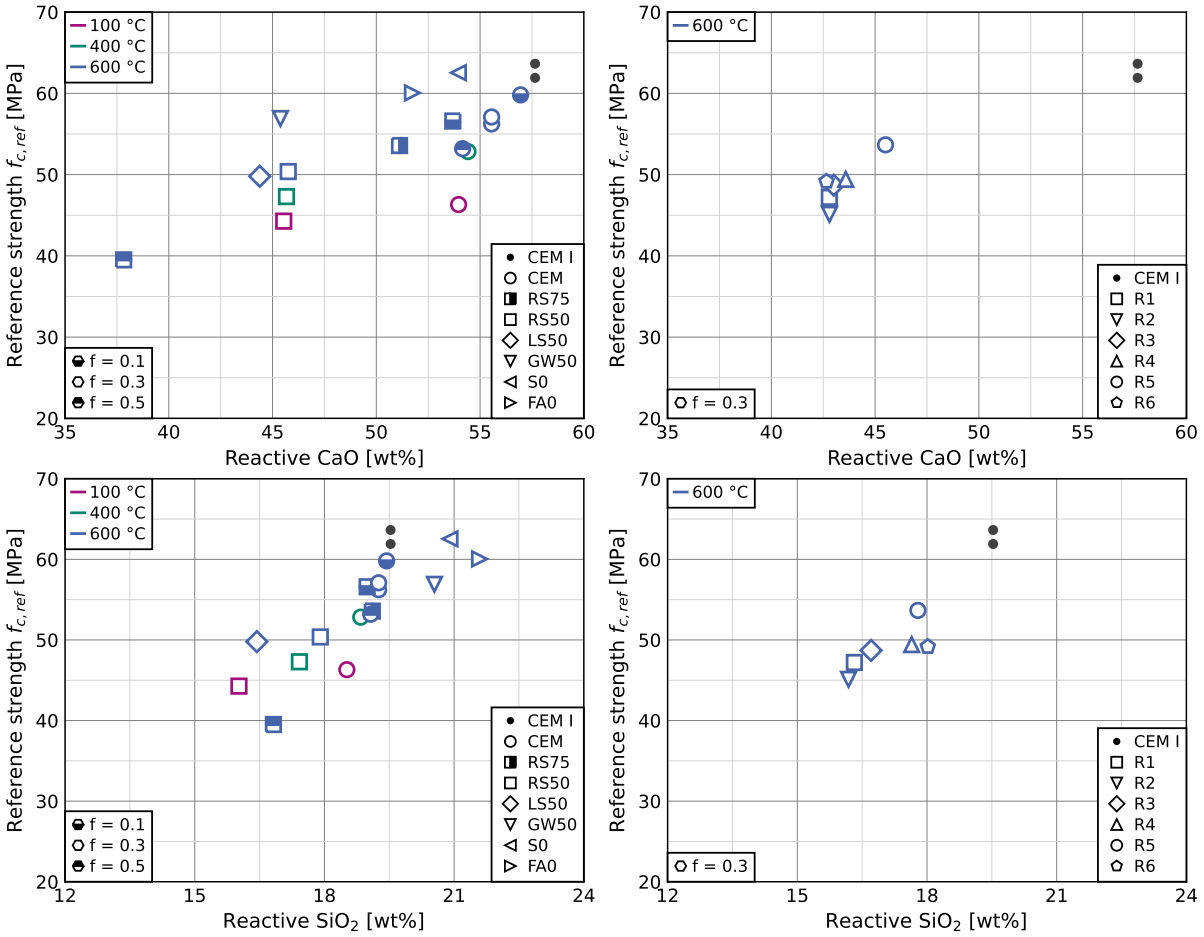

Fig. 5.1: Effect of reactive CaO (top) and SiO_2 (bottom) on compressive strength of concrete containing artificial (left) or industrial (right) concrete fines as SCM at a fixed water-binder ratio of $w/b = 0.5$.

[5, 24, 38, 75, 170, 187, 190, 206, 238]. By simplifying this to a weight ratio of 2, the weighted amount of reactive components (rC) is calculated with eq. (5.1).

$$rC = \frac{1}{3} \cdot r\mathrm{CaO} + \frac{2}{3} \cdot r\mathrm{SiO_2} \tag{5.1}$$

The relationship between rC and compressive strength in fig. 5.2 shows a good agreement between concrete containing artificial or industrial fines, and with the CEM I base mix. Figure 5.2 also partially explains the reduction of compressive strength with increasing substitution rates, indicating that this effect cannot be entirely ascribed to the loosening effect on microstructure hypothesized in [38, 203].

Figure 5.1 and fig. 5.2 also highlight a shortcoming of this setup: the experimental procedure for the determination of reactive phases fails to distinguish hydrated and dehydrated phases, as exemplified by CEM-100 and CEM-600.

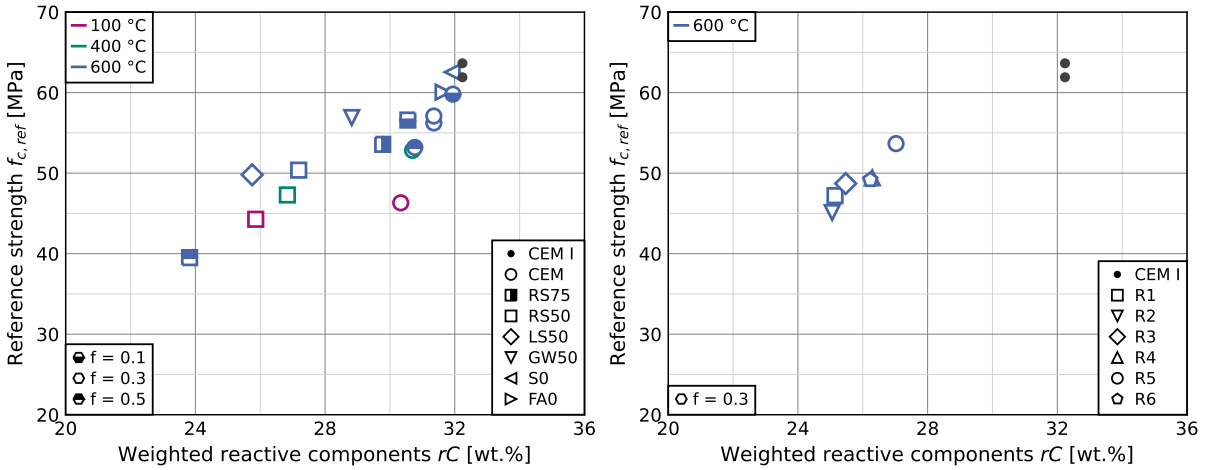

Fig. 5.2: Relationship between weighted reactive components rC (eq. (5.1)) and compressive strength of concrete containing artificial (left) or industrial (right) concrete fines as SCM at a fixed water-binder ratio of $w/b = 0.5$.

5.2.2 Porosity

P3 and P4 discuss two different kinds of material porosity: fines porosity and paste porosity, determined through N_2-adsorption with the Barrett-Joyner-Halenda (BJH), and, respectively, mercury intrusion porosimetry (MIP). The experimental analyses were more extensive than the results presented in P3 and P4. The following section presents additional results on processed fines used as binders and blended cement paste.

The evaluation of mercury intrusion porosimetry requires the postprocessing of the raw data, which offers two options: either the calibration through a "blank measurement" or postprocessing via an inherent "formula". The samples in P3 all used a blank measurement. To measure the samples used in P4, a different device with identical configuration had to be used. Since no blank measurement was available for this alternative device, the P4 results were processed using the formula method. For comparison, fig. 5.3 illustrated results for samples CEM I-1 and CEM I-2, which were used for both publications and therefore applied both postprocessing methods. For reducing pore size, the blank method delivers lower porosity than the formula method, which ultimately reflects in a reduced total porosity. However, for a pore radius $r_p > 25\,\text{nm}$, which was determined as most relevant in P3, the deviations are negligible.

For the artificial fines CEM-600 and RS50-600, as well as CEM I paste, MIP was performed on samples, where the hydration was stopped at different ages of 2 d and 56 d, in addition to 28 d used for all other samples. Figure 5.4 illustrates the resulting pore size distributions. The temporal effect is similar for all the binders. With higher sample age, specimens exhibit a smaller pore size. Compared to CEM I, paste containing either type of artificial fines exhibits a coarser pore structure at 2 d, while porosity does not evolve much at later ages.

In addition to MIP, paste samples CEM I-2, CEM-600-2, and RS50-600-2 were assessed through N_2-adsorption. Results in fig. 5.5 detail a higher porosity of artificial fines for pore diameters $d_p < 13\,\text{nm}$, and lower porosity for $d_p > 13\,\text{nm}$ compared to the paste containing pure CEM I.

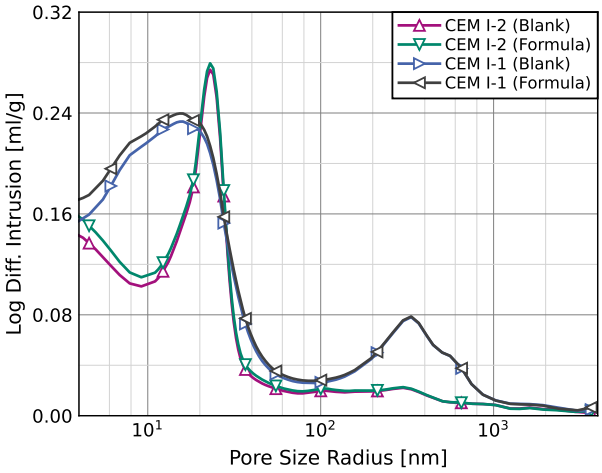

Fig. 5.3: Effect of the analysis procedure (blank or formula) on mercury intrusion pore size distribution.

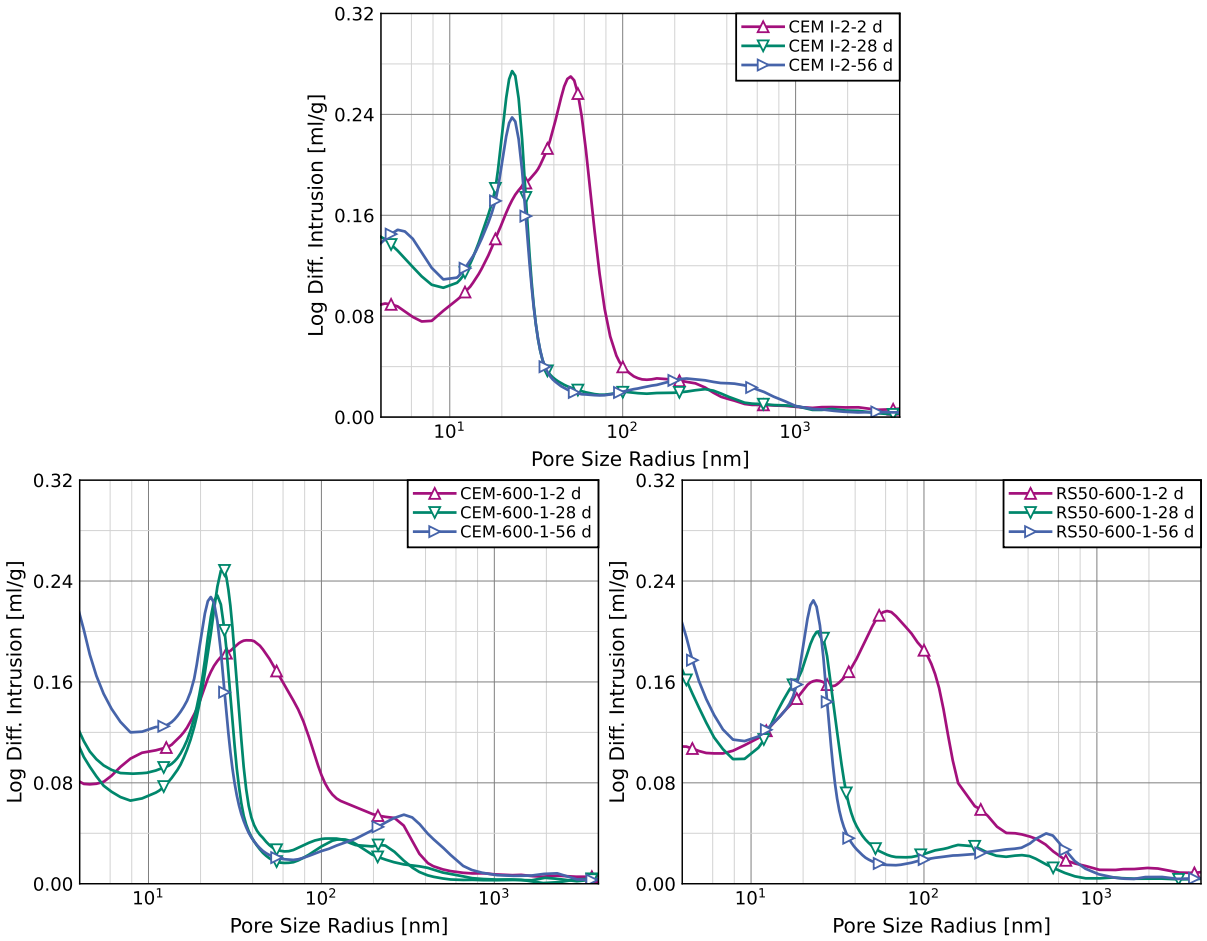

Fig. 5.4: Temporal development of the pore size distribution (MIP) of selected (blended) cement pastes.

While P3 and P4 provide tabulated results for binder porosity (P3, table 3; P4, table 1), results from the BJH method enable a more detailed assessment of binder composition.

Compared to CEM I, fly ash and limestone powder exhibit an increased incremental pore volume, with slag having the opposite effect (see fig. 5.6). Industrial concrete fines, which contain dehydrated cement paste in addition to finely milled aggregate particles, exhibit an even higher

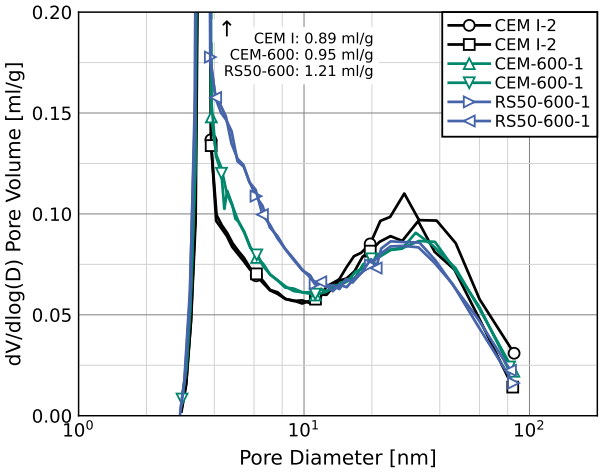

Fig. 5.5: Pore diameter distribution (N_2-BJH) of selected (blended) cement paste (double determination).

porosity across the entire pore-size range. This effect increases with higher precursor fineness and, hypothetically, with increased cement paste content.

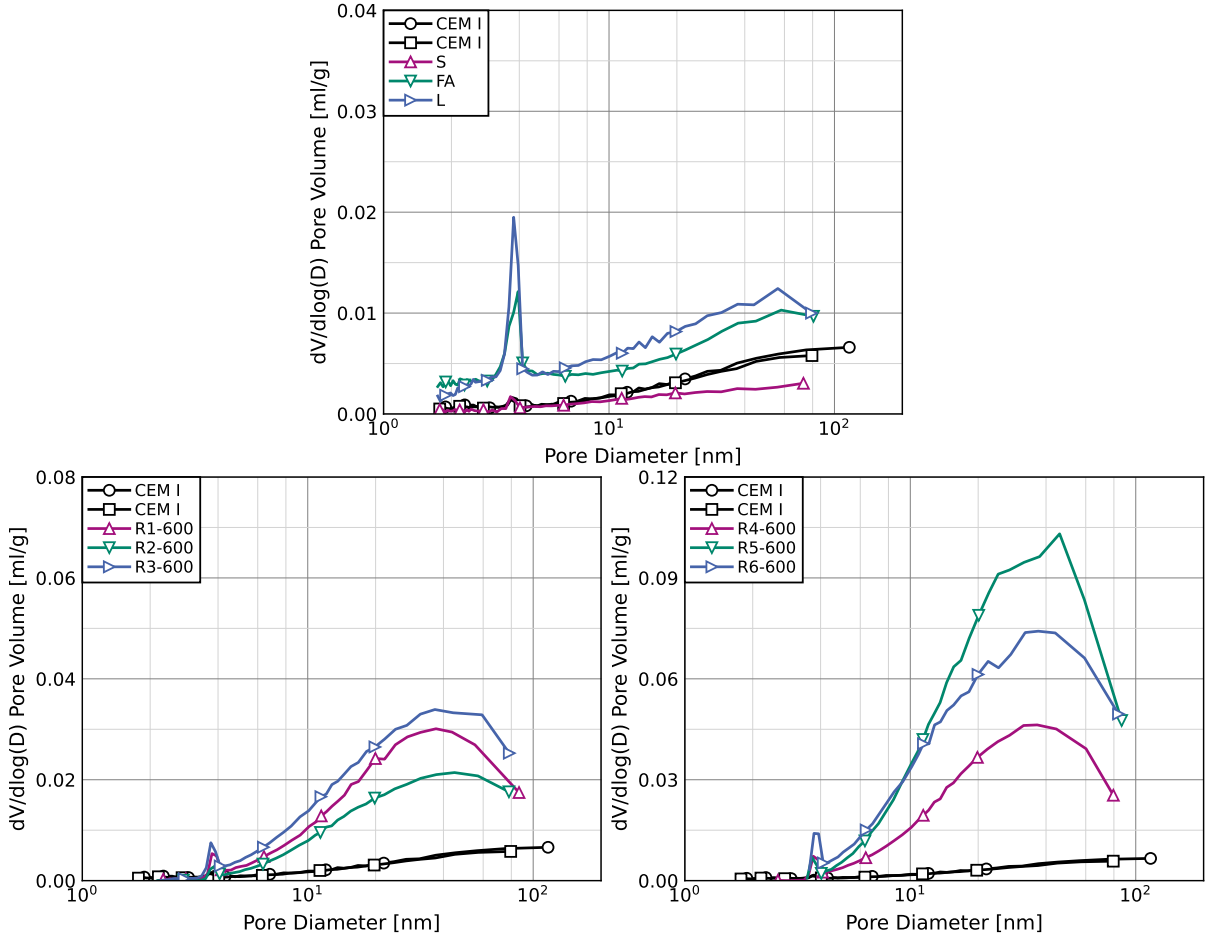

Fig. 5.6: Pore diameter distribution (N_2-BJH) of established supplementary cementitious materials (S, FA, L, top), processed industrial fines (bottom), and CEM I. Note the individual scaling of the vertical axes.

The investigation of artificial fines in fig. 5.7 corroborates these findings: fines containing aggregates exhibit a significantly reduced pore volume, which is similar to industrial fines. The

substitution of CEM I through slag of fly ash results in a reduced porosity, where the reaction of fly ash or slag particles with $Ca(OH)_2$ densifies the paste. Contrarily, when greywacke is used as aggregates instead of limestone or river sand, porosity increases. This can be attributed to the partial incorporation of amorphous SiO_2 in greywacke into paste hydration products, while limestone and river sand remain inert.

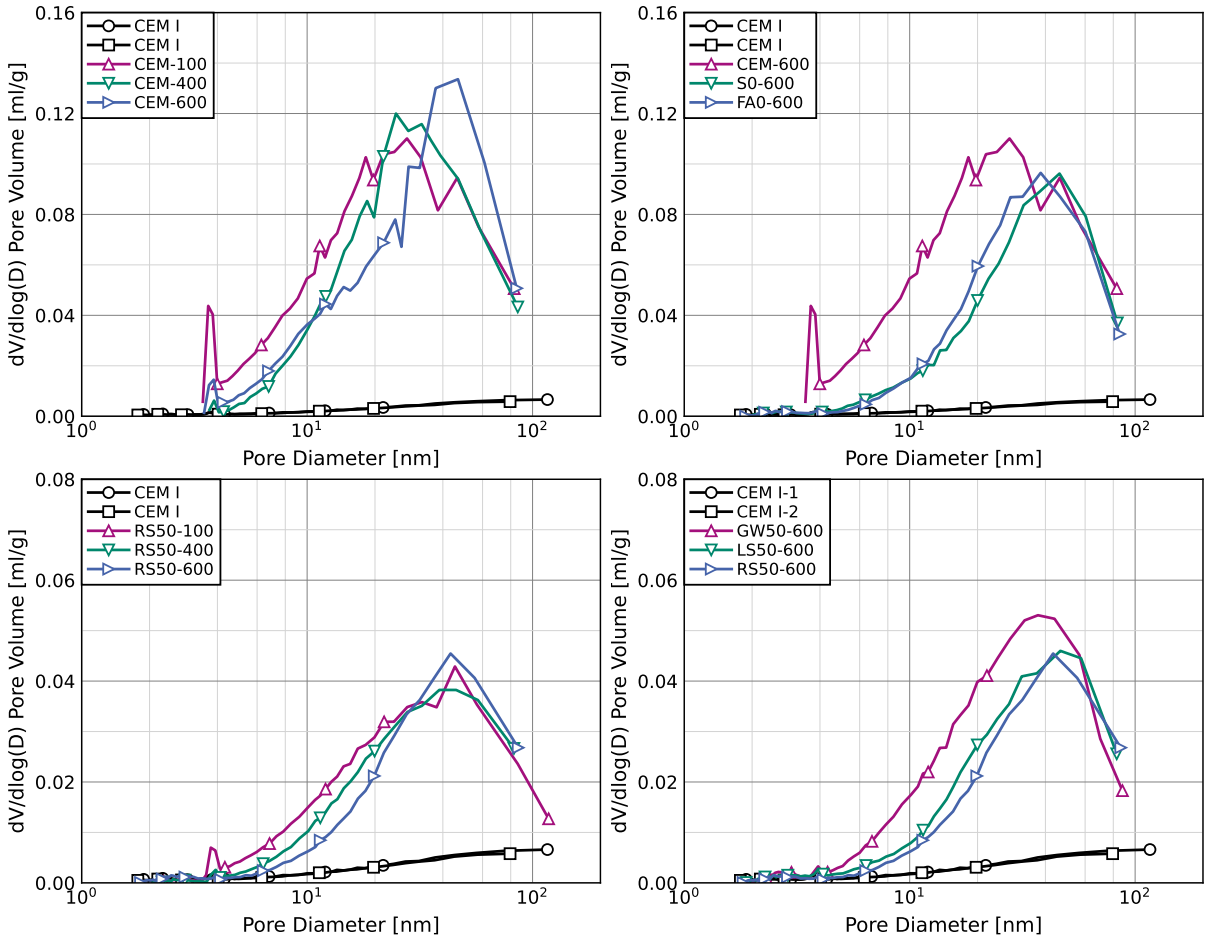

Fig. 5.7: Pore diameter distribution (N_2-BJH) of processed artificial fines and CEM I. Note the individual scaling of the vertical axes.

5.2.3 Freeze-Thaw-Resistance

Due to a device malfunction, freeze-thaw tests for P4 had to be abolished. Only series R5-600-2 and R6-600-2, in addition to CEM I-2 and FA 2, were carried out successfully up to 28 freeze-thaw-cycles (FTC). Figure 5.8 illustrates the evolution of the mass loss of the four series. The results for 28 FTC fall within the range of concrete containing artificial fines (P3, fig. 13), although a more thorough analysis requires a longer test duration.

5.2.4 Leaching

P4 analyzes the elution of harmful substances and concludes that the practical applicability requires the individual consideration of local regulations. In Germany, the Ersatzbaustoffverordnung [33] regulates application limits and individual threshold values for different material cat-

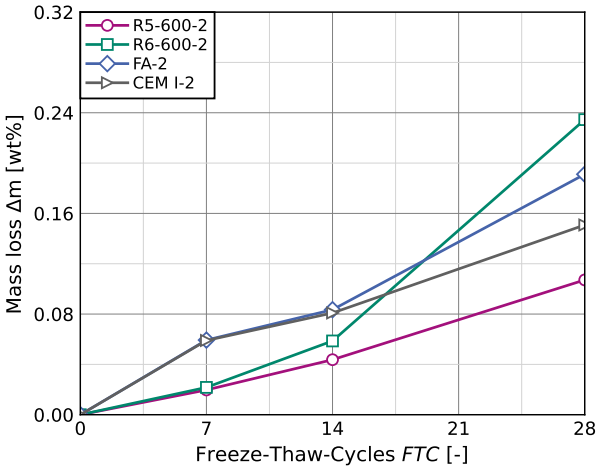

Fig. 5.8: Development of the cumulative mass loss after increasing freeze-thaw-cycles of concrete mixes R5-600-2, and R6-600-2 in comparison to references mixes FA-2 and CEMI-2.

egories and use cases. Figure 5.9 compares selected results from the six processed concrete fines (R1–R6) in P4 to these thresholds.

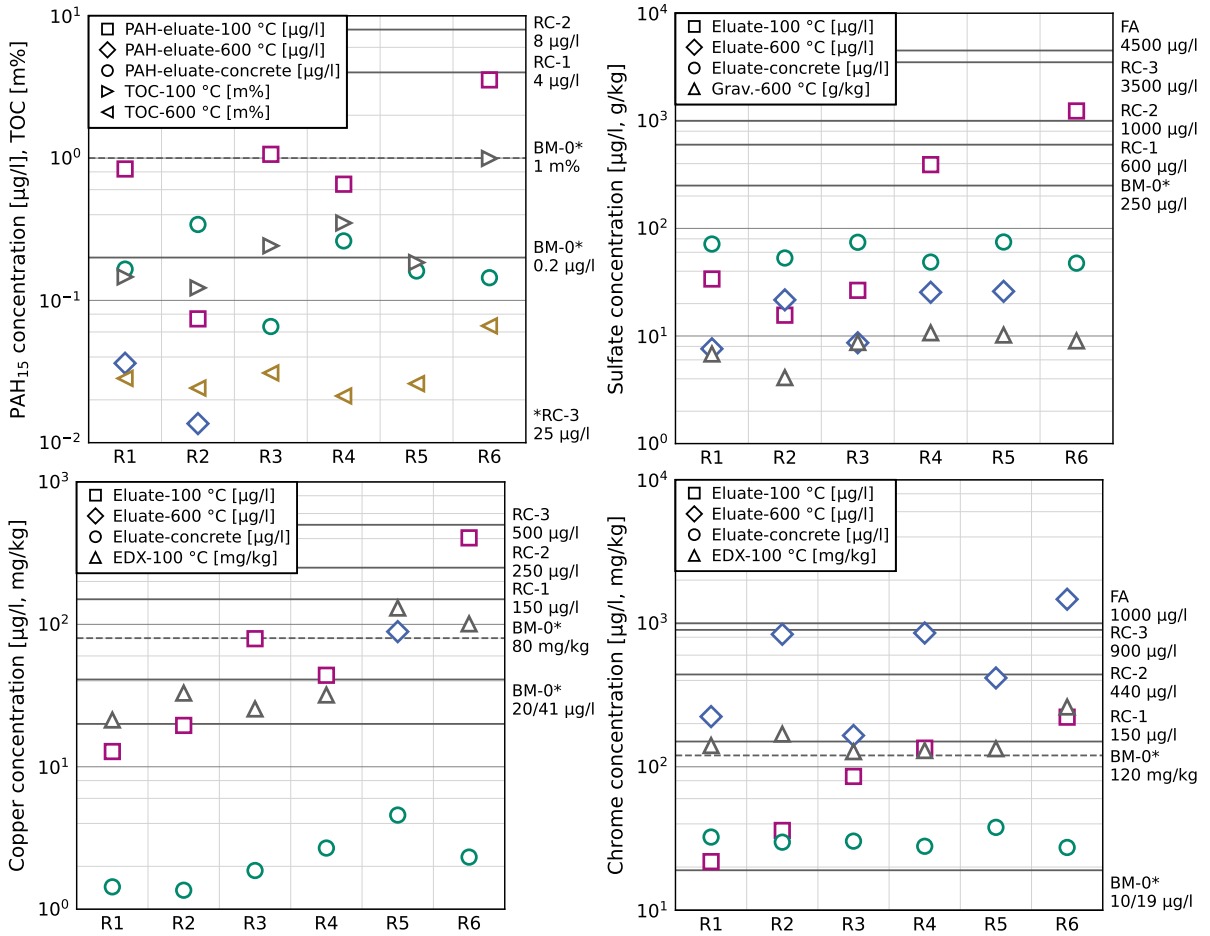

Fig. 5.9: Comparison of selected results of harmful substances (total content and eluate fractions). Top left: polycyclic aromatic carbohydrates (PAH_{15}) and total organic carbon (TOC), top right: sulfate, bottom left: copper, bottom right: total chromium. Threshold values for different material categories according to Ersatzbaustoffverordnung [33].

Except for total chromium content, thermally activated concrete fines consistently meet the requirements for RC-1, thereby allowing a broad range of applications. A classification in the harsher category BM-0* fails for heavy metals. For chromium, even a classification as fly ash is not possible for all samples.

However, for all eluate fractions, the question remains whether the decisive criterion is the concrete fines composition or the eluate from the concrete produced with such concrete fines. The analysis of PAH exemplifies this: while PAH in thermally activated concrete fines is insignificant or below the detection limit, PAH in the corresponding concrete mixes may exceed the threshold for BM-0*. Inversely, the total chromium concentration, which increases during thermal activation, decreases to low levels when concrete fines are used as a binder.

5.2.5 Concrete Design Proposal

The design of concrete structures according to Eurocode 2 assumes concrete of the same strength to exhibit similar mechanical properties. Concrete design further considers durability requirements by defining upper thresholds for the water-cement ratio and lower thresholds of the cement content and compressive strength. While P3 and P4 have shown that mechanical properties are consistent with standardized empirical relationships, partial cement substitution affects concrete durability beyond compressive strength. Subsequently, the application of the k-value concept to achieve a target compressive strength does not fully compensate for alterations of the resistance to chloride ingress or carbonation.

As both properties are significantly affected by concrete mix design and compressive strength, the magnitude of the impact of cement substitution may be assessed through comparing k-values for individual concrete properties. Applying the procedure for the calculation of k detailed in P1 on the individual results for concrete given in P3 and P4 yields k-values for compressive strength (k_S), chloride penetration (k_C), and carbonation (k_K). Results must be interpreted with caution, as the procedure uses a very small dataset. Four concrete mixes at two water-binder ratios deliver the reference curve, and k-values are calculated as the average of two concrete mixes at two water-binder ratios. For mixes with a 10 wt% substitution rate, only a single mix was produced. Fly ash (FA), however, yields two distinct k-values per parameter, as these series were repeated throughout the experimental program. The determination of k_C deviates from this protocol, as the reference curves were split into two, based on the assumption that a change in the raw material properties may have triggered the deviating chloride penetration depth between the two sets for CEM I. The subsequent conformity of the two k_C for FA substantiates this procedure.

Figure 5.10 details the results for k_C and k_K over k_S. The diverging composition of artificial fines causes a wide variation of k-values for both durability properties (see P3 for a discussion of the effect of individual artificial fines compositions).

The comparison of k-values for thermally activated industrial fines with established SCMs shows that the former perform better than limestone powder. Therefore, a conservative concrete design approach may adopt the model only for compressive strength contribution, as detailed in P1 (and validated in P4). To satisfy the requirements for exposure (resistance) classes, in terms of an upper threshold for the water-cement ratio or the minimum cement content, processed

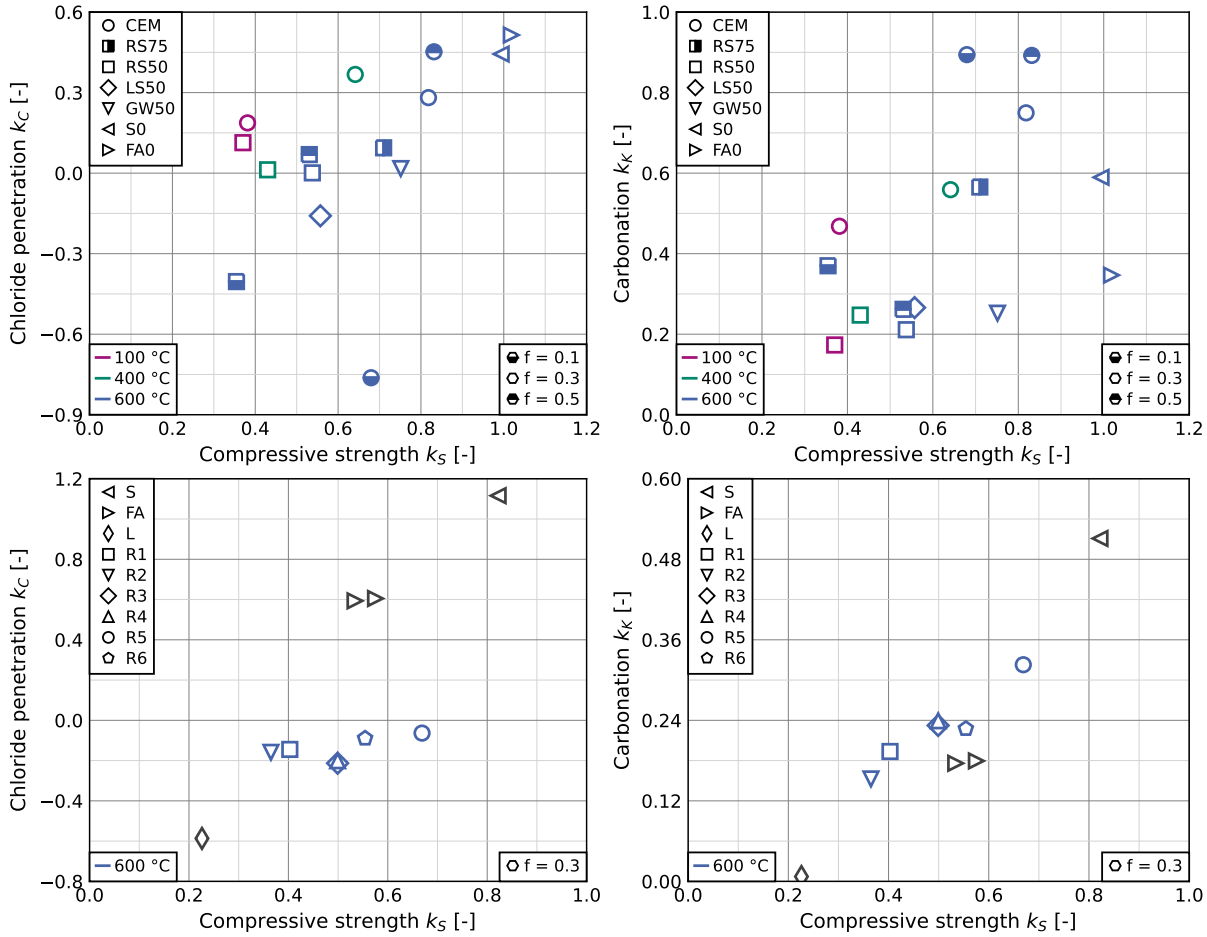

Fig. 5.10: Comparison of k-values for chloride penetration (k_C, left) and carbonation (k_K, right) with k-values for strength (k_S) for artificial fines (top) as well as industrial fines and reference SCMs (bottom). Note the individual axes scaling.

concrete fines can be regarded as inert ($k = 0$). A less conservative approach may instead use an adjusted k-value which considers only the mass loss from dehydration and forgoes all composition-dependent constant parameters. However, elaborating this concept requires further analyses.

Chapter 6

Conclusions and Outlook

6.1 Conclusions

This thesis investigates and discusses the impact of thermally activated concrete waste as supplementary cementitious materials.

The literature indicates that the activation of hardened cement paste is a promising approach for recycling waste fractions with increased paste content. However, the practical implementation has been lacking a method for predicting the concrete performance of waste with unknown composition. To address this issue, this thesis focuses on assessing the impact of concrete waste composition and thereby compares 12 artificial concrete fines with known compositions to 25 industrial concrete fines procured from waste-processing plants.

After the extensive literature review, the first experimental and analytical part of the thesis focuses on the activation procedure, the rehydration, and the compressive strength contribution of these materials as supplementary cementitious materials. The starting point for all investigations are ground and dried precursors. Thermal activation relied on a processing temperature of 600 °C, where hardened cement paste dehydration is nearly complete. Additionally, an intermediary temperature of 400 °C was selected to provide results for a partial dehydration. Compared to the hydration of CEM I, rehydration is a rapid process, exemplified by increased initial hydration heat flow and high early strength. The strength contribution of ground concrete waste of different origins exhibits substantial scatter. Thermal activation of these precursors reduces variability by establishing a linear relationship between the strength contribution and mass loss during the dehydration of hardened cement paste. Constants take different contributions of supplementary cementitious materials or amorphous aggregates into account. The slope of the relationship corresponds to the long-established amount of chemically bound water in hydrated cement, and is almost identical for artificial and industrial fines. The substitution of 30 wt% of cement through thermally activated artificial cement paste has no adverse effect on compressive strength. Compressive strength declines as the activation temperature decreases, or the aggregate content increases, in both artificial and industrial fines. Still, a replacement of up to 50 wt% of cement delivers sufficient compressive strength for structural design.

In the second experimental and analytical part of the thesis, a selection of artificial and industrial fines is used for assessing concrete durability and mechanical properties besides compressive strength. In contrast to previous findings, concrete compositions apply the model for

strength prediction to compensate for the effect of activated concrete waste on compressive strength. Results show that flexural strength, elastic moduli, or shrinkage generally change alongside compressive strength, and applying the newly developed model also compensates for alterations to other mechanical concrete properties. Thus, empirical design specifications can be applied. Durability, on the other hand, is affected beyond compressive strength. In particular, carbonation and chloride ingress increase, which can be attributed to a reduced binding capacity of rehydrated cement paste.

6.2 Outlook

The presented model provides a simplified method for predicting the strength contribution of processed concrete waste as supplementary cementitious materials. While the impact of the discharge of chemically bound water is consistent with the established literature, particularly the introduced constants for aggregates and binder composition, it may benefit from further refinement through additional research. This includes a detailed consideration of microscopic and thermodynamic processes of the de- and rehydration processes that may explain the currently identified macroscopic effects on rehydration, strength development, and durability.

Furthermore, the proposed model may benefit from expanding the database by incorporating additional concrete compositions and cement substitution rates. Here, concrete durability requires additional research beyond the microscopic investigation of the binding capacity of hydrated phases. The results within this thesis have shown an insufficient applicability of the model for carbonation and chloride ingress. Therefore, the definition of individual upper limits for the substitution rate and the (equivalent) water-cement ratio, and lower limits for the (effective) cement content remains paramount for a future application. However, the equivalent concrete performance concept offers a more straightforward approach than the k-value concept, which is the foundation of the presently proposed model. Nonetheless, the latter provides a simple method for screening and selecting concrete waste of varying compositions for potential use as a thermally activated supplementary cementitious material.

As EN 197-6:2023 only regulates mechanically processed concrete waste as a cement main constituent, the broad application of thermally activated concrete waste in the cement or concrete industry requires additional certification and a technical approval. The material performance reported in the literature and in this thesis is promising for a broad range of applications. Accelerated development of compressive strength is particularly advantageous for the precast concrete industry. Furthermore, activated concrete waste can be used as a supplementary cementitious material in non-concrete applications, such as ground improvement. Here, the substitution of up to 50 wt% has proven effective for achieving a sufficiently high material stiffness (A2).

A2 Jan P. Höffgen, Lukas Knittel, Manuel Bauer, Hans Henning Stutz, and Frank Dehn. „Baugrundverbesserung mit thermisch-mechanisch aufbereitetem Betonbrechsand“. Bautechnik 102, No. 9 (2025): 515–522. https://doi.org/10.1002/bate.202400038.

In a broader context, the activation of hardened cement paste enables more advanced processing methods for concrete waste. Techniques that focus on a more thorough separation of

hardened cement paste from natural aggregates are economically inefficient for producing recycled aggregates. However, by implementing a second processing output in the form of a (more valuable) supplementary cementitious material, these procedures may become economically feasible and subsequently improve the production of recycled aggregates. Here, both thermal and carbonation activation are promising procedures, and a comprehensive comparison of these approaches across technical, ecological, and economic dimensions is required to highlight their respective advantages in achieving the goal of a veritable material circularity in concrete production.

References

[1] A. Abidar et al. “Restoration of Hydraulic Properties in Recycled Cement Pastes via Thermal Treatment”. In: *Cement and Concrete Composites* 164 (2025), p. 106265. ISSN: 09589465. DOI: 10.1016/j.cemconcomp.2025.106265.

[2] H. M. Ai et al. “Properties of Recycled-Cement Produced from Waste Concrete”. In: *Advanced Materials Research* 194–196 (2011), pp. 1170–1175. ISSN: 1662-8985. DOI: 10.4028/www.scientific.net/AMR.194-196.1170.

[3] N. Algourdin et al. “Durability of Recycled Fine Mortars under Freeze–Thaw Cycles”. In: *Construction and Building Materials* 291 (2021), p. 123330. ISSN: 09500618. DOI: 10.1016/j.conbuildmat.2021.123330.

[4] N. Algourdin et al. “Experimental and Numerical Investigation of Accelerated Carbonation of Recycled Fines”. In: *Construction and Building Materials* 382 (2023), p. 131286. ISSN: 09500618. DOI: 10.1016/j.conbuildmat.2023.131286.

[5] C. Alonso and L. Fernandez. “Dehydration and Rehydration Processes of Cement Paste Exposed to High Temperature Environments”. In: *Journal of Materials Science* 39.9 (2004), pp. 3015–3024. ISSN: 0022-2461. DOI: 10.1023/B:JMSC.0000025827.65956.18.

[6] A. Alvarez-Coscojuela et al. “Insights into Mechanothermal Activation of Kaolinite: A Novel Multistep Process for Cement Precursors”. In: *Construction and Building Materials* 492 (2025), p. 142848. ISSN: 09500618. DOI: 10.1016/j.conbuildmat.2025.142848.

[7] S. Amroun et al. “Mechanochemical Activation of Basaltic Fines”. In: *Cement and Concrete Research* 195 (2025), p. 107923. ISSN: 00088846. DOI: 10.1016/j.cemconres.2025.107923.

[8] R. M. Andrew and G. P. Peters. *The Global Carbon Project’s Fossil CO2 Emissions Dataset*. 2025. DOI: 10.5281/ZENODO.5569234.

[9] S. C. Angulo et al. “The Role of Calcium Silicates and Quicklime on the Reactivity of Rehydrated Cements”. In: *Construction and Building Materials* 340 (2022), p. 127625. ISSN: 09500618. DOI: 10.1016/j.conbuildmat.2022.127625.

[10] M. Antunes et al. “Alternative Clinker Technologies for Reducing Carbon Emissions in Cement Industry: A Critical Review”. In: *Materials* 15.1 (2021), p. 209. ISSN: 1996-1944. DOI: 10.3390/ma15010209.

[11] J. H. Aquino Rocha and R. D. Toledo Filho. “Physical-Mechanical Assessment to Mortars Including Recycled Concrete Powder and Metakaolin”. In: *Case Studies in Construction Materials* 21 (2024), e03996. ISSN: 22145095. DOI: 10.1016/j.cscm.2024.e03996.

[12] J. H. Aquino Rocha and R. D. Toledo Filho. "The Utilization of Recycled Concrete Powder as Supplementary Cementitious Material in Cement-Based Materials: A Systematic Literature Review". In: *Journal of Building Engineering* 76 (2023), p. 107319. ISSN: 2352-7102. DOI: 10.1016/j.jobe.2023.107319.

[13] T. F. Baggio, E. Possan, and J. J. De Oliveira Andrade. "Physical-Chemical Characterization of Construction and Demolition Waste Powder with Thermomechanical Activation for Use as Supplementary Cementitious Material". In: *Construction and Building Materials* 437 (2024), p. 136907. ISSN: 09500618. DOI: 10.1016/j.conbuildmat.2024.136907.

[14] V. A. Baki et al. "The Impact of Mechanochemical Activation on the Physicochemical Properties and Pozzolanic Reactivity of Kaolinite, Muscovite and Montmorillonite". In: *Cement and Concrete Research* 162 (2022), p. 106962. ISSN: 0008-8846. DOI: 10.1016/j.cemconres.2022.106962.

[15] R. Baldusco et al. "Dehydration and Rehydration of Blast Furnace Slag Cement". In: *Journal of Materials in Civil Engineering* 31.8 (2019), p. 04019132. ISSN: 0899-1561, 1943-5533. DOI: 10.1061/(ASCE)MT.1943-5533.0002725.

[16] L. G. Baquerizo, T. Matschei, and K. L. Scrivener. "Impact of Water Activity on the Stability of Ettringite". In: *Cement and Concrete Research* 79 (2016), pp. 31–44. ISSN: 0008-8846. DOI: 10.1016/j.cemconres.2015.07.008.

[17] M. Barthel et al. "From Waste Materials to Products for Use in the Cement Industry". In: *Advances in Cement Research* 28.7 (2016), pp. 458–468. ISSN: 0951-7197, 1751-7605. DOI: 10.1680/jadcr.15.00149.

[18] D. Bastian et al. *Deutschland - Rohstoffsituation 2022*. Tech. rep. Bundesanstalt für Geowissenschaften und Rohstoffe, 2023. DOI: 10.25928/DERO-SI22.

[19] D. Bastian et al. *Deutschland - Rohstoffsituation 2023*. Tech. rep. Bundesanstalt für Geowissenschaften und Rohstoffe, 2024. DOI: 10.25928/DERO-SI23.

[20] R. Benedix. *Bauchemie: Einführung in die Chemie für Bauingenieure und Architekten*. 7. Auflage. Lehrbuch. Wiesbaden; Heidelberg: Springer Vieweg, 2020. ISBN: 978-3-658-26441-3.

[21] J. A. Bogas, A. Carriço, and M. Pereira. "Mechanical Characterization of Thermal Activated Low-Carbon Recycled Cement Mortars". In: *Journal of Cleaner Production* 218 (2019), pp. 377–389. ISSN: 09596526. DOI: 10.1016/j.jclepro.2019.01.325.

[22] J. A. Bogas, A. Carriço, and S. Real. "Durability of Concrete Produced with Recycled Cement from Waste Concrete". In: *Materials Today: Proceedings*. 3rd International Congress on Materials & Structural Stability 58 (2022), pp. 1149–1154. ISSN: 2214-7853. DOI: 10.1016/j.matpr.2022.01.280.

[23] J. A. Bogas, A. Carriço, and A. J. Tenza-Abril. "Microstructure of Thermoactivated Recycled Cement Pastes". In: *Cement and Concrete Research* 138 (2020), p. 106226. ISSN: 00088846. DOI: 10.1016/j.cemconres.2020.106226.

[24] J. A. Bogas et al. “Hydration and Phase Development of Recycled Cement”. In: *Cement and Concrete Composites* 127 (2022), p. 104405. ISSN: 09589465. DOI: 10.1016/j.cemconcomp.2022.104405.

[25] B. Bookhagen et al. *Deutschland - Rohstoffsituation 2021*. Tech. rep. Hannover: Bundesanstalt für Geowissenschaften und Rohstoffe, 2022.

[26] A. Bordy et al. “Cement Substitution by a Recycled Cement Paste Fine: Role of the Residual Anhydrous Clinker”. In: *Construction and Building Materials* 132 (2017), pp. 1–8. ISSN: 0950-0618. DOI: 10.1016/j.conbuildmat.2016.11.080.

[27] W. Brameshuber et al. *Verbundforschungsvorhaben Nachhaltig Bauen mit Beton: Potenziale des Sekundärstoffeinsatzes im Betonbau - Teilprojekt B Effiziente Sicherstellung der Umweltverträglichkeit von Beton - Teilprojekt E*. Vol. 584. DAfStb-Heft. Berlin: Beuth, 2011. ISBN: 978-3-410-65094-2.

[28] H. Brouwers. “The Work of Powers and Brownyard Revisited: Part 1”. In: *Cement and Concrete Research* 34.9 (2004), pp. 1697–1716. ISSN: 00088846. DOI: 10.1016/j.cemconres.2004.05.031.

[29] C. Bu et al. “The Durability of Recycled Fine Aggregate Concrete: A Review”. In: *Materials* 15.3 (2022), p. 1110. ISSN: 1996-1944. DOI: 10.3390/ma15031110.

[30] Bundesanstalt für Geowissenschaften und Rohstoffe. *Deutschland - Rohstoffsituation 2014*. Tech. rep. Hannover, 2015.

[31] Bundesanstalt für Geowissenschaften und Rohstoffe. *Deutschland - Rohstoffsituation 2018*. Tech. rep. Hannover, 2019.

[32] Bundesanstalt für Geowissenschaften und Rohstoffe. *Deutschland - Rohstoffsituation 2019*. Tech. rep. Hannover, 2020.

[33] Bundesrepublik Deutschland. *Verordnung über Anforderungen an den Einbau von mineralischen Ersatzbaustoffen in technische Bauwerke (Ersatzbaustoffverordnung): ErsatzbaustoffV*. 2023.

[34] B. Cantero et al. “Durability of Concretes Bearing Construction and Demolition Waste as Cement and Coarse Aggregate Substitutes”. In: *Cement and Concrete Composites* 134 (2022), p. 104722. ISSN: 09589465. DOI: 10.1016/j.cemconcomp.2022.104722.

[35] B. Cantero et al. “Inclusion of Construction and Demolition Waste as a Coarse Aggregate and a Cement Addition in Structural Concrete Design”. In: *Archives of Civil and Mechanical Engineering* 19.4 (2019), pp. 1338–1352. ISSN: 16449665. DOI: 10.1016/j.acme.2019.08.004.

[36] B. Cantero et al. “Water Transport and Shrinkage in Concrete Made with Ground Recycled Concrete-Additioned Cement and Mixed Recycled Aggregate”. In: *Cement and Concrete Composites* 118 (2021), p. 103957. ISSN: 09589465. DOI: 10.1016/j.cemconcomp.2021.103957.

[37] A. Carriço, S. Real, and J. A. Bogas. “Durability Performance of Thermoactivated Recycled Cement Concrete”. In: *Cement and Concrete Composites* 124 (2021). ISSN: 09589465. DOI: 10.1016/j.cemconcomp.2021.104270.

[38] A. Carriço et al. “Mortars with Thermo Activated Recycled Cement: Fresh and Mechanical Characterisation”. In: *Construction and Building Materials* 256 (2020), p. 119502. ISSN: 0950-0618. DOI: 10.1016/j.conbuildmat.2020.119502.

[39] A. Carriço et al. “Novel Separation Process for Obtaining Recycled Cement and High-Quality Recycled Sand from Waste Hardened Concrete”. In: *Journal of Cleaner Production* 309 (2021), p. 127375. ISSN: 09596526. DOI: 10.1016/j.jclepro.2021.127375.

[40] A. Carriço et al. “Shrinkage and Sorptivity of Mortars with Thermoactivated Recycled Cement”. In: *Construction and Building Materials* 333 (2022), p. 127392. ISSN: 09500618. DOI: 10.1016/j.conbuildmat.2022.127392.

[41] D. Chen et al. “Development of an Environmental Foamed Concrete Incorporating Recycled Cement Concrete Powder with Carbonation”. In: *Construction and Building Materials* 422 (2024), p. 135833. ISSN: 09500618. DOI: 10.1016/j.conbuildmat.2024.135833.

[42] J. Chen and J. Plank. “Alkali-Activated Calcined Clay Blended Cement: Effect of NaOH Activator on Performance of HPEG PCEs and on Early Strength”. In: *Cement and Concrete Research* 183 (2024), p. 107588. ISSN: 00088846. DOI: 10.1016/j.cemconres.2024.107588.

[43] L. Chen et al. “Effect of Chemical–Thermal Activation on the Properties of Recycled Fine Powder Cementitious Materials”. In: *Case Studies in Construction Materials* 20 (2024), e02956. ISSN: 2214-5095. DOI: 10.1016/j.cscm.2024.e02956.

[44] P. Chen et al. “Toward Net Negative Carbon for Bricks Using Mechano-Alkaline Activated Carbonated Recycled Concrete Fines”. In: *Construction and Building Materials* 452 (2024), p. 138947. ISSN: 09500618. DOI: 10.1016/j.conbuildmat.2024.138947.

[45] G.-C. Cho, J. Dodds, and J. C. Santamarina. “Particle Shape Effects on Packing Density, Stiffness, and Strength: Natural and Crushed Sands”. In: *Journal of Geotechnical and Geoenvironmental Engineering* 132.5 (2006), pp. 591–602. ISSN: 1090-0241, 1943-5606. DOI: 10.1061/(ASCE)1090-0241(2006)132:5(591).

[46] M. Cisiński et al. “Carbonated Calcium Silicates as Pozzolanic Supplementary Cementitious Materials”. In: *Construction and Building Materials* 443 (2024), p. 137764. ISSN: 09500618. DOI: 10.1016/j.conbuildmat.2024.137764.

[47] D. Coffetti et al. “Pathways towards Sustainable Concrete”. In: *Cement and Concrete Research* 154 (2022), p. 106718. ISSN: 00088846. DOI: 10.1016/j.cemconres.2022.106718.

[48] F. N. Costa and D. V. Ribeiro. “Reduction in CO2 Emissions during Production of Cement, with Partial Replacement of Traditional Raw Materials by Civil Construction Waste (CCW)”. In: *Journal of Cleaner Production* 276 (2020), p. 123302. ISSN: 09596526. DOI: 10.1016/j.jclepro.2020.123302.

[49] M. Cyr et al. “Recycled Concrete as Cement Main Constutient (CMC) or Supplementary Cementitious Materials (SCM)”. In: *Concrete Recycling: Research and Practice*. Ed. by F. Larrard and H. Colina. Boca Raton, FL: CRC Press/Taylor & Francis Group, 2019, pp. 83–95. ISBN: 1-351-05282-9.

[50] S. Dai et al. “Thermochemical Activation of Low-Grade Sand Washing Sludge and Its Application in Cement-Based Materials”. In: *Construction and Building Materials* 445 (2024), p. 137517. ISSN: 09500618. DOI: 10.1016/j.conbuildmat.2024.137517.

[51] D. O. De Lima et al. “Assessment of the Potential Use of Construction and Demolition Waste (CDW) Fines as Eco-Pozzolan in Binary and Ternary Cements”. In: *Construction and Building Materials* 411 (2024), p. 134320. ISSN: 09500618. DOI: 10.1016/j.conbuildmat.2023.134320.

[52] I. F. Del Sáez Bosque et al. “Carbonation of Concrete with Construction and Demolition Waste Based Recycled Aggregates and Cement with Recycled Content”. In: *Construction and Building Materials* 234 (2020), p. 117336. ISSN: 09500618. DOI: 10.1016/j.conbuildmat.2019.117336.

[53] Q. Deng et al. “Rheological Properties of Mortar with Recycled Fine Aggregate: From the Perspective of Particle Packing”. In: *Construction and Building Materials* 465 (2025), p. 140237. ISSN: 09500618. DOI: 10.1016/j.conbuildmat.2025.140237.

[54] Deutsche Rohstoffagentur (DERA) in der Bundesanstalt für Geowissenschaften und Rohstoffe. *Deutschland - Rohstoffsituation 2010*. Tech. rep. Hannover, 2011.

[55] T. Ding et al. “Engineering Aluminosilicates with High Surface Area Extracted from Waste Concrete to Form a Viable Supplementary Cementitious Material”. In: *Construction and Building Materials* 462 (2025), p. 139981. ISSN: 09500618. DOI: 10.1016/j.conbuildmat.2025.139981.

[56] B. Dora. “Hydraulisch Erhärtende Baustoffe Aus Betonbrechsand”. PhD thesis. TU Braunschweig, 2001.

[57] J. Du et al. “Phase Separation of Recycled Concrete Powder during Grinding and Consequent Influences on Its Hydration Behaviors in Cement Paste”. In: *Cement and Concrete Composites* 142 (2023), p. 105203. ISSN: 09589465. DOI: 10.1016/j.cemconcomp.2023.105203.

[58] C. F. Dunant et al. “Electric Recycling of Portland Cement at Scale”. In: *Nature* 629 (2024), pp. 1055–1061. ISSN: 0028-0836, 1476-4687. DOI: 10.1038/s41586-024-07338-8.

[59] C. Durastanti and L. Moretti. “Environmental Impacts of Cement Production: A Statistical Analysis”. In: *Applied Sciences* 10.22 (2020), p. 8212. ISSN: 2076-3417. DOI: 10.3390/app10228212.

[60] N. Ekin and O. Uyanik. “Comparison of Static and Dynamic Elastic Moduli in Concrete: Effects of Compressive Strength, Curing Conditions and Reinforcement”. In: *Iranian Journal of Science and Technology, Transactions of Civil Engineering* 45.4 (2021), pp. 2327–2343. ISSN: 2228-6160, 2364-1843. DOI: 10.1007/s40996-020-00513-7.

[61] C. J. Engelsen et al. “Leaching Characterisation and Geochemical Modelling of Minor and Trace Elements Released from Recycled Concrete Aggregates”. In: *Cement and Concrete Research* 40.12 (2010), pp. 1639–1649. ISSN: 00088846. DOI: 10.1016/j.cemconres.2010.08.001.

[62] L. Evangelista and J. De Brito. "Concrete with Fine Recycled Aggregates: A Review". In: *European Journal of Environmental and Civil Engineering* 18.2 (2014), pp. 129–172. ISSN: 1964-8189, 2116-7214. DOI: 10.1080/19648189.2013.851038.

[63] Y. Fan, H. Niu, and X. Zhang. "Impact of the Properties of Old Mortar on Creep Prediction Model of Recycled Aggregate Concrete". In: *Construction and Building Materials* 239 (2020), p. 117772. ISSN: 09500618. DOI: 10.1016/j.conbuildmat.2019.117772.

[64] G. Fang et al. "Microstructure and Micromechanical Properties of Interfacial Transition Zone in Green Recycled Aggregate Concrete". In: *Journal of Building Engineering* 66 (2023), p. 105860. ISSN: 23527102. DOI: 10.1016/j.jobe.2023.105860.

[65] X. Fang et al. "Characterization and Optimization of a Two-Step Carbonation Process for Valorization of Recycled Cement Paste Fine Powder". In: *Construction and Building Materials* 278 (2021), p. 122343. ISSN: 09500618. DOI: 10.1016/j.conbuildmat.2021.122343.

[66] C. Feng et al. "Enhancement Technologies of Recycled Aggregate – Enhancement Mechanism, Influencing Factors, Improvement Effects, Technical Difficulties, Life Cycle Assessment". In: *Construction and Building Materials* 317 (2022), p. 126168. ISSN: 09500618. DOI: 10.1016/j.conbuildmat.2021.126168.

[67] M. V. A. Florea. "Secondary Materials Applied in Cement-Based Products : Treatment, Modelling and Environmental Interaction". PhD thesis. Technische Universiteit Eindhoven, 2014. ISBN: 978-90-386-3609-2. DOI: 10.6100/IR772902.

[68] M. V. A. Florea, Z. Ning, and H. J. H. Brouwers. "Activation of Liberated Concrete Fines and Their Application in Mortars". In: *Construction and Building Materials* 50 (2014), pp. 1–12. ISSN: 0950-0618. DOI: 10.1016/j.conbuildmat.2013.09.012.

[69] M. Frías et al. "Reactivity in Cement Pastes Bearing Fine Fraction Concrete and Glass from Construction and Demolition Waste: Microstructural Analysis of Viability". In: *Cement and Concrete Research* 148 (2021), p. 106531. ISSN: 00088846. DOI: 10.1016/j.cemconres.2021.106531.

[70] F. Friol Guedes de Paiva et al. "Utilization of Inorganic Solid Wastes in Cementitious Materials – A Systematic Literature Review". In: *Construction and Building Materials* 285 (2021), p. 122833. ISSN: 09500618. DOI: 10.1016/j.conbuildmat.2021.122833.

[71] Y. Gao et al. "Accelerated Carbonation of Recycled Concrete Aggregate in Semi-Wet Environments: A Promising Technique for CO2 Utilization". In: *Cement and Concrete Research* 180 (2024), p. 107486. ISSN: 00088846. DOI: 10.1016/j.cemconres.2024.107486.

[72] Y. Gao et al. "Mechanical, Freeze-Thaw Resistance and Heavy Metals Leaching Properties of Alkali-Activated Recycled Concrete Powder Solidified Sludge". In: *Construction and Building Materials* 447 (2024), p. 138154. ISSN: 09500618. DOI: 10.1016/j.conbuildmat.2024.138154.

[73] Y. Gao et al. “A Microscopic Study on Ternary Blended Cement Based Composites”. In: *Construction and Building Materials* 46 (2013), pp. 28–38. ISSN: 09500618. DOI: 10.1016/j.conbuildmat.2013.04.021.

[74] P. Ge et al. “A Method for Separating Gravel Aggregates, Sand and Hardened Cement by High-Temperature Heating, Ball Milling and Sieving”. In: *Construction and Building Materials* 466 (2025), p. 140300. ISSN: 0950-0618. DOI: 10.1016/j.conbuildmat.2025.140300.

[75] P. Ge et al. “Study on the Activity, Phase, Thermal Decomposition Characteristics, Microstructure, and Chemical Element of Hardened Cement Powder under Heating Temperature of 100°C~1200°C”. In: *Structural Concrete* (2024), pp. 1–25. DOI: 10.1002/suco.202301108.

[76] A. T. Gebremariam et al. “Innovative Technologies for Recycling End-of-Life Concrete Waste in the Built Environment”. In: *Resources, Conservation and Recycling* 163 (2020), p. 104911. ISSN: 0921-3449. DOI: 10.1016/j.resconrec.2020.104911.

[77] E. M. Getachew et al. “Enhancing Mortar Properties through Thermoactivated Recycled Concrete Cement”. In: *Buildings* 13.9 (2023), p. 2209. ISSN: 2075-5309. DOI: 10.3390/buildings13092209.

[78] E. M. Getachew et al. “Performance Evaluation of Mortar with Ground and Thermo-Activated Recycled Concrete Cement”. In: *Cogent Engineering* 11.1 (2024), p. 2357726. ISSN: 2331-1916. DOI: 10.1080/23311916.2024.2357726.

[79] A. Gholizadeh-Vayghan et al. “Thermal Reactivation of Hydrated Cement Paste: Properties and Impact on Cement Hydration”. In: *Materials* 17.11 (2024), p. 2659. ISSN: 1996-1944. DOI: 10.3390/ma17112659.

[80] S. Greve-Dierfeld et al. “Understanding the Carbonation of Concrete with Supplementary Cementitious Materials: A Critical Review by RILEM TC 281-CCC”. In: *Materials and Structures* 53.6 (2020). ISSN: 1871-6873. DOI: 10.1617/s11527-020-01558-w.

[81] X. Guan et al. “Chloride Ion Permeability of Concrete Containing Recycled Composite Powder from Building Demolition Waste”. In: *Construction and Building Materials* 424 (2024), p. 135934. ISSN: 09500618. DOI: 10.1016/j.conbuildmat.2024.135934.

[82] E. Güneyisi and M. Gesoğlu. “A Study on Durability Properties of High-Performance Concretes Incorporating High Replacement Levels of Slag”. In: *Materials and Structures* 41.3 (2008), pp. 479–493. ISSN: 1359-5997, 1871-6873. DOI: 10.1617/s11527-007-9260-y.

[83] S. Gupta, H. Agrawal, and S. Chaudhary. “Thermo-Mechanical Treatment as an Upcycling Strategy for Mixed Recycled Aggregate”. In: *Construction and Building Materials* 398 (2023), p. 132471. ISSN: 09500618. DOI: 10.1016/j.conbuildmat.2023.132471.

[84] X. He et al. “Feasibility of Incorporating Autoclaved Aerated Concrete Waste for Cement Replacement in Sustainable Building Materials”. In: *Journal of Cleaner Production* 250 (2020), p. 119455. ISSN: 09596526. DOI: 10.1016/j.jclepro.2019.119455.

[85] Z. He et al. “Properties and Deformation Behavior of Concrete Containing Thermally Activated Recycled Cement”. In: *Construction and Building Materials* 509 (2026), p. 145230. ISSN: 09500618. DOI: 10.1016/j.conbuildmat.2026.145230.

[86] Z. He et al. “Reusing Thermoactivated Construction Waste Spoil as Sustainable Binder for Durable Concrete: Microstructure and Chloride Transport”. In: *Construction and Building Materials* 398 (2023), p. 132553. ISSN: 09500618. DOI: 10.1016/j.conbuildmat.2023.132553.

[87] Z. He et al. “Comparison of CO2 Emissions from OPC and Recycled Cement Production”. In: *Construction and Building Materials* 211 (2019), pp. 965–973. ISSN: 0950-0618. DOI: 10.1016/j.conbuildmat.2019.03.289.

[88] C. Herget. “Kalksteinmehl als Betonzusatzstoff für umweltfreundliche Betone”. PhD thesis. Darmstadt, 2022.

[89] C. Herget et al. “Kalksteinmehl als Betonzusatzstoff – Vorschlag für die Anrechenbarkeit auf den Zementgehalt und Potenzial zur CO_2 -Reduktion im Betonbau”. In: *Beton- und Stahlbetonbau* 117.2 (2022), pp. 109–118. ISSN: 0005-9900, 1437-1006. DOI: 10.1002/best.202100073.

[90] A. Herrmann, A. Koenig, and F. Dehn. “Structural Concrete Based on Alkali-Activated Binders: Terminology, Reaction Mechanisms, Mix Designs and Performance”. In: *Structural Concrete* 19.3 (2018), pp. 918–929. ISSN: 14644177. DOI: 10.1002/suco.201700016.

[91] J. P. Höffgen, M. Bauer, and F. Dehn. *Entwicklung einer Strategie zum Umgang mit Betonbrechsanden in Baden-Württemberg. THINKTANK Industrielle Ressourcenstrategien.* Tech. rep. Karlsruhe: Karlsruher Institut für Technologie (KIT), 2022. DOI: 10.5445/IR/1000169796.

[92] J. P. Höffgen et al. “Entwicklung thermisch-mechanisch aktivierter Betonbrechsande als Betonzusatzstoff – Projektvorstellung und erste Ergebnisse”. In: *Beton- und Stahlbetonbau* 118.4 (2023), pp. 239–246. ISSN: 00059900. DOI: 10.1002/best.202200127.

[93] I. Horváth, I. Proks, and I. Nerád. “Activation Energies of the Thermal Decompositions of C3AH6 and C3AD6 by the Isothermal TG Method”. In: *Journal of thermal analysis* 12.1 (1977), pp. 105–110. ISSN: 1572-8943. DOI: 10.1007/BF01909862.

[94] S. Hou et al. “Mechanical Properties and Pore Structure of 3D Printed Mortar with Recycled Powder”. In: *Construction and Building Materials* 394 (2023), p. 132068. ISSN: 09500618. DOI: 10.1016/j.conbuildmat.2023.132068.

[95] S. Hou et al. “Understanding the Chloride Migration in Recycled Powder Concrete: Effects of Recycled Powder Type, Replacement Rate and Substitution Pattern”. In: *Construction and Building Materials* 436 (2024), p. 136825. ISSN: 09500618. DOI: 10.1016/j.conbuildmat.2024.136825.

[96] H.-B. Hu et al. “Properties Enhancement of Recycled Coarse Aggregates by Pre-Coating/Pre-Soaking with Zeolite Powder/Calcium Hydroxide”. In: *Construction and Building Materials* 286 (2021), p. 122888. ISSN: 09500618. DOI: 10.1016/j.conbuildmat.2021.122888.

[97] S. Hu et al. “Performance of Limestone Calcined Clay Cement (LC3) Made with CO2-mineralized Concrete Slurry Waste”. In: *Journal of Cleaner Production* 472 (2024), p. 143476. ISSN: 09596526. DOI: 10.1016/j.jclepro.2024.143476.

[98] R. Huang et al. “A Review on Concrete Superplasticizers and Their Potential Applications for Enhancing the Performance of Thermally Activated Recycled Cement”. In: *Materials* 17.17 (2024), p. 4170. ISSN: 1996-1944. DOI: 10.3390/ma17174170.

[99] S. Ismail and M. Ramli. “Engineering Properties of Treated Recycled Concrete Aggregate (RCA) for Structural Applications”. In: *Construction and Building Materials* 44 (2013), pp. 464–476. ISSN: 09500618. DOI: 10.1016/j.conbuildmat.2013.03.014.

[100] L. Izoret et al. “Recycled Concrete Sand as Alternative Raw Material for Portland Clinker Production”. In: *Concrete Recycling: Research and Practice*. Ed. by F. Larrard and H. Colina. Boca Raton, FL: CRC Press/Taylor & Francis Group, 2019, pp. 63–81. ISBN: 1-351-05282-9.

[101] A. A. Jhatial, I. Nováková, and E. Gjerløw. “A Review on Emerging Cementitious Materials, Reactivity Evaluation and Treatment Methods”. In: *Buildings* 13.2 (2023), p. 526. ISSN: 2075-5309. DOI: 10.3390/buildings13020526.

[102] J. Jiang et al. “Multiscale Investigation of Hydration and Hardening Mechanism in Cementitious Composite Containing CO2-activation Recycled Cement Paste Powder with Aragonite Whiskers”. In: *Journal of Building Engineering* 112 (2025), p. 113888. ISSN: 23527102. DOI: 10.1016/j.jobe.2025.113888.

[103] Y. Jiang et al. “Ultra-Green Cement: Limestone Calcined Clay Cement (LC3) with Recycled Cement”. In: *Cement and Concrete Composites* 163 (2025), p. 106210. ISSN: 0958-9465. DOI: 10.1016/j.cemconcomp.2025.106210.

[104] M. S. Juan and P. A. Gutiérrez. “Study on the Influence of Attached Mortar Content on the Properties of Recycled Concrete Aggregate”. In: *Construction and Building Materials* 23.2 (2009), pp. 872–877. ISSN: 09500618. DOI: 10.1016/j.conbuildmat.2008.04.012.

[105] K. Kalinowska-Wichrowska, M. Kosior-Kazberuk, and E. Pawluczuk. “The Properties of Composites with Recycled Cement Mortar Used as a Supplementary Cementitious Material”. In: *Materials* 13.1 (2020), p. 64. ISSN: 1996-1944. DOI: 10.3390/ma13010064.

[106] S. K. Kaliyavaradhan, L. Li, and T.-C. Ling. “Response Surface Methodology for the Optimization of CO2 Uptake Using Waste Concrete Powder”. In: *Construction and Building Materials* 340 (2022), p. 127758. ISSN: 09500618. DOI: 10.1016/j.conbuildmat.2022.127758.

[107] Y. Katsuyama et al. “Development of a Process for Producing High-purity Calcium Carbonate (CaCO3) from Waste Cement Using Pressurized CO2”. In: *Environmental Progress* 24.2 (2005), pp. 162–170. ISSN: 0278-4491, 1547-5921. DOI: 10.1002/ep.10080.

[108] M. Keppert et al. “Recycling of Fresh Concrete Slurry Waste as Supplementary Cementing Material: Characterization, Application and Leaching of Selected Elements”. In: *Construction and Building Materials* 300 (2021), p. 124061. ISSN: 09500618. DOI: 10.1016/j.conbuildmat.2021.124061.

[109] H. Kim, S. Park, and H. Kim. "The Optimum Production Method for Quality Improvement of Recycled Aggregates Using Sulfuric Acid and the Abrasion Method". In: *International journal of environmental research and public health* 13.8 (2016). DOI: 10.3390/ijerph13080769.

[110] J.-H. Kim et al. "Utilization of Recycled Cement Powder as a Solidifying Agent for Radioactive Waste Immobilization". In: *Construction and Building Materials* 289 (2021), p. 123126. ISSN: 09500618. DOI: 10.1016/j.conbuildmat.2021.123126.

[111] J. Kim and N. Kim. "Exploring the Role of Thermal Activation of Cement Exposed to the External Environment on the Improvement of Concrete Properties". In: *Journal of Materials Research and Technology* 24 (2023), pp. 2868–2878. ISSN: 2238-7854. DOI: 10.1016/j.jmrt.2023.03.195.

[112] J. Kim and A. Ubysz. "Thermal Activation of Multi-Recycled Concrete Powder as Supplementary Cementitious Material for Repeated and Waste-Free Recycling". In: *Journal of Building Engineering* 98 (2024), p. 111169. ISSN: 2352-7102. DOI: 10.1016/j.jobe.2024.111169.

[113] J. Kim et al. "Characteristics of Waste Concrete Powders from Multi-Recycled Coarse Aggregate Concrete and Their Effects as Cement Replacements". In: *Construction and Building Materials* 398 (2023), p. 132525. ISSN: 09500618. DOI: 10.1016/j.conbuildmat.2023.132525.

[114] E. W. Klingsch. "Explosive Spalling of Concrete in Fire". PhD thesis. ETH Zurich, 2014. DOI: 10.3929/ethz-a-010243000.

[115] K. A. Knight, P. R. Cunningham, and S. A. Miller. "Optimizing Supplementary Cementitious Material Replacement to Minimize the Environmental Impacts of Concrete". In: *Cement and Concrete Composites* 139 (2023), p. 105049. ISSN: 09589465. DOI: 10.1016/j.cemconcomp.2023.105049.

[116] D. Kong et al. "Effect and Mechanism of Surface-Coating Pozzalanics Materials around Aggregate on Properties and ITZ Microstructure of Recycled Aggregate Concrete". In: *Construction and Building Materials* 24 (2010), pp. 701–708. ISSN: 09500618. DOI: 10.1016/j.conbuildmat.2009.10.038.

[117] G. Kotsay and R. Jaskulski. "Belite Cement as an Ecological Alternative to Portland Cement – a Review". In: *Materials Structures Technology* 2.1 (2019), pp. 70–76. DOI: 10.31448/mstj.02.01.2019.70-76.

[118] S.-C. Kou and C.-S. Poon. "Properties of Concrete Prepared with PVA-impregnated Recycled Concrete Aggregates". In: *Cement and Concrete Composites* 32 (2010), pp. 649–654. ISSN: 09589465. DOI: 10.1016/j.cemconcomp.2010.05.003.

[119] J. Krithika and G. Ramesh Kumar. "Influence of Fly Ash on Concrete – A Systematic Review". In: *Materials Today: Proceedings* 33 (2020), pp. 906–911. ISSN: 22147853. DOI: 10.1016/j.matpr.2020.06.425.

[120] H. Krour et al. “Incorporation Rate of Recycled Aggregates in Cement Raw Meals”. In: *Construction and Building Materials* 248 (2020), p. 118217. ISSN: 09500618. DOI: 10.1016/j.conbuildmat.2020.118217.

[121] H. Krour et al. “Industrial-Scale Valorization of Fine Recycled Aggregates in Cement Raw Meal: Towards Sustainable Mixtures”. In: *Journal of Cleaner Production* 362 (2022), p. 132231. ISSN: 09596526. DOI: 10.1016/j.jclepro.2022.132231.

[122] A. Kwan, V. Wong, and W. Fung. “A 3-Parameter Packing Density Model for Angular Rock Aggregate Particles”. In: *Powder Technology* 274 (2015), pp. 154–162. ISSN: 00325910. DOI: 10.1016/j.powtec.2014.12.054.

[123] E. Kwon et al. “A Study on Development of Recycled Cement Made from Waste Cementitious Powder”. In: *Construction and Building Materials* 83 (2015), pp. 174–180. ISSN: 09500618. DOI: 10.1016/j.conbuildmat.2015.02.086.

[124] V. Letelier et al. “Combined Effects of Recycled Hydrated Cement and Recycled Aggregates on the Mechanical Properties of Concrete”. In: *Construction and Building Materials* 132 (2017), pp. 365–375. ISSN: 09500618. DOI: 10.1016/j.conbuildmat.2016.12.010.

[125] J. Li et al. “Recycled Concrete Fines as a Supplementary Cementitious Material: Mechanical Performances, Hydration, and Microstructures in Cementitious Systems”. In: *Case Studies in Construction Materials* 21 (2024), e03575. ISSN: 2214-5095. DOI: 10.1016/j.cscm.2024.e03575.

[126] L. Li et al. “Mineralization and Utilization of CO2 in Construction and Demolition Wastes Recycling for Building Materials: A Systematic Review of Recycled Concrete Aggregate and Recycled Hardened Cement Powder”. In: *Separation and Purification Technology* 298 (2022), p. 121512. ISSN: 1383-5866. DOI: 10.1016/j.seppur.2022.121512.

[127] S. Li et al. “Investigation of Using Recycled Powder from the Preparation of Recycled Aggregate as a Supplementary Cementitious Material”. In: *Construction and Building Materials* 267 (2021), p. 120976. ISSN: 09500618. DOI: 10.1016/j.conbuildmat.2020.120976.

[128] T. Li et al. “Effect of Recycled Concrete Powder on the Evolution of the Static Yield Stress of Cement Paste”. In: *Cement and Concrete Composites* 162 (2025), p. 106158. ISSN: 09589465. DOI: 10.1016/j.cemconcomp.2025.106158.

[129] T. Li et al. “Effect of Recycled Concrete Powder on the Rheological Properties of Cement Paste: New Findings”. In: *Cement and Concrete Composites* 156 (2025), p. 105873. ISSN: 09589465. DOI: 10.1016/j.cemconcomp.2024.105873.

[130] X. Li et al. “Study on the Properties and Carbon Footprint of Low Heat Cement Clinker Prepared by Recycled Concrete Powder and Calcium Carbide Slag”. In: *Construction and Building Materials* 441 (2024), p. 137542. ISSN: 09500618. DOI: 10.1016/j.conbuildmat.2024.137542.

[131] W. Lian et al. “Transforming Waste Powder into Two Types of Supplementary Cementitious Materials through a Wet Carbonation Process”. In: *Construction and Building Materials* 489 (2025), p. 140644. ISSN: 09500618. DOI: 10.1016/j.conbuildmat.2025.140644.

[132] C. Liang et al. “Effect of Additional Water Content and Adding Methods on the Performance of Recycled Aggregate Concrete”. In: *Construction and Building Materials* 423 (2024), p. 135868. ISSN: 09500618. DOI: 10.1016/j.conbuildmat.2024.135868.

[133] C. Liang et al. “The Utilization of Active Recycled Powder from Various Construction Wastes in Preparing Ductile Fiber-Reinforced Cementitious Composites: A Case Study”. In: *Case Studies in Construction Materials* 15 (2021), p. 00650. ISSN: 22145095. DOI: 10.1016/j.cscm.2021.e00650.

[134] C. Liang et al. “Utilization of CO2 Curing to Enhance the Properties of Recycled Aggregate and Prepared Concrete: A Review”. In: *Cement and Concrete Composites* 105 (2020), p. 103446. ISSN: 09589465. DOI: 10.1016/j.cemconcomp.2019.103446.

[135] A. Lipowsky and A. Müller. “Gesteinsmehl Als Zuschlagstoffe in Hydraulischen Bindemitteln”. In: *Aufbereitungs-Technik/Mineral Processing* 58.12 (2017), pp. 52–64.

[136] J. Liu, P. Rauwoens, and Ö. Cizer. “Transforming Construction Waste into Low-Carbon Cementitious Materials through Co-Calcination of Recycled Concrete Fines and Kaolinite”. In: *Environmental Research* (2025), p. 123530. ISSN: 00139351. DOI: 10.1016/j.envres.2025.123530.

[137] M. Liu et al. “Reusing Thermoactivated Waste Paste/Concrete Powder for Sustainable Alkali-Activated Materials: Effects of Thermoactivated Temperature”. In: *Construction and Building Materials* 437 (2024), p. 136973. ISSN: 09500618. DOI: 10.1016/j.conbuildmat.2024.136973.

[138] Q. Liu, J. Xiao, and A. Singh. “Quantification of Plastic Shrinkage and Cracking in Mortars Containing Different Recycled Powders Using Digital Image Correlation Technique”. In: *Construction and Building Materials* 293 (2021), p. 123509. ISSN: 09500618. DOI: 10.1016/j.conbuildmat.2021.123509.

[139] Y. Liu et al. “Evaluation on Recycled Clinker Production and Properties from Regeneration of Completely Recycle Concrete”. In: *Construction and Building Materials* 301 (2021), p. 123882. ISSN: 09500618. DOI: 10.1016/j.conbuildmat.2021.123882.

[140] Y. Liu et al. “Performance Evaluation of Regenerated Clinker from Completely Recyclable Mortar”. In: *Construction and Building Materials* 309 (2021), p. 125184. ISSN: 09500618. DOI: 10.1016/j.conbuildmat.2021.125184.

[141] F. W. Locher. *Cement Principles of Production and Use*. Düsseldorf: Verl. Bau und Technik, 2006. ISBN: 978-3-7640-0420-0.

[142] L. Lu, Y. He, and S. Hu. “Binding Materials of Dehydrated Phases of Waste Hardened Cement Paste and Pozzolanic Admixture”. In: *Journal of Wuhan University of Technology-Mater. Sci. Ed.* 24.1 (2009), pp. 140–144. ISSN: 1000-2413, 1993-0437. DOI: 10.1007/s11595-009-1140-6.

[143] S. Luo et al. “Investigation into the Impact of Autoclaved Curing on the Properties of Recycled Concrete Powder”. In: *Construction and Building Materials* 496 (2025), p. 143758. ISSN: 09500618. DOI: 10.1016/j.conbuildmat.2025.143758.

[144] P. Lura, F. Winnefeld, and X. Fang. “A Simple Method for Determining the Total Amount of Physically and Chemically Bound Water of Different Cements”. In: *Journal of Thermal Analysis and Calorimetry* 130.2 (2017), pp. 653–660. ISSN: 1588-2926. DOI: 10.1007/s10973-017-6513-z.

[145] Q. Ma et al. “Influence of the Effect of Recycled Fine Aggregate and Powder on the Frost Resistance of Recycled Concrete”. In: *Low-carbon Materials and Green Construction* 3.1 (2025), p. 6. ISSN: 2731-6319. DOI: 10.1007/s44242-025-00067-9.

[146] Z. Ma et al. “Chloride Diffusion and Binding Capacity of Sustainable Cementitious Materials with Construction Waste Powder as Cement Replacement”. In: *Construction and Building Materials* 368 (2023), p. 130352. ISSN: 09500618. DOI: 10.1016/j.conbuildmat.2023.130352.

[147] Z. Ma et al. “Properties and Activation Modification of Eco-Friendly Cementitious Materials Incorporating High-Volume Hydrated Cement Powder from Construction Waste”. In: *Construction and Building Materials* 316 (2022), p. 125788. ISSN: 09500618. DOI: 10.1016/j.conbuildmat.2021.125788.

[148] Z. Ma et al. “Understanding the Micro-Characteristics and Mechanical Behavior of More Sustainable UHP-ECC with Both Recycled Aggregate and Recycled Powder from Concrete Waste”. In: *Journal of Building Engineering* 112 (2025), p. 113705. ISSN: 23527102. DOI: 10.1016/j.jobe.2025.113705.

[149] V. Malárics. “Ermittlung der Betonzugfestigkeit aus dem Spaltzugversuch an zylindrischen Betonproben”. PhD thesis. Karlsruher Institut für Technologie (KIT), 2011.

[150] Y. Mao et al. “Chloride Binding of Cement Paste Containing Wet Carbonated Recycled Concrete Fines”. In: *Cement and Concrete Research* 191 (2025), p. 107823. ISSN: 0008-8846. DOI: 10.1016/j.cemconres.2025.107823.

[151] Y. Mao et al. “Effect of Conditions on Wet Carbonation Products of Recycled Cement Paste Powder”. In: *Cement and Concrete Composites* 144 (2023), p. 105307. ISSN: 09589465. DOI: 10.1016/j.cemconcomp.2023.105307.

[152] Y. Mao et al. “Effect of Wet Carbonated Recycled Cement Paste Powder on the Rheology of Cement Paste”. In: *Cement and Concrete Research* 181 (2024), p. 107553. ISSN: 00088846. DOI: 10.1016/j.cemconres.2024.107553.

[153] Y. Mao et al. “Quantifying the Effects of Wet Carbonated Recycled Cement Paste Powder on the Properties of Cement Paste”. In: *Cement and Concrete Research* 175 (2024), p. 107381. ISSN: 0008-8846. DOI: 10.1016/j.cemconres.2023.107381.

[154] A. I. Marques et al. “Modulus of Elasticity of Mortars: Static and Dynamic Analyses”. In: *Construction and Building Materials* 232 (2020), p. 117216. ISSN: 09500618. DOI: 10.1016/j.conbuildmat.2019.117216.

[155] J. V. Martins et al. “Influence of Replacing Portland Cement with Three Different Concrete Sludge Wastes”. In: *Construction and Building Materials* 303 (2021), p. 124519. ISSN: 09500618. DOI: 10.1016/j.conbuildmat.2021.124519.

[156] L. Medeghini et al. “The Secret of Ancient Roman Hydraulic Mortar: The Lesson Learnt from the Past for Future Cements”. In: *Cement and Concrete Composites* 148 (2024), p. 105484. ISSN: 09589465. DOI: 10.1016/j.cemconcomp.2024.105484.

[157] H. Mehdizadeh et al. “Effect of Particle Size and CO2 Treatment of Waste Cement Powder on Properties of Cement Paste”. In: *Canadian Journal of Civil Engineering* 48.5 (2021), pp. 522–531. ISSN: 0315-1468. DOI: 10.1139/cjce-2019-0574.

[158] Y. Menard et al. “Innovative Process Routes for a High-Quality Concrete Recycling”. In: *Waste management* 33 (2013), pp. 1561–1565. DOI: 10.1016/j.wasman.2013.02.006.

[159] D. Meng et al. “A Strength-Based Mix Design Method for Recycled Aggregate Concrete and Consequent Durability Performance”. In: *Construction and Building Materials* 281 (2021), p. 122616. ISSN: 09500618. DOI: 10.1016/j.conbuildmat.2021.122616.

[160] T. Meng et al. “Comparison of Technical Properties of Cement Pastes with Different Activated Recycled Powder from Construction and Demolition Waste”. In: *Cement and Concrete Composites* 120 (2021), p. 104065. ISSN: 09589465. DOI: 10.1016/j.cemconcomp.2021.104065.

[161] S. A. Miller et al. “Carbon Dioxide Reduction Potential in the Global Cement Industry by 2050”. In: *Cement and Concrete Research* 114 (2018), pp. 115–124. ISSN: 00088846. DOI: 10.1016/j.cemconres.2017.08.026.

[162] Ministerium für Umwelt, Klima und Energiewirtschaft and Baden-Württemberg. *Abfallbilanz 2024*. Tech. rep. Stuttgart, 2025.

[163] A. Mistri et al. “A Review on Different Treatment Methods for Enhancing the Properties of Recycled Aggregates for Sustainable Construction Materials”. In: *Construction and Building Materials* 233 (2020), p. 117894. ISSN: 09500618. DOI: 10.1016/j.conbuildmat.2019.117894.

[164] A. Müller. *Baustoffrecycling: Entstehung - Aufbereitung - Verwertung*. Wiesbaden: Springer Fachmedien Wiesbaden, 2018. ISBN: 978-3-658-22987-0. DOI: 10.1007/978-3-658-22988-7.

[165] C. Müller and B. Dora. *Verwertung von Brechsand aus Bauschutt*. Vol. 506. Deutscher Ausschuss Für Stahlbeton. Berlin: Beuth, 2000. ISBN: 3-410-65706-1.

[166] A. Naghizadeh et al. “Effective Recycled Binder Produced upon Thermal Activation to Enhance Mechanical Properties of Fly Ash – Based Geopolymer Mortars”. In: *Developments in the Built Environment* 23 (2025), p. 100688. ISSN: 2666-1659. DOI: 10.1016/j.dibe.2025.100688.

[167] A. Naghizadeh et al. “Re – Activation of Recycled Fly Ash – Based Geopolymer Binder to Enhance Mechanical Properties”. In: *Case Studies in Construction Materials* 23 (2025), e04967. ISSN: 22145095. DOI: 10.1016/j.cscm.2025.e04967.

[168] National Minerals Information Center. *U.S. Geological Survey Mineral Commodity Summaries 2025 Data Release (Ver. 2.0, April 2025) – with Major Processing by Our World in Data*. Our World in Data, 2025. DOI: 10.5066/P13XCP3R.

[169] M. Nedeljković et al. "Use of Fine Recycled Concrete Aggregates in Concrete: A Critical Review". In: *Journal of Building Engineering* 38 (2021), p. 102196. ISSN: 23527102. DOI: 10.1016/j.jobe.2021.102196.

[170] N. Noel et al. "Chemical Transformations during the Preparation and Rehydration of Reactivated Virgin Cements". In: *CEMENT* 19 (2025), p. 100129. ISSN: 2666-5492. DOI: 10.1016/j.cement.2025.100129.

[171] E. A. Ohemeng and S. O. Ekolu. "A Review on the Reactivation of Hardened Cement Paste and Treatment of Recycled Aggregates". In: *Magazine of Concrete Research* 72.10 (2020), pp. 526–539. ISSN: 0024-9831. DOI: 10.1680/jmacr.18.00452.

[172] S. Omary, E. Ghorbel, and G. Wardeh. "Relationships between Recycled Concrete Aggregates Characteristics and Recycled Aggregates Concretes Properties". In: *Construction and Building Materials* 108 (2016), pp. 163–174. ISSN: 09500618. DOI: 10.1016/j.conbuildmat.2016.01.042.

[173] C. Orozco et al. "Comparison of Environmental Impacts of Fly Ash and Slag as Cement Replacement Materials for Mass Concrete and the Impact of Transportation". In: *Sustainable Materials and Technologies* 39 (2024), e00796. ISSN: 22149937. DOI: 10.1016/j.susmat.2023.e00796.

[174] X. Ouyang et al. "Multiscale Microstructure and Reactivity Evolution of Recycled Concrete Fines under Gas-Solid Carbonation". In: *Cement and Concrete Composites* 157 (2025), p. 105903. ISSN: 09589465. DOI: 10.1016/j.cemconcomp.2024.105903.

[175] E. Özbay, M. Erdemir, and H. İ. Durmuş. "Utilization and Efficiency of Ground Granulated Blast Furnace Slag on Concrete Properties – A Review". In: *Construction and Building Materials* 105 (2016), pp. 423–434. ISSN: 09500618. DOI: 10.1016/j.conbuildmat.2015.12.153.

[176] D. K. Panesar and R. Zhang. "Performance Comparison of Cement Replacing Materials in Concrete: Limestone Fillers and Supplementary Cementing Materials – A Review". In: *Construction and Building Materials* 251 (2020), p. 118866. ISSN: 09500618. DOI: 10.1016/j.conbuildmat.2020.118866.

[177] K. S. Park et al. "The Fate of Heavy Metals in Recycled Concrete Paste upon Enforced Carbonation: A Review". In: *Resources, Conservation & Recycling Advances* 28 (2025), p. 200289. ISSN: 26673789. DOI: 10.1016/j.rcradv.2025.200289.

[178] C. S. Poon et al. "Total Recycling of Concrete Waste Using Accelerated Carbonation: A Review". In: *Cement and Concrete Research* 173 (2023), p. 107284. ISSN: 00088846. DOI: 10.1016/j.cemconres.2023.107284.

[179] T. C. Powers and T. L. Brownyard. "Studies of the Physical Properties of Hardened Portland Cement Paste". In: *ACI Journal Proceedings* 43.9 (1946), pp. 249–336. ISSN: 0002-8061. DOI: 10.14359/15301.

[180] R. Prajapati, R. Gettu, and S. Singh. "Thermomechanical Beneficiation of Recycled Concrete Aggregates (RCA)". In: *Construction and Building Materials* 310 (2021), p. 125200. ISSN: 09500618. DOI: 10.1016/j.conbuildmat.2021.125200.

[181] Z. Prošek et al. "Recovery of Residual Anhydrous Clinker in Finely Ground Recycled Concrete". In: *Resources, Conservation and Recycling* 155 (2020), p. 104640. ISSN: 09213449. DOI: 10.1016/j.resconrec.2019.104640.

[182] Y. Pu et al. "Accelerated Carbonation Technology for Enhanced Treatment of Recycled Concrete Aggregates: A State-of-the-Art Review". In: *Construction and Building Materials* 282 (2021), p. 122671. ISSN: 09500618. DOI: 10.1016/j.conbuildmat.2021.122671.

[183] M. Purton. *Cement Is a Big Problem for the Environment. Here's How to Make It More Sustainable*. https://www.weforum.org/stories/2024/09/cement-production-sustainable-concrete-co2-emissions/. 2024. (Visited on 06/18/2025).

[184] D. Qian et al. "A Novel Development of Green Ultra-High Performance Concrete (UHPC) Based on Appropriate Application of Recycled Cementitious Material". In: *Journal of Cleaner Production* 261 (2020), p. 121231. ISSN: 0959-6526. DOI: 10.1016/j.jclepro.2020.121231.

[185] M. Rajczakowska et al. "Recycled and Mechanically Activated Concrete Fines as a Complete Substitute for Portland Cement - Feasibility and Life Cycle Assessment". In: *Case Studies in Construction Materials* 22 (2025), e04798. ISSN: 22145095. DOI: 10.1016/j.cscm.2025.e04798.

[186] J. V. M. Raman and V. Ramasamy. "Various Treatment Techniques Involved to Enhance the Recycled Coarse Aggregate in Concrete: A Review". In: *Materials Today: Proceedings* 45 (2021), pp. 6356–6363. ISSN: 22147853. DOI: 10.1016/j.matpr.2020.10.935.

[187] S. Real et al. "Influence of the Treatment Temperature on the Microstructure and Hydration Behavior of Thermoactivated Recycled Cement". In: *Materials* 13.18 (2020), p. 3937. ISSN: 1996-1944. DOI: 10.3390/ma13183937.

[188] S. Real et al. "Life Cycle Assessment of Thermoactivated Recycled Cement Production". In: *Materials* 15.19 (2022). ISSN: 1996-1944. DOI: 10.3390/ma15196766.

[189] S. Real et al. "Mechanical Characterisation and Shrinkage of Thermoactivated Recycled Cement Concrete". In: *Applied Sciences* 11.6 (2021), p. 2454. ISSN: 2076-3417. DOI: 10.3390/app11062454.

[190] I. G. Richardson. "The Nature of the Hydration Products in Hardened Cement Pastes". In: *Cement and Concrete Composites* 22.2 (2000), pp. 97–113. ISSN: 0958-9465. DOI: 10.1016/S0958-9465(99)00036-0.

[191] R. A. Robayo-Salazar and R. Mejía De Gutiérrez. "Natural Volcanic Pozzolans as an Available Raw Material for Alkali-Activated Materials in the Foreseeable Future: A Review". In: *Construction and Building Materials* 189 (2018), pp. 109–118. ISSN: 09500618. DOI: 10.1016/j.conbuildmat.2018.08.174.

[192] D. Ruth Bola Oliveira et al. “Concrete Powder Waste as a Substitution for Portland Cement for Environment-Friendly Cement Production”. In: *Construction and Building Materials* 397 (2023), p. 132382. ISSN: 09500618. DOI: 10.1016/j.conbuildmat.2023.132382.

[193] N. Saca et al. “An Investigation of the Physic-Mechanical Properties of the Expanded Perlite Mortars with Thermal-Activated Concrete Waste and Microencapsulated Paraffin”. In: *Heliyon* 10.21 (2024), e39720. ISSN: 24058440. DOI: 10.1016/j.heliyon.2024.e39720.

[194] E. K. Sadik et al. “Valorization of Industrial Wastes as Promising Alternatives in Eco-Friendly LC3”. In: *Construction and Building Materials* 500 (2025), p. 144129. ISSN: 09500618. DOI: 10.1016/j.conbuildmat.2025.144129.

[195] G. Santha Kumar and A. K. Minocha. “Studies on Thermo-Chemical Treatment of Recycled Concrete Fine Aggregates for Use in Concrete”. In: *Journal of Material Cycles and Waste Management* 20.1 (2018), pp. 469–480. ISSN: 1438-4957. DOI: 10.1007/s10163-017-0604-6.

[196] J. Scheidt. “Einfluss der Wasseraufnahme von rezyklierten Gesteinskörnungen auf den Wasserzementwert von R-Beton: Ergebnisse einer Dissertation”. In: *beton* 70.4 (2020), pp. 126–132.

[197] M. Schepper et al. “Life Cycle Assessment of Completely Recyclable Concrete”. In: *Materials* 7.8 (2014), pp. 6010–6027. ISSN: 1996-1944. DOI: 10.3390/ma7086010.

[198] M. Schepper et al. “The Hydration of Cement Regenerated from Completely Recyclable Concrete”. In: *Construction and Building Materials* 60 (2014), pp. 33–41. ISSN: 09500618. DOI: 10.1016/j.conbuildmat.2014.02.067.

[199] U. Schneider. *Verhalten von Beton bei hohen Temperaturen*. Vol. 337. DAfStb-Heft. Berlin: Wilhelm Ernst und Sohn, 1982.

[200] J. Schoon et al. “Fines Extracted from Recycled Concrete as Alternative Raw Material for Portland Cement Clinker Production”. In: *Cement and Concrete Composites* 58 (2015), pp. 70–80. ISSN: 09589465. DOI: 10.1016/j.cemconcomp.2015.01.003.

[201] K. L. Scrivener, A. K. Crumbie, and P. Laugesen. “The Interfacial Transition Zone (ITZ) Between Cement Paste and Aggregate in Concrete”. In: *Interface Science* 12.4 (2004), pp. 411–421. ISSN: 0927-7056, 1573-2746. DOI: 10.1023/B:INTS.0000042339.92990.4c.

[202] K. L. Scrivener, P. Juilland, and P. J. Monteiro. “Advances in Understanding Hydration of Portland Cement”. In: *Cement and Concrete Research* 78 (2015), pp. 38–56. ISSN: 00088846. DOI: 10.1016/j.cemconres.2015.05.025.

[203] G. Semugaza et al. “Reactivation of Hydrated Cement Powder by Thermal Treatment for Partial Replacement of Ordinary Portland Cement”. In: *Materials and Structures* 56.3 (2023). ISSN: 1871-6873. DOI: 10.1617/s11527-023-02133-9.

[204] R. Serpell and M. Lopez. “Properties of Mortars Produced with Reactivated Cementitious Materials”. In: *Cement and Concrete Composites* 64 (2015), pp. 16–26. ISSN: 0958-9465. DOI: 10.1016/j.cemconcomp.2015.08.003.

[205] R. Serpell and M. Lopez. "Reactivated Cementitious Materials from Hydrated Cement Paste Wastes". In: *Cement and Concrete Composites* 39 (2013), pp. 104–114. ISSN: 09589465. DOI: 10.1016/j.cemconcomp.2013.03.020.

[206] R. Serpell and F. Zunino. "Recycling of Hydrated Cement Pastes by Synthesis of α'H-C2S". In: *Cement and Concrete Research* 100 (2017), pp. 398–412. ISSN: 00088846. DOI: 10.1016/j.cemconres.2017.08.001.

[207] W. M. Shaban et al. "Quality Improvement Techniques for Recycled Concrete Aggregate: A Review". In: *Journal of Advanced Concrete Technology* 17 (2019), pp. 151–167. ISSN: 1346-8014. DOI: 10.3151/jact.17.151.

[208] I. H. Shah et al. "Cement Substitution with Secondary Materials Can Reduce Annual Global CO2 Emissions by up to 1.3 Gigatons". In: *Nature Communications* 13.1 (2022), p. 5758. ISSN: 2041-1723. DOI: 10.1038/s41467-022-33289-7.

[209] P. Shen et al. "Phase Assemblance Evolution during Wet Carbonation of Recycled Concrete Fines". In: *Cement and Concrete Research* 154 (2022), p. 106733. ISSN: 00088846. DOI: 10.1016/j.cemconres.2022.106733.

[210] P. Shen et al. "Synthesis of Amorphous Nano-Silica from Recycled Concrete Fines by Two-Step Wet Carbonation". In: *Cement and Concrete Research* 147 (2021), p. 106526. ISSN: 00088846. DOI: 10.1016/j.cemconres.2021.106526.

[211] C. Shi et al. "Performance Enhancement of Recycled Concrete Aggregate – A Review". In: *Journal of Cleaner Production* 112 (2016), pp. 466–472. ISSN: 09596526. DOI: 10.1016/j.jclepro.2015.08.057.

[212] C. Shi et al. "Performance of Mortar Prepared with Recycled Concrete Aggregate Enhanced by CO2 and Pozzolan Slurry". In: *Cement and Concrete Composites* 86 (2018), pp. 130–138. ISSN: 09589465. DOI: 10.1016/j.cemconcomp.2017.10.013.

[213] Z. Shui et al. "Cementitious Characteristics of Hydrated Cement Paste Subjected to Various Dehydration Temperatures". In: *Construction and Building Materials* 23.1 (2009), pp. 531–537. ISSN: 09500618. DOI: 10.1016/j.conbuildmat.2007.10.016.

[214] Z. Shui et al. "Rehydration Reactivity of Recycled Mortar from Concrete Waste Experienced to Thermal Treatment". In: *Construction and Building Materials* 22.8 (2008), pp. 1723–1729. ISSN: 09500618. DOI: 10.1016/j.conbuildmat.2007.05.012.

[215] R. V. Silva, J. Brito, and R. K. Dhir. "Comparative Analysis of Existing Prediction Models on the Creep Behaviour of Recycled Aggregate Concrete". In: *Engineering Structures* 100 (2015), pp. 31–42. ISSN: 01410296. DOI: 10.1016/j.engstruct.2015.06.004.

[216] R. V. Silva, J. Brito, and R. K. Dhir. "Fresh-State Performance of Recycled Aggregate Concrete: A Review". In: *Construction and Building Materials* 178 (2018), pp. 19–31. ISSN: 09500618. DOI: 10.1016/j.conbuildmat.2018.05.149.

[217] R. V. Silva, J. Brito, and R. K. Dhir. "Prediction of the Shrinkage Behavior of Recycled Aggregate Concrete: A Review". In: *Construction and Building Materials* 77 (2015), pp. 327–339. ISSN: 09500618. DOI: 10.1016/j.conbuildmat.2014.12.102.

[218] R. V. Silva, J. Brito, and R. K. Dhir. "Properties and Composition of Recycled Aggregates from Construction and Demolition Waste Suitable for Concrete Production". In: *Construction and Building Materials* 65 (2014), pp. 201–217. ISSN: 09500618. DOI: 10.1016/j.conbuildmat.2014.04.117.

[219] R. V. Silva, J. Brito, and R. K. Dhir. "Tensile Strength Behaviour of Recycled Aggregate Concrete". In: *Construction and Building Materials* 83 (2015), pp. 108–118. ISSN: 09500618. DOI: 10.1016/j.conbuildmat.2015.03.034.

[220] R. V. Silva, J. Brito, and R. K. Dhir. "The Influence of the Use of Recycled Aggregates on the Compressive Strength of Concrete: A Review". In: *European Journal of Environmental and Civil Engineering* 19.7 (2015), pp. 825–849. ISSN: 1964-8189. DOI: 10.1080/19648189.2014.974831.

[221] R. V. Silva et al. "Carbonation Behaviour of Recycled Aggregate Concrete". In: *Cement and Concrete Composites* 62 (2015), pp. 22–32. ISSN: 09589465. DOI: 10.1016/j.cemconcomp.2015.04.017.

[222] R. V. Silva, J. Brito, and R. K. Dhir. "Establishing a Relationship between Modulus of Elasticity and Compressive Strength of Recycled Aggregate Concrete". In: *Journal of Cleaner Production* 112 (2016), pp. 2171–2186. ISSN: 09596526. DOI: 10.1016/j.jclepro.2015.10.064.

[223] R. V. Silva et al. "Prediction of Chloride Ion Penetration of Recycled Aggregate Concrete". In: *Materials Research* 18.2 (2015), pp. 427–440. DOI: 10.1590/1516-1439.000214.

[224] R. Snellings, P. Suraneni, and J. Skibsted. "Future and Emerging Supplementary Cementitious Materials". In: *Cement and Concrete Research* 171 (2023), p. 107199. ISSN: 00088846. DOI: 10.1016/j.cemconres.2023.107199.

[225] L. N. Sousa et al. "Improving the Reactivity of Industrial Recycled Concrete Fines: Exploring Mechanical and Hydrothermal Activation". In: *Construction and Building Materials* 442 (2024), p. 137594. ISSN: 09500618. DOI: 10.1016/j.conbuildmat.2024.137594.

[226] V. Sousa and J. A. Bogas. "Comparison of Energy Consumption and Carbon Emissions from Clinker and Recycled Cement Production". In: *Journal of Cleaner Production* 306 (2021), p. 127277. ISSN: 09596526. DOI: 10.1016/j.jclepro.2021.127277.

[227] V. Sousa et al. "Industrial Production of Recycled Cement: Energy Consumption and Carbon Dioxide Emission Estimation". In: *Environmental Science and Pollution Research* 30.4 (2022), pp. 8778–8789. ISSN: 1614-7499. DOI: 10.1007/s11356-022-20887-7.

[228] V. Sousa et al. "Recycled Cement Production Energy Consumption Optimization". In: *Sustainable Chemistry and Pharmacy* 32 (2023), p. 101010. ISSN: 23525541. DOI: 10.1016/j.scp.2023.101010.

[229] V. Spaeth and A. Djerbi Tegguer. "Improvement of Recycled Concrete Aggregate Properties by Polymer Treatments". In: *International Journal of Sustainable Built Environment* 2 (2013), pp. 143–152. ISSN: 22126090. DOI: 10.1016/j.ijsbe.2014.03.003.

[230] R. Springenschmid. *Betontechnologie für die Praxis*. 2., aktualisierte und erweiterte Auflage. Bauwerk. Berlin; Wien; Zürich: Beuth Verlag GmbH, 2018. ISBN: 978-3-410-24466-0.

[231] Statistisches Bundesamt. *Abfallbilanz (Abfallaufkommen /-Verbleib, Abfallintensität, Abfallaufkommen Nach Wirtschaftszweigen) - 2023*. Tech. rep. EVAS Number 32171. Wiesbaden, 2025.

[232] P. Stemmermann et al. "Recycling Belite Cement Clinker from Post-Demolition Autoclaved Aerated Concrete – Assessing a New Process". In: *Resources, Conservation and Recycling* 203 (2024), p. 107404. ISSN: 09213449. DOI: 10.1016/j.resconrec.2023.107404.

[233] P. Stemmermann et al. "Belite Cement Clinker from Autoclaved Aerated Concrete Waste – A Contribution towards CO2-reduced Circular Building Materials". In: *ce/papers* 5.5 (2022), pp. 17–26. ISSN: 2509-7075. DOI: 10.1002/cepa.1879.

[234] P. Stemmermann et al. "Belite Cement Clinker from Autoclaved Aerated Concrete Waste Fines with High Sulfate Content". In: *ce/papers* 6.2 (2023), pp. 203–208. ISSN: 2509-7075. DOI: 10.1002/cepa.2096.

[235] Y. Sui et al. "Study on Properties of Waste Concrete Powder by Thermal Treatment and Application in Mortar". In: *Applied Sciences* 10.3 (2020), p. 998. ISSN: 2076-3417. DOI: 10.3390/app10030998.

[236] C. Sun et al. "Compound Utilization of Construction and Industrial Waste as Cementitious Recycled Powder in Mortar". In: *Resources, Conservation and Recycling* 170 (2021), p. 105561. ISSN: 09213449. DOI: 10.1016/j.resconrec.2021.105561.

[237] H. Sun et al. "Developing Sustainable Engineered Cementitious Composites with Carbonated Recycled Concrete Fines: Feasibility and Engineering Properties". In: *Cement and Concrete Composites* 166 (2026), p. 106378. ISSN: 09589465. DOI: 10.1016/j.cemconcomp.2025.106378.

[238] E. Tajuelo Rodriguez et al. "Thermal Stability of C-S-H Phases and Applicability of Richardson and Groves' and Richardson C-(A)-S-H(I) Models to Synthetic C-S-H". In: *Cement and Concrete Research* 93 (2017), pp. 45–56. ISSN: 00088846. DOI: 10.1016/j.cemconres.2016.12.005.

[239] V. W. Tam et al. "Utilising CO2 Technologies for Recycled Aggregate Concrete: A Critical Review". In: *Construction and Building Materials* 250 (2020), p. 118903. ISSN: 09500618. DOI: 10.1016/j.conbuildmat.2020.118903.

[240] X. Tan et al. "Effects of Particle Shape and Packing Density on the Mechanical Performance of Recycled Aggregates for Construction Purposes". In: *Buildings* 13.9 (2023), p. 2153. ISSN: 2075-5309. DOI: 10.3390/buildings13092153.

[241] S. Tao et al. "Activation of Recycled Concrete Powder with High Content of Inert Phase Based on Triethanolamine-Incorporated Wet Grinding Technique". In: *Construction and Building Materials* 479 (2025), p. 141505. ISSN: 09500618. DOI: 10.1016/j.conbuildmat.2025.141505.

[242] Y. Tian et al. “Quantitative Influence of Conditions on CO2-activation Quality in Recycled Cement Paste Powder: Content, Morphology and Chemical Reactivity of Target Product and CO2 Sequestration Capacity”. In: *Cement and Concrete Composites* 162 (2025), p. 106120. ISSN: 09589465. DOI: 10.1016/j.cemconcomp.2025.106120.

[243] A. Tokareva, S. Kaassamani, and D. Waldmann. “Fine Demolition Wastes as Supplementary Cementitious Materials for CO2 Reduced Cement Production”. In: *Construction and Building Materials* 392 (2023), p. 131991. ISSN: 0950-0618. DOI: 10.1016/j.conbuildmat.2023.131991.

[244] A. Tokareva and D. Waldmann. “Durability of Cement Mortars Containing Fine Demolition Wastes as Supplementary Cementitious Materials”. In: *Construction and Building Materials* 477 (2025), p. 141316. ISSN: 09500618. DOI: 10.1016/j.conbuildmat.2025.141316.

[245] I. Tole et al. “Enhancement of the Pozzolanic Activity of Natural Clays by Mechanochemical Activation”. In: *Construction and Building Materials* 352 (2022), p. 128739. ISSN: 0950-0618. DOI: 10.1016/j.conbuildmat.2022.128739.

[246] P. Vashistha et al. “Effect of Thermo-Mechanical Activation of Waste Concrete Powder (WCP) on the Characteristics of Cement Mixtures”. In: *Construction and Building Materials* 362 (2023), p. 129713. ISSN: 09500618. DOI: 10.1016/j.conbuildmat.2022.129713.

[247] E. Vázquez et al. “Improvement of the Durability of Concrete with Recycled Aggregates in Chloride Exposed Environment”. In: *Construction and Building Materials* 67 (2014), pp. 61–67. ISSN: 09500618. DOI: 10.1016/j.conbuildmat.2013.11.028.

[248] Verein Deutscher Zementwerke e.V., ed. *Dekarbonisierung von Zement und Beton – Minderungspfade und Handlungsstrategien*. Düsseldorf, 2020.

[249] Verein Deutscher Zementwerke e.V., ed. *Ressourcen der Zukunft für Zement und Beton – Potenziale und Handlungsstrategien*. Düsseldorf, 2022.

[250] Verein Deutscher Zementwerke e.V., ed. *Umweltdaten der deutschen Zementindustrie 2016*. Düsseldorf, 2017.

[251] Verein Deutscher Zementwerke e.V., ed. *Umweltdaten der deutschen Zementindustrie 2023*. Düsseldorf, 2024.

[252] Verein Deutscher Zementwerke e.V., ed. *Zement Taschenbuch*. 51. Ausgabe. Düsseldorf: Verlag Bau+Technik, 2008. ISBN: 978-3-7640-0499-6.

[253] Verein Deutscher Zementwerke e.V., ed. *Zementindustrie im Überblick 2013*. Berlin, 2013.

[254] Verein Deutscher Zementwerke e.V., ed. *Zementindustrie im Überblick 2017/2018*. Berlin, 2017.

[255] Verein Deutscher Zementwerke e.V., ed. *Zementindustrie im Überblick 2020/2021*. Berlin, 2020.

[256] Verein Deutscher Zementwerke e.V., ed. *Zementindustrie im Überblick 2023/2024*. Berlin, 2023.

[257] K. P. Verian, W. Ashraf, and Y. Cao. "Properties of Recycled Concrete Aggregate and Their Influence in New Concrete Production". In: *Resources, Conservation and Recycling* 133 (2018), pp. 30–49. ISSN: 09213449. DOI: 10.1016/j.resconrec.2018.02.005.

[258] M. Vyšvařil et al. "Physico-Mechanical and Microstructural Properties of Rehydrated Blended Cement Pastes". In: *Construction and Building Materials* 54 (2014), pp. 413–420. ISSN: 09500618. DOI: 10.1016/j.conbuildmat.2013.12.021.

[259] H. Wang et al. "A Dehydration Kinetic Model of Calcium Silicate Hydrates at High Temperature". In: *Structural Concrete* 24.2 (2023), pp. 1997–2008. ISSN: 14644177. DOI: 10.1002/suco.202200038.

[260] H. Wang, X. Liu, and Z. Zhang. "Pozzolanic Activity Evaluation Methods of Solid Waste: A Review". In: *Journal of Cleaner Production* 402 (2023), p. 136783. ISSN: 09596526. DOI: 10.1016/j.jclepro.2023.136783.

[261] J. Wang et al. "Experimental Study on Chloride Ion Permeability of Carbonated Recycled Aggregate Concrete Considering the Effects of Multiple Factors". In: *Construction and Building Materials* 451 (2024), p. 138835. ISSN: 09500618. DOI: 10.1016/j.conbuildmat.2024.138835.

[262] J. Wang et al. "Microbial Carbonate Precipitation for the Improvement of Quality of Recycled Aggregates". In: *Journal of Cleaner Production* 156 (2017), pp. 355–366. ISSN: 09596526. DOI: 10.1016/j.jclepro.2017.04.051.

[263] J. Wang, L. Lacarrière, and A. Sellier. "Multicomponent Modelling of Cement Paste Dehydration under Different Heating Rates". In: *Materials and Structures* 52.1 (2019), p. 6. ISSN: 1359-5997, 1871-6873. DOI: 10.1617/s11527-018-1306-9.

[264] J. Wang, M. Mu, and Y. Liu. "Recycled Cement". In: *Construction and Building Materials* 190 (2018), pp. 1124–1132. ISSN: 09500618. DOI: 10.1016/j.conbuildmat.2018.09.181.

[265] J. Wang et al. "Investigations on Factors Influencing Physical Properties of Recycled Cement and the Related Carbon Emissions and Energy Consumptions". In: *Journal of Cleaner Production* 414 (2023), p. 137715. ISSN: 09596526. DOI: 10.1016/j.jclepro.2023.137715.

[266] R. Wang, N. Yu, and Y. Li. "Methods for Improving the Microstructure of Recycled Concrete Aggregate: A Review". In: *Construction and Building Materials* 242 (2020), p. 118164. ISSN: 09500618. DOI: 10.1016/j.conbuildmat.2020.118164.

[267] X. Wang and C. Song. "Carbon Capture From Flue Gas and the Atmosphere: A Perspective". In: *Frontiers in Energy Research* 8 (2020). DOI: 10.3389/fenrg.2020.560849.

[268] Z. Wang and Y.-F. Wu. "Improvement of Mechanical Properties of High-Volume Recycled Powder Concrete by a Novel Compression Casting Method". In: *Construction and Building Materials* 458 (2025), p. 139485. ISSN: 09500618. DOI: 10.1016/j.conbuildmat.2024.139485.

[269] M. Wei et al. “Experimental Investigation on Freeze–Thaw Resistance of Thermally Activated Recycled Fine Powder Concrete”. In: *Construction and Building Materials* 457 (2024), p. 139378. ISSN: 09500618. DOI: 10.1016/j.conbuildmat.2024.139378.

[270] M. Wei et al. “Mechanical Properties and Microstructures of Thermally Activated Ultrafine Recycled Fine Powder Cementitious Materials”. In: *Construction and Building Materials* 475 (2025), p. 141195. ISSN: 09500618. DOI: 10.1016/j.conbuildmat.2025.141195.

[271] T. Wei et al. “A Comparative Study of Dry and Wet Carbonation Treatment on the Recycled Mortar Powder: Material Characteristics, Hydration Kinetics and Sustainability”. In: *Construction and Building Materials* 490 (2025), p. 142505. ISSN: 0950-0618. DOI: 10.1016/j.conbuildmat.2025.142505.

[272] H. Wu, C. Wang, and Z. Ma. “Drying Shrinkage, Mechanical and Transport Properties of Sustainable Mortar with Both Recycled Aggregate and Powder from Concrete Waste”. In: *Journal of Building Engineering* 49 (2022), p. 104048. ISSN: 23527102. DOI: 10.1016/j.jobe.2022.104048.

[273] H. Wu, D. Yang, and Z. Ma. “Micro-Structure, Mechanical and Transport Properties of Cementitious Materials with High-Volume Waste Concrete Powder and Thermal Modification”. In: *Construction and Building Materials* 313 (2021), p. 125477. ISSN: 09500618. DOI: 10.1016/j.conbuildmat.2021.125477.

[274] H. Wu et al. “Utilizing Heat Treatment for Making Low-Quality Recycled Aggregate into Enhanced Recycled Aggregate, Recycled Cement and Their Fully Recycled Concrete”. In: *Construction and Building Materials* 394 (2023), p. 132126. ISSN: 09500618. DOI: 10.1016/j.conbuildmat.2023.132126.

[275] X. Xi et al. “Influence of Water Glass Modulus and Alkali Content on the Properties of Alkali-Activated Thermally Activated Recycled Cement”. In: *Construction and Building Materials* 452 (2024), p. 138867. ISSN: 09500618. DOI: 10.1016/j.conbuildmat.2024.138867.

[276] X. Xi et al. “Mechanical Properties and Hydration Mechanism of Nano-Silica Modified Alkali-Activated Thermally Activated Recycled Cement”. In: *Journal of Building Engineering* 98 (2024), p. 110998. ISSN: 2352-7102. DOI: 10.1016/j.jobe.2024.110998.

[277] X. Xi et al. “Study on the Hydration Characteristics, Mechanical Properties, and Microstructure of Thermally Activated Low-Carbon Recycled Cement”. In: *Construction and Building Materials* 447 (2024), p. 138042. ISSN: 09500618. DOI: 10.1016/j.conbuildmat.2024.138042.

[278] L. Xu et al. “Insight into Multi-Ionic Adsorption Behavior of Recycled Cement Paste Exposed to Chloride Solutions”. In: *Construction and Building Materials* 426 (2024), p. 136142. ISSN: 09500618. DOI: 10.1016/j.conbuildmat.2024.136142.

[279] L. Xu et al. “Investigations on Micro-Mechanical Properties of the ITZs between Recycled Aggregates and Recycled Cement Paste”. In: *Construction and Building Materials* 450 (2024), p. 138640. ISSN: 09500618. DOI: 10.1016/j.conbuildmat.2024.138640.

[280] L. Xu et al. “Investigations on the Rehydration of Recycled Blended SCMs Cement”. In: *Cement and Concrete Research* 163 (2023), p. 107036. ISSN: 00088846. DOI: 10.1016/j.cemconres.2022.107036.

[281] L. Xu et al. “New Insights on Dehydration at Elevated Temperature and Rehydration of GGBS Blended Cement”. In: *Cement and Concrete Composites* 139 (2023), p. 105068. ISSN: 09589465. DOI: 10.1016/j.cemconcomp.2023.105068.

[282] L. Xu et al. “Physical Performance, Durability, and Carbon Emissions of Recycled Cement Concrete and Fully Recycled Concrete”. In: *Construction and Building Materials* 447 (2024), p. 138128. ISSN: 0950-0618. DOI: 10.1016/j.conbuildmat.2024.138128.

[283] D. X. Xuan and Z. H. Shui. “Rehydration Activity of Hydrated Cement Paste Exposed to High Temperature”. In: *Fire and Materials* 35.7 (2011), pp. 481–490. ISSN: 03080501. DOI: 10.1002/fam.1067.

[284] D. Xuan, B. Zhan, and C. S. Poon. “Assessment of Mechanical Properties of Concrete Incorporating Carbonated Recycled Concrete Aggregates”. In: *Cement and Concrete Composites* 65 (2016), pp. 67–74. ISSN: 09589465. DOI: 10.1016/j.cemconcomp.2015.10.018.

[285] K. Yang et al. “Unravelling Determining Role of Recycled Powder Adsorbing Polycarboxylate Ethers in Recycled Cement Paste Dispersion”. In: *Construction and Building Materials* 485 (2025), p. 141535. ISSN: 09500618. DOI: 10.1016/j.conbuildmat.2025.141535.

[286] Y. Yang et al. “Study on Hydration Characteristics and Mechanism of Recycled Powder-Cement Binary and Multivariate Systems”. In: *Construction and Building Materials* 420 (2024), p. 135646. ISSN: 09500618. DOI: 10.1016/j.conbuildmat.2024.135646.

[287] Y. Yao et al. “Deterioration Mechanism Understanding of Recycled Powder Concrete under Coupled Sulfate Attack and Freeze–Thaw Cycles”. In: *Construction and Building Materials* 388 (2023), p. 131718. ISSN: 09500618. DOI: 10.1016/j.conbuildmat.2023.131718.

[288] T. Ye et al. “Quantifying Reactivity of Secondary Materials as Cement Substitutes: Modifications to Strength Activity Index Methodology”. In: *Cement and Concrete Research* 199 (2026), p. 108055. ISSN: 00088846. DOI: 10.1016/j.cemconres.2025.108055.

[289] A. Yonis et al. “Novel Activation Method of Waste Concrete Powder for Sustainable Clinker-Free Binder”. In: *Cement and Concrete Composites* 151 (2024), p. 105600. ISSN: 09589465. DOI: 10.1016/j.cemconcomp.2024.105600.

[290] A. Younsi et al. “Performance-Based Design and Carbonation of Concrete with High Fly Ash Content”. In: *Cement and Concrete Composites* 33.10 (2011), pp. 993–1000. ISSN: 09589465. DOI: 10.1016/j.cemconcomp.2011.07.005.

[291] R. Yu and Z. Shui. “Efficient Reuse of the Recycled Construction Waste Cementitious Materials”. In: *Journal of Cleaner Production* 78 (2014), pp. 202–207. ISSN: 09596526. DOI: 10.1016/j.jclepro.2014.05.003.

[292] R. Yu and Z. Shui. "Influence of Agglomeration of a Recycled Cement Additive on the Hydration and Microstructure Development of Cement Based Materials". In: *Construction and Building Materials* 49 (2013), pp. 841–851. ISSN: 0950-0618. DOI: 10.1016/j.conbuildmat.2013.09.004.

[293] M. Zajac et al. "CO2 Mineralization of Demolished Concrete Wastes into a Supplementary Cementitious Material – a New CCU Approach for the Cement Industry". In: *RILEM Technical Letters* 6 (2021), pp. 53–60. DOI: 10.21809/rilemtechlett.2021.141.

[294] M. Zajac et al. "Composite Cements with Aqueous and Semi-Dry Carbonated Recycled Concrete Pastes". In: *Construction and Building Materials* 407 (2023), p. 133362. ISSN: 09500618. DOI: 10.1016/j.conbuildmat.2023.133362.

[295] M. Zajac et al. "Effect of Carbonated Cement Paste on Composite Cement Hydration and Performance". In: *Cement and Concrete Research* 134 (2020), p. 106090. ISSN: 00088846. DOI: 10.1016/j.cemconres.2020.106090.

[296] M. Zajac et al. "Effect of Temperature on Carbon Dioxide Mineralisation in Recycled Cement Paste". In: *Advances in Cement Research* 35.9 (2023), pp. 384–395. ISSN: 0951-7197. DOI: 10.1680/jadcr.22.00129.

[297] M. Zajac et al. "Enforced Carbonation of Cementitious Materials". In: *Cement and Concrete Research* 174 (2023), p. 107285. ISSN: 00088846. DOI: 10.1016/j.cemconres.2023.107285.

[298] M. Zajac et al. "High Early Pozzolanic Reactivity of Alumina-Silica Gel: A Study of the Hydration of Composite Cements with Carbonated Recycled Concrete Paste". In: *Cement and Concrete Research* 175 (2024), p. 107345. ISSN: 00088846. DOI: 10.1016/j.cemconres.2023.107345.

[299] M. Zanovello et al. "Strength-Porosity Correlation and Environmental Analysis of Recycled Portland Cement". In: *Resources, Conservation and Recycling* 190 (2023), p. 106763. ISSN: 09213449. DOI: 10.1016/j.resconrec.2022.106763.

[300] J. Zelic, L. Ugrina, and D. Jozic. "Application of Thermal Methods in the Chemistry of Cement: Kinetic Analysis of Portlandite from Non-Isothermal Thermogravimetric Data". In: *The First International Proficiency Testing Conference*. Sinaia, Romania, 2007, pp. 420–429.

[301] W. Zeng et al. "Using Microbial Carbonate Precipitation to Improve the Properties of Recycled Aggregate". In: *Construction and Building Materials* 228 (2019), p. 116743. ISSN: 09500618. DOI: 10.1016/j.conbuildmat.2019.116743.

[302] W.-Q. Zhai et al. "Thermal-Activated Recycled Cement Powder Synergized with Fly Ash as Supplementary Cementitious in Portland Cement: Strength, Microstructure and Environmental Benefits". In: *Construction and Building Materials* 474 (2025), p. 141018. ISSN: 09500618. DOI: 10.1016/j.conbuildmat.2025.141018.

[303] D. Zhang et al. “Comparison of Mechanical, Chemical, and Thermal Activation Methods on the Utilisation of Recycled Concrete Powder from Construction and Demolition Waste”. In: *Journal of Building Engineering* 61 (2022), p. 105295. ISSN: 23527102. DOI: 10.1016/j.jobe.2022.105295.

[304] H. Zhang et al. “Analysis of Two Processing Techniques Applied on Powders from Recycling of Clay Bricks and Concrete, in Terms of Efficiency, Energy Consumption, and Cost”. In: *Construction and Building Materials* 385 (2023), p. 131517. ISSN: 09500618. DOI: 10.1016/j.conbuildmat.2023.131517.

[305] K. Zhang et al. “Effects of Different Fine Aggregates as Sand Replacements on the Carbonation Properties of Recycled Aggregate Concrete”. In: *Construction and Building Materials* 468 (2025), p. 140416. ISSN: 0950-0618. DOI: 10.1016/j.conbuildmat.2025.140416.

[306] L. Zhang et al. “Effect of Retarders on the Early Hydration and Mechanical Properties of Reactivated Cementious Material”. In: *Construction and Building Materials* 212 (2019), pp. 192–201. ISSN: 09500618. DOI: 10.1016/j.conbuildmat.2019.03.323.

[307] L. Zhang et al. “Modification and Enhancement of Mechanical Properties of Dehydrated Cement Paste Using Ground Granulated Blast-Furnace Slag”. In: *Construction and Building Materials* 164 (2018), pp. 525–534. ISSN: 09500618. DOI: 10.1016/j.conbuildmat.2017.12.232.

[308] L. Zhang et al. “Effect of Borax on Early Hydration and Rheological Properties of Reactivated Cementitious Material”. In: *Advances in Cement Research* 31.5 (2019), pp. 235–242. ISSN: 0951-7197. DOI: 10.1680/jadcr.18.00051.

[309] S. Zhang et al. “Effect of Roughness on Bonding Performance between Portland Cement Concrete and Magnesium Phosphate Cement Concrete”. In: *Construction and Building Materials* 323 (2022), p. 126585. ISSN: 09500618. DOI: 10.1016/j.conbuildmat.2022.126585.

[310] Z. Zhang et al. “Mechanical Behavior of Sustainable Engineered Cementitious Composites with Construction Waste Powder as Binder and Sand Replacement”. In: *Construction and Building Materials* 404 (2023), p. 133185. ISSN: 09500618. DOI: 10.1016/j.conbuildmat.2023.133185.

[311] Y. Zhao et al. “Highly Reactive Carbonated Recycled Concrete Fines Prepared via Mechanochemical Carbonation: Influence on the Early Performance of Cement Composites”. In: *Cement and Concrete Composites* 152 (2024), p. 105636. ISSN: 09589465. DOI: 10.1016/j.cemconcomp.2024.105636.

[312] Y. Zhao et al. “Mechanochemical Carbonation of Recycled Concrete Fines: Towards a High-Efficiency Recycling and CO2 Sequestration”. In: *Cement and Concrete Research* 185 (2024), p. 107654. ISSN: 00088846. DOI: 10.1016/j.cemconres.2024.107654.

[313] Q. Zhou and F. P. Glasser. “Thermal Stability and Decomposition Mechanisms of Ettringite at <120°C”. In: *Cement and Concrete Research* 31.9 (2001), pp. 1333–1339. ISSN: 0008-8846. DOI: 10.1016/S0008-8846(01)00558-0.

[314] Q. Zhou, E. E. Lachowski, and F. P. Glasser. "Metaettringite, a Decomposition Product of Ettringite". In: *Cement and Concrete Research* 34.4 (2004), pp. 703–710. ISSN: 0008-8846. DOI: 10.1016/j.cemconres.2003.10.027.

[315] Q. Zhou, W. Wang, and T. Noguchi. "Recyclable Calcium Carbonate-Based Concrete: Utilizing Calcium Carbonate to Bond Recycled Concrete Fines through an in-Situ Heterogeneous Dual-Precipitation Approach". In: *Cement and Concrete Research* 186 (2024), p. 107679. ISSN: 00088846. DOI: 10.1016/j.cemconres.2024.107679.

[316] L. Zhu et al. "Binary Solid Wastes Derived Clinker: Raw Feed System Design Validation and Thermodynamic Simulation Investigation". In: *Cement and Concrete Research* 183 (2024), p. 107597. ISSN: 00088846. DOI: 10.1016/j.cemconres.2024.107597.

[317] S. Zhutovsky and A. Shishkin. "Recycling of Hydrated Portland Cement Paste into New Clinker". In: *Construction and Building Materials* 280 (2021), p. 122510. ISSN: 09500618. DOI: 10.1016/j.conbuildmat.2021.122510.

Paper P1

Influence of Thermally Activated Industrial Concrete Fines of Different Origin on Mortar Strength Development

Jan P. Höffgen
Sebastian Bruckschlögl
Bernhard Wetz
Frank Dehn

Case Studies in Construction Materials 23

October 2025, e05427

DOI: 10.1016/j.cscm.2025.e05427

Publisher's version

Case Studies in Construction Materials 23 (2025) e05427

Contents lists available at ScienceDirect

Case Studies in Construction Materials

journal homepage: www.elsevier.com/locate/cscm

Full length article

Influence of thermally activated industrial concrete fines of different origin on mortar strength development

Jan P. Höffgen *, Sebastian Bruckschlögl, Bernhard Wetz, Frank Dehn

Karlsruhe Institute of Technology (KIT), Institute for Concrete Structures and Building Materials (IMB), Gotthard-Franz-Str. 3, Karlsruhe, 76131, Germany

ARTICLE INFO

Keywords:
Concrete
Cement
Construction waste
Recycling
Thermal activation
Supplementary cementitious material

ABSTRACT

Thermal activation of recycled concrete fines (RCFs) has gained traction as a promising method for mineral waste recycling and the substitution of Portland cement, thereby reducing CO_2 emissions. However, as the composition of concrete fines varies, their performance as supplementary cementitious materials (SCMs) also changes. The present work compares 25 industrial concrete fines from various sources and compositions concerning their thermal decomposition and their influence on hydration heat and mortar compressive strength development. RCFs were processed at 100 °C, 400 °C, and 600 °C, and tested for their hydration heat development and compressive strength. Findings show that blended cements exhibit fast rehydration, which results in high early strength. Compressive strength of mortar containing processed RCFs increases with activation temperature. However, the mass loss from the disintegration of hydraulic hardened cement paste phases is a more significant parameter for assessing the strength contribution. Based on these findings, the study presents a new model for predicting compressive strength alongside current provisions for established SCMs. While compressive strength contribution of RCFs processed at 100 °C on average assumes about 10 % of CEM I reactivity and may be even negative, the same RCFs show an in increase to 41 % for 600 °C, with some RCFs even exceeding 60 %. This allows for the substitution of increasingly scarce fly ash, which exhibits strength contribution around 40 %-50 %.

1. Introduction

The production of cement is one of the most significant contributors to climate change, accounting for 8 % of global CO_2-emissions [1]. Emissions are attributed to two major sources: fossil fuels required for cement clinker processing temperatures up to 1450 °C and the calcination of carbonates from clinker raw meal. While the former can be abated through alternative fuels, the latter requires a switch to carbon-free calcitic feedstocks [2,3].

The hardening process of ordinary Portland cement (OPC, or CEM I according to EN 197-1:2011) based concrete relies on the hydraulic reaction of cement clinker, which forms high amounts of calcium-silicate-hydrates (C-S-H) responsible for strength development, and calcium hydroxide for high alkalinity from the hydration of alite (C_3S) and belite (C_2S), as well as hydration products of aluminous and ferrous clinker phases [4,5].

For ecological reasons, clinker can be partially substituted through alternative binders, so-called supplementary cementitious materials (SCMs), such as limestone powder, ground granulated blast-furnace slag (GGBS), amorphous silica, or fly ash [5–10]. These exhibit a different, in general lower, reactivity (compared to OPC) [3,11–13]. This depends on their mineralogical and chemical

* Corresponding author.
E-mail address: jan.hoeffgen@kit.edu (J.P. Höffgen).

https://doi.org/10.1016/j.cscm.2025.e05427
Received 23 July 2025; Received in revised form 18 September 2025; Accepted 13 October 2025
Available online 16 October 2025

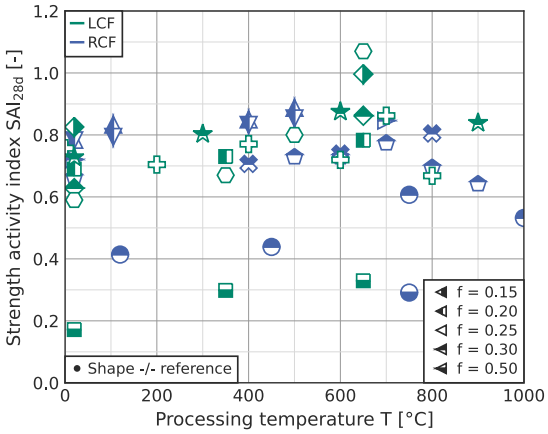

Fig. 1. Strength activity indices (SAI) over processing temperatures for different concrete fines and substitution rates (f) from various exemplary references.
LCF: fines from laboratory-made concrete, RCF: fines from concrete recycling plants.
Marker shapes: ⬠: [73], △, ▽: [58], ⊳: [74], ∘: [49], ×: [75], □: [76], ◇: [54], ⬡: [77], +: [66], ★: [71].

composition, where SCMs may react with hydration products from the OPC reaction, or are inert. Facing the high demand for sustainable building materials, research focuses on identifying potential SCMs [7,14].

Among these, recycled concrete fines (RCFs) are particularly promising [15–19]. Their application is identified as closed circularity, especially since the use as fine concrete aggregates is impeded through their high porosity and water absorption, which results in weak concrete performance [20,21]. This is associated with the enrichment of hardened cement paste (HCP) with decreasing particle size during mechanical processing of recycled concrete aggregates [22]. Alternatively, RCFs can be ground and serve as SCMs, where they act as fillers and nuclei for the hydration of OPC [23–25]. However, material properties can be enhanced by thermal activation. HCP dehydrates at elevated temperatures: Calcium silicate hydrates (C-S-H) start to decompose at 110 °C [26]. The upper limit of C-S-H decomposition lies between 300 °C and 500 °C [26–28]. Calcium hydroxide disintegrates in a smaller range between 400 °C and 550 °C [26,27,29]. Aluminous hydration products are anhydrous at temperatures higher than 400 °C [27,30–34]. Favored by the lower processing temperatures compared to clinker production, this process can be almost emission-free, as long as fossil fuels are avoided in favor of renewable energy [35–39]. Only when processing temperature exceeds 650 °C, carbonates start to disintegrate with the subsequent emission of CO_2. Dehydrated cement paste (DCP) is a reactive SCM: dehydrated C-S-H forms different variations of $\alpha'C_2S$ with C/S-ratio between 1.73 and 1.90 [4,40–47]. C-S-H from the rehydration of $\alpha'C_2S$ mainly forms within the porous structure of DCP-particles, resulting in a loose microstructure with weak interparticle connectivity [46,48,49]. However, when used as a partial Portland cement substitute, the water uptake and consumption in the DCP-pores reduce the water available for clinker hydration, which subsequently enhances the strength of the surrounding matrix [27,50–52]. The rehydration of $\alpha'C_2S$ exhibits a high velocity, more so when free lime from disintegrated calcium hydroxide or calcium carbonates is present in the DCP. This results in an accelerated hydration with high initial hydration heat release and high early strength development [27,28,40,43,46,50,52,53]. DCP can replace up to 40 wt% of OPC with no significant negative impact on compressive strength [45,52,54–60]. Optimum processing temperatures mostly lie within the range of 350 °C–800 °C [43,49,56,60–69]. Higher temperatures induce the reformation of $\alpha'C_2S$ to less reactive phases [43,46,51,68].

However, besides HCP, RCFs consist of fine natural aggregates, which are mostly inert after processing below calcination temperature (> 650 °C, depending on mineral composition) [70,71]. Inert aggregates in dehydrated concrete fines mostly exhibit no strength contribution aside from the nucleation and filler effect [49]. However, natural aggregates may contain amorphous siliceous or other pozzolanic phases [72]. Aside from different aggregate compositions and matrix porosity, RCFs vary in terms of the chemical composition of the original cement and SCMs used for the production of the source concrete.

For the assessment of the strength contribution of SCMs, the strength activity index (SAI) provides a single-point direct quantification method. SAI_t is defined through Eq. (1) as the relative compressive strength f_c of a reference mortar (or concrete) with OPC and a SCM-mortar with partial OPC substitution at a given age t. Requirements for mix composition and SAI-thresholds depend on individual SCM standards: European standard EN 15167-1:2006 requires $SAI_{7\,d} \geq 0.45$ and $SAI_{28\,d} \geq 0.70$ for standard mortar containing 50 wt% GGBS, and EN 450-1:2012 defines thresholds of $SAI_{28\,d} \geq 0.75$ and $SAI_{90\,d} \geq 0.85$ for a substitution rate of 25 wt% through fly ash.

$$SAI_t = \frac{f_{c,SCM,t}}{f_{c,ref,t}} \tag{1}$$

$SAI_{28\,d}$ for thermally activated concrete fines mostly lie within a range, which fulfills the aforementioned requirements for fly ash. However, the literature data presented in Fig. 1 also shows a great variation between results from different publications, where, besides concrete fines composition, different processing and testing approaches may negatively affect the comparability of these results.

Table 1
Overview of the investigated parameter combinations and processing temperatures for different precursors. RCF: Recycled concrete fines, RCA: Recycled concrete aggregates, FCR: Fresh concrete recycling, F: Filter cake.

Marker	Precursor		Variants		100 °C	400 °C	600 °C
□	RCF	0/2 mm	A1-	0/0.125 s	×		×
				0/0.25 s			×
				0/0.25	×		×
				0/0.5	×		×
				0/1	×		×
				0/2	×		×
◇	RCF	0/2 mm	A2-	0/0.25			×
				0/2			×
△	RCF	0/2 mm	B1-	0/0.25	×	×	×
				0/0.5	×		×
				0/1	×		×
				0/2	×	×	×
▽	RCA	0/45 mm	B2-	0/0.25	×		×
				0/2	×		×
▷	RCA	0/45 mm	C-	0/0.25	×		×
				0/2	×		×
○	RCA	0/16 mm	D-	0/0.25	×		×
				0/2	×	×	×
	FCR	F		F	×	×	×
×	RCF	0/2 mm	E-	0/0.25	×		×
				0/2	×		×
+	RCF	0/3 mm	F-	0/0.25	×		×
				0/2	×	×	×
⬠	RCF	F	G-	F	×	×	×
⬡	FCR	F	H-	F	×		×

Ultimately, for these variations, the present data is insufficient for providing a means for predicting compressive strength of mortar or concrete containing thermally processed RCFs. Besides the impact of different experimental procedures, the influence of varying RCF composition itself has rarely been investigated in the literature, where most studies focus on evaluating a single RCF. For the industrial application of thermally processed RCFs as SCMs, knowledge about fluctuating material properties is paramount. A direct comparison of the strength contribution of RCFs from different sources, and subsequently, a model for predicting compressive strength based on RCF properties, is lacking. Therefore, the present study investigates the influence of thermally activated RCFs of different compositions on compressive strength with the ultimate objective of providing a comprehensive model for predicting compressive strength of mortar or concrete containing therally processed RCFs as SCM.

2. Experimental program

The experimental program comprises two distinct goals: The first step is to analyze parameters of the thermal activation, followed by the evaluation of thermally activated concrete fines as supplementary cementitious materials (SCM) in comparison to ground granulated blast-furnace slag, black coal fly ash, and limestone powder as established concrete binders.

2.1. Materials

The experimental assessment uses and compares eleven different batches of waste concrete from eight different processing plants (labeled A – H). From two plants (A and B), two batches produced several months apart were procured. For batches of recycled concrete aggregates (RCA), where the maximum particle size exceeded 2 mm, larger particles were removed through dry-sieving before any further handling. In addition to the variant "0/2" [mm] from each recycled concrete fines (RCF) batch, an additional variant "0/0.25" [mm] was produced through a second dry-sieving step. From two batches, additional variants with different particle sizes were obtained in a similar procedure. Three batches had a different preprocessing: Batch G-F originated from a mineral waste processing plant, which used a wet-separation, where concrete fines smaller than 100 µm, rather than the typical 2 mm from the other batches, can be obtained as residue filter-cake (F). In contrast, D-F and H-F denote filter cakes from two fresh-concrete recycling (FCR) plants. Following the subsequent thermal activation, concrete fines were ground to a maximum particle size of 125 µm, except for the variants A1-0/0.125s and A1-0.25s, which were left without grinding after thermal processing ("s"). Activation temperature was 400 °C or 600 °C, as hereinafter indicated through suffices "−400" and "−600". Additionally, concrete fines were dried at 105 °C and ground (suffix "−100"). Table 1 gives an overview of the, in total, 25 different concrete fines variations and 53 processed concrete fines combinations.

Besides concrete fines, the experimental analyses used OPC (CEM I 42.5 R, "CEM I") as base binder and ground granulated blast-furnace slag ("S"), fly ash ("FA"), as well as limestone powder ("L") as established SCMs for reference. Additionally, siliceous river sand (0/2 mm, "RS") served as fine aggregates.

CEM I was also used to produce an artificial hardened cement paste ("CEM") with a water-cement ratio of $w/c = 0.5$, which was used for the evaluation of thermal activation processing parameters. CEM was kept moist for 9 months, before drying at 105 °C and subsequent grinding ("CEM-100").

2.2. Experimental procedures

Initially, all materials, including thermally activated fines, were characterized for their chemical composition as well as their density and particle size distribution. Concrete fines were also investigated through thermogravimetric analyses before and after activation, using sample sizes of 160 mg and a heating rate of 10 K/min.

The evaluation of thermal activation processing parameters followed a three-step approach. First, the base material CEM-100 was examined for its thermal behavior in the same thermogravimetric test setup, but with varying heating rates (1 K/min, 5 K/min and 10 K/min) and sample sizes of 5 g. The test at 10 K/min was repeated in a different setup with a sample size of 60 mg, which included a mass spectrometer for measuring ion currents (IC) of H_2O and CO_2. The second step exploited the versatility of the thermogravimetric setup for processing CEM-100 at varying temperatures, heating and (passive) cooling rates, as well as holding times. Finally, the influence of varying sample sizes and holding times was analyzed with the ultimate goal of defining the thermal processing regimen for the subsequent RCF activation.

CEM I, reference SCMs, and select activated concrete fines were used for isothermal hydration heat measurements at 20 °C with internal mixing, which allowed the determination of the initial heat release. Following preliminary tests on mixing efficiency and homogeneity, the water-binder ratio was set to $w/b = 0.6$ for all materials. SCMs were investigated in combination with CEM I and a substitution rate of $f = 0.3$. For all mixes, a double determination was carried out, except for the base mix with pure CEM I, which consisted of eight single measurements.

Strength development tests used a mortar with 50 v% quartzitic river sand (0 mm-2 mm) as aggregates. For the assessment of SCM influence, from all SCMs two mixes with $w/b = 0.4$ and $w/b = 0.5$ at $f = 0.3$ were produced, with selected SCMs adding $w/b = 0.5$ at $f = 0.1$, and $f = 0.5$. Fourteen base mixes with pure CEM I used $w/b = 0.40$–0.65, which were produced in three series repeated over the experimental program. In case of stiff mortars, superplasticiser was added to ensure comparable workability. After mixing, mortar was placed in steel molds, which were moist-cured for 1 d, and, following demolding, stored under water at 20 °C. Strength testing used three prisms ($(20 \times 20 \times 80)\,mm^3$) at 2 d and 28 d. Since thermal activation and grinding of concrete fines was a resource-intensive process, this smaller specimen size was chosen, compared to standard mortar bars ($(40 \times 40 \times 160)\,mm^3$), to reduce the amount of binder required for each mix. First, flexural strength f_f was determined with a span of 50 mm at a loading rate of $\dot{f}_f = 10$ N/s. Compressive strength (f_c) testing used six prism halves at a loading rate of $\dot{f}_c = 600$ N/s.

Fig. A.14 in the appendix section gives a graphical illustration of the experimental procedures.

3. Results and discussion

3.1. Thermal activation parameters

The temperature-dependent mass loss (Δm) of CEM-100 in Fig. 2 shows the aforementioned segments, although all measurements produce unique results. With decreasing heating rate, decomposition processes occur at lower temperatures, resulting in increased mass losses at the same temperatures. In particular, the decomposition of calcium hydroxide shows a strong influence of the heating rate, with an offset of more than 50 K. This offset is interrelated with sample size, as with larger sizes, thermal conduction impedes a uniform temperature within the sample. Accordingly, Δm in the thermogravimetric measurement coupled with mass spectroscopy, which used a sample size of 60 mg and a heating rate of 10 K/min, is closest to Δm at 1 K/min and 5 g. Similar observations are made for the decomposition of carbonates, which starts at 550 °C and peaks at 720 °C, but is offset to higher temperatures for larger sample sizes.

Conversely, Fig. 2 allows for the determination of processing temperatures that are less susceptible to heating rate and/or sample size, thus enabling better reproducibility and comparability across different thermal processing setups. Subsequently, a processing temperature of 600 °C was chosen for the following analyses. Additionally, at 600 °C mass spectroscopy shows an almost complete loss of H_2O, while CO_2 emissions are still low.

In addition to the processing temperature of 600 °C, two other processing temperatures were identified from Fig. 2. At a temperature of 400 °C, apart from the decomposition of calcium hydroxide, the majority of the dehydration is complete. At a temperature of 800 °C, a high proportion of the carbonates in the cement paste is also decomposed. In combination with 600 °C, 400 °C, and 800 °C allow for evaluating the influence of calcium hydroxide and carbonates decomposition.

To investigate this preselection of processing temperatures in more detail, samples of CEM-100, each weighing 5 g, were activated in the same thermogravimetric setup. In particular, the different holding times, heating, and cooling rates allowed the influence of system inertia and thus control accuracy to be addressed. The core parameter combination was 5-600-0-10, which is an abbreviation for a heating rate of 5 K/min, target temperature of 600 °C, holding time of 0 h, and an initial cooling rate of 10 K/min. Parameter variations combine heating rates of 1 K/min, 5 K/min and 10 K/min, holding times of 0 h and 2 h and initial cooling rates of 5 K/min, 10 K/min and 20 K/min. The latter could not be actively controlled, but denotes the maximum rates during passive cooling.

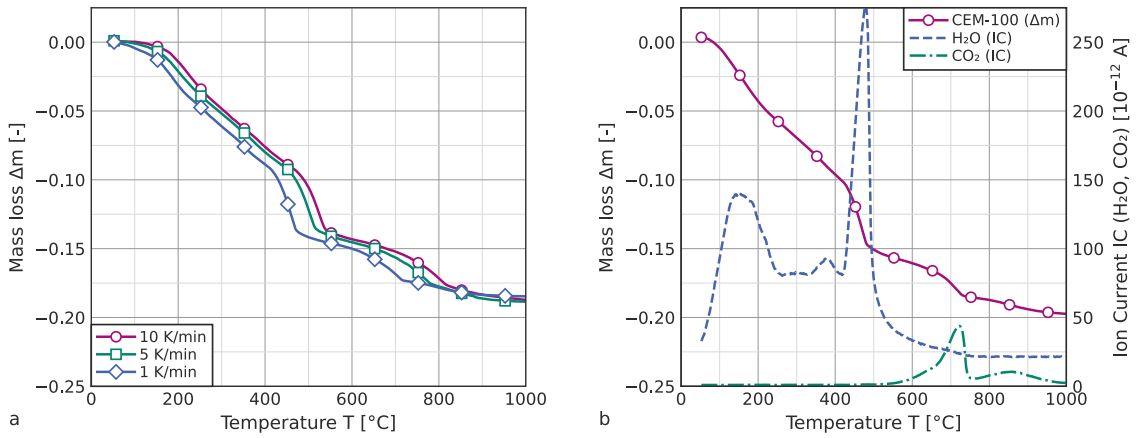

Fig. 2. Temperature-dependent mass loss of CEM-100. a: influence of different heating rates (sample size 5 g), b: additional ion current measurements at a heating rate of 10 K/min (sample size 60 mg).

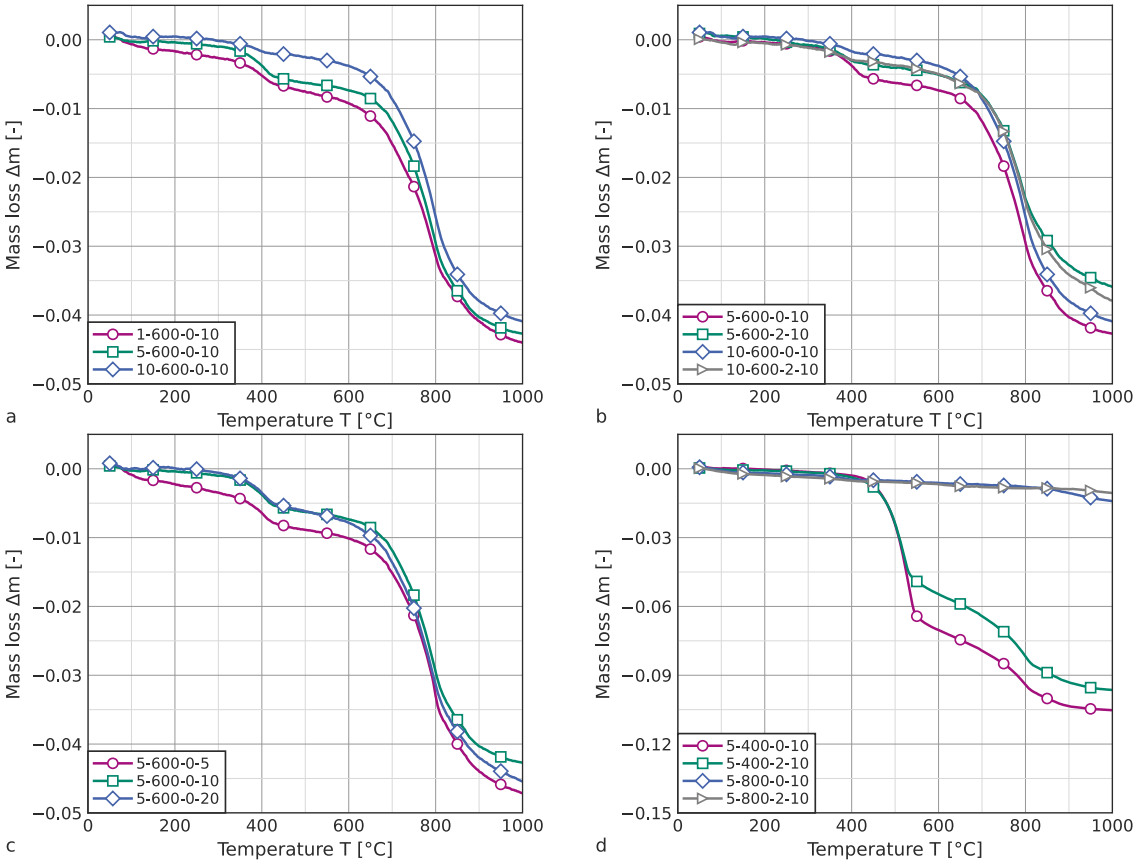

Fig. 3. Thermogravimetric analysis of CEM-100 activated at different processing parameters.

Additionally, for processing temperatures of 400 °C and 800 °C, the influence of different holding times (0 h and 2 h) was evaluated at a heating rate of 5 K/min and a cooling rate of 10 K/min.

From these samples, subsamples were taken and initially characterized in a repeated thermogravimetric investigation. For this purpose, sample masses of 160 mg were examined at a heating rate of 10 K/min. Fig. 3 shows the resulting mass losses as a function of temperature up to 1100 °C.

In an ideal thermal preparation, it would be expected that the curve progressions remain constant until the preparation temperature is reached again and only then show a mass loss with increasing temperature. Fig. 3 shows that this is not the case for any of the samples prepared at 600 °C – all samples show varying degrees of mass loss. However, no systematic influence of the processing parameters can be identified. An increased mass loss occurs at approximately 400 °C, while the decomposition of calcium hydroxide is complete in all cases at around 500 °C. This shift in the decomposition temperature suggests that the observed

mass losses are due to compounds formed after thermal processing (compare [43,78,79]). A probable reason is that the hot samples cannot be immediately removed from the test device after processing. At the same time, the results underscore the importance of rapid further processing of the samples.

The processing temperatures of 400 °C and 800 °C were only considered concerning different holding times. Here, it is shown that processing at 800 °C, in contrast to processing at 600 °C, results in very low mass losses for both parameter combinations during the repeated thermogravimetric measurements. Both samples prepared at 400 °C also show only a slight mass loss up to the previous preparation temperature. However, a plausible influence of the treatment duration is evident: A temperature of 400 °C is not sufficient to decompose calcium hydroxide. However, an extension of the processing duration can have a similar effect as a reduction of the heating rate (see Fig. 2), so that a small amount of calcium hydroxide is decomposed after a duration of 2 h. Similar, albeit less pronounced, observations can be made for the samples processed at 800 °C.

In the third step of the analysis of processing parameters, CEM-100 was activated in different crucibles for either 3 h or 6 h in a static high-temperature furnace. The target temperature was 600 °C, with a heating rate of 5 K/min. Finally, the results from the static furnace were compared to the activation in a rotary furnace. In contrast to processing in crucibles, a rotary furnace continuously agitates the sample, resulting in a homogeneous temperature distribution. Holding time was therefore reduced to 0 h and 1 h. Immediately after the preset test duration ended, the static furnace opened automatically, and the samples were cooled in their covered crucibles at a laboratory climate before storage in desiccators. The samples in the rotary furnace were cooled in their containers at laboratory climate and stored in desiccators after reaching a temperature of < 200 °C.

Subsequently, thermogravimetric measurements were carried out on subsamples, which are shown in Fig. 4. The measurements illustrate a mutual influence between crucible size and preparation duration: While small crucibles already show similarly successful preparation after 3 h as the samples in Fig. 3, larger samples (examined were 0.75 kg and 1.0 kg) show a significantly increased mass loss between 400 °C and 600 °C, suggesting that the samples were not heated homogenously. Consequently, longer preparation times are required for larger samples. However, 6 h proved sufficient for all sample sizes up to 1.5 kg. The rotary furnace allows for a strongly reduced holding time. It is evident that the sample, where the heat treatment was terminated immediately after reaching the target temperature of 600 °C (0 h), subsequently showed the lowest mass loss below 600 °C. Extending the preparation by 1 h brought no additional benefit, with the mass loss subsequently slightly increased. An influence of storage can be assumed here, analogous to the previous experiments in the static furnace. The deviation between the two samples from the rotary furnace is smaller than the deviation between the two repeated samples from the static furnace. All samples show different mass losses above 700 °C, with no systematic pattern evident.

Subsequently, the procedure where RCFs were treated for 6 h in a static furnace at the target temperature following a heating ramp at 5 K/min was elected for the main analyses.

3.2. Precursors characterization

Fig. 5 presents the chemical compositions of RCFs (sieved to 2 mm and 0.25 mm) measured by WDXRF, the corresponding filter cakes, as well as CEM I, reference SCMs, and siliceous river sand (RS). It becomes apparent that the examined RCFs contain a similarly low amount of Al_2O_3 and Fe_2O_3. In contrast, RCFs contain high amounts of SiO_2, indicating the presence of siliceous aggregates. CaO- and MgO-content, on the other hand, increases with decreasing particle size, thus implying the concentration of hydrated cement in smaller particles.

Fig. 6 shows the mass loss of selected RCFs before thermal processing. The finer materials generally exhibit greater mass losses than the corresponding variants with a maximum grain size of 2 mm. However, the difference does not follow any apparent systematics and varies in magnitude for individual RCFs. The highest mass loss at 600 °C is observed for the RCF "D-F", a filter cake from fresh concrete recycling. None of the examined samples shows an increased mass loss at around 500 °C, which would be associated with the decomposition of calcium hydroxide. It can therefore be assumed that calcium hydroxide has been converted to other compounds such as $CaCO_3$ through natural carbonation. Regarding the mass losses between 650 °C and 850 °C, which are associated with the decomposition of carbonates, the samples also show significant differences among each other. The RCFs from plant A and the filter cake from plant G show the highest mass losses here, while RCFs from plant D show only slight mass losses, which also end at lower temperatures of around 800 °C. This, in conjunction with the WDXRF results, which indicate a high CaO-content in RCFs from plants A and G, suggests that the RCFs contain different primary aggregates with varying calcium carbonate contents and variations.

The particle size distribution of processed RCFs shows a generally good comparability between different samples, except processed filter cakes (see Table 2). The latter exhibits smaller particle sizes, which are similar to limestone powder. Processing at 600 °C before grinding has a minor effect on the particle size distribution.

3.3. Concrete fines performance as SCM

3.3.1. Hydration heat

The hydration heat flow calorimetry measurements were limited to CEM I, S, FA, L, and selected RCFs processed at 600 °C. Fig. 7 includes the span obtained from eight single measurements, as well as the average of the double determinations performed for all measurements, where 30 wt% of CEM I was substituted through SCMs. The released hydration heat in Fig. 7 shows a great similarity between the processed RCFs and a great similarity to the mixture of CEM I with blast-furnace slag, exceeding the values for fly ash and limestone powder. Additionally, the heat release of finer raw materials (0/0.25 mm) is slightly increased compared to coarser

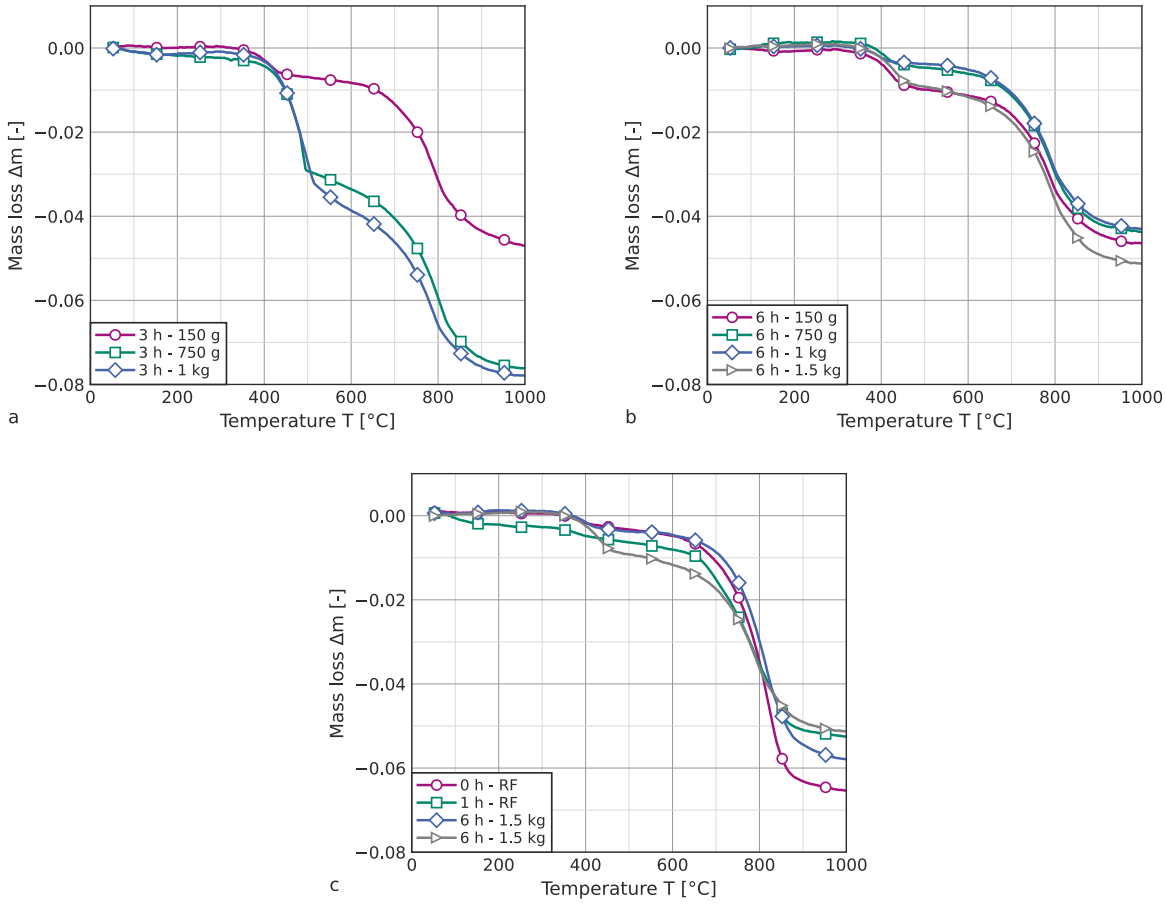

Fig. 4. Thermogravimetric analysis of CEM-100 activated in a static furnace with different sample sizes and holding times (a: 3 h, b: 6 h) and a rotary furnace "RF" (c).

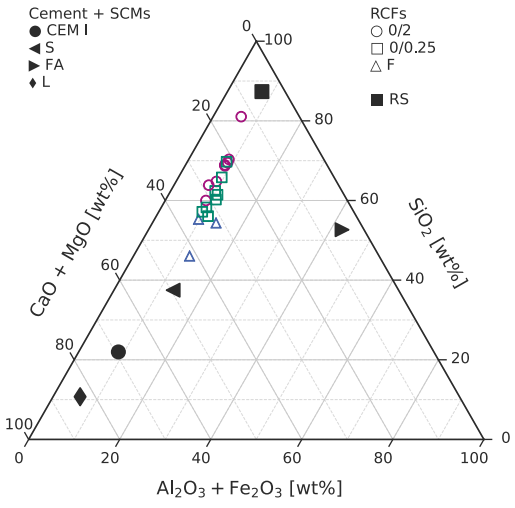

Fig. 5. Relative chemical composition of base materials and recycled concrete fines (RCF) through WDXRF (see tabulated data in the appendix section Table A.5).

raw materials (0/2 mm). Noteworthy is the hydration heat release of D-F (filter cake from a fresh concrete recycling plant). Here, a significantly increased heat release is evident in the first minutes after water addition. Additionally, the subsequent local maximum

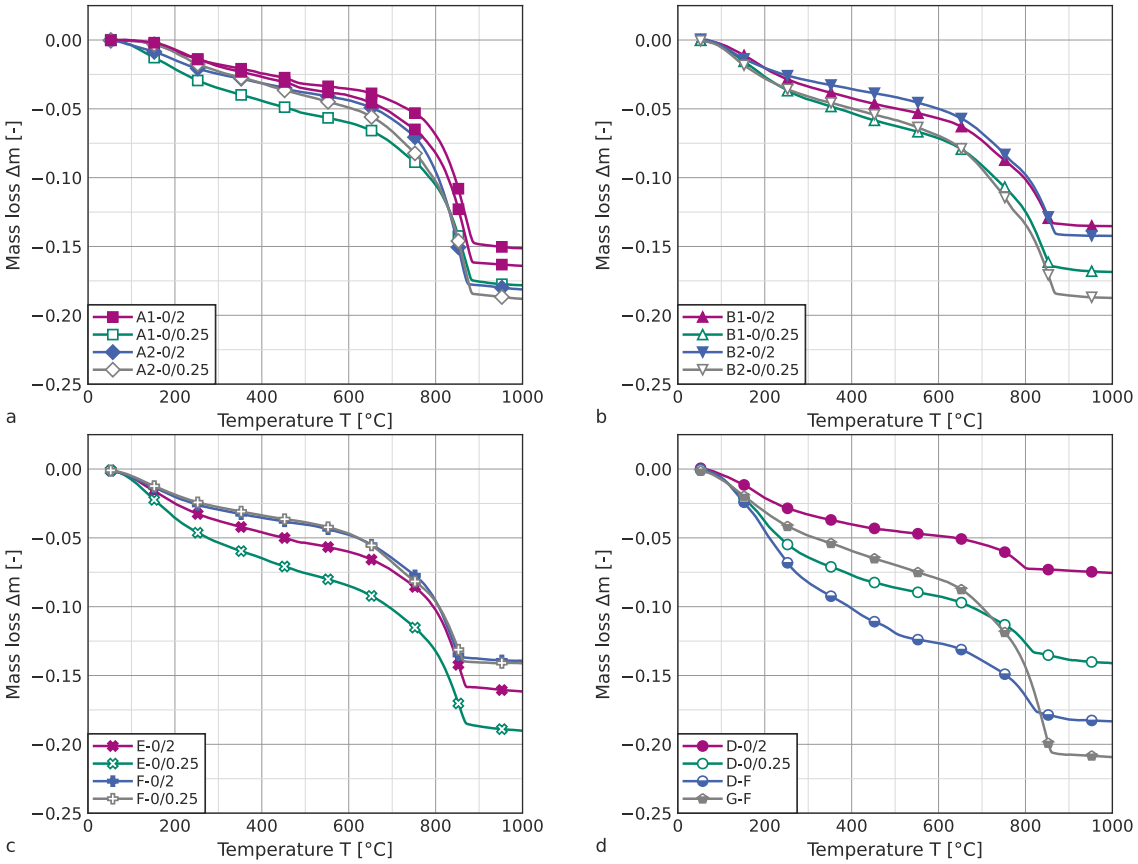

Fig. 6. Thermogravimetric characterization of select RCFs (sample size 160 mg, heating rate 10 K/min).

Table 2
Relevant characteristics (average and standard deviation at 10 v%, 50 v%, and 90 v% passing) of the particle size distribution of processed concrete fines and reference binders. Results only include values where pairs of RCFs were processed at both 100 °C and 600 °C.

	Qty.	d_{10} [µm]	d_{50} [µm]	d_{90} [µm]
CEM I	1	1.7	12.1	32.9
S	1	2.1	12.3	30.0
FA	1	2.9	21.6	83.4
L	1	1.9	12.5	44.4
0/2–100	7	1.8(3)	13.2(33)	54.1(83)
0/2–600		1.8(3)	14.1(33)	57.1(71)
0/0.25–100	7	1.8(3)	13.7(23)	55.2(58)
0/0.25–600		1.8(2)	14.0(16)	57.7(52)
F-100	3	2.2(6)	11.6(27)	44.7(109)
F-600		2.1(4)	10.1(13)	41.6(18)

of the hydration heat flow is lower and occurs earlier. However, the following decline in heat release is reduced, so this sample ultimately shows the highest heat release of all investigated mixtures of CEM I and processed RCFs.

3.3.2. *Compressive strength development*

The influence of cement, and SCMs, on compressive strength development can be characterized through the ratio of 2 d- to 28 d-strength (r_2). Fig. 8 shows results for the strength ratio r_2 for mortar with CEM I at different w/c-ratios and the partial replacement of CEM I through latent-hydraulic blast-furnace slag (S), pozzolanic fly ash (FA), or limestone powder (L). Particularly for CEM I, but also for mortar with SCMs, strength development accelerates with higher 28 d-compressive strength, i.e., for lower w/c-ratio and lower substitution rate through SCMs. Correspondingly, with the same strength, the partial substitution of CEM I through blast-furnace slag or fly ash leads to reduced strength at the age of 2 d. r_2 for these mixtures ranges from 0.4 to 0.5. The replacement of CEM I with inert limestone powder has the greatest impact on mortar compressive strength compared to blast-furnace slag or fly ash. Apart from that, the strength ratio r_2 is not additionally affected. Mixtures with CEM I and limestone powder, as well as

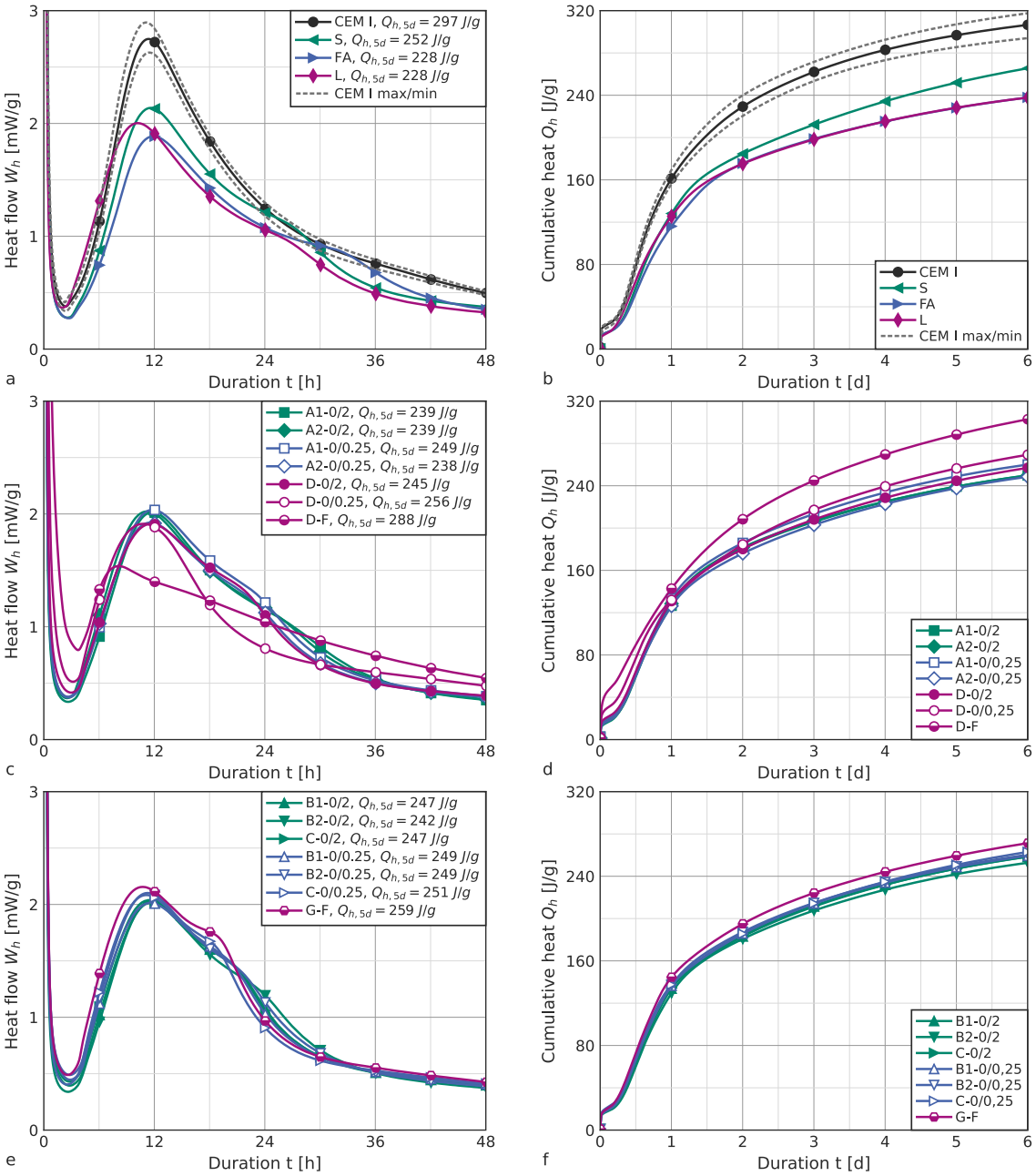

Fig. 7. Hydration heat of CEM I, including standard deviation, and mixtures of 70 wt% CEM I and 30 wt% reference SCMs, or RCFs processed at 600 °C.

mixtures with pure CEM I, show strength-dependent values of r_2 in the range of 0.5 to 0.7. With the same strength at the age of 28 d, these mixtures tend to have higher 2 d compressive strength than mixtures with fly ash or blast-furnace slag.

The compressive strength development of mixtures with thermally activated RCFs shows similar r_2 values to the pure CEM I mixtures, with even higher r_2 values up to 0.7 being achieved at the same 28 d compressive strength — regardless of the processing temperature. This indicates an accelerating effect of RCF on compressive strength development.

3.3.3. Compressive strength at 28 d

The assessment of compressive strength at a mortar age of 28 d uses both strength activity indices as well as the k-value approach.

Strength activity indices ($SAI_{28\,d}$) for processed concrete fines replacing 30 wt% of CEM I were calculated based on the average $f_{c,ref,28\,d}$ = 53.3 MPa. Results indicate a temperature dependence, with average $SAI_{28\,d}(100\,°C)$ = 0.64(7) and $SAI_{28\,d}(600\,°C)$ = 0.74(5). Fig. 9 illustrates individual results for different concrete fines variations. For comparison, the double determination of SAI for established SCMs yield $SAI_{28\,d}(S)$ = 0.91 for slag, $SAI_{28\,d}(FA)$ = 0.78 for fly ash, and $SAI_{28\,d}(L)$ = 0.66 for limestone powder.

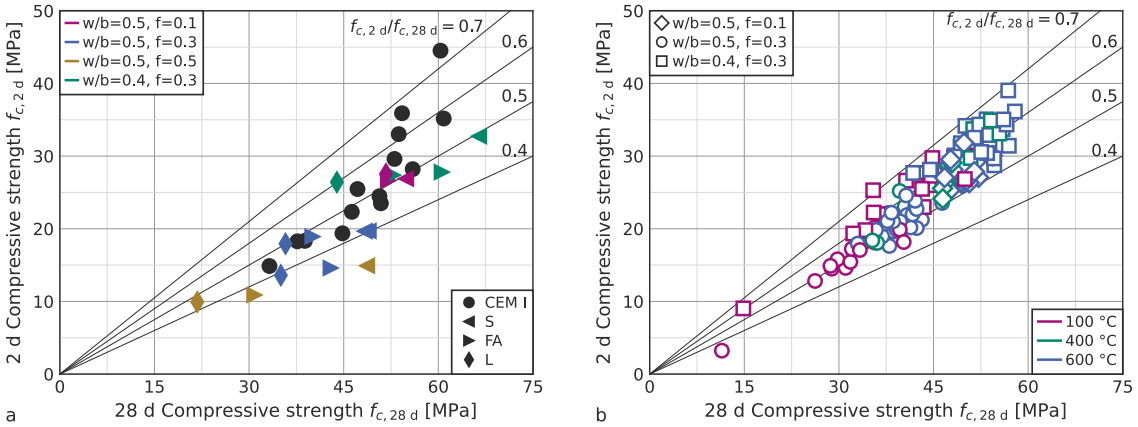

Fig. 8. Mortar compressive strength f_c at an age of 2 d over 28 d for different mix designs and CEM I substitution through reference SCMs (a) or processed concrete fines (b).

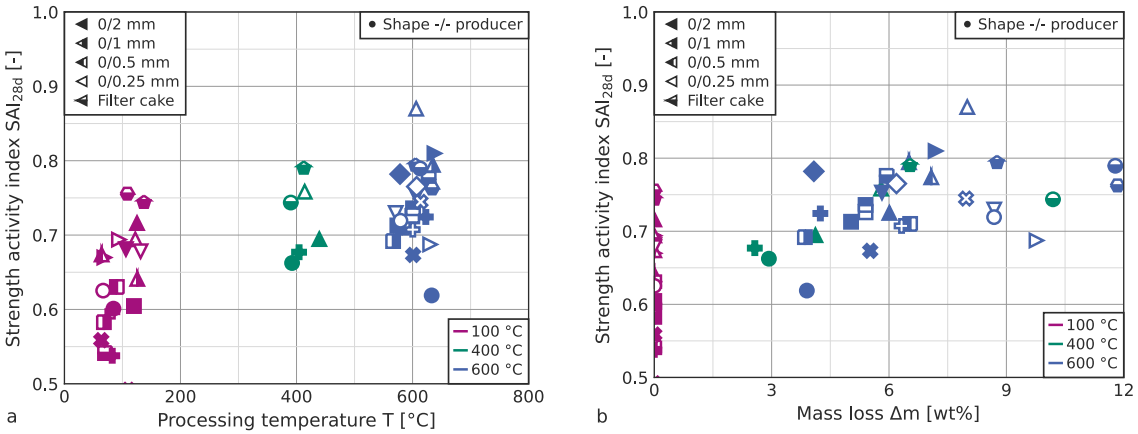

Fig. 9. Strength activity indices ($SAI_{28\,d}$) over processing temperatures (a) and mass loss (b) for different concrete fines at CEM I-substitution of $f = 0.3$ (see Table 1 for marker shapes). For better visualization only, results in (a) are randomly distributed around the activation temperatures of 100 °C, 400 °C, and 600 °C.

SAI for individual CEM I-series range between 0.95 and 1.05. While this uncertainty of the base mix strength is partially reflected in the scatter of SAI-results for processed concrete fines, the latter exhibit a high variation between different fines variations.

While investigating concrete fines from a single source, previous research found a logarithmic [63] or parabolic [49,64] relationship between processing temperature and compressive strength, or SAI, respectively. When applying the latter to the present data, the fit from Eq. (2) yields $SAI_0 = 0.59$, $SAI_1 = 5 \cdot 10^{-4}$, and $SAI_2 = -4 \cdot 10^{-7}$, albeit with a mediocre coefficient of variation ($R^2 = 0.44$)

$$SAI = SAI_0 + SAI_1 \cdot T + SAI_2 \cdot T^2 \qquad \text{with } SAI_{1,2,3}\text{: fit parameters} \tag{2}$$

When, instead of processing temperature, the relative mass loss during thermal activation is used as the horizontal axis, the bandwidth of the results for SAI reduces and shows a linear trend (see Fig. 9(b)). This can be expressed through Eq. (3), where the least squares method yields $SAI_n = 0.64$ and $SAI_m = 1.45$, with a slightly improved coefficient of determination ($R^2 = 0.47$).

$$SAI = SAI_n + SAI_m \cdot \Delta m \qquad \text{with } SAI_{n,m}\text{: fit parameters} \tag{3}$$

Due to the low coefficients of determination for both approaches, neither serves as a measure to predict compressive strength based on RCF properties or processing parameters. A more extensive, multipoint approach to account for the strength contribution of SCMs is the k-value concept as described in the European standard EN 206:2013, which uses these parameters to negate the impact of SCMs on relevant concrete properties, presently the compressive strength. The concept relies on the relationship between compressive strength and the water-cement ratio w/c, which is replaced through an equivalent water-cement ratio w/c_{eq} according

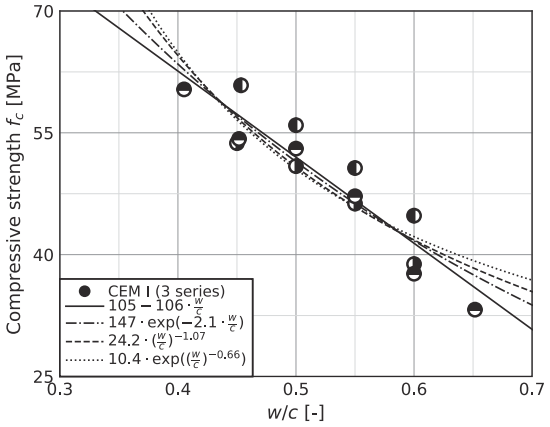

Fig. 10. Relationship between w/c and compressive strength f_c of base mixes without CEM I-substitution. Maker fill grades indicate results from three individual series.

to Eq. (4), where a concrete with partial cement substitution through an SCM has the same properties as a concrete without SCM with the same w/c-ratio.

$$\frac{w}{c_{\text{eq}}} = \frac{w}{c + k \cdot a} \qquad \text{with } a\text{: mass of the reactive SCM} \tag{4}$$

k-values serve as a measure of reactivity of the concrete additives and thus as an indication of their influence on compressive strength. Overall, k-values of a given SCM vary with concrete mix design, including water-cement ratio w/c and substitution rate. For most SCMs, k ranges between 0.0 and 1.0, where the former indicates an inert material, and the latter an SCM, which does not affect concrete properties when substituting CEM I.

The experimental determination of k-values uses the individual, mixture-dependent relationship between compressive strength f_c of mixtures without CEM I-substitution and the water-cement ratio w/c. For a mixture with SCMs, the equivalent water-cement ratio is then obtained by equating the resulting compressive strength with the relationship of w/c and f_c. Fig. 10 shows the individual results from three distinct series consisting of a total of 14 base mixes.

To represent the relationship mathematically, the experimental results were approximated by regression curves. Four approaches were examined for this purpose, which are shown in Fig. 10 with the respective optimized fit parameters (α_i, β_i).

$$f_{c,28\,\text{d}} = \alpha_1 - \beta_1 \cdot \frac{w}{c} \tag{5}$$

$$f_{c,28\,\text{d}} = \alpha_2 \cdot \exp\left(-\beta_2 \cdot \frac{w}{c}\right) \tag{6}$$

$$f_{c,28\,\text{d}} = \alpha_3 \cdot \left(\frac{w}{c}\right)^{-\beta_3} \tag{7}$$

$$f_{c,28\,\text{d}} = \alpha_4 \cdot \exp\left(\left[\frac{w}{c}\right]^{-\beta_4}\right) \tag{8}$$

The linear approach (Eq. (5)) – recommended in CEN/TR 16639:2014 – provides the best fit to the experimental results. Although linear material behavior is physically implausible, Eq. (6), Eq. (7), and Eq. (8) were discarded as empirical relationships for further analysis due to their insufficient fit. Furthermore, the comparison of the individual approaches illustrates that for mortar compressive strength between 43.4 MPa and 58.4 MPa, the linear approach yields higher values for w/c and thus lower values for k, corresponding to a conservative approach.

The subsequent determination of k calculates the individual equivalent water-cement ratio (Eq. (12)) and the respective k-value (Eq. (9)) for each mixture with the respective mixing parameters (w/b-ratio and cement substitution rate f) based on the compressive strength at the age of 28 d. The calculation of k requires additional input parameters such as the water-binder ratio w/b and the cement substitution rate f, as defined in Eq. (10) and (11).

$$k = \frac{1-f}{f} \cdot \left(\frac{\frac{w}{b}}{\frac{w}{z_{\text{eq}}}} \cdot \frac{1}{1-f} - 1\right) = 1 + \frac{1}{f} \cdot \left(\frac{\frac{w}{b}}{\frac{w}{z_{\text{eq}}}} - 1\right) \tag{9}$$

$$f = \frac{a}{b} = 1 - \frac{c}{b} \tag{10}$$

$$\frac{w}{b} = \frac{w}{c + a} \tag{11}$$

$$\frac{w}{c_{\text{eq}}} = \frac{\alpha_1 - f_{c,28\,\text{d}}}{\beta_1} \tag{12}$$

CEM I, by definition, has a k-value of $k = 1.0$. $k > 1.0$ can only be reached by highly reactive SCMS (as silica fume, according to EN 206:2013), where compressive strength increases when CEM I is substituted. Generally, the partial replacement of CEM I

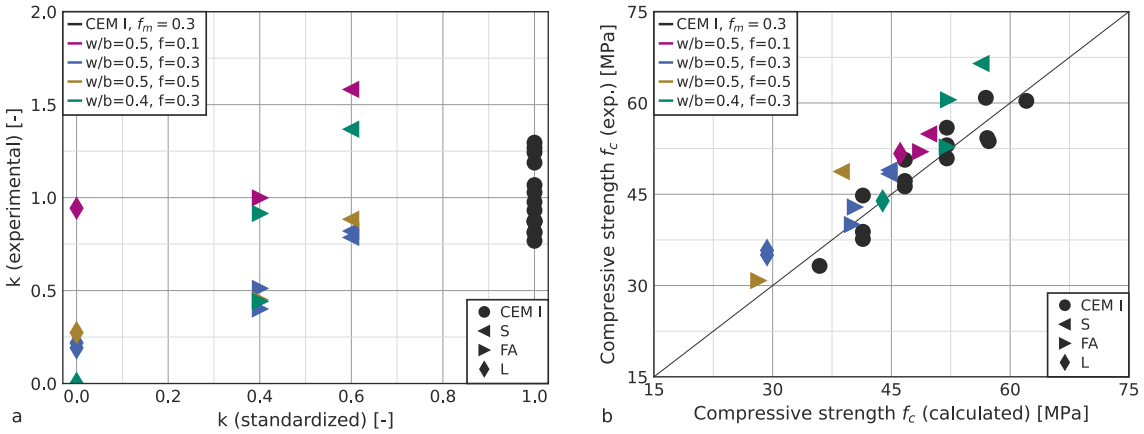

Fig. 11. a: k-values calculated for individual mortar mixes with CEM I substitution through established SCMs (slag (S), fly ash (FA), and limestone powder (L)) for different parameter combinations of the water-binder ratio w/b and the substitution rate f over respective design values in EN 206:2013.
b: measured compressive strength over calculated compressive strength using k from EN 206:2013.

Table 3
Average k-values for all processed RCF mixtures, clustered for different parameter combinations (excluding results from D-F-100 as outliers).

	100 °C	400 °C	600 °C	Total
$f = 0.1, w/b = 0.5$		0.20	0.61	0.51
$f = 0.3, w/b = 0.5$	0.17	0.36	0.39	0.30
$f = 0.3, w/b = 0.4$	0.01	0.40	0.43	0.26
$f = 0.3, w/b = 0.4/0.5$	0.09	0.38	0.41	0.28

through SCMs lowers compressive strength, which shows in $k < 1.0$. The magnitude of the strength reduction is represented by the value of k, where decreasing strength coincides with a reduction of k.

This behavior is exemplified by the reference SCMs (S, FA, and L) in Fig. 11. By definition in EN 206:2013, limestone powder (L) is an inert filler, consistent with $k = 0.0$, although slightly higher values for k have been proposed [80]. For $f = 0.3$, experimentally determined values for k range between 0.0 and 0.2. For fly ash and slag, experimental results in this study show a similar exceedance of conservative, standardized provisions, which are $k = 0.4$ for fly ash, and $k = 0.6$ for slag (EN 206:2013, CEN/TR 16639:2014). Experimental results yield $k = 0.4$–0.9 for fly ash and $k = 0.8$–1.4 for slag with $f = 0.3$, which reflects alternative standards and provisions [81,82]. For all tested SCMs, the substitution of 10 wt% of CEM I results in even higher k-values. However, when comparing the predicted compressive strength (by means of Eqs. (4) and (5)) to the experimentally measured compressive strength (Fig. 11(b)), this influence of the substitution rate f is mitigated. Nonetheless, f has a major influence on the scatter of k, which cannot be neglected for further analysis. Fig. 10 illustrates the three individual series for the determination of the fit parameters in Eq. (5). Between the different series, the measured strength has an apparent offset from the regression curve. The reason for this lies in deviating raw material properties, as the three series were produced with several months between them, so that all raw materials came from individual subsamples of the main batches. Fig. 11(b) compares these experimental results for CEM I to their prediction, which exhibits a similar scatter band as the reference SCMs, but lies around the bisector, while results for reference SCMs lie above. This is due to the aforementioned exceedance of standardized k-values, while $k = 1.0$ for CEM I is true by definition. Regardless, results for CEM I can be converted into individual k-values by assuming f in Eq. (9). For $f = 1.0$, k ranges between 0.9 and 1.0. This range increases hyperbolically with reducing f: For $f = 0.1$, the bandwidth of k for CEM I is 0.3 to 1.9, and for $f = 0.3$, k ranges between 0.8 and 1.3, with a standard deviation of 0.18.

For the second step of the analysis, 55 processed RCFs were used to produce 137 mortar mixtures, which were analyzed for their compressive strength and k-values. Generally, k-values increase with the processing temperature, whereby the difference between 400 °C and 600 °C is considerably smaller than the increase between 100 °C and 400 °C. The incorporation of RCFs processed at 100 °C can result in negative k-values, which is more pronounced for lower w/b-ratios. For 400 °C and 600 °C and the substitution rate $f = 0.3$, average k-values for different w/b-ratios deviate only slightly. Varying the substitution rate f at constant w/b has a higher, albeit ambiguous impact on k-values (see Table 3).

Fig. 12 shows the relationship between k-values calculated from the experimental results for $f = 0.3$ and the mass loss Δm during thermal processing. The RCFs in Fig. 12 were provided by the same manufacturer for each of the two upper diagrams. Batches A1 and A2, as well as B1 and B2, came from the same plants, so the same preparation technique for each pair can be assumed. However,

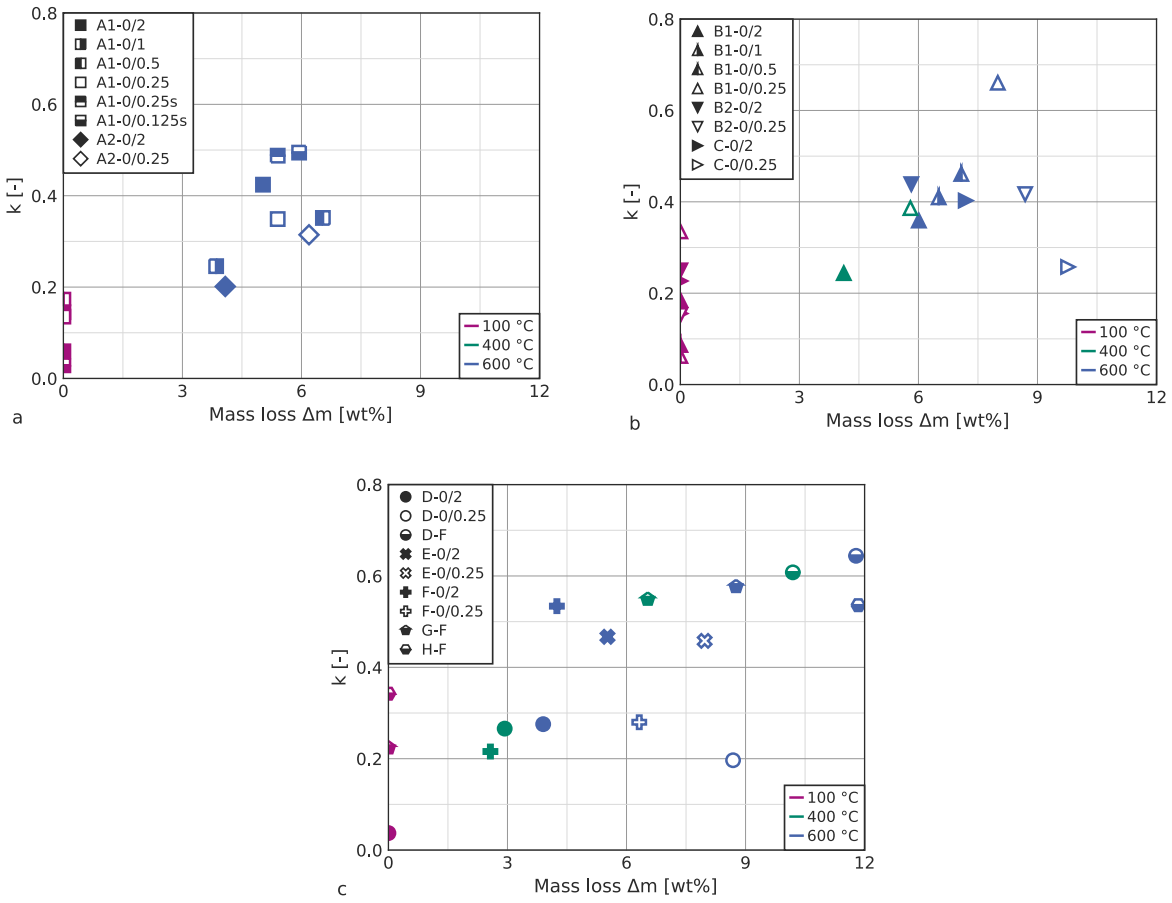

Fig. 12. k-values of select processed concrete fines over mass loss during thermal activation (averages for $w/b = 0.40$ and $w/b = 0.50$). Marker shapes and fill styles denote RCF producer and variation, and color indicates processing temperature.

the source concrete for A1 and A2, as well as B1 and B2, is for obvious reasons not the same, which includes different chemical compositions and mass losses. As mass loss also varies between variants of the same batch, a linear relationship between mass loss and k becomes apparent, notwithstanding scatter, especially for RCFs processed at 100 °C. Variants A1-0/0.25s and A1-0/0.125s, where the milling after the thermal activation was omitted, yielded higher k-values compared to milled variants at similar mass loss. Yet, this came with the side effect of impaired workability and higher superplasticiser demand, thus indicating an increased water demand. Two select variants from batch B1 were processed at 400 °C in addition to 100 °C and 600 °C, agreeing with the linear relationship between k and mass loss for batches B1 and B2.

Similar observations hold when considering the other RCF-variants illustrated in Fig. 12(c). Generally, RCFs processed at 400 °C yielded reduced mass losses and k-values compared to their 600 °C-counterparts. RCFs processed at 100 °C generally show low k-values, with some smaller than zero.

Variant D-F (filter cake from a fresh concrete recycling plant) showed the most noteworthy behavior: The RCF processed at 100 °C yielded a foam-like mortar with low density and low strength, resulting in $k = -0.55$, which is the lowest observed in this study. Mortars containing D-F-400 had a very stiff consistency, requiring the highest amount of superplasticizer within this study. However, the resulting k-values were among the highest, yet surpassed by D-F-600, which required less superplasticizer than its counterpart processed at 400 °C. Similar results for k were reached by other filter cake materials (G-F and H-F).

Subsequently, a linear model for the relationship between k and the mass loss Δm was fitted to the experimental results in Fig. 12 (Eq. (13)), excluding the variant D-F-100 as an outlier.

$$k = k_0 + k_m \cdot \Delta m k_0, \; k_m \text{ fit parameters} \tag{13}$$

Fit parameters k_0 and k_m were obtained through the least squares method. Predictably, $k_0 = 0.10$ roughly matches the average for RCFs processed at 100 °C (Table 3). $k_m = 4.55$ is based on direct mass loss measurements before and after thermal processing. These results, however, are possibly distorted by the decomposition of RCF components unrelated to hydration, such as organic material. The total organic carbon content (TOC) of the investigated RCFs ranges between 0.1 wt% (A2-0/2 and D-0/2) and 1.8 wt% (G-F).

Alternatively, the relevant mass loss can be obtained from thermogravimetric measurements, where the inert gas, in this case nitrogen (N_2), prevents the oxidation of carbons. By substituting Δm in Eq. (13) through the mass loss difference between

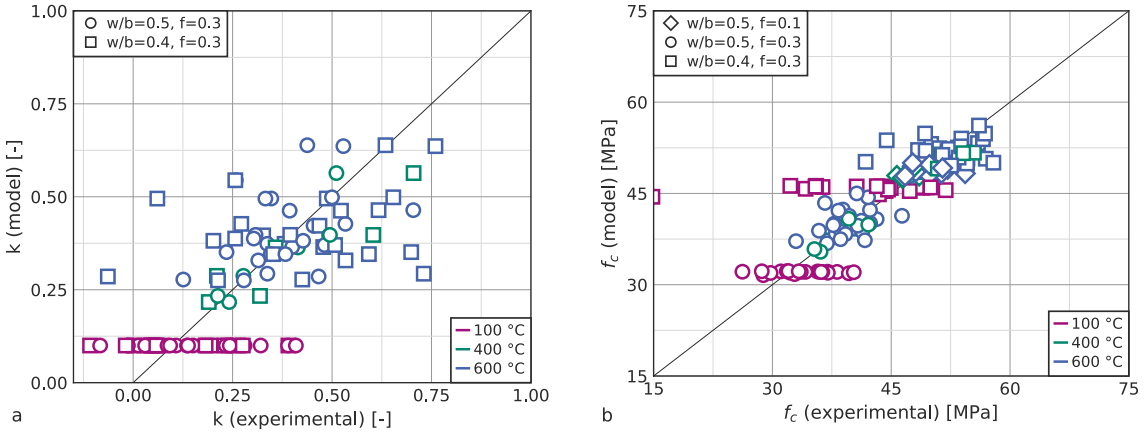

Fig. 13. Modeled k-values for a CEM I substitution rate through processed RCFs of $f = 0.3$ over k-values obtained from measurements (a) and modeled compressive strength over measured compressive strength (b). Marker shape indicates mix design, and color indicates activation temperature.

thermogravimetric measurements before and after thermal processing (Δm_{TG}), k_m increases to $k_{m,TG} = 5.30$. Eq. (15) provides an alternative interpretation of $k'_{m,TG}$. Under the assumption that Δm_{TG} comprises the total chemically bound water in cement hydration products, the parameter m_h illustrates the water consumption of one weight-unit of anhydrous cement. $k_{m,TG} = 5.30$ corresponds to $m_h = 0.23$, which agrees well with previous determinations of chemically bound water in OPC hydration products [83–85].

$$k = k_0 + k'_{m,TG} \cdot \Delta m_{TG} \tag{14}$$

$$= k_0 + \left(1 + \frac{1}{m_h}\right) \cdot \Delta m_{TG} \tag{15}$$

$$k_0,\ k'_{m,TG},\ m_h\ :\ \text{fit parameters} \tag{16}$$

Fig. 13 visualizes the individual comparison of the experimental results for compressive strength f_c and k versus their counterparts obtained from Eq. (13) in conjunction with Eq. (4) and (5). The coefficient of variation of the model for predicting k based on mass loss is mediocre with $R^2 = 0.60$. However, the scatter of the experimental and analytical results is to some extent due to the baseline scatter of the CEM I-series (compare Fig. 11). Consequently, the determination of the coefficient of determination for the extended model, which includes Eq. (5) for predicting compressive strength, yields an increase to $R^2 = 0.72$. This provides a significant improvement of the fit curve compared to SAI (Eq. (3)), even so, when only taking results for $w/b = 0.5$ and $f = 0.3$ into account, which yield $R^2 = 0.75$.

Table 4 lists the analysis of the model residuals $\Delta f_c = f_{c,\text{measured}} - f_{c,\text{modeled}}$ for different parameter combinations, which includes arithmetic means m and standard deviations s. For the reference SCMS (S, FA, and L), $m = 4.19$ means that measured compressive strength exceeds predicted compressive strength (based on k-valued from EN 206:2013) by more than 4 MPa, on average. For the base series with CEM I, and mortars including processed concrete fines, m is much smaller, since the model was fitted to the present data. The standard deviation of the residuals gives insight into the resulting deviations between measured strength results and the model, thereby allowing for a detailed analysis of the scatter. Since s for mixes containing processed concrete fines is higher than s for the CEM I base, the coefficient of variation cannot be completely explained through the scatter of CEM I. However, the present data imply this is mainly due to the high variations among RCFs processed at 100 °C. For RCFs, which were thermally activated, the residuals exhibit a lower scatter than the CEM I-mixes.

4. Conclusion and outlook

Thermal activation of recycled concrete fines (RCFs) is a promising procedure for construction and demolition waste recycling and CO_2-emission reduction as supplementary cementitious material (SCM). Industrial application requires a means for coping with variations in concrete fines composition. While usually focusing on a single precursor, comparing recent studies yields different strength activity indices (SAI), with processing temperature as the most important processing parameter.

The present study approaches this issue by processing 25 variations of 11 precursors and comparing their performance as SCM to reference materials, such as blast-furnace slag, fly ash, and limestone powder. Main findings include:

Table 4
Statistical parameters of the distribution of model residuals Δf_c for compressive strength. SCM: established SCMs (S, FA, L), f: substitution rate, T: activation temperature [°C], n: number of individual mortar mixes, m: arithmetic mean, and s: standard deviation directly calculated from Δf_c for the given parameter combinations.

	CEM I	SCM	RCF	RCF	RCF	RCF	RCF	RCF
f	–	0.3	0.3	0.3	0.1	0.3	0.1	0.3
T	–	–	all	100	400	400	600	600
n	14	10	103	41	7	12	23	50
m	−0.14	4.19	−0.18	−0.41	−0.87	0.65	1.07	−1.22
s	2.94	3.48	4.17	5.32	0.93	1.66	1.87	2.91

- Hydration heat development is accelerated and increased when CEM I is partially substituted through activated RCFs compared to reference SCMs like blast-furnace slag or fly ash. Subsequently, mortars containing processed concrete fines as SCM have a fast compressive strength development regardless of processing temperature, which is similar to CEM I and faster than fly ash or blast-furnace slag. This allows the application for structures, where fast demolding is required, e.g., in the precast industry.
- Compressive strength of mortar containing processed RCFs increases when RCFs are activated at 400 °C compared to processing at 100 °C. The positive influence of 600 °C over 400 °C is measurable, but smaller. Strength activity indices (SAI) from this study range from 0.67 to 0.81 (with two outliers) for 600 °C, and agree with findings in literature with regards to temperature dependence and scatter. Mass loss during processing is a better indicator for SAI, as RCFs with higher mass loss yield higher compressive strength.
- The present study proposes a model, which extends the k-value concept in the European standard EN 206:2013 for slag or fly ash. The compressive strength contribution of thermally processed RCFs with sufficiently high mass loss can exceed $k = 0.4$, which is the proposed k-value for fly ash, and even $k = 0.6$, which is applicable for slag.
- The determination of the mass loss of RCFs on samples in an inert atmosphere, e.g. in a thermogravimetric setup, provides a better agreement with theory, where k increases proportionally with the chemically bound water. This setup also allows for precursor screening and assessment before activation, where a lower boundary of the mass loss may serve as a compliance criterion.

However, the scatter of the obtained results underlines the necessity for additional research. The present study focuses on comparing thermally processed RCFs to established SCMs and proposing a simplified model approach for the strength contribution alongside existing provisions. The consideration of the influence of the chemical and mineralogical RCF composition may improve model accuracy for RCFs, where binder composition or aggregate reactivity varies. Besides, while the present study focuses on compressive strength development as a major concrete performance indicator, the influence of thermally activated RCFs on concrete long-term behavior requires additional research before practical application.

Furthermore, the presented model uses processed RCFs as a standalone SCM. Contemporary composite cements may consist of more than two different main constituents, which requires further development of the model. In the case of RCFs, blends with fly ash, slag, or nano silica have proven especially promising [51,53,67,86–92].

CRediT authorship contribution statement

Jan P. Höffgen: Writing – original draft, Visualization, Methodology, Funding acquisition, Formal analysis, Conceptualization. **Sebastian Bruckschlögl:** Writing – review & editing, Validation. **Bernhard Wetz:** Formal analysis. **Frank Dehn:** Writing – review & editing, Supervision, Project administration, Funding acquisition.

Declaration of Generative AI and AI-assisted technologies in the writing process

During the preparation of this work, the authors used Grammarly and DeepL in order to check for spelling and wording errors. After using these tools/services, the authors reviewed and edited the content as needed and take full responsibility for the content of the published article.

Funding

This work was supported by the Dres. Edith und Klaus Dyckerhoff-Stiftung, grant no. T0218/36374.

Declaration of competing interest

The authors declare that they have no known competing financial interests or personal relationships that could have appeared to influence the work reported in this paper.

Acknowledgments

The authors would like to thank Lukas Funk for his invaluable experimental work.

Appendix

See Fig. A.14 and Table A.5.

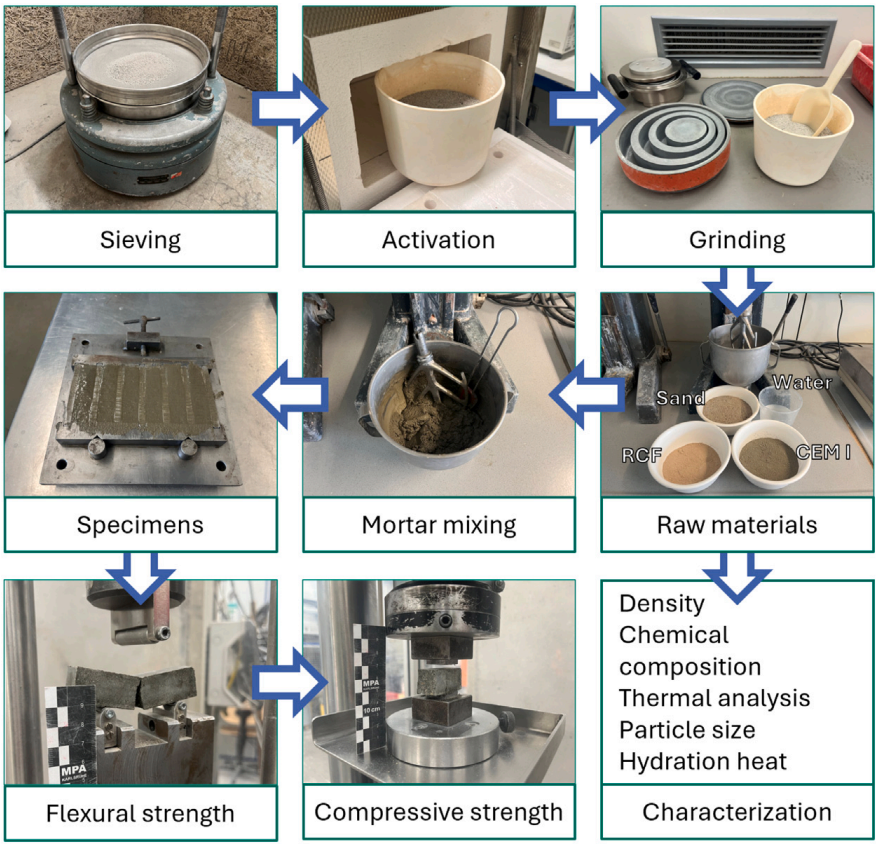

Fig. A.14. Graphical illustration of the experimental procedure.

Table A.5
Chemical composition and loss on ignition (LOI) of select RCF-variants (WDXRF in wt% according to EN 196-2:2013).

Variant	Na_2O wt%	MgO wt%	Al_2O_3 wt%	SiO_2 wt%	P_2O_5 wt%	K_2O wt%	CaO wt%	TiO_2 wt%	MnO wt%	Fe_2O_3 wt%	LOI wt%
A1-0/2	0.45	1.48	5.02	47.1	0.11	1.31	22.9	0.22	0.04	2.00	16.9
A1-0/0.25	0.48	1.64	5.48	45.2	0.12	1.33	23.1	0.25	0.04	2.22	17.4
A2-0/2	0.42	1.36	4.41	51.3	0.08	1.18	21.5	0.17	0.04	1.72	15.3
A2-0/0.25	0.41	1.72	5.10	43.1	0.10	1.19	23.4	0.22	0.05	2.10	21.2
B1-0/2	0.52	1.28	5.15	56.5	0.08	1.48	17.3	0.19	0.05	2.07	13.1
B1-0/0.25	0.51	1.49	5.48	49.0	0.10	1.44	20.4	0.22	0.05	2.19	16.2
B2-0/2	0.50	1.38	5.22	56.8	0.09	1.60	16.2	0.19	0.04	2.11	14.0
B2-0/0.25	0.52	1.86	5.99	47.7	0.10	1.63	19.7	0.25	0.05	2.37	17.3
C-0/2	0.50	1.73	5.34	56.8	0.09	1.44	15.1	0.19	0.07	1.80	14.3
C-0/0.25	0.51	2.51	6.23	45.5	0.11	1.45	19.2	0.25	0.10	2.10	19.1
D-0/2	0.61	0.76	4.36	71.7	0.05	1.11	10.5	0.18	0.03	1.08	7.3
D-0/0.25	0.73	1.41	6.04	54.1	0.09	1.22	18.9	0.34	0.05	1.79	13.2
D-F	0.43	1.86	5.84	42.7	0.09	0.76	25.1	0.27	0.06	1.60	17.6
E-0/2	0.51	1.22	5.21	51.5	0.10	1.44	19.7	0.20	0.04	1.82	15.4
E-0/0.25	0.50	1.63	6.37	42.9	0.14	1.40	23.3	0.28	0.05	2.33	18.4
F-0/2	0.63	0.94	5.27	56.3	0.10	1.61	17.4	0.21	0.04	1.75	13.7
F-0/0.25	0.70	0.91	5.23	56.7	0.10	1.58	16.7	0.22	0.05	1.78	13.9
G-F	0.70	2.02	7.23	41.1	0.15	1.46	21.9	0.31	0.10	3.31	19.8
H-F	0.34	1.65	6.00	32.7	0.22	1.07	27.8	0.26	0.04	2.72	23.3

Data availability

Data will be made available on request.

References

[1] M. Purton, Cement is a big problem for the environment. Here's how to make it more sustainable, 2024, https://www.weforum.org/stories/2024/09/cement-production-sustainable-concrete-co2-emissions/.
[2] Verein Deutscher Zementwerke, Environmental Data of the German Cement Industry 2023, Tech. rep., Düsseldorf, 2024.
[3] D. Coffetti, E. Crotti, G. Gazzaniga, M. Carrara, T. Pastore, L. Coppola, Pathways towards sustainable concrete, Cem. Concr. Res. 154 (2022) 106718, http://dx.doi.org/10.1016/j.cemconres.2022.106718.
[4] I.G. Richardson, The nature of the hydration products in hardened cement pastes, Cem. Concr. Compos. 22 (2) (2000) 97–113, http://dx.doi.org/10.1016/S0958-9465(99)00036-0.
[5] K.L. Scrivener, P. Juilland, P.J. Monteiro, Advances in understanding hydration of Portland cement, Cem. Concr. Res. 78 (2015) 38–56, http://dx.doi.org/10.1016/j.cemconres.2015.05.025.
[6] D.K. Panesar, R. Zhang, Performance comparison of cement replacing materials in concrete: Limestone fillers and supplementary cementing materials – A review, Constr. Build. Mater. 251 (2020) 118866, http://dx.doi.org/10.1016/j.conbuildmat.2020.118866.
[7] R. Snellings, P. Suraneni, J. Skibsted, Future and emerging supplementary cementitious materials, Cem. Concr. Res. 171 (2023) 107199, http://dx.doi.org/10.1016/j.cemconres.2023.107199.
[8] C. Orozco, S. Babel, S. Tangtermsirikul, T. Sugiyama, Comparison of environmental impacts of fly ash and slag as cement replacement materials for mass concrete and the impact of transportation, Sustain. Mater. Technol. 39 (2024) e00796, http://dx.doi.org/10.1016/j.susmat.2023.e00796.
[9] G.L. Golewski, Using digital image correlation to evaluate fracture toughness and crack propagation in the mode I testing of concretes involving fly ash and synthetic nano-SiO_2, Mater. Res. Express 11 (9) (2024) 095504, http://dx.doi.org/10.1088/2053-1591/ad755e.
[10] G.L. Golewski, Investigating the effect of using three pozzolans (including the nanoadditive) in combination on the formation and development of cracks in concretes using non-contact measurement method, Adv. Nano Res. 16 (3) (2024) 217–229, http://dx.doi.org/10.12989/ANR.2024.16.3.217.
[11] Y. Gao, G. Schutter, G. Ye, Z. Yu, Z. Tan, K. Wu, A microscopic study on ternary blended cement based composites, Constr. Build. Mater. 46 (2013) 28–38, http://dx.doi.org/10.1016/j.conbuildmat.2013.04.021.
[12] K.A. Knight, P.R. Cunningham, S.A. Miller, Optimizing supplementary cementitious material replacement to minimize the environmental impacts of concrete, Cem. Concr. Compos. 139 (2023) 105049, http://dx.doi.org/10.1016/j.cemconcomp.2023.105049.
[13] M. Barthel, K. Rübner, H.-C. Kühne, A. Rogge, F. Dehn, From waste materials to products for use in the cement industry, Adv. Cem. Res. 28 (7) (2016) 458–468, http://dx.doi.org/10.1680/jadcr.15.00149.
[14] F. Friol Guedes de Paiva, J.R. Tamashiro, L.H. Pereira Silva, A. Kinoshita, Utilization of inorganic solid wastes in cementitious materials – A systematic literature review, Constr. Build. Mater. 285 (2021) 122833, http://dx.doi.org/10.1016/j.conbuildmat.2021.122833.
[15] A. Carriço, J.A. Bogas, M. Guedes, Thermoactivated cementitious materials – A review, Constr. Build. Mater. 250 (2020) 118873, http://dx.doi.org/10.1016/j.conbuildmat.2020.118873.
[16] E.A. Ohemeng, S.O. Ekolu, A review on the reactivation of hardened cement paste and treatment of recycled aggregates, Mag. Concr. Res. 72 (10) (2020) 526–539, http://dx.doi.org/10.1680/jmacr.18.00452.
[17] L. Xu, J. Wang, K. Li, S. Lin, M. Li, T. Hao, Z. Ling, D. Xiang, T. Wang, A systematic review of factors affecting properties of thermal-activated recycled cement, Resour. Conserv. Recycl. 185 (2022) 106432, http://dx.doi.org/10.1016/j.resconrec.2022.106432.
[18] J.H. Aquino Rocha, R.D. Toledo Filho, The utilization of recycled concrete powder as supplementary cementitious material in cement-based materials: A systematic literature review, J. Build. Eng. 76 (2023) 107319, http://dx.doi.org/10.1016/j.jobe.2023.107319.
[19] Y. Zheng, X. Xi, H. Liu, C. Du, H. Lu, A review: Enhanced performance of recycled cement and CO2 emission reduction effects through thermal activation and nanosilica incorporation, Constr. Build. Mater. 422 (2024) 135763, http://dx.doi.org/10.1016/j.conbuildmat.2024.135763.
[20] R.V. Silva, J. Brito, R.K. Dhir, Properties and composition of recycled aggregates from construction and demolition waste suitable for concrete production, Constr. Build. Mater. 65 (2014) 201–217, http://dx.doi.org/10.1016/j.conbuildmat.2014.04.117.
[21] M. Nedeljković, J. Visser, B. Šavija, S. Valcke, E. Schlangen, Use of fine recycled concrete aggregates in concrete: A critical review, J. Build. Eng. 38 (2021) 102196, http://dx.doi.org/10.1016/j.jobe.2021.102196.
[22] S.K. Kaliyavaradhan, T.-C. Ling, K.H. Mo, Valorization of waste powders from cement-concrete life cycle: A pathway to circular future, J. Clean. Prod. 268 (2020) 122358, http://dx.doi.org/10.1016/j.jclepro.2020.122358.
[23] J. Li, X. Deng, Z. Lu, X. Li, L. Hou, J. Jiang, F. Yang, J. Zhang, K. He, Recycled concrete fines as a supplementary cementitious material: Mechanical performances, hydration, and microstructures in cementitious systems, Case Stud. Constr. Mater. 21 (2024) e03575, http://dx.doi.org/10.1016/j.cscm.2024.e03575.
[24] J.H.A. Rocha, R.D. Toledo Filho, Physical-mechanical assessment to mortars including recycled concrete powder and metakaolin, Case Stud. Constr. Mater. 21 (2024) e03996, http://dx.doi.org/10.1016/j.cscm.2024.e03996.
[25] Y. Yang, J. Xu, P. Gao, B. Zhan, Q. Yu, M. Ni, Y. Zhang, Study on the hydration characteristics and mechanical properties of recycled powder-slag powder-cement system, Case Stud. Constr. Mater. 21 (2024) e03952, http://dx.doi.org/10.1016/j.cscm.2024.e03952.
[26] T.F. Baggio, E. Possan, J.J. De Oliveira Andrade, Physical-chemical characterization of construction and demolition waste powder with thermomechanical activation for use as supplementary cementitious material, Constr. Build. Mater. 437 (2024) 136907, http://dx.doi.org/10.1016/j.conbuildmat.2024.136907.
[27] R. Baldusco, T.R.S. Nobre, S.C. Angulo, V.A. Quarcioni, M.A. Cincotto, Dehydration and rehydration of blast furnace slag cement, J. Mater. Civ. Eng. 31 (8) (2019) 04019132, http://dx.doi.org/10.1061/(ASCE)MT.1943-5533.0002725.
[28] S.C. Angulo, M.S. Guilge, V.A. Quarcioni, M.A. Cincotto, T.R. Nobre, H. Pöllmann, The role of calcium silicates and quicklime on the reactivity of rehydrated cements, Constr. Build. Mater. 340 (2022) 127625, http://dx.doi.org/10.1016/j.conbuildmat.2022.127625.
[29] J. Zelic, L. Ugrina, D. Jozic, Application of thermal methods in the chemistry of cement: kinetic analysis of portlandite from non-isothermal thermogravimetric data, in: The First International Proficiency Testing Conference, Sinaia, Romania, 2007, pp. 420–429.
[30] Q. Zhou, F.P. Glasser, Thermal stability and decomposition mechanisms of ettringite at <120°C, Cem. Concr. Res. 31 (9) (2001) 1333–1339, http://dx.doi.org/10.1016/S0008-8846(01)00558-0.
[31] Q. Zhou, E.E. Lachowski, F.P. Glasser, Metaettringite, a decomposition product of ettringite, Cem. Concr. Res. 34 (4) (2004) 703–710, http://dx.doi.org/10.1016/j.cemconres.2003.10.027.
[32] L.G. Baquerizo, T. Matschei, K.L. Scrivener, Impact of water activity on the stability of ettringite, Cem. Concr. Res. 79 (2016) 31–44, http://dx.doi.org/10.1016/j.cemconres.2015.07.008.
[33] J. Wang, L. Lacarrière, A. Sellier, Multicomponent modelling of cement paste dehydration under different heating rates, Mater. Struct. 52 (1) (2019) 6, http://dx.doi.org/10.1617/s11527-018-1306-9.

[34] I. Horváth, I. Proks, I. Nerád, Activation energies of the thermal decompositions of C3AH6 AND C3AD6 by the isothermal TG method, J. Therm. Anal. 12 (1) (1977) 105–110, http://dx.doi.org/10.1007/BF01909862.
[35] Z. He, X. Zhu, J. Wang, M. Mu, Y. Wang, Comparison of CO2 emissions from OPC and recycled cement production, Constr. Build. Mater. 211 (2019) 965–973, http://dx.doi.org/10.1016/j.conbuildmat.2019.03.289.
[36] V. Sousa, J.A. Bogas, Comparison of energy consumption and carbon emissions from clinker and recycled cement production, J. Clean. Prod. 306 (2021) 127277, http://dx.doi.org/10.1016/j.jclepro.2021.127277.
[37] S. Real, V. Sousa, I. Meireles, J.A. Bogas, A. Carriço, Life cycle assessment of thermoactivated recycled cement production, Mater. (Basel, Switzerland) 15 (19) (2022) http://dx.doi.org/10.3390/ma15196766.
[38] V. Sousa, J.A. Bogas, S. Real, I. Meireles, Industrial production of recycled cement: Energy consumption and carbon dioxide emission estimation, Environ. Sci. Pollut. Res. 30 (4) (2022) 8778–8789, http://dx.doi.org/10.1007/s11356-022-20887-7.
[39] V. Sousa, J.A. Bogas, S. Real, I. Meireles, A. Carriço, Recycled cement production energy consumption optimization, Sustain. Chem. Pharm. 32 (2023) 101010, http://dx.doi.org/10.1016/j.scp.2023.101010.
[40] J.A. Bogas, S. Real, A. Carriço, J. Abrantes, M. Guedes, Hydration and phase development of recycled cement, Cem. Concr. Compos. 127 (2022) 104405, http://dx.doi.org/10.1016/j.cemconcomp.2022.104405.
[41] C. Alonso, L. Fernandez, Dehydration and rehydration processes of cement paste exposed to high temperature environments, J. Mater. Sci. 39 (9) (2004) 3015–3024, http://dx.doi.org/10.1023/B:JMSC.0000025827.65956.18.
[42] P. Ge, Y. Song, J. Quan, Y. Wu, J. Zhou, Study on the activity, phase, thermal decomposition characteristics, microstructure, and chemical element of hardened cement powder under heating temperature of 100 °C~1200 °C, Struct. Concr. (2024) http://dx.doi.org/10.1002/suco.202301108, suco.202301108.
[43] N. Noel, T. Mielke, G. Semugaza, A.Z. Gierth, S. Helmich, S. Nawrath, D.C. Lupascu, Chemical transformations during the preparation and rehydration of reactivated virgin cements, Cement 19 (2025) 100129, http://dx.doi.org/10.1016/j.cement.2025.100129.
[44] E. Tajuelo Rodriguez, K. Garbev, D. Merz, L. Black, I.G. Richardson, Thermal stability of C-S-H phases and applicability of Richardson and Groves' and Richardson C-(A)-S-H(I) models to synthetic C-S-H, Cem. Concr. Res. 93 (2017) 45–56, http://dx.doi.org/10.1016/j.cemconres.2016.12.005.
[45] A. Carriço, S. Real, J.A. Bogas, M.F. Costa Pereira, Mortars with thermo activated recycled cement: Fresh and mechanical characterisation, Constr. Build. Mater. 256 (2020) 119502, http://dx.doi.org/10.1016/j.conbuildmat.2020.119502.
[46] S. Real, A. Carriço, J.A. Bogas, M. Guedes, Influence of the treatment temperature on the microstructure and hydration behavior of thermoactivated recycled cement, Materials 13 (18) (2020) 3937, http://dx.doi.org/10.3390/ma13183937.
[47] R. Serpell, F. Zunino, Recycling of hydrated cement pastes by synthesis of α'H-C2S, Cem. Concr. Res. 100 (2017) 398–412, http://dx.doi.org/10.1016/j.cemconres.2017.08.001.
[48] R. Yu, Z. Shui, Influence of agglomeration of a recycled cement additive on the hydration and microstructure development of cement based materials, Constr. Build. Mater. 49 (2013) 841–851, http://dx.doi.org/10.1016/j.conbuildmat.2013.09.004.
[49] X. Xi, Y. Zheng, C. Du, P. Zhang, M. Sun, Study on the hydration characteristics, mechanical properties, and microstructure of thermally activated low-carbon recycled cement, Constr. Build. Mater. 447 (2024) 138042, http://dx.doi.org/10.1016/j.conbuildmat.2024.138042.
[50] J.A. Bogas, A. Carriço, A.J. Tenza-Abril, Microstructure of thermoactivated recycled cement pastes, Cem. Concr. Res. 138 (2020) 106226, http://dx.doi.org/10.1016/j.cemconres.2020.106226.
[51] R. Serpell, M. Lopez, Properties of mortars produced with reactivated cementitious materials, Cem. Concr. Compos. 64 (2015) 16–26, http://dx.doi.org/10.1016/j.cemconcomp.2015.08.003.
[52] M. Wei, L. Chen, N. Lei, H. Li, L. Huang, Mechanical properties and microstructures of thermally activated ultrafine recycled fine powder cementitious materials, Constr. Build. Mater. 475 (2025) 141195, http://dx.doi.org/10.1016/j.conbuildmat.2025.141195.
[53] Z. Shui, D. Xuan, H. Wan, B. Cao, Rehydration reactivity of recycled mortar from concrete waste experienced to thermal treatment, Constr. Build. Mater. 22 (8) (2008) 1723–1729, http://dx.doi.org/10.1016/j.conbuildmat.2007.05.012.
[54] J.A. Bogas, A. Carriço, S. Real, Durability of concrete produced with recycled cement from waste concrete, Mater. Today: Proc. 58 (2022) 1149–1154, http://dx.doi.org/10.1016/j.matpr.2022.01.280.
[55] V. Letelier, E. Tarela, P. Muñoz, G. Moriconi, Combined effects of recycled hydrated cement and recycled aggregates on the mechanical properties of concrete, Constr. Build. Mater. 132 (2017) 365–375, http://dx.doi.org/10.1016/j.conbuildmat.2016.12.010.
[56] Z. Ma, J. Shen, H. Wu, P. Zhang, Properties and activation modification of eco-friendly cementitious materials incorporating high-volume hydrated cement powder from construction waste, Constr. Build. Mater. 316 (2022) 125788, http://dx.doi.org/10.1016/j.conbuildmat.2021.125788.
[57] D. Qian, R. Yu, Z. Shui, Y. Sun, C. Jiang, F. Zhou, M. Ding, X. Tong, Y. He, A novel development of green ultra-high performance concrete (UHPC) based on appropriate application of recycled cementitious material, J. Clean. Prod. 261 (2020) 121231, http://dx.doi.org/10.1016/j.jclepro.2020.121231.
[58] A. Tokareva, S. Kaassamani, D. Waldmann, Fine demolition wastes as supplementary cementitious materials for CO2 reduced cement production, Constr. Build. Mater. 392 (2023) 131991, http://dx.doi.org/10.1016/j.conbuildmat.2023.131991.
[59] P. Vashistha, Y. Oinam, H.-K. Kim, S. Pyo, Effect of thermo-mechanical activation of waste concrete powder (WCP) on the characteristics of cement mixtures, Constr. Build. Mater. 362 (2023) 129713, http://dx.doi.org/10.1016/j.conbuildmat.2022.129713.
[60] H. Wu, C. Liang, Z. Zhang, P. Yao, C. Wang, Z. Ma, Utilizing heat treatment for making low-quality recycled aggregate into enhanced recycled aggregate, recycled cement and their fully recycled concrete, Constr. Build. Mater. 394 (2023) 132126, http://dx.doi.org/10.1016/j.conbuildmat.2023.132126.
[61] J. Chen, J. Plank, Alkali-activated calcined clay blended cement: Effect of NaOH activator on performance of HPEG PCEs and on early strength, Cem. Concr. Res. 183 (2024) 107588, http://dx.doi.org/10.1016/j.cemconres.2024.107588.
[62] Z. He, R. Hu, Z. Ma, X. Liu, C. Wang, H. Wu, Reusing thermoactivated construction waste spoil as sustainable binder for durable concrete: Microstructure and chloride transport, Constr. Build. Mater. 398 (2023) 132553, http://dx.doi.org/10.1016/j.conbuildmat.2023.132553.
[63] J. Kim, N. Kim, Exploring the role of thermal activation of cement exposed to the external environment on the improvement of concrete properties, J. Mater. Res. Technol. 24 (2023) 2868–2878, http://dx.doi.org/10.1016/j.jmrt.2023.03.195.
[64] J. Kim, A. Ubysz, Thermal activation of multi-recycled concrete powder as supplementary cementitious material for repeated and waste-free recycling, J. Build. Eng. 98 (2024) 111169, http://dx.doi.org/10.1016/j.jobe.2024.111169.
[65] G. Semugaza, T. Mielke, M.E. Castillo, A.Z. Gierth, J.X. Tam, S. Nawrath, D.C. Lupascu, Reactivation of hydrated cement powder by thermal treatment for partial replacement of ordinary portland cement, Mater. Struct. 56 (3) (2023) http://dx.doi.org/10.1617/s11527-023-02133-9.
[66] Y. Sui, C. Ou, S. Liu, J. Zhang, Q. Tian, Study on properties of waste concrete powder by thermal treatment and application in mortar, Appl. Sci. 10 (3) (2020) 998, http://dx.doi.org/10.3390/app10030998.
[67] J. Wang, M. Mu, Y. Liu, Recycled cement, Constr. Build. Mater. 190 (2018) 1124–1132, http://dx.doi.org/10.1016/j.conbuildmat.2018.09.181.
[68] L. Xu, J. Wang, K. Li, T. Hao, Z. Li, L. Li, B. Ran, H. Du, New insights on dehydration at elevated temperature and rehydration of GGBS blended cement, Cem. Concr. Compos. 139 (2023) 105068, http://dx.doi.org/10.1016/j.cemconcomp.2023.105068.
[69] H. Zhang, B. Zhang, L. Tang, W. Zeng, Analysis of two processing techniques applied on powders from recycling of clay bricks and concrete, in terms of efficiency, energy consumption, and cost, Constr. Build. Mater. 385 (2023) 131517, http://dx.doi.org/10.1016/j.conbuildmat.2023.131517.
[70] E.W. Klingsch, Explosive Spalling of Concrete in Fire (Ph.D. thesis), ETH Zurich, Zürich, 2014, http://dx.doi.org/10.3929/ethz-a-010243000.
[71] H. Wu, D. Yang, Z. Ma, Micro-structure, mechanical and transport properties of cementitious materials with high-volume waste concrete powder and thermal modification, Constr. Build. Mater. 313 (2021) 125477, http://dx.doi.org/10.1016/j.conbuildmat.2021.125477.

[72] A. Lipowsky, A. Müller, Gesteinsmehl als Zuschlagstoffe in hydraulischen Bindemitteln, Aufbereitungs-Technik/Mineral Process. 58 (12) (2017) 52–64.
[73] L. Chen, M. Wei, N. Lei, H. Li, Effect of chemical–thermal activation on the properties of recycled fine powder cementitious materials, Case Stud. Constr. Mater. 20 (2024) e02956, http://dx.doi.org/10.1016/j.cscm.2024.e02956.
[74] M. Wei, L. Chen, N. Lei, H. Li, L. Huang, Experimental investigation on freeze–thaw resistance of thermally activated recycled fine powder concrete, Constr. Build. Mater. 457 (2024) 139378, http://dx.doi.org/10.1016/j.conbuildmat.2024.139378.
[75] D. Zhang, S. Zhang, B. Huang, Q. Yang, J. Li, Comparison of mechanical, chemical, and thermal activation methods on the utilisation of recycled concrete powder from construction and demolition waste, J. Build. Eng. 61 (2022) 105295, http://dx.doi.org/10.1016/j.jobe.2022.105295.
[76] J.A. Bogas, A. Carriço, M. Pereira, Mechanical characterization of thermal activated low-carbon recycled cement mortars, J. Clean. Prod. 218 (2019) 377–389, http://dx.doi.org/10.1016/j.jclepro.2019.01.325.
[77] K. Kalinowska-Wichrowska, M. Kosior-Kazberuk, E. Pawluczuk, The properties of composites with recycled cement mortar used as a supplementary cementitious material, Materials 13 (1) (2020) 64, http://dx.doi.org/10.3390/ma13010064.
[78] A. Carriço, S. Real, J.A. Bogas, Durability performance of thermoactivated recycled cement concrete, Cem. Concr. Compos. 124 (2021) http://dx.doi.org/10.1016/j.cemconcomp.2021.104270.
[79] S. Real, J.A. Bogas, A. Carriço, S. Hu, Mechanical characterisation and shrinkage of thermoactivated recycled cement concrete, Appl. Sci. 11 (6) (2021) 2454, http://dx.doi.org/10.3390/app11062454.
[80] C. Herget, A. Müller, T. Proske, M. Rezvani, C.-A. Graubner, Kalksteinmehl als Betonzusatzstoff – Vorschlag für die Anrechenbarkeit auf den Zementgehalt und Potenzial zur CO_2 -Reduktion im Betonbau, Beton- Und Stahlbetonbau 117 (2) (2022) 109–118, http://dx.doi.org/10.1002/best.202100073.
[81] W. Brameshuber, Sonderbetone für Tübbinge, in: R. Nothnagel, H. Twelmeier (Eds.), Baustoff Und Konstruktion, Springer Berlin Heidelberg, Berlin, Heidelberg, 2012, pp. 105–112, http://dx.doi.org/10.1007/978-3-642-29573-7.
[82] K. Weise, Die Reaktivität von Hüttensand als Betonzusatzstoff, Springer Fachmedien Wiesbaden, Wiesbaden, 2018, http://dx.doi.org/10.1007/978-3-658-20492-1.
[83] T.C. Powers, T.L. Brownyard, Studies of the physical properties of hardened portland cement paste, ACI J. Proc. 43 (9) (1946) 249–336, http://dx.doi.org/10.14359/15301.
[84] H. Brouwers, The work of powers and brownyard revisited: Part 1, Cem. Concr. Res. 34 (9) (2004) 1697–1716, http://dx.doi.org/10.1016/j.cemconres.2004.05.031.
[85] P. Lura, F. Winnefeld, X. Fang, A simple method for determining the total amount of physically and chemically bound water of different cements, J. Therm. Anal. Calorim. 130 (2) (2017) 653–660, http://dx.doi.org/10.1007/s10973-017-6513-z.
[86] L. Lu, Y. He, S. Hu, Binding materials of dehydrated phases of waste hardened cement paste and pozzolanic admixture, J. Wuhan Univ. Technol.-Mater. Sci. Ed. 24 (1) (2009) 140–144, http://dx.doi.org/10.1007/s11595-009-1140-6.
[87] R. Yu, Z. Shui, Efficient reuse of the recycled construction waste cementitious materials, J. Clean. Prod. 78 (2014) 202–207, http://dx.doi.org/10.1016/j.jclepro.2014.05.003.
[88] A. Yonis, Y. Oinam, P. Vashistha, A.B. Degefa, G.B. Belayneh, S. Park, S. Pyo, Novel activation method of waste concrete powder for sustainable clinker-free binder, Cem. Concr. Compos. 151 (2024) 105600, http://dx.doi.org/10.1016/j.cemconcomp.2024.105600.
[89] L. Zhang, J. Yongsheng, H. Guodong, J. Li, Y. Hu, Modification and enhancement of mechanical properties of dehydrated cement paste using ground granulated blast-furnace slag, Constr. Build. Mater. (164) (2018) 525–534, http://dx.doi.org/10.1016/j.conbuildmat.2017.12.232.
[90] Y. Jiang, Q. Ji, L. Feng, W. Luo, X. Wen, S. Chu, Ultra-green cement: Limestone calcined clay cement (LC3) with recycled cement, Cem. Concr. Compos. 163 (2025) 106210, http://dx.doi.org/10.1016/j.cemconcomp.2025.106210.
[91] X. Xi, Y. Zheng, J. Zhuo, P. Zhang, G.L. Golewski, C. Du, Influence of water glass modulus and alkali content on the properties of alkali-activated thermally activated recycled cement, Constr. Build. Mater. 452 (2024) 138867, http://dx.doi.org/10.1016/j.conbuildmat.2024.138867.
[92] X. Xi, Y. Zheng, J. Zhuo, P. Zhang, G.L. Golewski, C. Du, Mechanical properties and hydration mechanism of nano-silica modified alkali-activated thermally activated recycled cement, J. Build. Eng. 98 (2024) 110998, http://dx.doi.org/10.1016/j.jobe.2024.110998.

Supplementary Data to Paper P1

Tab. A1: Mass loss Δm of ground concrete fines at selected temperatures in a thermogravimetric setup (P1, fig. 6).

	200 °C	400 °C	600 °C	800 °C	1000 °C	1200 °C
A1-0/0.25	0.021	0.044	0.060	0.105	0.178	0.181
A1-0/2	0.007	0.027	0.040	0.082	0.164	0.166
A2-0/0.25	0.009	0.031	0.049	0.102	0.188	0.191
A2-0/2	0.015	0.031	0.044	0.095	0.181	0.185
B1-0/0.25	0.027	0.053	0.071	0.125	0.169	0.171
B1-0/2	0.020	0.042	0.057	0.101	0.135	0.137
B2-0/0.25	0.028	0.050	0.069	0.134	0.187	0.189
B2-0/2	0.020	0.036	0.050	0.098	0.142	0.144
C-0/0.25	0.034	0.060	0.080	0.146	0.202	0.204
C-0/2	0.025	0.043	0.058	0.106	0.149	0.150
D-0/0.25	0.038	0.077	0.092	0.126	0.141	0.144
D-0/2	0.021	0.040	0.049	0.072	0.075	0.077
D-F	0.045	0.101	0.126	0.165	0.183	0.187
E-0/0.25	0.035	0.065	0.085	0.132	0.190	0.193
E-0/2	0.025	0.046	0.060	0.102	0.162	0.164
F-0/0.25	0.019	0.034	0.047	0.096	0.141	0.143
F-0/2	0.020	0.035	0.048	0.096	0.139	0.141
G-F	0.031	0.059	0.080	0.144	0.209	0.213
H-F	0.027	0.058	0.093	0.203	0.246	0.251

Tab. A2: Particle size distributions of reference binders and processed concrete fines (P1, table 2). d_i: particle size at i % passing [µm].

	d_{10}	d_{30}	d_{50}	d_{70}	d_{90}
CEM I	1.7	5.9	12.1	20.6	32.9
S	2.1	6.6	12.3	19.5	30.0
FA	2.9	9.9	21.6	43.3	83.4
L	1.9	6.8	12.5	20.7	44.4
A1-0/0.25-100	1.9	6.6	15.6	31.8	58.8
A1-0/0.25-600	1.6	5.3	13.5	30.3	60.8
A1-0/2-100	2.3	8.1	18.2	35.2	65.9
A1-0/2-600	2.3	8.9	20.8	39.2	70.4
A2-0/0.25-600	1.4	3.9	8.5	17.5	36.9
A2-0/2-600	1.5	4.2	10.1	22.4	48.1
B1-0/0.25-100	1.6	4.9	11.6	25.4	50.4
B1-0/0.25-400	1.7	5.4	12.1	24.2	47.3
B1-0/0.25-600	1.7	5.6	13.9	32.3	63.7
B1-0/2-100	1.4	4.0	9.4	20.9	43.2
B1-0/2-400	1.7	5.3	11.8	23.7	46.4
B1-0/2-600	1.6	5.1	12.4	27.1	53.5
B2-0/0.25-100	1.5	4.8	11.4	24.9	49.3
B2-0/0.25-600	2.0	6.7	15.4	32.0	61.6
B2-0/2-100	1.5	4.7	11.4	25.4	50.2
B2-0/2-600	1.5	4.9	12.8	30.1	62.6
C-0/0.25-100	1.5	4.7	11.4	24.4	48.2
C-0/0.25-600	2.1	7.0	15.9	32.1	59.8
C-0/2-100	1.5	4.6	11.1	24.1	47.8
C-0/2-600	1.5	4.6	11.3	25.2	52.4
D-0/0.25-100	2.1	6.9	15.4	30.4	57.3
D-0/0.5-600	1.7	5.1	11.7	24.9	50.5
D-0/2-100	2.0	7.0	16.4	32.9	61.6
D-0/2-400	2.2	7.5	16.9	32.4	58.8
D-0/2-600	2.1	6.8	15.6	30.8	57.5
D-F-100	2.8	7.8	14.5	29.3	57.3
D-F-400	2.9	7.1	12.5	23.0	47.2
D-F-600	2.5	6.1	10.9	19.6	40.9
E-0/0.25-100	2.3	7.6	17.0	34.1	63.3
E-0/0.25-600	2.1	6.7	15.0	29.9	56.8
E-0/2-100	1.7	4.9	11.0	24.0	50.5
E-0/2-400	1.8	5.5	12.4	25.5	51.3
E-0/2-600	1.7	5.3	12.2	25.5	51.7
F-0/0.25-100	1.6	5.3	13.2	29.7	58.9
F-0/0.25-600	1.5	4.9	12.2	26.0	51.0
F-0/2-100	1.9	6.3	14.9	30.9	59.7
F-0/2-400	1.8	5.9	13.9	28.8	56.4
F-0/2-600	1.8	5.7	13.4	27.0	51.7
G-F-100	1.8	5.4	11.2	20.7	38.8
G-F-400	1.8	5.6	11.9	22.1	40.7
G-F-600	1.8	5.1	10.9	20.9	40.3
H-F-100	1.8	4.7	9.2	18.0	38.0
H-F-600	1.9	4.6	8.6	17.5	43.6

Tab. A3: Results of hydration heat measurements on blended cement paste containing established SCMs or processed industrial fines (P1, fig. 7). Double determinations; for CEM I: eightfold determination including standard deviation.

	$Q_{0.5\,\mathrm{h}}$ J/g	t_b h	W_{t_b} mW/g	Q_{t_b} J/g	t_p h	W_{t_p} mW/g	Q_{t_p} J/g	$Q_{5\,\mathrm{d}}$ J/g
CEM I	18.8	2.4	0.4	23.2	11.4	2.8	72.5	296.8
	±1.4	±0.1	±0.0	±1.2	±0.2	±0.1	±1.8	±8.3
S	12.5	2.6	0.3	15.9	11.6	2.1	55.4	251.9
FA	12.7	2.8	0.3	16.3	11.9	1.9	52.4	228.1
L	11.6	2.0	0.4	14.5	10.2	2.0	51.7	228.2
A1-0/0.25-600	15.5	2.7	0.4	19.8	11.8	2.0	61.5	248.9
A1-0/2-600	14.4	2.7	0.3	18.3	11.8	2.0	57.9	239.3
A2-0/0.25-600	13.1	2.6	0.4	17.5	11.5	1.9	56.7	237.7
A2-0/2-600	12.3	2.5	0.4	16.3	11.2	2.0	56.1	239.1
B1-0/0.25-600	16.3	2.9	0.4	22.1	11.6	2.0	63.8	248.6
B1-0/2-600	16.2	2.8	0.4	21.0	11.7	2.0	62.1	247.3
B2-0/0.25-600	14.5	2.6	0.4	18.8	11.3	2.1	61.1	249.3
B2-0/2-600	14.1	2.6	0.3	17.9	11.7	2.0	58.1	242.0
C-0/0.25-600	15.4	2.8	0.5	21.2	11.2	2.1	63.0	250.8
C-0/2-600	14.8	2.7	0.4	20.0	11.3	2.0	60.2	247.2
D-F-0/0.25-600	30.3	3.7	0.8	49.4	8.2	1.5	69.2	288.3
D-K-0/0.25-600	22.4	3.2	0.5	31.4	10.8	1.9	68.9	256.4
D-K-0/2-600	16.4	3.0	0.4	22.1	11.7	1.9	61.8	244.7
G-F-0/0.25-600	15.3	2.6	0.5	20.6	10.8	2.2	63.5	259.4

Tab. A4: Compressive strength of reference mortar mixes.

	f –	$\frac{w}{b}$ –	$\frac{w+FM}{b}$ –	$f_{c,2\,\mathrm{d}}$ MPa	$f_{c,28\,\mathrm{d}}$ MPa
CEM I		0.45	0.45	33.0(9)	53.7(16)
CEM I		0.50	0.50	23.5(20)	50.9(9)
CEM I		0.55	0.55	22.3(5)	46.3(12)
CEM I		0.60	0.60	18.3(4)	38.8(18)
CEM I		0.45	0.45	35.2(8)	60.9(16)
CEM I		0.50	0.50	28.2(13)	55.9(15)
CEM I		0.55	0.55	24.5(11)	50.7(16)
CEM I		0.60	0.60	19.4(5)	44.8(13)
CEM I		0.40	0.41	44.5(8)	60.3(32)
CEM I		0.45	0.45	35.9(6)	54.2(30)
CEM I		0.50	0.50	29.6(7)	53.1(14)
CEM I		0.55	0.55	25.5(2)	47.2(11)
CEM I		0.60	0.60	18.3(5)	37.7(8)
CEM I		0.65	0.65	14.9(7)	33.2(11)
FA	0.1	0.50	0.50	26.7(9)	52.0(11)
FA	0.3	0.40	0.41	27.8(4)	60.5(20)
FA	0.3	0.40	0.41	27.4(7)	52.8(10)
FA	0.3	0.50	0.50	14.6(18)	42.9(6)
FA	0.3	0.50	0.50	18.9(6)	40.0(7)
FA	0.5	0.50	0.51	10.9(2)	30.8(10)
S	0.1	0.50	0.50	26.9(8)	54.9(26)
S	0.3	0.40	0.40	32.7(9)	66.5(28)
S	0.3	0.45	0.45	27.1(3)	63.2(22)
S	0.3	0.50	0.50	19.7(5)	49.0(32)
S	0.3	0.50	0.50	19.7(6)	48.4(17)
S	0.5	0.50	0.50	14.9(3)	48.7(15)
L	0.1	0.50	0.50	27.5(7)	51.7(34)
L	0.3	0.35	0.36	36.2(5)	56.3(14)
L	0.3	0.40	0.40	26.4(7)	43.9(28)
L	0.3	0.50	0.50	13.6(9)	35.0(8)
L	0.3	0.50	0.50	17.9(5)	35.8(19)
L	0.5	0.50	0.50	9.9(3)	21.8(6)

Tab. A5: Compressive strength of mortar containing processed industrial fines (part 1).

	Temp. °C	f –	$\frac{w}{b}$ –	$\frac{w+FM}{b}$ –	Δm –	$f_{c,2\,\mathrm{d}}$ MPa	$f_{c,28\,\mathrm{d}}$ MPa
A1-0/0.125	100	0.3	0.5	0.50	0.000	14.5(5)	28.9(6)
A1-0/0.125	100	0.3	0.4	0.51	0.000	23.0(5)	43.4(13)
A1-0/0.125	600	0.1	0.5	0.41	0.059	27.4(6)	48.5(12)
A1-0/0.125	600	0.3	0.5	0.50	0.059	20.2(5)	41.3(18)
A1-0/0.125	600	0.3	0.4	0.50	0.059	30.4(8)	53.5(10)
A1-0/0.25u	600	0.1	0.5	0.50	0.054	27.0(9)	47.6(10)
A1-0/0.25u	600	0.3	0.5	0.50	0.054	19.8(4)	39.2(7)
A1-0/0.25u	600	0.3	0.4	0.50	0.054	29.7(5)	54.6(7)
A1-0/0.25	100	0.3	0.5	0.41	0.000	18.6(3)	32.8(12)
A1-0/0.25	600	0.1	0.5	0.41	0.054	30.1(10)	54.3(32)
A1-0/0.25	600	0.3	0.5	0.50	0.054	21.9(4)	38.7(7)
A1-0/0.25	600	0.3	0.4	0.50	0.054	32.5(4)	51.5(11)
A1-0/0.5	100	0.3	0.5	0.51	0.000	17.9(12)	33.6(5)
A1-0/0.5	100	0.3	0.4	0.51	0.000	30.0(13)	48.3(20)
A1-0/0.5	600	0.1	0.5	0.51	0.065	28.9(9)	47.5(23)
A1-0/0.5	600	0.3	0.5	0.51	0.065	22.2(7)	37.8(16)
A1-0/0.5	600	0.3	0.4	0.50	0.065	34.3(7)	52.2(23)
A1-0/1	100	0.3	0.5	0.51	0.000	14.6(5)	31.1(15)
A1-0/1	100	0.3	0.4	0.51	0.000	26.0(6)	44.3(18)
A1-0/1	600	0.1	0.5	0.52	0.038	26.6(9)	49.9(9)
A1-0/1	600	0.3	0.5	0.52	0.038	19.0(6)	36.9(14)
A1-0/1	600	0.3	0.4	0.41	0.038	29.6(2)	48.5(9)
A1-0/2	100	0.3	0.5	0.41	0.000	17.1(3)	32.2(18)
A1-0/2	100	0.3	0.4	0.42	0.000	27.1(9)	47.3(10)
A1-0/2	600	0.1	0.5	0.41	0.050	26.3(7)	50.6(6)
A1-0/2	600	0.3	0.5	0.41	0.050	17.6(7)	38.0(8)
A1-0/2	600	0.3	0.4	0.50	0.050	28.7(8)	54.6(20)
A2-0/0.25	600	0.3	0.5	0.50	0.034	21.9(5)	40.8(12)
A2-0/0.25	600	0.3	0.4	0.41	0.034	30.1(6)	48.4(17)
A2-0/2	600	0.3	0.5	0.51	0.021	22.0(4)	41.7(14)
A2-0/2	600	0.3	0.4	0.41	0.021	27.7(4)	41.8(21)
G-F	100	0.3	0.5	0.50	0.000	19.9(12)	39.7(11)
G-F	100	0.3	0.4	0.50	0.000	27.3(3)	44.6(12)
G-F	400	0.1	0.5	0.40	0.065	27.6(15)	48.0(10)
G-F	400	0.3	0.5	0.41	0.065	23.1(3)	42.1(7)
G-F	400	0.3	0.4	0.50	0.065	33.1(6)	55.4(17)
G-F	600	0.1	0.5	0.50	0.088	28.3(7)	50.5(22)
G-F	600	0.3	0.5	0.41	0.088	22.7(9)	42.3(10)
G-F	600	0.3	0.4	0.50	0.088	34.4(13)	56.6(21)
H-F	100	0.3	0.5	0.50	0.000	18.2(5)	40.3(18)
H-F	100	0.3	0.4	0.41	0.000	26.8(4)	50.0(15)
H-F	600	0.1	0.5	0.50	0.118	29.5(13)	47.7(8)
H-F	600	0.3	0.5	0.50	0.118	24.6(4)	40.6(7)
H-F	600	0.3	0.4	0.40	0.118	35.0(4)	56.1(30)

Tab. A6: Compressive strength of mortar containing processed industrial fines (part 2).

	Temp. °C	f –	$\frac{w}{b}$ –	$\frac{w+FM}{b}$ –	Δm –	$f_{c,2\,\mathrm{d}}$ MPa	$f_{c,28\,\mathrm{d}}$ MPa
B1-0/0.25	100	0.3	0.5	0.50	0.000	18.3(7)	37.0(12)
B1-0/0.25	100	0.3	0.4	0.41	0.000	30.0(9)	51.9(6)
B1-0/0.25	400	0.1	0.5	0.50	0.058	27.8(11)	48.2(23)
B1-0/0.25	400	0.3	0.5	0.41	0.058	23.1(5)	40.4(10)
B1-0/0.25	400	0.3	0.4	0.50	0.058	33.7(8)	51.3(29)
B1-0/0.25	600	0.1	0.5	0.41	0.080	27.1(5)	52.1(20)
B1-0/0.25	600	0.3	0.5	0.50	0.080	23.6(7)	46.4(8)
B1-0/0.25	600	0.3	0.4	0.41	0.080	33.7(16)	56.0(18)
B1-0/0.5	100	0.3	0.5	0.50	0.000	18.6(6)	35.9(10)
B1-0/0.5	100	0.3	0.4	0.41	0.000	26.6(6)	40.6(37)
B1-0/0.5	600	0.1	0.5	0.50	0.071	27.9(6)	49.4(15)
B1-0/0.5	600	0.3	0.5	0.50	0.071	21.6(4)	41.2(9)
B1-0/0.5	600	0.3	0.4	0.40	0.071	35.1(4)	53.4(15)
B1-0/1	100	0.3	0.5	0.50	0.000	18.6(9)	34.2(15)
B1-0/1	100	0.3	0.4	0.41	0.000	27.7(18)	43.7(12)
B1-0/1	600	0.1	0.5	0.50	0.065	26.2(10)	49.5(19)
B1-0/1	600	0.3	0.5	0.50	0.065	20.1(9)	42.3(10)
B1-0/1	600	0.3	0.4	0.50	0.065	30.1(8)	51.1(12)
B1-0/2	100	0.3	0.5	0.50	0.000	21.6(9)	38.2(19)
B1-0/2	100	0.3	0.4	0.40	0.000	29.7(8)	44.8(7)
B1-0/2	400	0.1	0.5	0.41	0.041	27.4(9)	45.7(19)
B1-0/2	400	0.3	0.5	0.50	0.041	20.2(3)	37.0(10)
B1-0/2	400	0.3	0.4	0.50	0.041	29.8(3)	48.3(6)
B1-0/2	600	0.1	0.5	0.50	0.060	26.4(9)	49.6(15)
B1-0/2	600	0.3	0.5	0.50	0.060	19.6(4)	38.6(11)
B1-0/2	600	0.3	0.4	0.41	0.060	32.7(6)	52.1(27)
B2-0/0.25	100	0.3	0.5	0.41	0.000	19.0(4)	36.1(6)
B2-0/0.25	100	0.3	0.4	0.50	0.000	26.6(8)	44.9(5)
B2-0/0.25	600	0.1	0.5	0.41	0.087	29.2(9)	51.7(23)
B2-0/0.25	600	0.3	0.5	0.50	0.087	20.3(12)	38.9(12)
B2-0/0.25	600	0.3	0.4	0.50	0.087	31.9(10)	53.9(6)
B2-0/2	100	0.3	0.5	0.50	0.000	19.1(5)	36.3(17)
B2-0/2	100	0.3	0.4	0.50	0.000	28.8(18)	49.5(21)
B2-0/2	600	0.1	0.5	0.40	0.058	27.7(6)	49.4(16)
B2-0/2	600	0.3	0.5	0.41	0.058	20.0(4)	40.1(7)
B2-0/2	600	0.3	0.4	0.50	0.058	33.4(6)	54.0(32)
C-0/0.2	100	0.3	0.5	0.50	0.000	19.1(3)	37.0(10)
C-0/0.2	100	0.3	0.4	0.50	0.000	26.8(6)	44.5(16)
C-0/0.2	600	0.1	0.5	0.50	0.098	25.4(5)	47.7(16)
C-0/0.2	600	0.3	0.5	0.41	0.098	19.3(8)	36.6(10)
C-0/0.2	600	0.3	0.4	0.41	0.098	31.3(4)	49.3(33)
C-0/2	100	0.3	0.5	0.50	0.000	18.1(3)	35.7(9)
C-0/2	100	0.3	0.4	0.41	0.000	28.9(5)	48.9(15)
C-0/2	600	0.1	0.5	0.50	0.072	26.6(6)	50.9(6)
C-0/2	600	0.3	0.5	0.50	0.072	21.2(6)	43.2(20)
C-0/2	600	0.3	0.4	0.41	0.072	34.2(6)	50.0(43)

Tab. A7: Compressive strength of mortar containing processed industrial fines (part 3).

	Temp. °C	f –	$\frac{w}{b}$ –	$\frac{w+FM}{b}$ –	Δm –	$f_{c,2\,\mathrm{d}}$ MPa	$f_{c,28\,\mathrm{d}}$ MPa
D-0/0.25	100	0.3	0.5	0.50	0.000	17.1(3)	33.3(13)
D-0/0.25	100	0.3	0.4	0.50	0.000	25.3(15)	35.4(44)
D-0/0.25	600	0.1	0.5	0.41	0.087	27.9(5)	51.5(22)
D-0/0.25	600	0.3	0.5	0.50	0.087	22.2(10)	38.3(9)
D-0/0.25	600	0.3	0.4	0.41	0.087	28.1(7)	44.4(18)
D-0/2	100	0.3	0.5	0.50	0.000	17.2(4)	32.0(6)
D-0/2	100	0.3	0.4	0.50	0.000	25.5(16)	43.2(11)
D-0/2	400	0.1	0.5	0.41	0.029	24.1(11)	46.5(12)
D-0/2	400	0.3	0.5	0.50	0.029	18.4(5)	35.3(7)
D-0/2	400	0.3	0.4	0.50	0.029	29.7(3)	50.9(18)
D-0/2	600	0.1	0.5	0.41	0.039	27.0(7)	46.7(13)
D-0/2	600	0.3	0.5	0.50	0.039	18.0(6)	33.0(15)
D-0/2	600	0.3	0.4	0.50	0.039	30.6(9)	52.6(5)
D-F	100	0.3	0.5	0.40	0.000	3.2(35)	11.4(5)
D-F	100	0.3	0.4	0.50	0.000	9.0(7)	14.8(18)
D-F	400	0.1	0.5	0.50	0.102	29.1(7)	47.9(24)
D-F	400	0.3	0.5	0.50	0.102	25.2(7)	39.6(11)
D-F	400	0.3	0.4	0.50	0.102	34.9(11)	54.1(15)
D-F	600	0.1	0.5	0.50	0.118	31.8(5)	49.8(15)
D-F	600	0.3	0.5	0.40	0.118	23.8(3)	42.1(13)
D-F	600	0.3	0.4	0.40	0.118	39.0(10)	56.8(9)
E-0/0.25	100	0.3	0.5	0.50	0.000	12.8(8)	26.2(14)
E-0/0.25	100	0.3	0.4	0.50	0.000	19.8(11)	34.2(16)
E-0/0.25	600	0.1	0.5	0.50	0.080	26.7(13)	50.3(13)
E-0/0.25	600	0.3	0.5	0.50	0.080	21.0(4)	39.7(9)
E-0/0.25	600	0.3	0.4	0.50	0.080	32.9(7)	53.8(9)
E-0/2	100	0.3	0.5	0.40	0.000	15.8(3)	29.8(3)
E-0/2	100	0.3	0.4	0.40	0.000	22.0(3)	36.3(35)
E-0/2	400	0.1	0.5	0.50	0.040	27.5(8)	48.5(30)
E-0/2	600	0.1	0.5	0.50	0.055	27.8(10)	51.3(12)
E-0/2	600	0.3	0.5	0.41	0.055	19.8(3)	35.9(41)
E-0/2	600	0.3	0.4	0.50	0.055	31.4(21)	56.9(13)
F-0/0.25	100	0.3	0.5	0.50	0.000	15.4(3)	31.8(10)
F-0/0.25	100	0.3	0.4	0.40	0.000	19.4(23)	32.3(19)
F-0/0.25	600	0.1	0.5	0.50	0.063	28.1(10)	48.1(16)
F-0/0.25	600	0.3	0.5	0.50	0.063	21.1(12)	37.7(11)
F-0/0.25	600	0.3	0.4	0.50	0.063	31.8(26)	49.3(14)
F-0/2	100	0.3	0.5	0.50	0.000	14.9(4)	28.7(19)
F-0/2	100	0.3	0.4	0.50	0.000	22.2(15)	35.5(12)
F-0/2	400	0.1	0.5	0.40	0.026	25.6(2)	46.4(13)
F-0/2	400	0.3	0.5	0.40	0.026	18.1(6)	36.1(13)
F-0/2	400	0.3	0.4	0.40	0.026	28.1(6)	47.9(24)
F-0/2	600	0.1	0.5	0.50	0.042	28.9(11)	49.8(10)
F-0/2	600	0.3	0.5	0.50	0.042	21.0(12)	38.6(34)
F-0/2	600	0.3	0.4	0.50	0.042	36.1(11)	57.9(39)

Paper P2

Influence of Thermally Activated Artificial Concrete Fines Composition on Mortar Strength Development

Jan P. Höffgen
Frank Dehn

Developments in the Built Environment 24

December 2025, 100775

DOI: 10.1016/j.dibe.2025.100775

Publisher's version

Developments in the Built Environment 24 (2025) 100775

Contents lists available at ScienceDirect

Developments in the Built Environment

journal homepage: www.sciencedirect.com/journal/developments-in-the-built-environment

Influence of thermally activated artificial concrete fines composition on mortar strength development

Jan P. Höffgen *, Frank Dehn

Karlsruhe Institute of Technology (KIT), Institute for Concrete Structures and Building Materials (IMB), Gotthard-Franz-Str. 3, Karlsruhe, 76131, Germany

ARTICLE INFO

Keywords:
Concrete
Cement
Mineral waste
Recycling
Thermal activation
Supplementary cementitious material

ABSTRACT

The study explores the use of thermally activated concrete fines as substitution for cement to recycle mineral waste and reduce emissions. Concrete fines from waste recycling have a significant impact on compressive strength, with considerable variation due to their varying compositions. In the present study, 12 artificial concrete fines with varying compositions are thermally activated and assessed for their strength contribution. Increasing aggregate content within artificial fines results in a decrease in compressive strength, with aggregate mineralogy and binder composition having a major impact. Ultimately, this study proposes a model for predicting the impact of fines composition on compressive strength based on mass loss during dehydration. For thermally activated cement paste, the new model proposes no influence on compressive strength compared to the reference ($k = 1.0$). Paste precursors containing hydration products from alternative binders may even surpass the reference ($k > 1.0$), while an increasing amount of inert aggregates reduces strength ($k < 1.0$).

1. Introduction

Concrete is essential for the production of infrastructure and housing, but faces challenges: The sourcing of aggregates already results in localized shortages, and the production of cement clinker as a hydraulic binder entails high CO_2-emissions (VDZ, 2024; Coffetti et al., 2022). Therefore, concrete and composite cements partially substitute clinker through supplementary cementitious materials (SCMs), or even avoid cement altogether as alkali-activated materials (Coffetti et al., 2022; Gao et al., 2013; Knight et al., 2023; Barthel et al., 2016; Shah et al., 2022; Herrmann et al., 2018; Wang et al., 2024; Ma et al., 2025; Wu et al., 2024). However, some of the most widely used SCMs – ground granulated blast-furnace slag and coal fly ash – already face regional shortages, which will only magnify when less coal is burned in steel production and power plants, thus raising the need for the identification of additional SCMs (Hafez et al., 2020; Knight et al., 2023; Snellings et al., 2023; Friol Guedes de Paiva et al., 2021).

Concrete recycling may provide an alleviation for both issues. However, while the application of recycled concrete aggregates is well established, cement recycling requires additional research and development. One pathway for cement recycling is thermal activation, where hydrated cement paste (HCP) retains reactivity after the loss of chemically bound water (Carriço et al., 2020a; Ohemeng and Ekolu, 2020; Xu et al., 2022; Aquino Rocha and Toledo Filho, 2023; Zheng et al., 2024). HCP mostly consists of cement clinker hydration products, namely calcium silicate hydrate and calcium hydroxide from the hydration of tricalcium silicate (C_3S) and dicalcium silicate (C_2S), as well as aluminous, ferrous, or sulfate hydrates (Richardson, 2000; Scrivener et al., 2015). The hydration of 1 g of ordinary Portland cement (OPC) requires about 0.4 g of water, of which 0.2 g–0.25 g is chemically bound in hydrates (Lura et al., 2017; Powers and Brownyard, 1946; Brouwers, 2004). The remainder is present as physically bound water in gel pores. While the latter evaporates at temperatures up to 105 °C, the disintegration of different hydraulic phases in HCP requires increased temperatures (see Table 1). Calcium silicate hydrate is transformed into reactive $\alpha'_L C_2S$ and $\alpha'_H C_2S$, with calcium oxide to silicon dioxide ratios ranging between 1.73 and 1.9 (Bogas et al., 2022b; Alonso and Fernandez, 2004; Richardson, 2000; Ge et al., 2024; Noel et al., 2025; Tajuelo Rodriguez et al., 2017; Carriço et al., 2020b; Real et al., 2020; Serpell and Zunino, 2017). Dehydrated cement paste (DCP) exhibits high specific surface areas and high porosity, which originates in porous HCP and increases with increasing temperature and phase decomposition (Baldusco et al., 2019; Bogas et al., 2019; Carriço et al., 2020b; Kim et al., 2021). For processing temperatures surpassing the dehydroxylation range of calcium hydroxide, DCP may contain finely distributed calcium oxide (Bogas et al., 2019; Serpell and Lopez, 2015).

When used as a recycled binder, rehydration begins with the reformation of calcium hydroxide from calcium oxide, and the reformation of calcium silicate hydrates from C_2S, which manifests in increased and

* Corresponding author.
E-mail address: jan.hoeffgen@kit.edu (J.P. Höffgen).

https://doi.org/10.1016/j.dibe.2025.100775
Received 13 August 2025; Received in revised form 29 September 2025; Accepted 4 October 2025
Available online 13 October 2025

Table 1
Temperature-dependent decomposition of concrete fines containing hardened cement paste and aggregates.
Source: Data from (Angulo et al., 2022; Baggio et al., 2024; Baldusco et al., 2019; Baquerizo et al., 2016; Florea, 2014; Horváth et al., 1977; Klingsch, 2014; Schneider, 1982; Wang et al., 2019; Zelic et al., 2007; Zhou and Glasser, 2001; Zhou et al., 2004).

Temperature [°C]			Process
	<	105	Loss of free and physically bound water
	<	115	Disintegration of ettringite
	<	250	Disintegration of monosulfate
260	–	400	Decomposition of calcium aluminate hydrates
110	–	500	Disintegration of calcium silicate hydrates
400	–	550	Dehydroxylation of calcium hydroxide
	573		Quartz inversion in siliceous aggregates
650	–	900	Calcination of carbonated cement phases or carbonatic aggregates

accelerated hydration heat development (Angulo et al., 2022; Bogas et al., 2020; Semugaza et al., 2023; Yu and Shui, 2013; Wei et al., 2025; Baldusco et al., 2019; Real et al., 2020). However, due to the porous nature of DCP, rehydrated C–S–H forms inside the particles, and exhibits weak interparticle connectivity after hydration, resulting in a low-strength material (Carriço et al., 2020b; Shui et al., 2008; Real et al., 2020; Xi et al., 2024a). Yet, when used as SCM, water consumption of DCP reduces the available water for clinker hydration, which forms a dense and interlocking microstructure (Qian et al., 2020; Tokareva et al., 2023; Wei et al., 2025). Small amounts of thermally activated cement paste may have a positive impact on compressive strength (Ma et al., 2022; Wei et al., 2025; Carriço et al., 2021b). However, with increasing substitution rate, strength declines (Carriço et al., 2020b; Semugaza et al., 2023). Overall, up to 40 wt% of clinker can be substituted through DCP with minimal adverse effects on concrete strength (Bogas et al., 2022a; Carriço et al., 2020b; Letelier et al., 2017; Ma et al., 2022; Qian et al., 2020; Tokareva et al., 2023; Vashistha et al., 2023; Wu et al., 2023).

When HCP contains hydration products from pozzolanic or latent-hydraulic SCMs, like fly ashes or ground granulated blast-furnace slag, dehydration and rehydration behavior changes. Prominently, the reduction of clinker reduces the amount of calcium hydroxides in HCP, in favor of an increased amount of calcium silicate hydrates and calcium aluminate silicate hydrates (Xu et al., 2023b). After processing, the rehydration potential increases, especially for ground granulated blast-furnace slag containing cement paste, which shows increased hydration heat development and higher compressive strength (Xu et al., 2023b,a). HCP containing fly ash exhibits reduced hydration heat and compressive strength, while inert limestone powder as part of SCM merely dilutes DCP performance, as long as the processing temperature is kept below calcination temperature (Xu et al., 2023b,a; Serpell and Lopez, 2013). While the dehydration and rehydration of HCP from OPC have been thoroughly investigated, the behavior of HCP from binary cements lacks a detailed analysis.

Similar shortcomings concerning the influence of aggregate type and content in recycled concrete fines need addressing. Fines from waste concrete processing never consist of pure HCP and always contain primary aggregates, which have an overall negative impact on performance as SCM following thermal activation (Bogas et al., 2019; Carriço et al., 2021a,b). However, the mineral composition of finely ground aggregates impacts their performance as SCM, especially when containing amorphous silicon dioxide, which exhibits a pozzolanic reactivity (Lipowsky and Müller, 2017). Regardless, no studies where the influence of aggregate type and concentration was assessed employing artificial fines could be identified.

Therefore, this study presents a systematic approach for assessing the influence of concrete fines composition regarding cement composition and aggregate content on the performance of thermally activated concrete fines as SCM.

Table 2
Composition of artificial fines used as precursors for thermal activation. w/b: water-binder ratio; v_p: paste volume; A: aggregates; FA: fly ash; S: blast-furnace slag; RS: river sand; LS: limestone sand; GW: greywacke.

	Binder	w/b	v_p [v%]	A
CEM	100 wt% CEM I	0.5	100	–
RS75	100 wt% CEM I	0.5	75	RS
RS62			62.5	
RS50			50	
LS75	100 wt% CEM I	0.5	75	LS
LS50			50	
GW75	100 wt% CEM I	0.5	75	GW
GW50			50	
FA0	70 wt% CEM I + 30 wt% FA	0.5	100	–
FA50			50	RS
S0	70 wt% CEM I + 30 wt% S	0.5	100	–
S50			50	RS

Table 3
Mix designs of artificial fines used as precursors for thermal activation [g/l]. W: Water; C: CEM I 42.5 R; FA: fly ash; S: blast-furnace slag; RS: river sand; LS: limestone sand; GW: greywacke.

[g/l]	W	C	FA	S	RS	LS	GW
CEM	610	1220					
RS75	458	915			658		
RS62	381	763			986		
RS50	305	610			1315		
LS75	458	915				670	
LS50	305	610				1340	
GW75	458	915					678
GW50	305	610					1355
FA0	583	816	350				
FA50	292	408	175		1315		
S0	605	847		363			
S50	303	424		182	1315		

2. Experimental program

The experimental program aims to assess the influencing parameters of concrete fines composition on the performance as supplementary cementitious materials. Thermally activated artificial fines were assessed for their rehydration behavior and compressive strength development.

2.1. Materials

To reflect the bandwidth of possible concrete fines from existing or demolished concrete structures, 12 artificial fines with known compositions were produced. Variations include aggregate composition and content as well as the partial substitution of OPC (CEM I 42.5 R, "CEM I") through reactive supplementary cementitious materials. Table 2 gives an overview of the artificial fines compositions and naming scheme. Table 3 details the corresponding mix designs.

The basis of the artificial fines is hardened cement paste (HCP) made from CEM I 42.5 R. The influence of the type of sand is to be investigated primarily on mortars with an aggregate content of 50 v%. A quartzitic river sand (RS) and a calcitic crushed limestone sand (LS), which are intended to represent the predominantly used types of aggregate, are used. In addition, two artificial fines were produced with greywacke (GW), whose alkali reactivity was known from a previous research project (Wiedmann, 2020). To investigate the influence of the aggregates content, additional artificial fines with an aggregates content of 25 v% – and in the case of RS 37.5 v% – were produced. Since the use of OPC has been declining in recent years, pure binder pastes and mortars with an aggregates content of 50 v% by volume, in which 30 wt% of CEM I was replaced by fly ash (FA) or ground

granulated blast-furnace slag (S), which are widely used pozzolanic or latent-hydraulic SCMs, complete the artificial fines matrix.

All artificial fines were manufactured with a fixed water-binder ratio of $w/b = 0.5$, as it can be assumed that at $w/b = 0.5$, the entire binder is hydrated, even if the local w/b-ratio may be slightly altered. Preliminary analyses showed that lower w/b-ratios were feasible for the production of paste materials, but required the undesired addition of superplasticizer for mortars with low paste content. Higher w/b-ratios, as often found in practice, do not lead to an increased degree of hydration, but affect the porosity of the cement matrix. On the other hand, the tendency of the fresh mortar to segregate increases with increasing w/b-ratio, especially with high paste content. Pure paste artificial fines (CEM, FA0, S0) nonetheless showed segregation, so these materials were repeatedly homogenized by hand after the original mixing until hydration had started. From all artificial fines, prisms ($(20 \times 20 \times 80)\,mm^3$) for strength testing were cast.

Bulk artificial fines were stored in sealed buckets to ensure a high degree of hydration. Prisms were demolded at 1 d and subsequently stored under water alongside bulk samples until the age of testing at 2 d, 7 d, 28 d, and 356 d. At an age of at least 9 months, bulk specimens were crushed and dried at 105 °C, followed by grinding in an industrial mill. Ground and dried artificial fines were labeled with the suffix "−100". Subsequent thermal activation used a static oven with a crucible size of 1.5 kg. The thermal activation procedure was obtained from preliminary analyses, with a heating rate of 5 K/min and a holding time of 6 h at the individual processing temperature (400 °C, 600 °C or 800 °C), before cooling in laboratory climate. Afterwards, samples were stored in a sealed container containing a drying agent. Similar to ground artificial fines, the naming scheme for thermally activated samples added the temperature as a suffix to the artificial fines, i.e., "GW75-400" for a mortar containing 25 v% greywacke, which was activated at 400 °C.

The artificial fines matrix was complemented by RS0 and LS0, which denote the respective aggregates used for mortars, after grinding in a laboratory mill.

2.2. Experimental procedures

Raw materials as well as artificial fines were characterized for their chemical composition through Wavelength Dispersive X-ray Fluorescence (WDXRF), their particle size distribution, and density. The thermal decomposition behavior of artificial fines was assessed through thermogravimetric analyses before and after activation (sample sizes: 160 mg, heating rate: 10 K/min).

Isothermal hydration heat measurements were conducted on blends of CEM I and artificial fines at 20 °C with internal mixing, enabling the determination of the initial heat release. Preliminary tests on mixing efficiency and homogeneity led to setting the water-binder ratio to $w/b = 0.6$ for all samples. Artificial fines were generally investigated in combination with CEM I at a substitution rate of $f = 0.3$. Double determinations were performed for all mixes, except for the base mix with pure CEM I, which comprised eight single measurements. Additionally, activated paste artificial fines (CEM, FA0, S0) were tested at different CEM I-substitution rates.

For strength development tests, a mortar with 50 v% quartzitic river sand (0 mm–2 mm) as aggregates was used, matching the composition of RS50. To assess the influence of artificial fines on SCM, two mixes with $w/b = 0.4$ and $w/b = 0.5$ at $f = 0.3$ were produced for each SCM, with selected SCMs also having $w/b = 0.5$ at $f = 0.1$ and $f = 0.5$. Fourteen base mixes with pure CEM I were produced with $w/b = 0.40$–0.65 and were repeated in three series throughout the experimental program. 159 mixes, including repetitions, were tested for the assessment of CEM I-substitution through processed artificial fines. In stiff mortars, superplasticizer was added to ensure comparable workability. After mixing, the mortar was placed in steel molds, which were moist-cured for 1 d, and then stored underwater at 20 °C after demolding. Strength testing was performed on three prisms each ($(20{\times}20{\times}80)\,mm^3$) at 2 d and 28 d. The small specimen size (half of a standard mortar prism according to EN 196:2016) was chosen for the reduced amount of raw materials required for one mix. This allowed for the production of up to four different mortar compositions from one batch of thermally activated artificial fines. For CEM I, as well as CEM and different RS-artificial fines, additional strength measurements were conducted at 1 d and 7 d. First, flexural strength f_f was determined with a span of 50 mm at a loading rate of $\dot{F}_f = 10\,N/s$. Compressive strength (f_c) testing used six prism halves at a loading rate of $\dot{F}_c = 600\,N/s$.

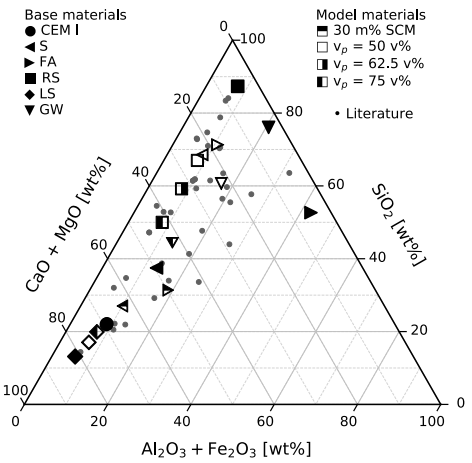

Fig. 1. Ternary illustration of raw materials and artificial fines composition determined through WDXRF (EN 196-2:2013) as well as literature (Baggio et al., 2024; Chen et al., 2024; Gebremariam et al., 2020; Kim and Ubysz, 2024; Sousa et al., 2024; Tokareva et al., 2023; Vashistha et al., 2023; Sui et al., 2020; Wei et al., 2024, 2025; Xi et al., 2024b; Yonis et al., 2024; Zhang et al., 2023; Cyr et al., 2019; Florea, 2014; Frías et al., 2021; Brameshuber et al., 2011; Izoret et al., 2019; Li et al., 2021; Liang et al., 2021; Liu et al., 2021; Müller and Dora, 2000; Shen et al., 2021; Sun et al., 2021). See Table 2 for artificial fines composition.

3. Results and discussion

3.1. Precursors characterization

Table 4 lists the results of the strength development of artificial fines prisms. Overall, strength increases with reduced paste content, while aggregate composition does not exhibit a systematic influence. Materials, where CEM I was partially substituted through reactive SCMs, show a slower strength development, but exhibit similar 356 d-compressive strength as equivalent materials without CEM I-substitution, with S50 reaching the highest ultimate compressive strength of all artificial fines prisms.

Fig. 1 illustrates the chemical composition of raw and artificial fines in a ternary diagram. Results show the expected difference between individual artificial fines.

The chemical composition reflects variations between individual RCFs from the literature, which consist of different kinds of binders and aggregates. Fig. 1 also implies that the chemical composition is not suited as a standalone assessment parameter of RCF potential.

The thermal behavior of artificial fines was determined on samples that had been dried at 105 °C to eliminate free and physically bound water. Instead of industrial grinding, samples were ground in a laboratory ball mill immediately after drying (Fig. 2).

Here, the influence of the type and content of the aggregates is shown, which is in good agreement with the XRF results. Regardless of aggregate composition, mass loss up to 600 °C scales with paste content, as pure aggregates exhibit almost no mass loss for lower temperatures. Mass loss of artificial fines with different aggregate types

Table 4
Flexural (f_f) and compressive strength (f_c) of artificial fines prisms at 2 d, 7 d, 28 d and 365 d on prisms with $(20 \times 20 \times 80)\,mm^3$.

	f_f at the age of				f_c at the age of			
	2 d	7 d	28 d	365 d	2 d	7 d	28 d	365 d
CEM	4.6	7.1	7.4	8.1	20.3	36.8	42.5	53.6
RS75		7.4	8.5	8.5		38.7	46.7	55.9
RS62	6.0	8.0	8.6	6.3	27.1	46.1	50.4	53.6
RS50	6.1	7.7	8.5	8.9	26.5	48.3	50.0	60.5
LS75		6.7	7.1	7.4		41.5	45.6	53.1
LS50	6.2	7.9	8.7	10.1	29.7	49.8	56.5	64.1
GW75		7.0	8.6	7.9		43.0	50.4	60.3
GW50	6.1	8.3	9.9	11.2	32.9	52.8	47.6	65.4
FA0	2.8	4.4[a]	6.7	9.2	11.0	22.9	35.1	56.8
FA50	3.9	5.6	5.7	9.6	18.0	32.9	37.9	56.6
S0	3.8	4.5[a]	7.2	8.9	13.3	24.2	37.4	53.9
S50	4.6	6.9	8.9	11.2	21.8	39.0	54.3	73.8

[a] At 7 d, FA0 and S0 were tested with $\dot{F}_f = 1\,N/s$.

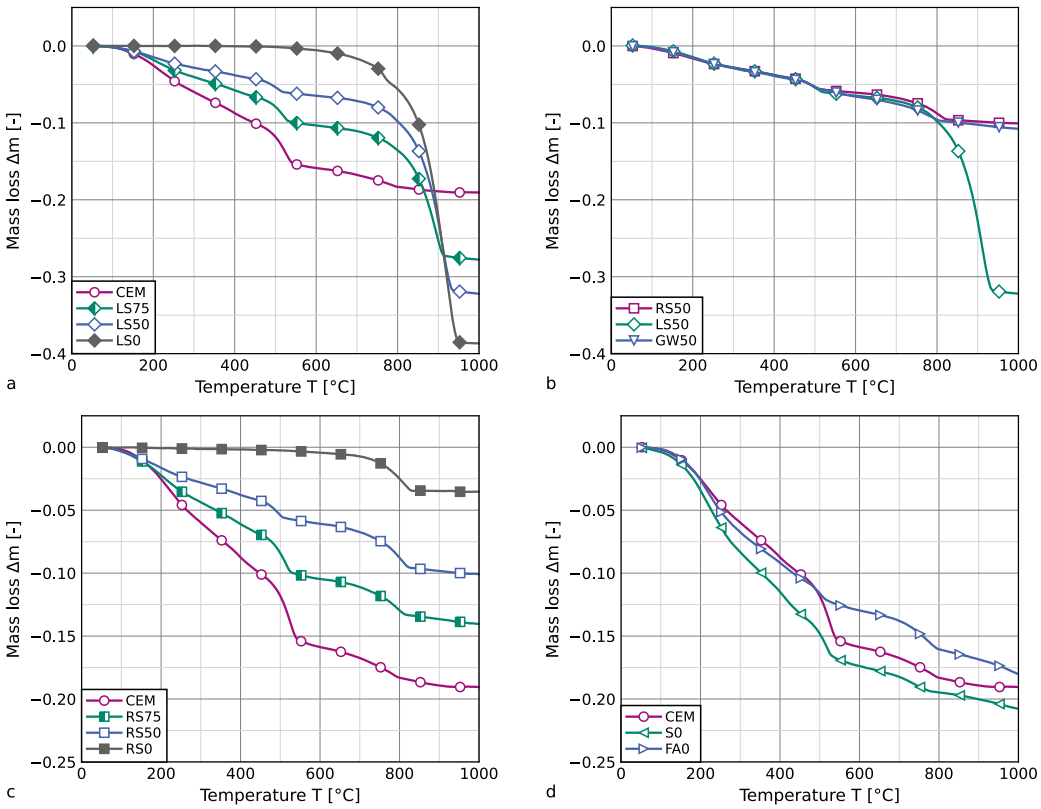

Fig. 2. Thermogravimetric characterization of artificial fines (sample size 160 mg, heating rate 10 K/min). See Table 2 for artificial fines composition.

but the same aggregate content is almost identical. The artificial fines with limestone aggregate (LS) show a high mass loss at temperatures above 810 °C, which is only slightly present in the artificial fines with greywacke and not present in samples with siliceous river sand. This is due to the decomposition of calcium carbonate ($CaCO_3$) in the aggregate particles. However, all artificial fines exhibit a mass loss between 700 °C and 800 °C, which is also caused by the decomposition of calcium carbonate. The different decomposition temperatures can be explained by different mineralogical and petrographic compositions or configurations of $CaCO_3$.

In addition to the obvious influence of the aggregate content on the mass loss, Fig. 2 also shows differences between cement pastes with different binder compositions. FA0, in which 30 wt% of the hydraulically reactive CEM I was replaced by pozzolanic coal fly ash, shows a similar mass loss up to temperatures of around 500 °C as CEM. However, the subsequent increased mass loss, which is due to the decomposition of calcium hydroxide ($Ca(OH)_2$), is significantly lower. This can be explained by the fact that $Ca(OH)_2$ is consumed by the pozzolanic reaction of the fly ash. Since the $Ca(OH)_2$ content of FA0 is reduced to almost zero, it is also possible that FA0 contains undetermined amounts of primary, unreacted fly ash, which affects its usability as a concrete additive. Compared to FA0, S0 shows an increased mass loss at 500 °C, but this is lower than that of CEM. Since latent-hydraulic blast-furnace slag replaces 30 wt% of the CEM I here, less $Ca(OH)_2$ is produced in favor of calcium silicate hydrates

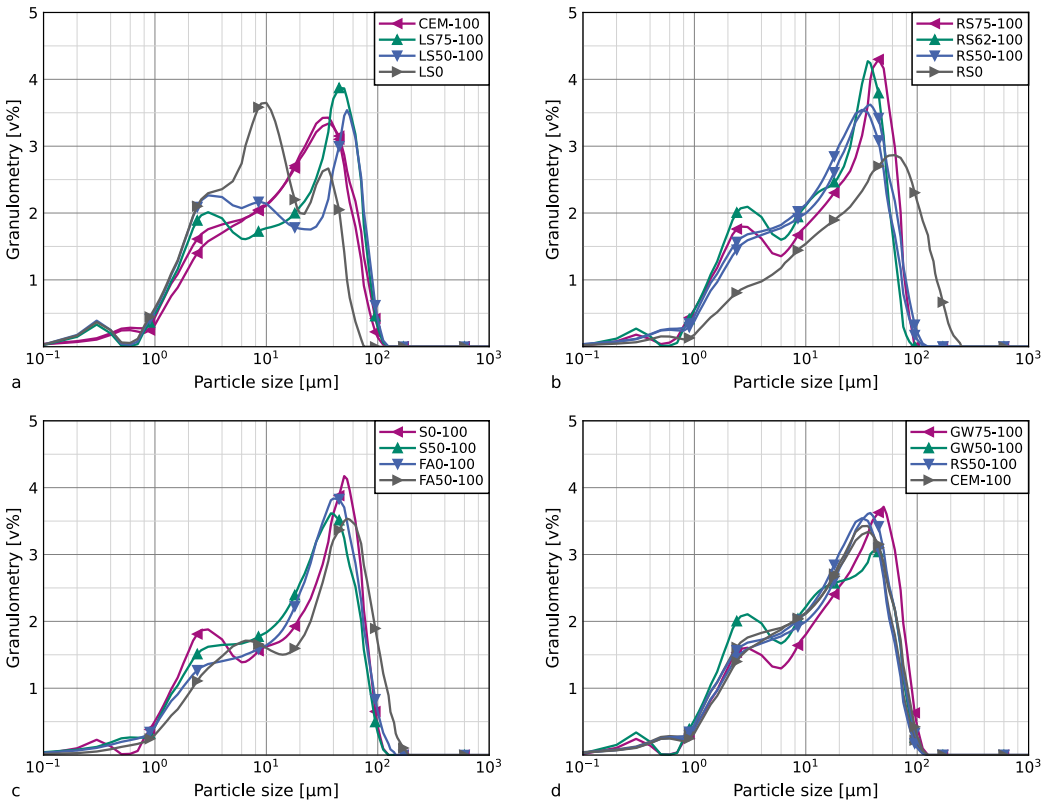

Fig. 3. Particle size distribution of ground artificial fines determined through laser diffraction.

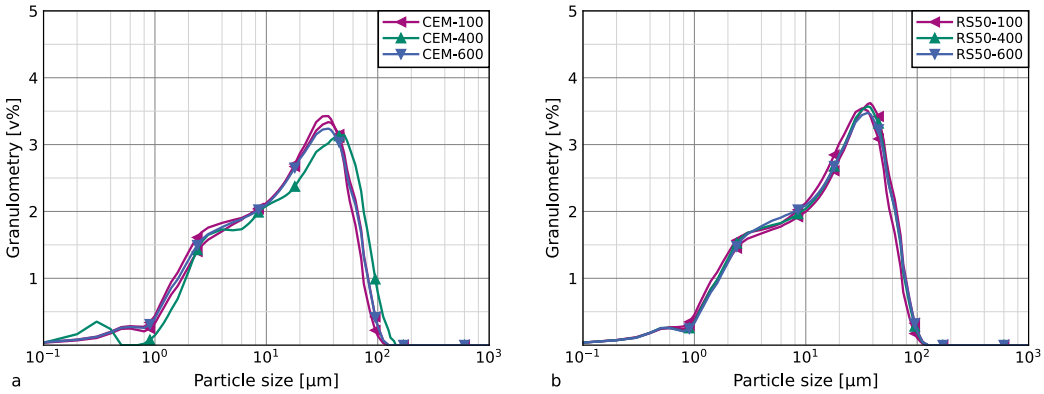

Fig. 4. Particle size distribution of artificial fines CEM and RS50 after thermal activation at different temperatures determined through laser diffraction.

(C–S–H) during hydration. This explains the increased mass loss at temperatures below 500 °C compared to CEM, which is mainly due to the decomposition of C–S–H.

The ultimate goal of using an industrial mill for grinding before thermal activation was to achieve good comparability between individual samples, allowing the exclusion of particle size influence on experimental results. Overall, ground artificial fines have similar particle size distributions, with the exception of LS0 and RS0, which is due to the diverging milling process (see Fig. 3).

To rule out the impact of thermal processing on particle size distribution, artificial fines CEM and RS50 were measured after processing at 400 °C and 600 °C. Laser diffraction measurements yielded no systematic influence of thermal activation on particle size, so the comprehensive determination of particle size distributions for all activated artificial fines combinations was forgone (see Fig. 4).

3.2. Artificial fines performance as SCM

3.2.1. Hydration heat

The assessment of the rehydration behavior of processed artificial fines comprises four individual steps: The influence of activation temperature, the influence of paste content, the influence of aggregate composition, and, finally, the influence of CEM I-substitution rate.

The effect of the processing temperature on hydration heat development in Fig. 5 used three paste artificial fines (CEM, FA0, and S0) as well as mortar RS50 at a CEM I-substitution rate of 30 wt% in comparison to the average results from the eightfold determination of pure CEM I.

The results show a significant influence of the activation temperature for CEM: In the first minutes after water addition, the mixtures of CEM I with thermally activated CEM exhibit a significantly increased

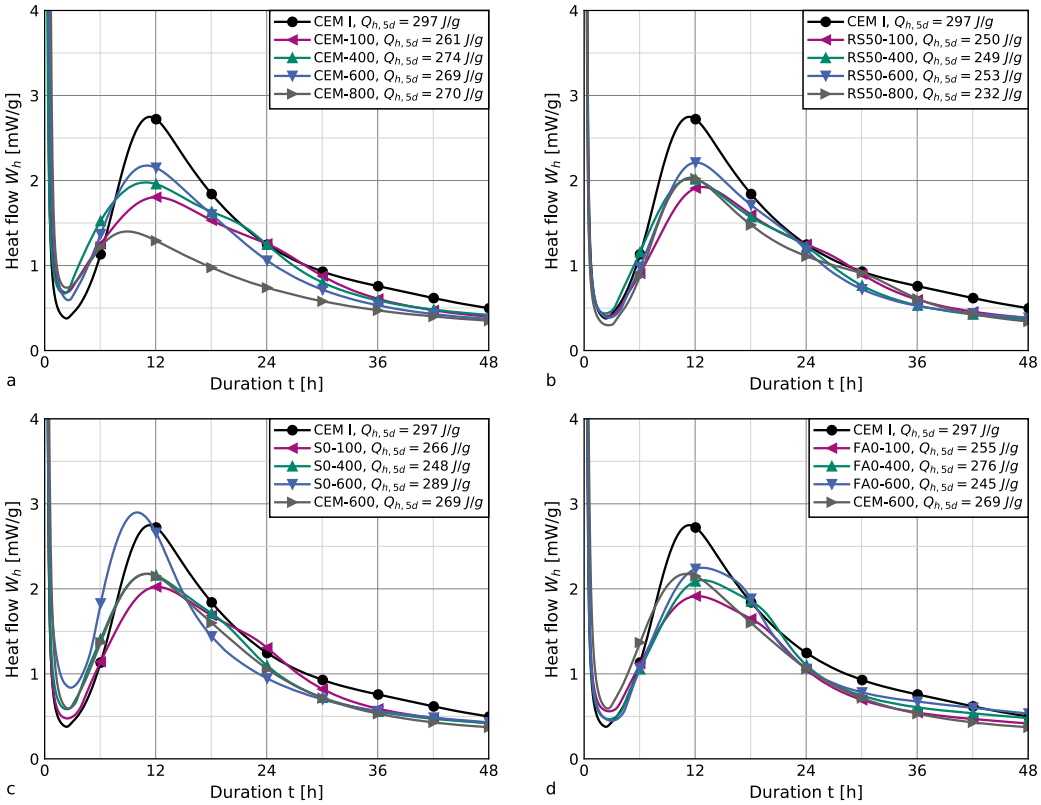

Fig. 5. Hydration heat development of blended binders with 70 wt% CEM I and 30 wt% artificial fines activated at different temperatures. See Table 2 for artificial fines composition.

heat release with rising temperature. Subsequently, the heat release decreases for all mixtures. Compared to pure CEM I, mixtures with all four processed CEM samples exhibit increased heat release during the induction period in the first 6 h of measurement. Subsequently, the curves show a flatter progression than the reference sample made of pure CEM I – the heat release is reduced depending on the processing temperature. CEM-600 shows the highest local maximum after the acceleration period, while the total heat released within 5 days between CEM-600 and CEM-400 hardly differs. CEM-100 exhibits the lowest hydration heat release. However, the behavior stemming from CEM-800 is particularly striking: Although only 30 wt% of CEM I was replaced, the initial heat release during the first 30 min increases by a factor of 4. The height of the local maximum of the hydration heat flow is reduced by about 50% and also occurs significantly earlier. Subsequently, the hydration heat flow curve of the mixture of CEM I and CEM-800 runs significantly flatter than that of the other investigated mixtures. Overall, none of the investigated mixtures of CEM I and thermally activated CEM reach the cumulative heat released by pure CEM I.

These observations are only partially transferable to RS50, although analogous tendencies are shown. The analysis is made more difficult by the fact that in the calorimetry measurements, reactive CEM I makes up 70 wt% of the solid quantity. Furthermore, RS50 consists of CEM I and river sand in a mass ratio of 0.46, so that the proportion of potentially reactivated cement paste in the solid quantity of the calorimetry balance is reduced from 30 wt% for CEM to 9.4 wt% for RS50. The hydration heat release is accordingly influenced to a lesser extent by the treatment temperature. The artificial fines RS50-100, RS50-400, and RS50-600 exhibit almost the same hydration heat release, with RS50-600 showing the highest local maximum, analogous to CEM-600. RS50-800 has a less pronounced effect on the hydration heat release compared to CEM-800, but results in a lower overall heat release than RS50-100. All mixtures of CEM I with thermally processed model materials RS50 release less heat cumulatively than the corresponding mixtures of CEM I with CEM.

Artificial fines whose cement paste matrix consists of hydration products of CEM I and blast-furnace slag (S0) or coal fly ash (FA0) show a behavior deviating from the processed CEM. Compared to CEM-600, the cumulative hydration heat release of S0-600 is significantly increased and reaches the level of pure CEM I, with the increased local maximum of the hydration heat flow being reached earlier (compare Baldusco et al., 2019; Xu et al., 2023b,a). S0-100 and S0-400 also show a slightly increased heat release compared to CEM-100 and CEM-400, respectively. However, the heat release in the first minutes after water addition is significantly reduced compared to CEM-600 and is similar to that of pure CEM I. The same applies to FA0, where, apart from the initial heat release in the first 24 h after water addition, no increased heat release is detectable. Subsequently, the processed materials, regardless of the activation temperature, exhibit an increased hydration heat flow.

Fig. 6(a) illustrates the corresponding results for artificial fines prepared at 600 °C with different contents of river sand. Here, a decrease in hydration heat release can be observed with decreasing cement paste content. However, further details cannot be inferred due to the scatter of the experimental results.

Fig. 6 shows the heat flow curves of artificial fines with different types of aggregate in comparison. The individual measurement results are close to each other, making interpretations difficult due to the scatter of the experimental results. On the one hand, it can be observed that the processing temperature has only a minor influence on the hydration heat release. The same applies to the type of aggregates. It can be seen that the artificial fines with 50 v% greywacke (GW50) show a reduced hydration heat release at the beginning of hydration, which is, however, compensated for in the further course. Artificial fines with 75 v% cement paste content show slightly increased cumulative hydration heat releases.

In Fig. 7, the results of hydration heat flow measurements on the processed artificial fines CEM-400, CEM-600, S0-600, and FA0-600 are

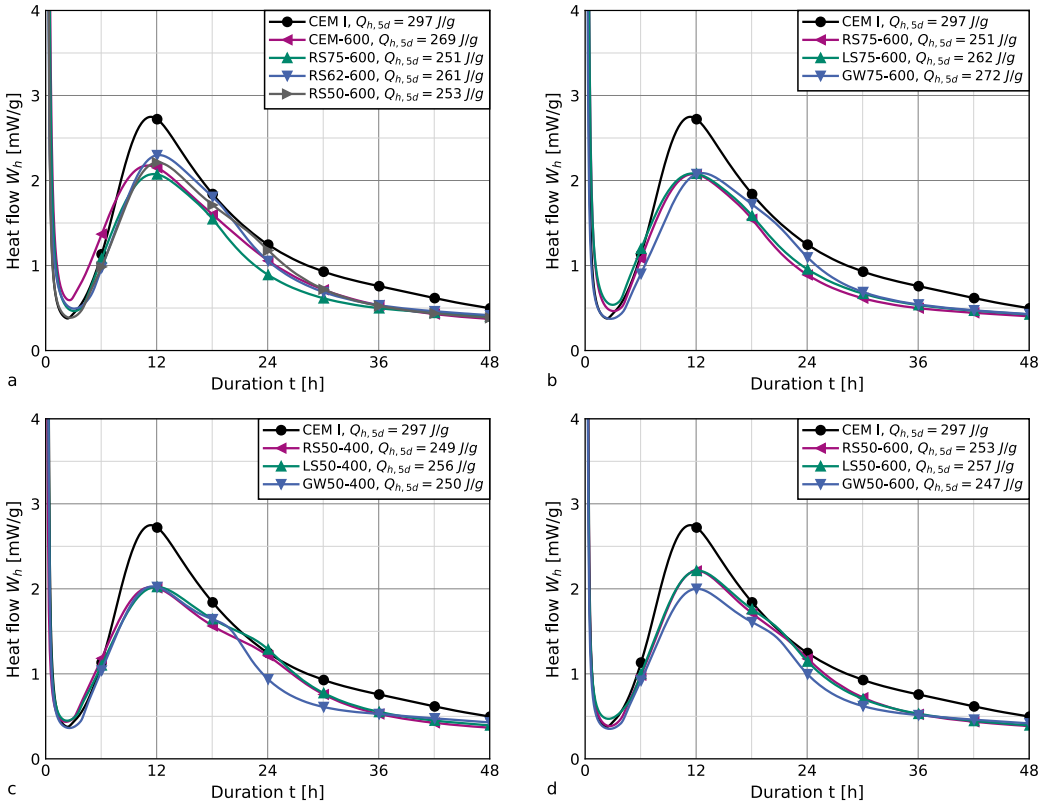

Fig. 6. Hydration heat development of select blends of 70 wt% CEM I and 30 wt% artificial fines with different aggregate contents and compositions, activated at 400 °C and 600 °C. See Table 2 for artificial fines composition.

compared for different substitution rates of CEM I (10 wt%, 30 wt%, 50 wt% and 100 wt%). The experimental results show, on the one hand, clear differences between the individual artificial fines among themselves, as well as between the substitution rates of respective processed artificial fines.

Activation of CEM at 400 °C produces a binder with hydraulic reactivity. The cumulative hydration heat release of pure CEM-400 corresponds to 55% of the heat release of CEM I after 5 d. Based on the results for pure CEM I, the hydration heat release decreases with increasing substitution rate. Considering the heat flows reveals a nuanced picture: CEM-400 releases more heat in the first minutes after water addition than CEM I. The difference stems from the near omission of the acceleration and deceleration phases between 2 h and 48 h present in CEM I-containing binder blends. While the heat flow of pure CEM-400 plateaus, blends with CEM I increase to a local maximum after an induction period with increased heat flow compared to CEM I. When replacing 50 wt% of CEM I with CEM-400, the hydration heat flow decreases more strongly after reaching the maximum than when replacing 30 wt%.

CEM-600 is also hydraulically reactive, with a cumulative hydration heat release after 5 d corresponding to 84% of CEM I. The difference to CEM-400 is approximately equal to the hydration heat release within the first hour after water addition. However, the heat flow of CEM-600, in contrast to CEM-400, shows a recognizable maximum after 10 h. Subsequently, the hydration heat flow decreases more strongly than that of CEM-400. Blends of CEM I and CEM-600 are arranged according to their replacement rates between the pure binders.

S0-600 also shows hydraulic reactivity, which is associated with a larger cumulative hydration heat release than CEM-600 and reaches 98% of the hydration heat of CEM I after 5 d. The evaluation of the hydration heat flows shows a more balanced course than CEM I, with a significantly increased local minimum after 3 h and a reduced and temporally shifted maximum after 15 h, so that the heat flow before the minimum and after the maximum is each higher than CEM I. The position of the minima and maxima of mixtures with 30 wt% and 50 wt% S0-600 is also changed, but no systematic relationship with the substitution rate can be identified.

When considering FA0-600, no hydraulic behavior is recognizable after the initial heat flow has subsided within the first hours after water addition. Only after several days does the hydration heat release increase measurably; a local maximum is reached after 163 h with W_h = 0.4 mW/g. The substitution of 30 wt% of CEM I through FA0-600 behaves similarly to corresponding blends containing CEM-600 and S0-600 except for a reduced initial hydration heat within the first minutes. The substitution of 50 wt% of CEM I through FA0-600 results in a reduced peak after the shortened acceleration phase and a plateauing deceleration phase.

In the overall view, the present results of the hydration heat flow measurements show a clear influence of the processing temperature, the binder composition, and, to a lesser extent, the aggregate content. Findings for the temperature-dependence agree with results in literature, where heat-release is partially attributed to the reaction of free lime as well as the reformation of calcium silicate hydrate and other hydrate phases (Angulo et al., 2022; Bogas et al., 2020; Semugaza et al., 2023; Real et al., 2020). The effect of hydration products from blast-furnace slag corroborates results presented in Baldusco et al. (2019), Xu et al. (2023b) and Xu et al. (2023a). Xu et al. (2023b) also reports a hydration heat release for a blended paste containing 30 wt% fly ash, which is considerably higher than the present results for FA0. However, the precursor in Xu et al. (2023b) contains a higher amount of $Ca(OH)_2$ compared to FA0, which supports the hypothesis of the importance of calcium hydroxide for fines rehydration. The effects observed here cannot be conclusively clarified with the available results, particularly the hypothesis of incomplete reaction of the fly ash in connection with the reduction of the $Ca(OH)_2$ content, as discussed in Section 3.1. The type of aggregate is of lesser importance for the hydration heat

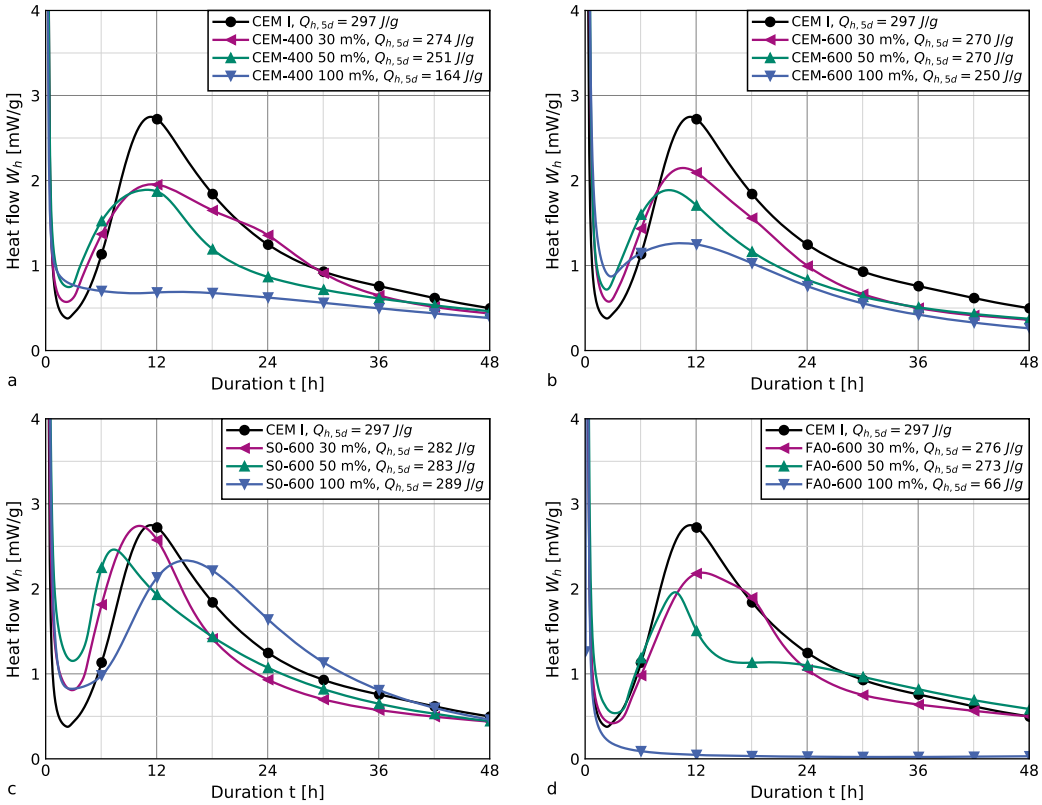

Fig. 7. Hydration heat flow of select blends of CEM I and CEM-400, CEM-600, S0-600 or FA0-600 at different substitution rates. See Table 2 for artificial fines composition.

release, while the general presence of inert particles generally reduces the hydration heat release, which agrees with previous findings for limestone-blended cement pastes (Serpell and Lopez, 2013; Xu et al., 2023b). The ratio of CEM I to thermally activated artificial fines brings additional effects that overlap and interact with the previously mentioned factors (compare Zhang et al., 2018).

3.2.2. Compressive strength development

To analyze the strength development of the manufactured mortar mixtures, two approaches were used. The quotient r according to Eq. (1) describes the ratio of the mortar compressive strength at the ages of 2 d and 28 d, and was determined for all mixtures.

$$r = \frac{f_{c,2\,\mathrm{d}}}{f_{c,28\,\mathrm{d}}} \tag{1}$$

Fig. 8 shows results for the mortar compressive strength f_c at the age of 2 d and 28 d for different compositions in which thermo-mechanically activated model fines partially substitute CEM I. The quotient in the present representation is illustrated through lines of different slopes. The mortar compressive strength at the age of 28 d, which in turn strongly depends on the SCM content and the w/b-ratio, significantly influences r, which increases with higher $f_{c,28\,\mathrm{d}}$. For similar $f_{c,28\,\mathrm{d}}$, artificial fines activated at 400 °C or 600 °C exhibit similar r, while increasing activation temperature to 800 °C leads to reduced r and mortar with artificial fines processed at 100 °C show increased r. These results mirror findings in literature, where compressive strength development of dehydrated cement paste is similar to Portland cement up to 3 d, but falls behind at later ages (Bogas et al., 2020; Real et al., 2020).

The resulting values for r correspond to the results for CEM I-mortar with different w/c-ratios (here, respective mean values from three series). These range from r = 0.46 for w/c = 0.60 (with $f_{c,28\,\mathrm{d}}$ = 40.4 MPa) to r = 0.50 for w/c = 0.55 (with $f_{c,28\,\mathrm{d}}$ = 48.0 MPa) and

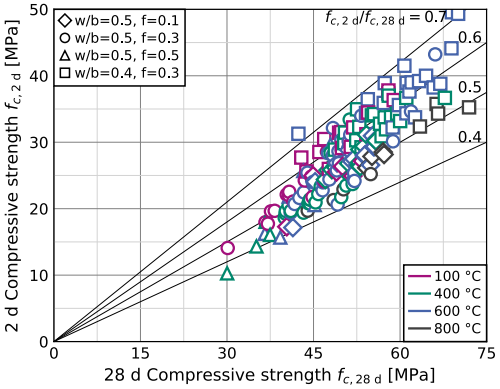

Fig. 8. Mortar compressive strength f_c at the age of 2 d over mortar compressive strength at 28 d for different mixes with partial CEM I-substitution through processed artificial fines. Marker shapes indicate mix composition, and colors indicate the activation temperature. (For interpretation of the references to color in this figure legend, the reader is referred to the web version of this article.)

r = 0.51 for w/c = 0.50 (with $f_{c,28\,\mathrm{d}}$ = 53.3 MPa) to r = 0.62 for w/c = 0.45 (with $f_{c,28\,\mathrm{d}}$ = 56.3 MPa).

Additionally, Eq. (2) was adapted from fib Model Code (2023) and adjusted to the results of mixtures that were tested at the ages of 1 d, 2 d, 7 d and 28 d using the least squares method.

$$f_c(t) = \beta_{cc}(t) \cdot f_{c,28\,\mathrm{d}} \quad \text{with} \tag{2}$$

$$\beta_{cc}(t) = \exp\left\{ s_c \cdot \left[1 - \left(\frac{28}{t} \right)^{l} \right] \right\} \tag{3}$$

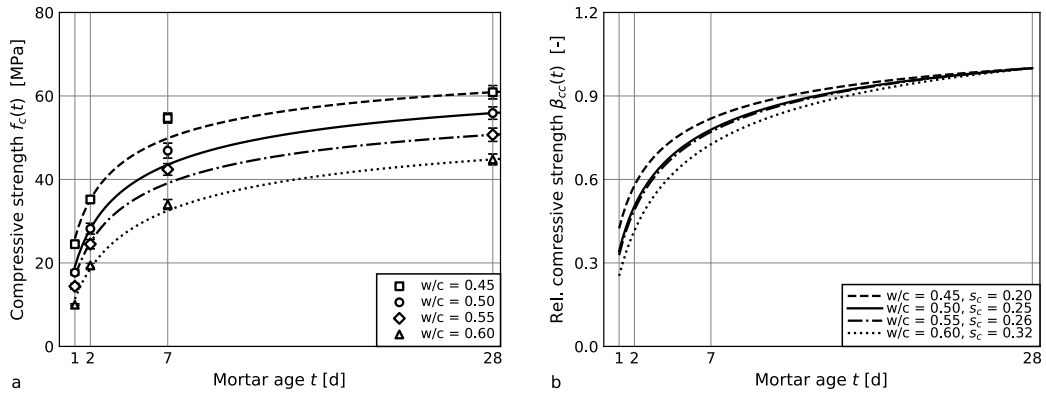

Fig. 9. Temporal compressive strength development (absolute (a) and relative (b)) of CEM I-mortar with different w/c ratio at the age of 1 d, 2 d, 7 d and 28 d, (mean and standard deviation from six prism halves for each data point as well as regression curves following Eq. (2)).

The parameter $l = 0.5$ is independent of the binder. A global analysis showed that these results in an underestimation of the strength development of the examined mortars at the age of 7 d. $l = 0.85$ would allow a better overall fit to the experimental data. However, for the following evaluation of the activated artificial fines, $l = 0.5$ was applied to enable better comparison with the values given in fib Model Code (2023). Subsequently, the parameter s_c was calculated for each individual mixture.

Fig. 9 illustrates the results for $f_c(t)$ and $\beta_{cc}(t)$, which were measured or calculated for mortars with CEM I with different w/c-ratios. The expected increase in compressive strength with decreasing w/c-ratios was shown, as well as a faster initial strength development with increasing strength. The calculated parameters s_c using regression analysis lie between 0.20 for $w/c = 0.45$ and 0.32 for $w/c = 0.60$. Thus, the values for s_c correspond to the values in fib Model Code (2023) of 0.3 and 0.2 for CEM I 42,5 R for characteristic concrete compressive strength $f_{ck} \leq 35$ MPa and 35 MPa $< f_{ck} <$ 60 MPa, respectively.

In Fig. 10, the corresponding calculated curves of $\beta_{cc}(t)$ are shown for eight mixtures with CEM I-substitution by thermally activated artificial fines ($f = 0.3$ at $w/b = 0.50$). The artificial fines CEM, RS75, RS62, and RS50 were used as SCMs, which were thermally activated at 400 °C or 600 °C. Strength tests were performed at the age of 1 d, 2 d, 7 d and 28 d on three prisms each. The replacement of CEM I by activated artificial fines generally leads to decreasing strengths at the age of 28 d. Apart from this, the relative temporal strength development, illustrated by the time functions $\beta_{cc}(t)$, is not affected. The determined values for s_c range from 0.19 for RS62-400 to 0.32 for RS75-600, with no systematic influence of activated artificial fines composition. Activation at 800 °C exhibits similar, yet slightly increased results for s_c, with $s_c = 0.32$ for CEM-800 and $s_c = 0.30$ for RS75-800, indicating a decelerated strength development.

3.2.3. Compressive strength at 28 d

The analysis of the test results regarding the influence of using processed artificial fines on the mortar compressive strength at the age of 28 d was based on the so-called k-value concept, which is described in CEN/TR 16639:2014. In this approach, the w/b-ratio (Eq. (4)) is replaced by an equivalent water-cement ratio (w/c_{eq}) according to Eq. (5). The k-values serve as a measure of the reactivity of the supplementary cementitious materials and thus as an indication of their influence on the compressive strength. The European concrete standard EN 206:2017 defines k-values for individual types of SCM, such as $k = 0.4$ for fly ash or $k = 0.6$ for blast-furnace slag.

$$\frac{w}{b} = \frac{w}{c+a} \quad \text{with } a\text{: mass of (reactive) SCMs} \tag{4}$$

$$\frac{w}{c_{eq}} = \frac{w}{c + k \cdot a} \tag{5}$$

Rather than the application of preset values for k to produce concrete with a target compressive strength, the present research uses Eq. (5) to calculate k-values for all activated artificial fines individually. Subsequently, k-values can serve as a measure for the analysis of the reactivity and compressive strength contribution of mode materials composition. Essential for determining equivalent water-cement ratios is the knowledge of the relationship between compressive strength f_c and the water-cement ratio w/c, which was first established for the 14 base mixtures from three series without SCMs (see Fig. 11).

For further computation, the test results were approximated using regression curves based on the least squares method. While normally convex curves are used for analyzing this material behavior, the present data are best represented by a linear approach (Eq. (6)), which is also proposed in CEN/TR 16639:2014.

$$f_{c,28\,d} = \alpha - \beta \cdot \frac{w}{c} \quad \text{with } \alpha = 105 \text{ and } \beta = 106 \tag{6}$$

The subsequent calculation of k uses the measured compressive strength to compute the corresponding equivalent water-cement ratio w/c_{eq} (Eq. (7)). With the additional input of mix parameters (substitution rate f and the water-binder ratio w/b), Eq. (8) gives the individual k-value of a specific mortar mix.

$$\frac{w}{c_{eq}} = \frac{\alpha - f_{c,28\,d}}{\beta} \tag{7}$$

$$k = 1 - \frac{1}{f} \cdot \left(1 - \frac{w/b}{w/c_{eq}}\right) \tag{8}$$

To evaluate the k-values of the mixtures with processed artificial fines as SCMs, it is first investigated to what extent the binder content f and the water-binder ratio w/b influence the overall results. For this purpose, pairs of mixtures from a sample set are considered. For $w/b = 0.50$, 37 successful test pairs are available, which result in arithmetic means of $k(f = 0.1) = 1.07$ and $k(f = 0.3) = 0.65$, suggesting an influence of the SCM content on the analysis results. 53 test pairs for $f = 0.3$ yield $k\,(w/b = 0.40) = 0.72$ and $k\,(w/b = 0.50) = 0.68$, whereby the influence of the water-binder ratio on the calculated k-values can be considered negligible.

Therefore, in the next step, these 53 test pairs for $f = 0.3$ were used to determine influencing factors of processing parameters as well as artificial fines composition. Fig. 12 illustrates the arithmetic mean values of the 53 test pairs.

By comparing the artificial fines CEM, LS75, and LS50 (Fig. 12(a)), it becomes apparent that the treatment temperature only indirectly influences the reactivity. Instead, the mass loss due to dehydration is the decisive criterion for the reactivity resulting from thermal processing. CEM activated at 400 °C (CEM-400) shows a similar mass loss of $\Delta m = 9.4$ wt% as LS75-600 with $\Delta m = 9.7$ wt%, resulting in $k = 0.66$ for both artificial fines (mean values over two test pairs). LS75-400 and

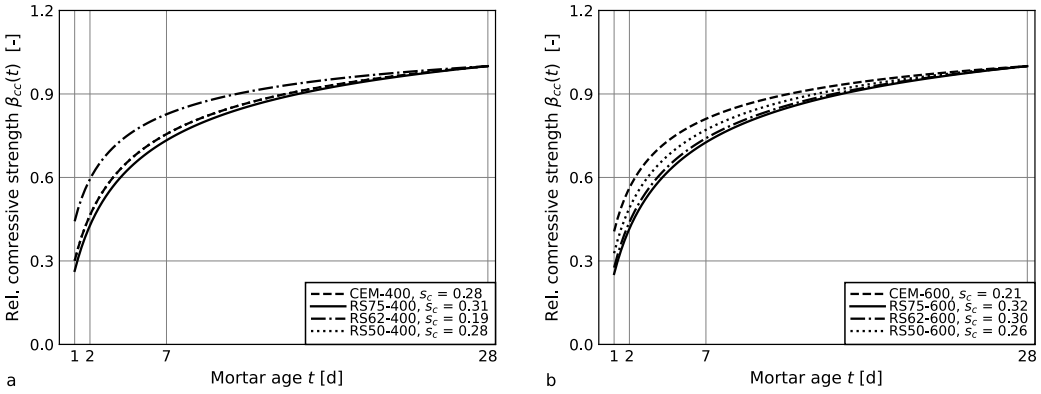

Fig. 10. Relative temporal compressive strength development of mortar containing artificial fines with different river sand content activated at 400 °C (a) and 600 °C (b).

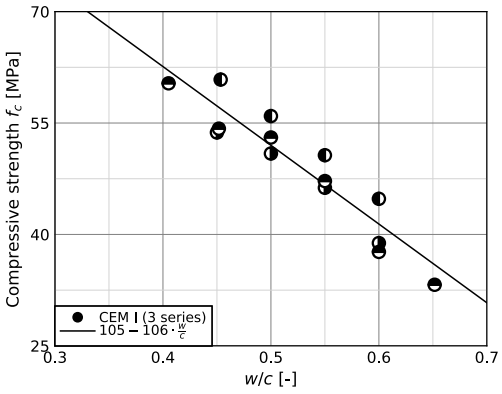

Fig. 11. Relationship between compressive strength f_c and water-cement ratio for mortar mixes without CEM I-substitution for $0.40 \leq w/c \leq 0.65$.

LS50-600 behave similarly (with an outlier due to material scattering being plausible). For all examined test series with the artificial fines CEM, LS75, LS50, and LS0, a linear relationship between k and Δm can be observed. A plausible deviation is CEM-800 with $\Delta m = 18.0\,\mathrm{wt\%}$, as the mass loss can only be attributed to dehydration up to processing temperatures of approximately 650 °C, after which the decomposition of carbonates with the release of CO_2 begins (Klingsch, 2014). The high k-values for thermally activated CEM corroborate findings in Bogas et al. (2022a), Carriço et al. (2020b), Letelier et al. (2017), Ma et al. (2022), Qian et al. (2020), Tokareva et al. (2023), Vashistha et al. (2023) and Wu et al. (2023), where the substitution of Portland cement through thermally activated cement paste has only minor negative effects on compressive strength. Paste precursors containing limestone powder, which is similar to LS75, exhibit reduced strength (Xu et al., 2023b; Serpell and Lopez, 2013).

When considering artificial fines with river sand instead of limestone as aggregate (Fig. 12(b)), a slight increase in k-values can be observed, regardless of the mass loss. The same applies more pronouncedly to artificial fines with greywacke (Fig. 12(d)). Ground limestone (or limestone powder) acts as an inert SCM, whereas SiO_2 from the aggregate contained in the artificial fines can exhibit pozzolanic reactivity. Prerequisites for this are that SiO_2 is amorphous or that crystalline quartzitic SiO_2 has been very finely ground. While it can be assumed that artificial fines with river sand and greywacke contain some particles with sufficient fineness, greywacke also contains amorphous SiO_2.

Additional positive effects on the reactivity of thermally activated artificial fines become apparent when they contain reaction products of blast-furnace slag or fly ash (Fig. 12(c)), which corroborates findings in Xu et al. (2023b,a).

Based on these observations, various model approaches are subsequently investigated to predict k-values based on the artificial fines composition and mass loss during thermal processing. The analysis is based on 49 test pairs with a CEM I-substitution rate of $f = 0.3$ through artificial fines processed at 100 °C, 400 °C or 600 °C.

The best fit is defined in Eq. (9). Model parameters are determined using the method of least squares from 98 individual results of the 49 test pairs with $f = 0.3$. As a result, the sum of the squared errors amounts to $\Delta^2 = 14.8$ and the coefficient of determination for the compressive strength is $R^2 = 0.75$. The results are illustrated in Fig. 13.

$$k = k_h \cdot \Delta m + k_a + k_b \tag{9}$$

$$k_h = 5.70 \tag{10}$$

$$k_a = \begin{cases} 0.00 & \text{for LS} \\ 0.10 & \text{for RS} \\ 0.30 & \text{for GW} \end{cases} \tag{11}$$

$$k_b = \begin{cases} 0.15 & \text{for CEM I} \\ 0.30 & \text{for CEM I + S} \\ 0.45 & \text{for CEM I + FA} \end{cases} \tag{12}$$

For ground artificial fines, the k-value comprises a binder-dependent and an aggregate-dependent constant parameter. The mass loss Δm during thermal activation increases k linearly. Alongside the interpretation of Δm as chemically bound water, k_h can be transformed into the amount of water bound per unit-weight of cement, m_h (see Eq. (13)). $k_h = 5.70$ corresponds to $m_h = 0.21$. Despite the indirect determination method, this agrees with the amount of chemically bound water from Power's model (Powers and Brownyard, 1946; Brouwers, 2004; Lura et al., 2017).

$$k_h = 1 + \frac{1}{m_h} \tag{13}$$

A simplified model, where artificial fines composition is not accounted for ($k_a = k_b = 0.00$) yields an increased $k_h = 8.80$ at a higher sum of the squared errors ($\Delta^2 = 20.4$) and a reduced coefficient of determination for the compressive strength ($R^2 = 0.40$). Similarly, when using the exact artificial fines composition to alter Eq. (9) to directly account for the aggregate and paste content, the sum of squared errors increases slightly to $\Delta^2 = 14.9$. The coefficient of determination for the compressive strength decreases insignificantly ($R^2 = 0.73$).

Subsequently, an extension of Eq. (9) for k to account for the CEM I-substitution rate (f) is investigated. The best approach (Eq. (14)) yields $R^2 = 0.77$ (starting from $R^2 = 0.75$ without considering f).

$$k = (k_h \cdot \Delta m + k_a + k_b) \cdot \left(\frac{f_{ref}}{f}\right)^{k_f} \tag{14}$$

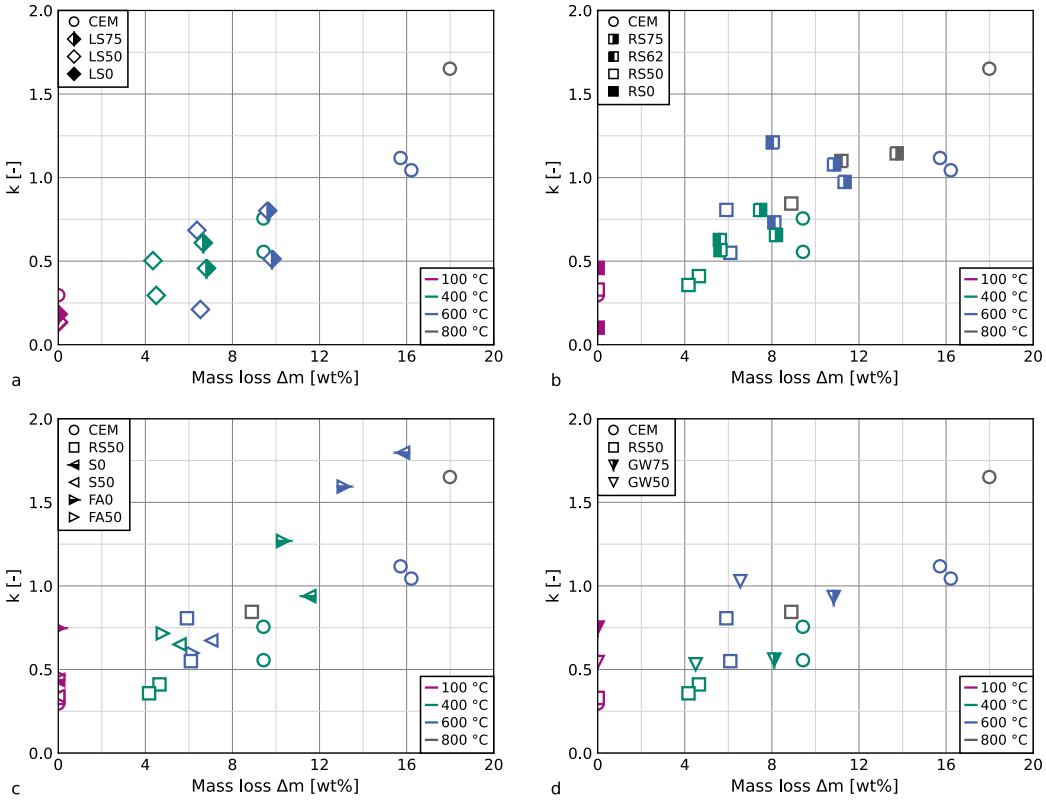

Fig. 12. Relationship between k-values of processed artificial fines and mass loss during thermal activation (arithmetic means for $w/b = 0.40$ and $w/b = 0.50$ at $f = 0.3$).

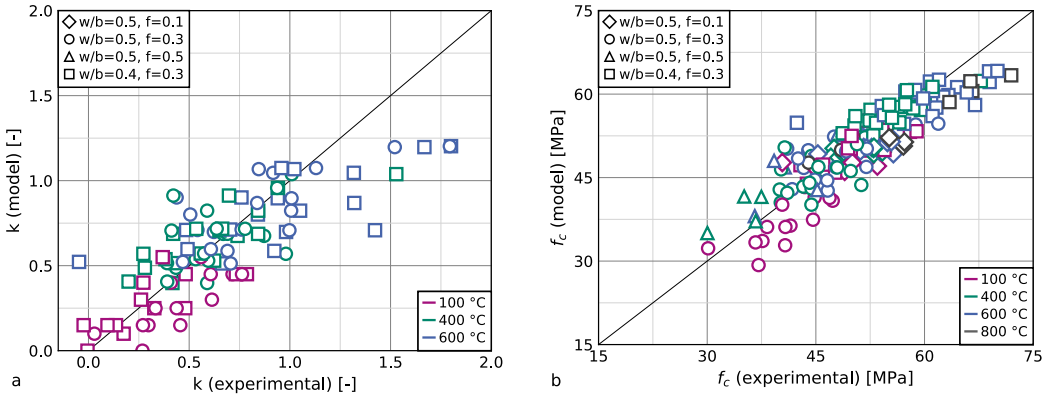

Fig. 13. Modeled over measured k-values for $f = 0.3$ (a), modeled over measured compressive strength f_c for all mix compositions (b).

$$k_f = 0.5 \tag{15}$$

f_{ref} denotes the CEM I-substitution rate for which the basic model was calibrated; presently $f_{ref} = 0.3$. The nonetheless relatively poor model fit is due to incomplete data: For $f = 0.1$, no experiments were conducted with the artificial fines S0, S50, FA0, and FA50. For $f = 0.5$, the scope of the experiments was further significantly reduced, making it impossible to analyze the influence of the binder content in conjunction with some artificial fines parameters. Furthermore, the results for $f = 0.1$ are subject to significantly increased scatter, which results from the calculation procedure (see Eq. (8)). Fig. 14 confirms that the scatter of theoretical k-values increases with decreasing substitution rate f, since all material scatter is projected onto a decreasing proportion of the binder. Nevertheless, it becomes apparent that the model adaptation leads to a significantly improved prediction of the k-value, in that k-values for $f = 0.1$ are no longer underestimated and for $f = 0.5$ are no longer overestimated. However, only the latter has a notable influence on the prediction of the mortar compressive strength, since a cement substitution of 10 wt% generally only shows minor effects on compressive strength.

4. Conclusions

The present results detail the impact of concrete fines composition on compressive strength contribution after thermal activation. The substitution of 30 wt% OPC through pure cement paste activated at 600 °C does not affect compressive strength ($k = 1.0$). When cement paste contains hydration products from blast-furnace slag or fly ash, compressive strength at 28 d can even exceed the reference ($k > 1.0$). Compressive strength contribution decreases with increasing aggregate content in the fines, but also depends on the aggregate composition, with limestone sand performing worse than quartzitic sand.

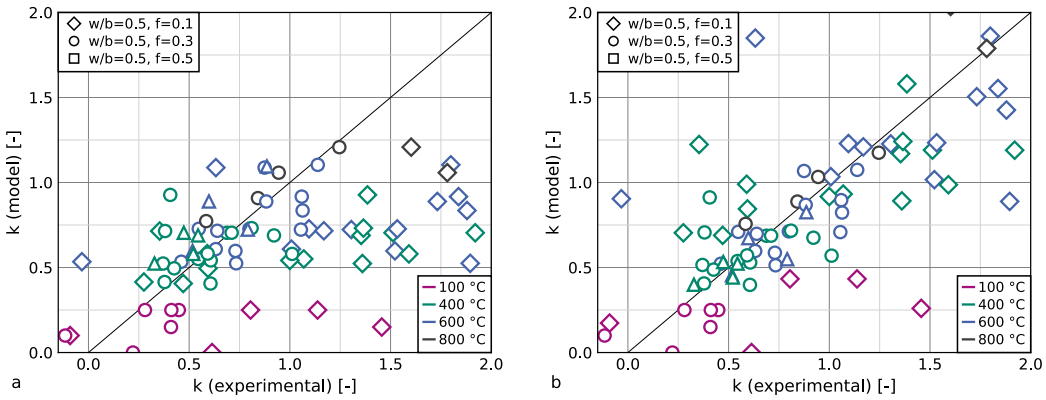

Fig. 14. Modeled k-values without consideration of the substitution rate f (a) and with consideration of f through Eq. (14) (b).

Fines containing greywacke with amorphous silicates exhibit increased compressive strength contribution, even without thermal activation.

While the activation temperature remains the most important processing parameter for achieving high compressive strength, the present analysis finds an overall good correlation between mass loss during thermal activation and compressive strength contribution, regardless of fines composition and aggregate content. The proposed model for strength contribution is based on the k-value approach in EN:206:2017 and reflects binder and aggregate composition through fixed parameters. The linear influence of the mass loss agrees with theoretical assumptions for the chemically bound water content in hardened cement paste.

While these findings are mostly based on a CEM I-substitution of 30 wt%, a model extension reflects findings from both the present experimental work as well as literature, where compressive strength contribution reduces with increasing substitution rate. This allows for increasing compressive strength when up to 10 wt% of CEM I is substituted through thermally activated concrete fines.

The temporal compressive strength development of mortar containing thermally activated concrete fines is independent of their composition or processing temperature. Overall, besides the aforementioned impact on absolute strength, relative strength development is similar to CEM I. Only when fines are processed at 800 °C, relative strength development slows.

High early strength is caused by fast rehydration of fines, which exhibit an increased and accelerated hydration heat development during the first 6 h after mixing. While fines composition has a minor impact on hydration heat development, results for different substitution rates suggest interactions between activated fines and Portland cement, which require additional research.

While the proposed model for strength contribution has been calibrated for the extensive present experimental data, an industrial application requires an even broader dataset, which includes cement, SCMs, and aggregates from different geographical sources, with a more detailed analysis of their compositions. This dataset may then serve as a benchmark and model validation for industrially processed concrete fines, where the composition is generally unknown. As the present analysis focuses on compressive strength, further studies also require the investigation of concrete durability and the applicability of empirical provisions in structural design codes.

CRediT authorship contribution statement

Jan P. Höffgen: Writing – original draft, Visualization, Methodology, Funding acquisition, Formal analysis, Conceptualization. **Frank Dehn:** Writing – review & editing, Supervision, Project administration, Funding acquisition.

Declaration of Generative AI and AI-assisted technologies in the writing process

During the preparation of this work the authors used Grammarly and DeepL in order to check for spelling and wording errors. After using these tools/services, the authors reviewed and edited the content as needed and take full responsibility for the content of the published article.

Funding

This work was supported by the Dres. Edith und Klaus Dyckerhoff-Stiftung, grant no. T0218/36374.

Declaration of competing interest

The authors declare that they have no known competing financial interests or personal relationships that could have appeared to influence the work reported in this paper.

Acknowledgments

The authors would like to thank Jakob Grigo and Jonas Vormschlag for their invaluable experimental work.

Data availability

Data will be made available on request.

References

Alonso, C., Fernandez, L., 2004. Dehydration and rehydration processes of cement paste exposed to high temperature environments. J. Mater. Sci. 39 (9), 3015–3024. http://dx.doi.org/10.1023/B:JMSC.0000025827.65956.18.

Angulo, S.C., Guilge, M.S., Quarcioni, V.A., Cincotto, M.A., Nobre, T.R., Pöllmann, H., 2022. The role of calcium silicates and quicklime on the reactivity of rehydrated cements. Constr. Build. Mater. 340, 127625. http://dx.doi.org/10.1016/j.conbuildmat.2022.127625.

Aquino Rocha, J.H., Toledo Filho, R.D., 2023. The utilization of recycled concrete powder as supplementary cementitious material in cement-based materials: A systematic literature review. J. Build. Eng. 76, 107319. http://dx.doi.org/10.1016/j.jobe.2023.107319.

Baggio, T.F., Possan, E., De Oliveira Andrade, J.J., 2024. Physical-chemical characterization of construction and demolition waste powder with thermomechanical activation for use as supplementary cementitious material. Constr. Build. Mater. 437, 136907. http://dx.doi.org/10.1016/j.conbuildmat.2024.136907.

Baldusco, R., Nobre, T.R.S., Angulo, S.C., Quarcioni, V.A., Cincotto, M.A., 2019. Dehydration and rehydration of blast furnace slag cement. J. Mater. Civ. Eng. 31 (8), 04019132. http://dx.doi.org/10.1061/(ASCE)MT.1943-5533.0002725.

Baquerizo, L.G., Matschei, T., Scrivener, K.L., 2016. Impact of water activity on the stability of ettringite. Cem. Concr. Res. 79, 31–44. http://dx.doi.org/10.1016/j.cemconres.2015.07.008.

Barthel, M., Rübner, K., Kühne, H.-C., Rogge, A., Dehn, F., 2016. From waste materials to products for use in the cement industry. Adv. Cem. Res. 28 (7), 458–468. http://dx.doi.org/10.1680/jadcr.15.00149.

Bogas, J.A., Carriço, A., Pereira, M., 2019. Mechanical characterization of thermal activated low-carbon recycled cement mortars. J. Clean. Prod. 218, 377–389. http://dx.doi.org/10.1016/j.jclepro.2019.01.325.

Bogas, J.A., Carriço, A., Real, S., 2022a. Durability of concrete produced with recycled cement from waste concrete. Mater. Today: Proc. 58, 1149–1154. http://dx.doi.org/10.1016/j.matpr.2022.01.280.

Bogas, J.A., Carriço, A., Tenza-Abril, A.J., 2020. Microstructure of thermoactivated recycled cement pastes. Cem. Concr. Res. 138, 106226. http://dx.doi.org/10.1016/j.cemconres.2020.106226.

Bogas, J.A., Real, S., Carriço, A., Abrantes, J., Guedes, M., 2022b. Hydration and phase development of recycled cement. Cem. Concr. Compos. 127, 104405. http://dx.doi.org/10.1016/j.cemconcomp.2022.104405.

Brameshuber, W., Hannawald, J., Hauer, B., Herbst, T., Meng, B., Nebel, H., Pierkes, R., Rübner, K., Schäfer, S., Seidel, M., Vollpracht, A., DAfStb, 2011. Verbundforschungsvorhaben nachhaltig bauen mit beton: potenziale des sekundärstoffeinsatzes im betonbau - teilprojekt b effiziente sicherstellung der umweltverträglichkeit von beton - teilprojekt e. DAfStb-Heft, vol. 584, Beuth, Berlin.

Brouwers, H., 2004. The work of powers and Brownyard revisited: Part 1. Cem. Concr. Res. 34 (9), 1697–1716. http://dx.doi.org/10.1016/j.cemconres.2004.05.031.

Carriço, A., Bogas, J.A., Guedes, M., 2020a. Thermoactivated cementitious materials – a review. Constr. Build. Mater. 250, 118873. http://dx.doi.org/10.1016/j.conbuildmat.2020.118873.

Carriço, A., Bogas, J.A., Hu, S., Real, S., Costa Pereira, M.F., 2021a. Novel separation process for obtaining recycled cement and high-quality recycled sand from waste hardened concrete. J. Clean. Prod. 309, 127375. http://dx.doi.org/10.1016/j.jclepro.2021.127375.

Carriço, A., Real, S., Bogas, J.A., 2021b. Durability performance of thermoactivated recycled cement concrete. Cem. Concr. Compos. 124, http://dx.doi.org/10.1016/j.cemconcomp.2021.104270.

Carriço, A., Real, S., Bogas, J.A., Costa Pereira, M.F., 2020b. Mortars with thermo activated recycled cement: Fresh and mechanical characterisation. Constr. Build. Mater. 256, 119502. http://dx.doi.org/10.1016/j.conbuildmat.2020.119502.

Chen, L., Wei, M., Lei, N., Li, H., 2024. Effect of chemical–thermal activation on the properties of recycled fine powder cementitious materials. Case Stud. Constr. Mater. 20, e02956. http://dx.doi.org/10.1016/j.cscm.2024.e02956.

Coffetti, D., Crotti, E., Gazzaniga, G., Carrara, M., Pastore, T., Coppola, L., 2022. Pathways towards sustainable concrete. Cem. Concr. Res. 154, 106718. http://dx.doi.org/10.1016/j.cemconres.2022.106718.

Cyr, M., Diliberto, C., Lecomte, A., Izoret, L., 2019. Recycled concrete as cement main constutient (CMC) or supplementary cementitious materials (SCM). In: Larrard, F.c., Colina, H. (Eds.), Concrete Recycling: Research and Practice. CRC Press/Taylor & Francis Group, Boca Raton, FL, pp. 83–95.

fib Model Code, 2023. fib model code for concrete structures (2020), Version 1. In: International Federation for Structural Concrete (Ed.), International Federation for Structural Concrete (fib), Lausanne, ISBN: 978-2-88394-175-5.

Florea, M.V.A., 2014. Secondary Materials Applied in Cement-Based Products : Treatment, Modelling and Environmental Interaction (Ph.D. thesis). Technische Universiteit Eindhoven, http://dx.doi.org/10.6100/IR772902.

Frías, M., Martínez-Ramírez, S., La Villa, R.V., Fernández-Carrasco, L., García, R., 2021. Reactivity in cement pastes bearing fine fraction concrete and glass from construction and demolition waste: microstructural analysis of viability. Cem. Concr. Res. 148, 106531. http://dx.doi.org/10.1016/j.cemconres.2021.106531.

Friol Guedes de Paiva, F., Tamashiro, J.R., Pereira Silva, L.H., Kinoshita, A., 2021. Utilization of inorganic solid wastes in cementitious materials – a systematic literature review. Constr. Build. Mater. 285, 122833. http://dx.doi.org/10.1016/j.conbuildmat.2021.122833.

Gao, Y., Schutter, G., Ye, G., Yu, Z., Tan, Z., Wu, K., 2013. A microscopic study on ternary blended cement based composites. Constr. Build. Mater. 46, 28–38. http://dx.doi.org/10.1016/j.conbuildmat.2013.04.021.

Ge, P., Song, Y., Quan, J., Wu, Y., Zhou, J., 2024. Study on the activity, phase, thermal decomposition characteristics, microstructure, and chemical element of hardened cement powder under heating temperature of 100°c˜1200°c. Struct. Concr. http://dx.doi.org/10.1002/suco.202301108.

Gebremariam, A.T., Di Maio, F., Vahidi, A., Rem, P., 2020. Innovative technologies for recycling End-of-Life concrete waste in the built environment. Resour. Conserv. Recycl. 163, 104911. http://dx.doi.org/10.1016/j.resconrec.2020.104911.

Hafez, H., Kurda, R., Cheung, W.M., Nagaratnam, B., 2020. Comparative life cycle assessment between imported and recovered fly ash for blended cement concrete in the UK. J. Clean. Prod. 244, 118722. http://dx.doi.org/10.1016/j.jclepro.2019.118722.

Herrmann, A., Koenig, A., Dehn, F., 2018. Structural concrete based on alkali-activated binders: terminology, reaction mechanisms, mix designs and performance. Struct. Concr. 19 (3), 918–929. http://dx.doi.org/10.1002/suco.201700016.

Horváth, I., Proks, I., Nerád, I., 1977. Activation energies of the thermal decompositions of C3AH6 AND C3AD6 by the isothermal TG method. J. Therm. Anal. 12 (1), 105–110. http://dx.doi.org/10.1007/BF01909862.

Izoret, L., Diliberto, C., Mechling, J.M., Lecomte, A., Natin, P., 2019. Recycled concrete sand as alternative raw material for Portland clinker production. In: Larrard, F.c., Colina, H. (Eds.), Concrete Recycling: Research and Practice. CRC Press/Taylor & Francis Group, Boca Raton, FL, pp. 63–81.

Kim, J.-H., Seo, E.-A., Kim, D.-G., Chung, C.-W., 2021. Utilization of recycled cement powder as a solidifying agent for radioactive waste immobilization. Constr. Build. Mater. 289, 123126. http://dx.doi.org/10.1016/j.conbuildmat.2021.123126.

Kim, J., Ubysz, A., 2024. Thermal activation of multi-recycled concrete powder as supplementary cementitious material for repeated and waste-free recycling. J. Build. Eng. 98, 111169. http://dx.doi.org/10.1016/j.jobe.2024.111169.

Klingsch, E.W., 2014. Explosive Spalling of Concrete in Fire (Ph.D. thesis). ETH Zurich, Zürich, http://dx.doi.org/10.3929/ethz-a-010243000.

Knight, K.A., Cunningham, P.R., Miller, S.A., 2023. Optimizing supplementary cementitious material replacement to minimize the environmental impacts of concrete. Cem. Concr. Compos. 139, 105049. http://dx.doi.org/10.1016/j.cemconcomp.2023.105049.

Letelier, V., Tarela, E., Muñoz, P., Moriconi, G., 2017. Combined effects of recycled hydrated cement and recycled aggregates on the mechanical properties of concrete. Constr. Build. Mater. 132, 365–375. http://dx.doi.org/10.1016/j.conbuildmat.2016.12.010.

Li, S., Gao, J., Li, Q., Zhao, X., 2021. Investigation of using recycled powder from the preparation of recycled aggregate as a supplementary cementitious material. Constr. Build. Mater. 267, 120976. http://dx.doi.org/10.1016/j.conbuildmat.2020.120976.

Liang, C., Zhang, Y., Wu, R., Yang, D., Ma, Z., 2021. The utilization of active recycled powder from various construction wastes in preparing ductile fiber-reinforced cementitious composites: A case study. Case Stud. Constr. Mater. 15, 00650. http://dx.doi.org/10.1016/j.cscm.2021.e00650.

Lipowsky, A., Müller, A., 2017. Gesteinsmehl als Zuschlagstoffe in hydraulischen Bindemitteln. Aufbereitungs-Technik/Mineral Process. 58 (12), 52–64.

Liu, Q., Xiao, J., Singh, A., 2021. Quantification of plastic shrinkage and cracking in mortars containing different recycled powders using digital image correlation technique. Constr. Build. Mater. 293, 123509. http://dx.doi.org/10.1016/j.conbuildmat.2021.123509.

Lura, P., Winnefeld, F., Fang, X., 2017. A simple method for determining the total amount of physically and chemically bound water of different cements. J. Therm. Anal. Calorim. 130 (2), 653–660. http://dx.doi.org/10.1007/s10973-017-6513-z.

Ma, Z., Shen, J., Wu, H., Zhang, P., 2022. Properties and activation modification of eco-friendly cementitious materials incorporating high-volume hydrated cement powder from construction waste. Constr. Build. Mater. 316, 125788. http://dx.doi.org/10.1016/j.conbuildmat.2021.125788.

Ma, Z., Wu, Y., Fang, K., Zhang, Y., Wang, C., 2025. Developing fully recycled alkali-activated mortar made with waste concrete fines as a substitute for both binder and sand: multi-properties evaluation. Constr. Build. Mater. 477, 141323. http://dx.doi.org/10.1016/j.conbuildmat.2025.141323.

Müller, C., Dora, B., 2000. Verwertung von brechsand aus bauschutt. Deutscher Ausschuss Für Stahlbeton, vol. 506, Beuth, Berlin.

Noel, N., Mielke, T., Semugaza, G., Gierth, A.Z., Helmich, S., Nawrath, S., Lupascu, D.C., 2025. Chemical transformations during the preparation and rehydration of reactivated virgin cements. CEMENT 19, 100129. http://dx.doi.org/10.1016/j.cement.2025.100129.

Ohemeng, E.A., Ekolu, S.O., 2020. A review on the reactivation of hardened cement paste and treatment of recycled aggregates. Mag. Concr. Res. 72 (10), 526–539. http://dx.doi.org/10.1680/jmacr.18.00452.

Powers, T.C., Brownyard, T.L., 1946. Studies of the physical properties of hardened portland cement paste. ACI J. Proc. 43 (9), 249–336. http://dx.doi.org/10.14359/15301.

Qian, D., Yu, R., Shui, Z., Sun, Y., Jiang, C., Zhou, F., Ding, M., Tong, X., He, Y., 2020. A novel development of green ultra-high performance concrete (UHPC) based on appropriate application of recycled cementitious material. J. Clean. Prod. 261, 121231. http://dx.doi.org/10.1016/j.jclepro.2020.121231.

Real, S., Carriço, A., Bogas, J.A., Guedes, M., 2020. Influence of the treatment temperature on the microstructure and hydration behavior of thermoactivated recycled cement. Materials 13 (18), 3937. http://dx.doi.org/10.3390/ma13183937.

Richardson, I.G., 2000. The nature of the hydration products in hardened cement pastes. Cem. Concr. Compos. 22 (2), 97–113. http://dx.doi.org/10.1016/S0958-9465(99)00036-0.

Schneider, U., 1982. Verhalten von Beton bei hohen temperaturen. DAfStb-Heft, vol. 337, Wilhelm Ernst und Sohn, Berlin.

Scrivener, K.L., Juilland, P., Monteiro, P.J., 2015. Advances in understanding hydration of Portland cement. Cem. Concr. Res. 78, 38–56. http://dx.doi.org/10.1016/j.cemconres.2015.05.025.

Semugaza, G., Mielke, T., Castillo, M.E., Gierth, A.Z., Tam, J.X., Nawrath, S., Lupascu, D.C., 2023. Reactivation of hydrated cement powder by thermal treatment for partial replacement of ordinary portland cement. Mater. Struct. 56 (3), http://dx.doi.org/10.1617/s11527-023-02133-9.

Serpell, R., Lopez, M., 2013. Reactivated cementitious materials from hydrated cement paste wastes. Cem. Concr. Compos. 39, 104–114. http://dx.doi.org/10.1016/j.cemconcomp.2013.03.020.

Serpell, R., Lopez, M., 2015. Properties of mortars produced with reactivated cementitious materials. Cem. Concr. Compos. 64, 16–26. http://dx.doi.org/10.1016/j.cemconcomp.2015.08.003.

Serpell, R., Zunino, F., 2017. Recycling of hydrated cement pastes by synthesis of α′H-C2S. Cem. Concr. Res. 100, 398–412. http://dx.doi.org/10.1016/j.cemconres.2017.08.001.

Shah, I.H., Miller, S.A., Jiang, D., Myers, R.J., 2022. Cement substitution with secondary materials can reduce annual global CO2 emissions by up to 1.3 gigatons. Nat. Commun. 13 (1), 5758. http://dx.doi.org/10.1038/s41467-022-33289-7.

Shen, P., Sun, Y., Liu, S., Jiang, Y., Zheng, H., Xuan, D., Lu, J., Poon, C.S., 2021. Synthesis of amorphous nano-silica from recycled concrete fines by two-step wet carbonation. Cem. Concr. Res. 147, 106526. http://dx.doi.org/10.1016/j.cemconres.2021.106526.

Shui, Z., Xuan, D., Wan, H., Cao, B., 2008. Rehydration reactivity of recycled mortar from concrete waste experienced to thermal treatment. Constr. Build. Mater. 22 (8), 1723–1729. http://dx.doi.org/10.1016/j.conbuildmat.2007.05.012.

Snellings, R., Suraneni, P., Skibsted, J., 2023. Future and emerging supplementary cementitious materials. Cem. Concr. Res. 171, 107199. http://dx.doi.org/10.1016/j.cemconres.2023.107199.

Sousa, L.N., Zepper, J., Schollbach, K., Brouwers, H., 2024. Improving the reactivity of industrial recycled concrete fines: exploring mechanical and hydrothermal activation. Constr. Build. Mater. 442, 137594. http://dx.doi.org/10.1016/j.conbuildmat.2024.137594.

Sui, Y., Ou, C., Liu, S., Zhang, J., Tian, Q., 2020. Study on properties of waste concrete powder by thermal treatment and application in mortar. Appl. Sci. 10 (3), 998. http://dx.doi.org/10.3390/app10030998.

Sun, C., Chen, L., Xiao, J., Singh, A., Zeng, J., 2021. Compound utilization of construction and industrial waste as cementitious recycled powder in mortar. Resour. Conserv. Recycl. 170, 105561. http://dx.doi.org/10.1016/j.resconrec.2021.105561.

Tajuelo Rodriguez, E., Garbev, K., Merz, D., Black, L., Richardson, I.G., 2017. Thermal stability of C-S-H phases and applicability of Richardson and Groves' and richardson C-(A)-S-H(I) models to synthetic C-S-H. Cem. Concr. Res. 93, 45–56. http://dx.doi.org/10.1016/j.cemconres.2016.12.005.

Tokareva, A., Kaassamani, S., Waldmann, D., 2023. Fine demolition wastes as supplementary cementitious materials for CO2 reduced cement production. Constr. Build. Mater. 392, 131991. http://dx.doi.org/10.1016/j.conbuildmat.2023.131991.

Vashistha, P., Oinam, Y., Kim, H.-K., Pyo, S., 2023. Effect of thermo-mechanical activation of waste concrete powder (WCP) on the characteristics of cement mixtures. Constr. Build. Mater. 362, 129713. http://dx.doi.org/10.1016/j.conbuildmat.2022.129713.

VDZ, 2024. Environmental Data of the German Cement Industry 2023. Tech. rep., Verein Deutscher Zementwerke e.V., Düsseldorf.

Wang, J., Lacarrière, L., Sellier, A., 2019. Multicomponent modelling of cement paste dehydration under different heating rates. Mater. Struct. 52 (1), 6. http://dx.doi.org/10.1617/s11527-018-1306-9.

Wang, C., Zhang, Z., Liu, X., Zhang, Y., Ma, Z., 2024. Elucidating the role of recycled concrete aggregate in ductile engineered geopolymer composites: Effects of recycled concrete aggregate content and size. J. Build. Eng. 95, 110150. http://dx.doi.org/10.1016/j.jobe.2024.110150.

Wei, M., Chen, L., Lei, N., Li, H., Huang, L., 2024. Experimental investigation on freeze–thaw resistance of thermally activated recycled fine powder concrete. Constr. Build. Mater. 457, 139378. http://dx.doi.org/10.1016/j.conbuildmat.2024.139378.

Wei, M., Chen, L., Lei, N., Li, H., Huang, L., 2025. Mechanical properties and microstructures of thermally activated ultrafine recycled fine powder cementitious materials. Constr. Build. Mater. 475, 141195. http://dx.doi.org/10.1016/j.conbuildmat.2025.141195.

Wiedmann, A., 2020. Schadensrisiko und Schadensentwicklung in Betonfahrbahndecken als Folge einer Alkali-Kieselsäure-Reaktion. KIT-Bibliothek, Karlsruhe, http://dx.doi.org/10.5445/IR/1000125632.

Wu, H., Liang, C., Zhang, Z., Yao, P., Wang, C., Ma, Z., 2023. Utilizing heat treatment for making low-quality recycled aggregate into enhanced recycled aggregate, recycled cement and their fully recycled concrete. Constr. Build. Mater. 394, 132126. http://dx.doi.org/10.1016/j.conbuildmat.2023.132126.

Wu, H., Liu, X., Wang, C., Zhang, Y., Ma, Z., 2024. Micro-properties and mechanical behavior of high-ductility engineered geopolymer composites (EGC) with recycled concrete and paste powder as green precursor. Cem. Concr. Compos. 152, 105672. http://dx.doi.org/10.1016/j.cemconcomp.2024.105672.

Xi, X., Zheng, Y., Du, C., Zhang, P., Sun, M., 2024a. Study on the hydration characteristics, mechanical properties, and microstructure of thermally activated low-carbon recycled cement. Constr. Build. Mater. 447, 138042. http://dx.doi.org/10.1016/j.conbuildmat.2024.138042.

Xi, X., Zheng, Y., Zhuo, J., Zhang, P., Golewski, G.L., Du, C., 2024b. Influence of water glass modulus and alkali content on the properties of alkali-activated thermally activated recycled cement. Constr. Build. Mater. 452, 138867. http://dx.doi.org/10.1016/j.conbuildmat.2024.138867.

Xu, L., Wang, J., Li, K., Hao, T., Li, Z., Li, L., Ran, B., Du, H., 2023a. New insights on dehydration at elevated temperature and rehydration of GGBS blended cement. Cem. Concr. Compos. 139, 105068. http://dx.doi.org/10.1016/j.cemconcomp.2023.105068.

Xu, L., Wang, J., Li, K., Li, M., Lin, S., Hao, T., Wang, T., Guo, Y., Ling, Z., 2023b. Investigations on the rehydration of recycled blended SCMs cement. Cem. Concr. Res. 163, 107036.

Xu, L., Wang, J., Li, K., Lin, S., Li, M., Hao, T., Ling, Z., Xiang, D., Wang, T., 2022. A systematic review of factors affecting properties of thermal-activated recycled cement. Resour. Conserv. Recycl. 185, 106432. http://dx.doi.org/10.1016/j.resconrec.2022.106432.

Yonis, A., Oinam, Y., Vashistha, P., Degefa, A.B., Belayneh, G.B., Park, S., Pyo, S., 2024. Novel activation method of waste concrete powder for sustainable clinker-free binder. Cem. Concr. Compos. 151, 105600. http://dx.doi.org/10.1016/j.cemconcomp.2024.105600.

Yu, R., Shui, Z., 2013. Influence of agglomeration of a recycled cement additive on the hydration and microstructure development of cement based materials. Constr. Build. Mater. 49, 841–851. http://dx.doi.org/10.1016/j.conbuildmat.2013.09.004.

Zelic, J., Ugrina, L., Jozic, D., 2007. Application of thermal methods in the chemistry of cement: Kinetic Analysis of Portlandite from non-isothermal thermogravimetric data. In: The First International Proficiency Testing Conference. n. d., Sinaia, Romania, pp. 420–429.

Zhang, L., Yongsheng, J., Guodong, H., Li, J., Hu, Y., 2018. Modification and enhancement of mechanical properties of dehydrated cement paste using ground granulated blast-furnace slag. Constr. Build. Mater. (164), 525–534. http://dx.doi.org/10.1016/j.conbuildmat.2017.12.232.

Zhang, H., Zhang, B., Tang, L., Zeng, W., 2023. Analysis of two processing techniques applied on powders from recycling of clay bricks and concrete, in terms of efficiency, energy consumption, and cost. Constr. Build. Mater. 385, 131517. http://dx.doi.org/10.1016/j.conbuildmat.2023.131517.

Zheng, Y., Xi, X., Liu, H., Du, C., Lu, H., 2024. A review: enhanced performance of recycled cement and CO2 emission reduction effects through thermal activation and nanosilica incorporation. Constr. Build. Mater. 422, 135763. http://dx.doi.org/10.1016/j.conbuildmat.2024.135763.

Zhou, Q., Glasser, F.P., 2001. Thermal stability and decomposition mechanisms of ettringite at <120°c. Cem. Concr. Res. 31 (9), 1333–1339. http://dx.doi.org/10.1016/S0008-8846(01)00558-0.

Zhou, Q., Lachowski, E.E., Glasser, F.P., 2004. Metaettringite, a decomposition product of ettringite. Cem. Concr. Res. 34 (4), 703–710. http://dx.doi.org/10.1016/j.cemconres.2003.10.027.

Supplementary Data to Paper P2

Tab. A8: Apparent density (ρ_a), density on oven-dry basis (ρ_{rd}), density on saturated, surface-dry basis (ρ_{ssd}), and water absorption after submersion for 24 h (WA_{24}) of the aggregates used for the production of artificial fines (river sand, RS, limestone sand, LS, and greywacke, GW) according to EN 1097-7:2008.

		RS	LS	GW
ρ_a	g/cm^3	2.66	2.73	2.75
ρ_{rd}	g/cm^3	2.63	2.68	2.71
ρ_{ssd}	g/cm^3	2.64	2.69	2.72
WA_{24}	wt%	0.38	0.67	0.48

Tab. A9: Particle density (ρ_p) according to EN 1097-7:2008 and specific surface area (S_{BET} and S_{Blaine}) according to the BET- and Blaine-method for the reference binders CEM I 42.5 R (CEM I), ground granulated blast-furnace slag (S), fly ash (FA), and limestone powder (L).

		CEM I	S	FA	L
ρ_p	g/cm^3	3.13	2.92	2.24	2.70
S_{BET}	m^2/g	1.282	0.926	7.683	5.998
S_{Blaine}	cm^2/g	4336	3406	4664	4276

Tab. A10: Hydration heat ($Q_{h,7\,\mathrm{d}}$) for $w/b = 0.4$, water demand (w_n), and setting times (t_{si}, t_{se}) of (blended) cement paste, according to EN 196-11:2019 and EN 196-6:2019. "-S" and "-FA" indicate a 30 wt% substitution of CEM I through slag or fly ash.

		CEM I	CEM I-S	CEM I-FA
$Q_{h,7\,\mathrm{d}}$	J/g	312.8	269.3	241.7
w_n	wt%	29.2	29.5	30.0
t_{si}	min	240	235	265
t_{se}	min	320	295	320

Tab. A11: Chemical composition of the raw materials used for the production of artificial fines through WDXRF in wt% according to EN 196-2:2013 (P2, fig. 1).

	Na_2O wt%	MgO wt%	Al_2O_3 wt%	SiO_2 wt%	P_2O_5 wt%	K_2O wt%	CaO wt%	TiO_2 wt%	MnO wt%	Fe_2O_3 wt%	LOI wt%	Div. wt%
CEM I	0.06	1.85	4.65	19.82	0.22	0.79	60.67	0.21	0.22	3.22	2.4	5.9
S	0.20	5.54	10.97	35.50	0.05	0.68	41.36	0.98	0.60	1.34	-0.3	3.1
FA	0.43	1.27	29.66	48.09	0.31	1.27	3.14	3.40	0.07	9.16	1.8	1.4
L	0.01	1.07	2.45	6.20	0.05	0.60	47.11	0.11	0.02	0.99	39.0	2.4
GW	0.78	1.89	13.29	68.77	0.12	3.15	1.11	0.89	0.07	5.36	3.8	0.7
LS	0.02	2.99	2.33	7.65	0.10	0.79	44.26	0.09	0.02	0.94	38.5	2.3
RS	1.16	0.58	5.84	80.61	0.06	1.96	4.12	0.15	0.02	1.15	3.8	0.6

Tab. A12: Chemical composition of artificial fines before milling ("-R") and of two selectef fines after milling ("-100") through WDXRF in wt% according to EN 196-2:2013 (P2, fig. 1). LOD: Limit of detection.

Variante	Na_2O wt%	MgO wt%	Al_2O_3 wt%	SiO_2 wt%	P_2O_5 wt%	K_2O wt%	CaO wt%	TiO_2 wt%	MnO wt%	Fe_2O_3 wt%	LOI wt%	Div. wt%
CEM-R	<LOD	1.52	3.84	16.8	0.18	0.62	50.7	0.19	0.19	2.76	18.2	5.1
FA0-R	0.12	1.46	10.64	25.0	0.21	0.80	38.2	1.01	0.16	4.39	14.5	3.5
FA50-R	0.75	0.82	7.14	61.7	0.10	1.56	14.7	0.42	0.07	2.19	7.6	3.0
GW50-R	0.49	1.73	9.91	51.3	0.13	2.24	17.2	0.66	0.11	4.47	9.2	2.5
GW75-R	0.26	1.65	7.13	35.7	0.15	1.46	32.4	0.45	0.14	3.64	14.3	2.7
LS50-R	<LOD	2.39	2.91	11.1	0.13	0.77	46.9	0.14	0.09	1.62	31.2	2.8
LS75-R	<LOD	2.03	3.16	13.6	0.15	0.68	47.7	0.15	0.12	1.95	26.6	3.8
RS50-R	0.74	0.93	5.21	58.0	0.10	1.53	20.7	0.17	0.08	1.77	9.0	1.8
RS62-R	0.61	1.07	4.94	50.0	0.11	1.36	26.5	0.17	0.10	1.95	10.8	2.4
RS75-R	0.41	1.17	4.55	41.1	0.13	1.14	33.3	0.18	0.13	2.12	12.8	3.1
S0-R	0.03	2.43	5.38	20.5	0.14	0.61	45.2	0.38	0.27	2.20	18.8	4.1
S50-R	0.74	1.21	5.60	58.6	0.08	1.51	18.5	0.24	0.11	1.56	9.7	2.1
LS50-100	<LOD	2.42	2.82	11.3	0.12	0.72	46.8	0.13	0.08	1.54	31.0	3.0
RS50-100	0.71	0.92	5.06	57.7	0.09	1.51	20.8	0.17	0.08	1.80	8.8	2.4

Tab. A13: Mass loss Δm of artificial fines at selected temperatures in a thermogravimetric setup (P2, fig. 2).

	200 °C	400 °C	600 °C	800 °C	1000 °C	1200 °C
CEM	0.025	0.087	0.159	0.183	0.190	0.192
FA0	0.026	0.092	0.130	0.160	0.180	0.185
FA50	0.012	0.032	0.044	0.066	0.082	0.084
GW50	0.016	0.039	0.066	0.096	0.108	0.110
GW75	0.020	0.058	0.100	0.134	0.147	0.151
LS50	0.015	0.038	0.065	0.098	0.322	0.327
LS75	0.018	0.058	0.103	0.136	0.278	0.280
RS50	0.016	0.038	0.061	0.088	0.101	0.101
RS62	0.018	0.046	0.079	0.102	0.114	0.114
RS75	0.022	0.061	0.105	0.130	0.140	0.142
S0	0.034	0.115	0.174	0.195	0.208	0.212
S50	0.015	0.041	0.060	0.083	0.095	0.096

Tab. A14: Results of hydration heat measurements on blended cement paste containing different artificial fines (P2, fig. 6, fig. 7).

	$Q_{0.5\,\mathrm{h}}$ J/g	t_b h	W_{t_b} mW/g	Q_{t_b} J/g	t_p h	W_{t_p} mW/g	Q_{t_p} J/g	$Q_{5\,\mathrm{d}}$ J/g
CEM I	18.8	2.4	0.4	23.2	11.4	2.8	72.5	296.8
CEM-100	18.4	2.3	0.7	24.7	12.1	1.8	72.5	260.7
CEM-400	19.2	2.0	0.7	23.8	10.9	2.0	72.0	274.2
CEM-600	27.1	2.6	0.6	35.4	11.0	2.2	80.9	269.4
CEM-600	37.3	2.5	0.6	45.0	11.0	2.2	90.2	285.9
CEM-800	73.7	2.4	0.7	84.9	9.0	1.4	111.6	270.2
FA0-100	17.6	2.7	0.6	24.0	12.3	1.9	70.0	255.0
FA0-400	17.4	2.8	0.5	22.9	12.8	2.1	73.0	276.2
FA0-600	16.7	2.9	0.4	22.6	12.8	2.2	74.6	287.2
FA50-100	13.7	2.4	0.4	17.2	12.0	2.0	59.7	243.6
FA50-400	14.4	2.2	0.3	17.6	11.7	2.0	60.6	250.1
FA50-600	14.5	2.5	0.3	18.1	12.0	2.0	59.4	244.9
GW50-400	15.0	2.6	0.4	19.1	11.6	2.0	59.9	250.4
GW50-600	15.0	2.7	0.4	19.1	12.1	2.0	60.7	247.4
GW75-400	12.8	2.5	0.4	16.7	12.1	2.2	63.7	268.1
GW75-600	14.2	2.6	0.4	18.6	12.1	2.2	64.5	271.8
GW75-600	14.6	2.7	0.4	19.1	12.7	2.1	64.6	257.1
LS50-100	15.1	2.8	0.4	20.9	13.5	1.8	65.7	245.8
LS50-400	15.5	2.3	0.4	19.7	12.1	2.0	65.8	256.4
LS50-600	15.3	2.6	0.5	20.2	12.2	2.2	67.3	257.2
LS75-100	13.4	4.0	0.4	21.5	18.5	1.7	74.6	254.4
LS75-400	16.2	3.1	0.4	21.8	15.9	1.9	77.5	269.2
LS75-600	20.0	3.0	0.5	28.2	11.7	2.1	73.0	262.0
RS50-100	15.8	2.6	0.4	20.3	12.8	1.9	65.2	250.0
RS50-400	15.6	2.2	0.4	19.1	11.4	2.0	62.8	248.9
RS50-600	14.0	2.7	0.4	18.7	12.1	2.2	63.7	253.0
RS50-800	12.9	2.6	0.3	16.5	11.5	2.0	54.4	232.4
RS62-100	15.9	2.5	0.4	20.6	12.2	2.0	65.8	255.7
RS62-400	15.4	2.8	0.5	21.1	13.1	2.1	71.6	265.2
RS62-600	15.1	3.1	0.5	22.1	12.3	2.3	69.1	261.2
RS62-800	13.7	3.3	0.4	21.0	11.7	2.0	60.0	238.6
RS75-100	15.9	2.3	0.5	20.8	12.1	1.9	65.6	254.4
RS75-400	15.7	2.5	0.5	21.4	12.4	2.1	71.2	266.7
RS75-600	19.7	3.1	0.5	27.7	11.7	2.1	69.8	250.6
RS75-800	14.8	3.7	0.5	26.8	11.2	2.0	64.7	240.6
S0-100	16.5	2.5	0.5	21.4	12.2	2.0	68.6	265.5
S0-400	17.4	2.3	0.6	22.3	11.1	2.2	70.1	273.2
S0-600	16.8	2.8	0.8	26.9	10.0	2.9	76.5	288.6
S50-100	14.6	2.4	0.4	18.7	11.8	2.0	61.5	245.6
S50-400	14.8	2.2	0.4	17.8	11.6	2.1	60.9	248.2
S50-600	14.2	2.6	0.3	17.9	11.9	2.1	59.2	248.2

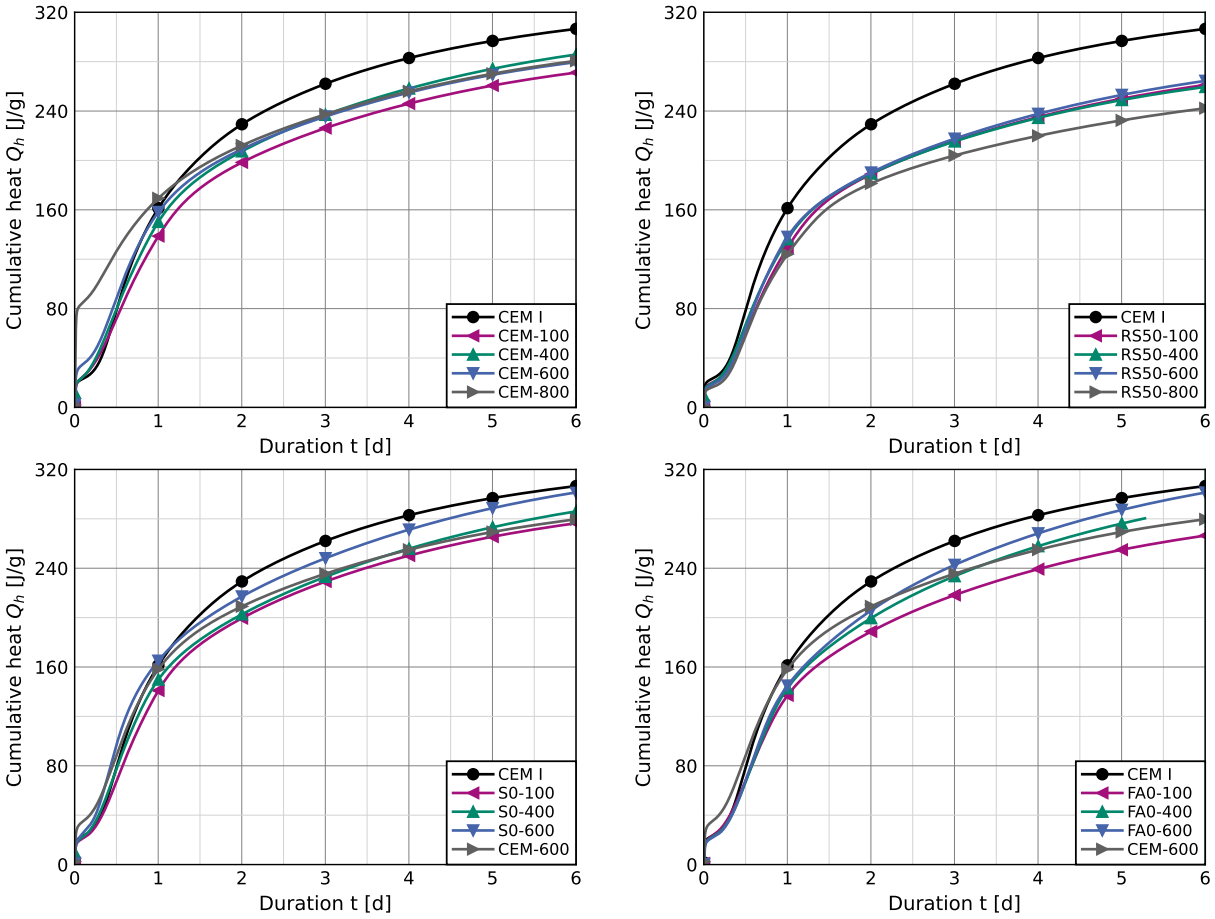

Fig. A1: Cumulative hydration heat development of blended binders with 70 wt% CEM I and 30 wt% artificial fines activated at different temperatures (P2, fig. 5).

Tab. A15: Results of hydration heat measurements on blended cement paste containing artificial fines with varying substitution rates (P2, fig. 7).

	$Q_{0.5\,\mathrm{h}}$ J/g	t_b h	W_{t_b} mW/g	Q_{t_b} J/g	t_p h	W_{t_p} mW/g	Q_{t_p} J/g	$Q_{5\,\mathrm{d}}$ J/g
CEM-400-100	13.2	9.7	0.7	38.2	14.7	0.7	50.6	164.2
CEM-400-50	15.4	2.5	0.7	22.3	11.0	1.9	68.2	251.2
CEM-400-30	14.6	2.2	0.6	19.4	11.5	2.0	66.9	273.6
CEM-600-100	88.7	2.8	0.9	100.4	10.3	1.3	131.2	249.8
CEM-600-50	54.7	2.3	0.7	62.9	9.1	1.9	97.6	270.5
CEM-600-30	33.0	2.6	0.6	41.1	10.7	2.1	84.5	270.0
CEM-600-10	18.4	2.2	0.5	23.8	10.3	2.6	70.9	285.3
S0-600-100	18.1	2.8	0.8	28.4	15.2	2.3	97.8	289.4
S0-600-50	17.0	2.9	1.2	31.3	7.4	2.5	60.2	283.4
S0-600-30	15.2	2.8	0.8	24.8	10.2	2.7	74.4	282.1
FA0-600-100	15.1	30.3	0.0	23.6	136.1	0.4	87.6	65.7
FA0-600-50	17.8	3.2	0.5	26.3	9.7	2.0	55.9	272.6
FA0-600-30	14.9	3.0	0.4	20.7	12.6	2.2	68.4	275.6

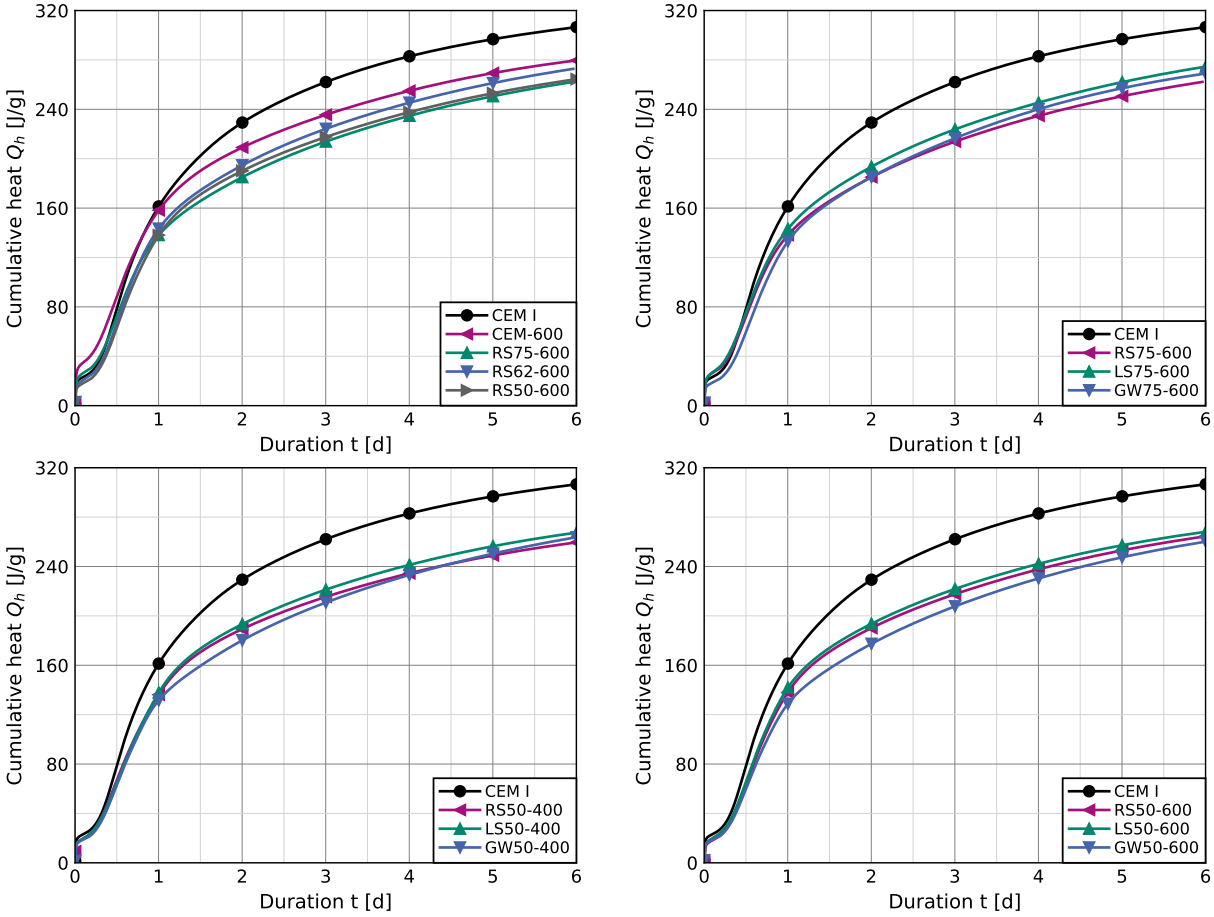

Fig. A2: Cumulative hydration heat development of select blends of 70 wt% CEM I and 30 wt% artificial fines with different aggregate contents and compositions, activated at 400 °C and 600 °C (P2, fig. 6).

Tab. A16: Mortar compressive strength of selected mixtures at 1 d, 2 d, 7 d and 28 d (P2, fig. 9).

	Temp. °C	f –	$\frac{w}{b}$ –	$f_{c,1\,d}$ MPa	$f_{c,2\,d}$ MPa	$f_{c,7\,d}$ MPa	$f_{c,28\,d}$ MPa
CEM I			0.45	24.5(5)	35.2(8)	54.7(12)	60.9(16)
CEM I			0.50	17.7(6)	28.2(13)	46.9(18)	55.9(15)
CEM I			0.55	14.4(7)	24.5(11)	42.4(14)	50.7(16)
CEM I			0.60	10.0(2)	19.4(5)	34.0(12)	44.8(13)
RS50	400	0.3	0.50	9.7(3)	18.6(5)	32.2(7)	40.0(20)
RS62	400	0.3	0.50	19.1(12)	33.4(15)	43.6(15)	51.3(24)
RS75	400	0.3	0.50	10.2(4)	21.7(4)	40.0(9)	49.8(19)
CEM	400	0.3	0.50	10.4(3)	22.2(7)	39.4(12)	45.8(19)
RS50	600	0.3	0.50	12.5(3)	22.8(12)	40.0(20)	46.6(16)
RS62	600	0.3	0.50	10.9(4)	24.4(8)	42.3(9)	52.0(18)
RS75	600	0.3	0.50	9.6(1)	20.6(4)	40.2(14)	49.2(56)
CEM	600	0.3	0.50	17.8(3)	30.2(4)	45.4(26)	51.1(11)
RS75	800	0.3	0.50	11.9(2)	22.9(7)	38.2(17)	50.2(18)
CEM	800	0.3	0.50	9.6(4)	25.2(8)	43.5(11)	54.9(31)

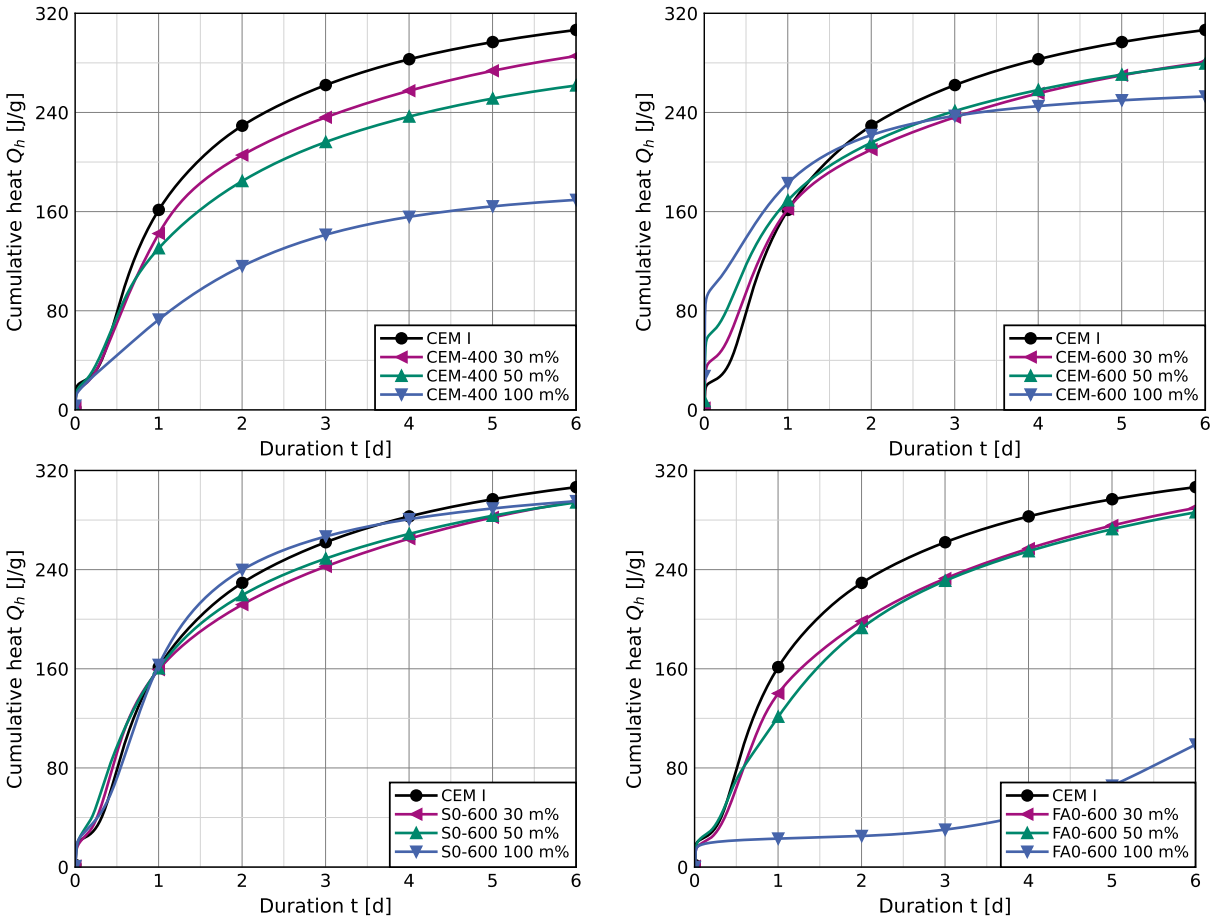

Fig. A3: Cumulative hydration heat development of select blends of CEM I and CEM-400, CEM-600, S0-600 or FA0-600 at different substitution rates (P2, fig. 7).

Tab. A17: Compressive strength of mortar containing processed artificial fines (part 1).

	Temp. °C	f –	$\frac{w}{b}$ –	$\frac{w+FM}{b}$ –	Δm –	$f_{c,2\,\mathrm{d}}$ MPa	$f_{c,28\,\mathrm{d}}$ MPa
CEM	100	0.1	0.5	0.50	0.000	27.2(5)	53.5(13)
CEM	100	0.3	0.5	0.51	0.000	22.0(4)	40.8(9)
CEM	100	0.3	0.4	0.41	0.000	30.5(8)	46.9(16)
CEM	400	0.1	0.5	0.50	0.094	30.2(9)	55.8(11)
CEM	400	0.1	0.5	0.50	0.094	29.4(10)	53.8(13)
CEM	400	0.3	0.5	0.50	0.094	22.2(7)	45.8(19)
CEM	400	0.3	0.5	0.50	0.094	23.3(8)	46.2(16)
CEM	400	0.5	0.5	0.50	0.094	14.3(4)	35.1(4)
CEM	400	0.3	0.4	0.41	0.094	34.3(8)	59.5(17)
CEM	400	0.3	0.4	0.41	0.094	35.0(2)	52.5(16)
CEM	600	0.1	0.5	0.50	0.161	17.2(9)	41.4(12)
CEM	600	0.1	0.5	0.50	0.162	31.0(15)	55.2(17)
CEM	600	0.3	0.5	0.51	0.161	43.2(12)	66.1(21)
CEM	600	0.3	0.5	0.51	0.162	34.0(3)	53.3(42)
CEM	600	0.3	0.5	0.51	0.162	30.2(4)	51.1(11)
CEM	600	0.3	0.5	0.51	0.157	28.9(6)	49.9(7)
CEM	600	0.3	0.5	0.50	0.131	25.4(5)	44.0(26)
CEM	600	0.3	0.5	0.51	0.139	28.0(7)	48.3(12)
CEM	600	0.5	0.5	0.51	0.161	29.6(5)	47.9(17)
CEM	600	0.5	0.5	0.52	0.131	21.8(8)	40.7(10)
CEM	600	0.5	0.5	0.52	0.139	25.7(5)	43.2(15)
CEM	600	0.3	0.4	0.41	0.161	49.6(17)	69.0(16)
CEM	600	0.3	0.4	0.41	0.162	41.5(13)	60.7(37)
CEM	600	0.3	0.4	0.42	0.157	40.0(26)	64.5(22)
CEM	600	0.3	0.4	0.41	0.131	39.2(10)	63.3(13)
CEM	600	0.3	0.4	0.41	0.139	38.9(6)	57.3(18)
CEM	800	0.1	0.5	0.50	0.180	26.1(8)	54.2(7)
CEM	800	0.3	0.5	0.50	0.180	25.2(8)	54.9(31)
CEM	800	0.3	0.4	0.41	0.180	35.2(8)	72.0(20)
FA0	100	0.3	0.5	0.51	0.000	28.6(5)	47.3(35)
FA0	100	0.3	0.4	0.41	0.000	37.8(8)	58.0(23)
FA0	400	0.3	0.5	0.50	0.103	23.7(7)	51.8(10)
FA0	400	0.3	0.4	0.41	0.103	36.7(6)	67.8(24)
FA0	600	0.3	0.5	0.50	0.131	30.1(9)	58.8(11)
FA0	600	0.3	0.4	0.41	0.131	44.1(11)	68.9(10)
S0	100	0.3	0.5	0.50	0.000	24.8(10)	44.6(11)
S0	100	0.3	0.4	0.41	0.000	31.4(8)	49.4(33)
S0	400	0.3	0.5	0.50	0.115	23.5(5)	50.7(12)
S0	400	0.3	0.4	0.41	0.115	36.7(7)	61.1(18)
S0	600	0.3	0.5	0.50	0.158	34.6(9)	61.9(27)
S0	600	0.3	0.4	0.41	0.158	49.3(9)	70.1(12)

Tab. A18: Compressive strength of mortar containing processed artificial fines (part 2).

	Temp. °C	f –	$\frac{w}{b}$ –	$\frac{w+FM}{b}$ –	Δm –	$f_{c,2\,\mathrm{d}}$ MPa	$f_{c,28\,\mathrm{d}}$ MPa
LS0		0.1	0.5	0.50	0.000	25.5(10)	49.0(24)
LS0		0.3	0.5	0.50	0.000	17.7(14)	37.1(26)
LS0		0.3	0.4	0.40	0.000	25.6(7)	43.8(18)
LS50	100	0.3	0.5	0.50	0.000	19.6(4)	37.6(7)
LS50	100	0.3	0.4	0.41	0.000	27.7(6)	42.9(23)
LS50	400	0.1	0.5	0.50	0.045	24.4(5)	47.1(11)
LS50	400	0.1	0.5	0.50	0.044	25.9(10)	48.2(24)
LS50	400	0.3	0.5	0.50	0.045	19.3(6)	40.2(14)
LS50	400	0.3	0.5	0.50	0.044	21.4(6)	44.4(9)
LS50	400	0.3	0.4	0.40	0.045	28.9(4)	48.7(27)
LS50	400	0.3	0.4	0.41	0.044	32.3(6)	52.9(21)
LS50	600	0.1	0.5	0.50	0.065	24.0(9)	45.3(11)
LS50	600	0.1	0.5	0.50	0.064	30.3(7)	55.7(15)
LS50	600	0.3	0.5	0.50	0.065	20.7(4)	41.7(16)
LS50	600	0.3	0.5	0.50	0.064	24.0(9)	46.6(15)
LS50	600	0.3	0.4	0.41	0.065	31.3(8)	42.4(55)
LS50	600	0.3	0.4	0.41	0.064	35.9(10)	57.2(28)
LS75	100	0.3	0.5	0.50	0.000	18.0(10)	36.7(13)
LS75	100	0.3	0.4	0.41	0.000	28.5(11)	46.0(25)
LS75	400	0.1	0.5	0.50	0.068	24.8(16)	51.5(12)
LS75	400	0.1	0.5	0.50	0.067	26.8(5)	51.1(17)
LS75	400	0.3	0.5	0.50	0.068	19.4(6)	43.3(12)
LS75	400	0.3	0.5	0.50	0.067	21.4(5)	44.4(12)
LS75	400	0.3	0.4	0.40	0.068	30.3(6)	52.4(8)
LS75	400	0.3	0.4	0.41	0.067	32.8(8)	56.5(17)
LS75	600	0.1	0.5	0.50	0.098	27.2(5)	51.6(14)
LS75	600	0.1	0.5	0.50	0.096	27.5(11)	52.0(6)
LS75	600	0.3	0.5	0.50	0.098	22.5(3)	43.3(10)
LS75	600	0.3	0.5	0.50	0.096	24.0(3)	45.0(14)
LS75	600	0.3	0.4	0.41	0.098	34.4(7)	54.1(26)
LS75	600	0.3	0.4	0.41	0.096	37.6(5)	61.6(18)
GW50	100	0.3	0.5	0.50	0.000	21.8(5)	44.8(6)
GW50	100	0.3	0.4	0.41	0.000	31.2(32)	54.2(64)
GW50	400	0.1	0.5	0.50	0.045	25.8(8)	47.5(44)
GW50	400	0.3	0.5	0.50	0.045	19.6(3)	40.2(13)
GW50	400	0.3	0.4	0.41	0.045	30.9(5)	56.8(31)
GW50	600	0.1	0.5	0.50	0.066	29.3(7)	55.6(12)
GW50	600	0.3	0.5	0.50	0.066	24.2(8)	52.1(4)
GW50	600	0.3	0.4	0.41	0.066	33.7(15)	62.6(17)
GW75	100	0.3	0.5	0.50	0.000	24.1(7)	46.9(19)
GW75	100	0.3	0.4	0.41	0.000	36.3(8)	58.9(17)
GW75	400	0.1	0.5	0.50	0.081	26.3(7)	53.1(10)
GW75	400	0.3	0.5	0.50	0.081	20.5(8)	40.7(21)
GW75	400	0.3	0.4	0.41	0.081	31.9(16)	57.6(33)
GW75	600	0.1	0.5	0.50	0.108	26.9(4)	49.1(7)
GW75	600	0.3	0.5	0.50	0.108	25.8(7)	49.0(15)
GW75	600	0.3	0.4	0.41	0.108	39.0(10)	62.0(31)

Tab. A19: Compressive strength of mortar containing processed artificial fines (part 3).

	Temp. °C	f –	$\frac{w}{b}$ –	$\frac{w+FM}{b}$ –	Δm –	$f_{c,2\,\mathrm{d}}$ MPa	$f_{c,28\,\mathrm{d}}$ MPa
RS62	100	0.1	0.5	0.50	0.000	17.3(4)	40.4(12)
RS62	100	0.3	0.5	0.50	0.000	21.1(6)	41.5(8)
RS62	100	0.3	0.4	0.40	0.000	31.5(4)	49.8(14)
RS62	400	0.1	0.5	0.50	0.056	31.1(6)	54.2(24)
RS62	400	0.1	0.5	0.50	0.056	26.5(9)	48.8(18)
RS62	400	0.3	0.5	0.50	0.056	33.4(15)	51.3(24)
RS62	400	0.3	0.5	0.50	0.056	20.8(6)	44.1(10)
RS62	400	0.5	0.5	0.50	0.056	18.0(6)	36.7(13)
RS62	400	0.3	0.4	0.40	0.056	31.4(12)	50.5(19)
RS62	400	0.3	0.4	0.40	0.056	34.2(5)	55.5(21)
RS62	600	0.1	0.5	0.50	0.080	26.6(11)	52.7(26)
RS62	600	0.1	0.5	0.50	0.081	28.1(7)	53.9(14)
RS62	600	0.3	0.5	0.50	0.080	24.4(8)	52.0(18)
RS62	600	0.3	0.5	0.50	0.081	24.4(6)	47.8(13)
RS62	600	0.5	0.5	0.50	0.080	20.5(7)	45.2(19)
RS62	600	0.3	0.4	0.40	0.080	38.8(6)	67.0(22)
RS62	600	0.3	0.4	0.40	0.081	37.3(10)	58.0(25)
RS62	800	0.1	0.5	0.50	0.112	28.2(7)	57.2(20)
RS62	800	0.3	0.5	0.50	0.112	21.3(4)	48.5(12)
RS62	800	0.3	0.4	0.41	0.112	34.3(9)	66.6(19)
RS75	100	0.1	0.5	0.50	0.000	26.4(7)	50.0(18)
RS75	100	0.3	0.5	0.50	0.000	22.5(4)	40.8(8)
RS75	100	0.3	0.4	0.40	0.000	34.5(12)	54.5(25)
RS75	400	0.1	0.5	0.50	0.075	26.5(4)	53.0(9)
RS75	400	0.1	0.5	0.50	0.082	28.9(14)	53.0(27)
RS75	400	0.3	0.5	0.50	0.075	21.7(4)	49.8(19)
RS75	400	0.3	0.5	0.50	0.082	28.4(9)	48.0(24)
RS75	400	0.5	0.5	0.50	0.075	16.1(3)	37.5(11)
RS75	400	0.3	0.4	0.40	0.074	37.0(14)	58.0(29)
RS75	400	0.3	0.4	0.40	0.075	33.8(14)	58.4(26)
RS75	400	0.3	0.4	0.40	0.082	34.0(11)	55.1(19)
RS75	600	0.1	0.5	0.50	0.109	26.6(6)	54.9(26)
RS75	600	0.1	0.5	0.50	0.113	29.3(10)	55.4(15)
RS75	600	0.3	0.5	0.50	0.109	20.6(4)	49.2(56)
RS75	600	0.3	0.5	0.50	0.113	25.4(6)	52.0(19)
RS75	600	0.5	0.5	0.50	0.109	15.7(3)	39.2(15)
RS75	600	0.3	0.4	0.40	0.109	38.2(28)	65.8(15)
RS75	600	0.3	0.4	0.41	0.113	38.9(6)	61.2(19)
RS75	800	0.1	0.5	0.50	0.137	27.9(6)	55.1(16)
RS75	800	0.3	0.5	0.50	0.137	22.9(7)	50.2(18)
RS75	800	0.3	0.4	0.41	0.137	35.8(6)	66.3(22)

Tab. A20: Compressive strength of mortar containing processed artificial fines (part 4).

	Temp. °C	f –	$\frac{w}{b}$ –	$\frac{w+FM}{b}$ –	Δm –	$f_{c,2\,\mathrm{d}}$ MPa	$f_{c,28\,\mathrm{d}}$ MPa
RS0		0.1	0.5	0.50	0.000	25.0(6)	44.9(10)
RS0		0.3	0.5	0.50	0.000	14.1(5)	30.1(10)
RS0		0.3	0.4	0.41	0.000	26.0(5)	47.7(12)
RS50	100	0.1	0.5	0.50	0.000	24.9(4)	51.8(14)
RS50	100	0.3	0.5	0.50	0.000	19.7(5)	38.3(9)
RS50	100	0.3	0.4	0.40	0.000	29.3(10)	51.5(13)
RS50	400	0.1	0.5	0.50	0.046	27.0(8)	53.0(17)
RS50	400	0.1	0.5	0.50	0.042	26.2(8)	48.9(24)
RS50	400	0.3	0.5	0.50	0.046	18.6(5)	40.0(20)
RS50	400	0.3	0.5	0.50	0.042	19.7(7)	41.1(37)
RS50	400	0.5	0.5	0.50	0.046	10.3(3)	30.0(6)
RS50	400	0.3	0.4	0.40	0.046	29.2(4)	53.3(28)
RS50	400	0.3	0.4	0.40	0.042	29.9(9)	50.3(26)
RS50	600	0.1	0.5	0.50	0.059	27.9(34)	53.8(8)
RS50	600	0.1	0.5	0.50	0.061	28.8(10)	51.1(25)
RS50	600	0.3	0.5	0.50	0.059	22.8(12)	46.6(16)
RS50	600	0.3	0.5	0.50	0.061	24.0(6)	44.9(31)
RS50	600	0.5	0.5	0.50	0.059	16.2(3)	36.6(11)
RS50	600	0.3	0.4	0.40	0.059	34.3(6)	61.1(23)
RS50	600	0.3	0.4	0.40	0.061	36.5(8)	54.4(33)
RS50	800	0.1	0.5	0.50	0.089	28.5(7)	57.1(13)
RS50	800	0.3	0.5	0.50	0.089	19.7(6)	44.0(13)
RS50	800	0.3	0.4	0.41	0.089	32.4(8)	63.4(19)
FA50	100	0.3	0.5	0.50	0.000	24.2(5)	43.5(5)
FA50	100	0.3	0.4	0.41	0.000	32.2(5)	51.9(19)
FA50	400	0.3	0.5	0.50	0.048	20.8(6)	44.4(11)
FA50	400	0.3	0.4	0.40	0.048	33.2(10)	60.0(15)
FA50	600	0.3	0.5	0.50	0.062	19.4(5)	41.0(13)
FA50	600	0.3	0.4	0.41	0.062	32.2(6)	58.7(13)
S50	100	0.3	0.5	0.50	0.000	22.1(8)	40.4(15)
S50	100	0.3	0.4	0.41	0.000	29.1(12)	49.9(13)
S50	400	0.3	0.5	0.50	0.056	20.9(6)	45.3(8)
S50	400	0.3	0.4	0.40	0.056	33.7(4)	57.3(11)
S50	600	0.3	0.5	0.50	0.070	21.6(6)	42.6(9)
S50	600	0.3	0.4	0.41	0.070	35.6(9)	59.8(18)

Paper P3

Influence of Thermally Activated Artificial Concrete Fines Composition on Concrete Long-Term Behavior

Jan P. Höffgen
Marius Schmitt
Frank Dehn

Journal of Building Engineering 122

March 2026, 115767

DOI: 10.1016/j.jobe.2026.115767

Publisher's version

Journal of Building Engineering 122 (2026) 115767

Contents lists available at ScienceDirect

Journal of Building Engineering

journal homepage: www.elsevier.com/locate/jobe

Full length article

Influence of thermally activated artificial concrete fines composition on concrete long-term behavior

Jan P. Höffgen *, Marius Schmitt, Frank Dehn

Karlsruhe Institute of Technology (KIT), Institute for Concrete Structures and Building Materials (IMB), Gotthard-Franz-Str. 3, Karlsruhe, 76131, Germany

ARTICLE INFO

Keywords:
Concrete
Cement
Mineral waste
Recycling
Thermal activation
Supplementary cementitious material

ABSTRACT

Thermal activation of concrete fines is a promising method for the simultaneous reduction of CO_2 emissions and mineral waste. Hydrated cement paste, a major component of these recycled materials, can be used as a reactive supplementary cementitious material after dehydration at elevated temperatures and grinding. This affects concrete strength, especially when fines contain a higher proportion of aggregates. While strength loss can be mitigated by adjusting the water-binder ratio, the combined effect on other mechanical properties and durability remains unclear. This study utilizes seven different artificial concrete fines with varying binder compositions, aggregate contents, and aggregate mineralogies to produce concrete with varying compressive strengths. These concretes are then assessed for their flexural strength, elastic modulus, shrinkage, water absorption, chloride diffusion, carbonation, and freeze-thaw-resistance. Results highlight that with increasing compressive strength, mechanical properties and durability also improve. However, while strength development and the elastic modulus are similar to the reference concrete, the substitution of Portland cement through activated fines increases shrinkage as well as carbonation and chloride ingress, especially for fines with a high amount of reactive SiO_2.

1. Introduction

Thermal activation of concrete fines is a promising process for mineral construction and demolition waste recycling, as well as reducing the carbon footprint of cement production [1–9]. The activation process relies on the dehydration of hydrated cement paste (HCP) within these fines. With increasing temperature, different cement hydration products gradually release chemically bound water. Most prominently, calcium hydroxide disintegrates to free lime in the temperature range of 400 °C to 550 °C, and calcium silicate hydrates decompose between 110 °C and 500 °C to form reactive $\alpha'_H C_2S$ and $\alpha'_L C_2S$ [10–23]. Upon re-wetting, the activated paste rapidly rehydrates, recreating the original cement phases [10,12,13,16,17,19,24–27]. Because both the hydrated and the dehydrated paste remain porous, the rehydrated product primarily occupies the existing pore network, resulting in limited inter-particle bonding and reduced strength [17,18,25,28–30].

When used as a supplementary cementitious material (SCM), thermally activated cement paste can replace up to 25 wt% – 40 wt% of ordinary Portland cement (OPC) without significantly compromising compressive strength [14,29,31–36]. The behavior stems from the high water consumption of the activated particles, which lowers the free water available for OPC hydration and thus densifies the matrix [29,34,37]. For higher substitution rates, total porosity increases alongside decreasing compressive strength [14,18]. Similarly, incomplete dehydration at activation temperatures below 400 °C leads to increased porosity [18,37].

* Corresponding author.
E-mail address: jan.hoeffgen@kit.edu (J.P. Höffgen).

https://doi.org/10.1016/j.jobe.2026.115767
Received 7 October 2025; Received in revised form 12 December 2025; Accepted 1 March 2026
Available online 4 March 2026

While compressive strength is the central material property, durability and deformation behavior are major factors in concrete design. Besides affecting compressive strength, the substitution of Portland cement through activated concrete fines as supplementary cementitious materials (SCMs) also changes material resistance to corrosion (e.g., carbonation, chloride ingress, or freeze-thaw action) as well as elastic or shrinkage deformations.

Substituting OPC with activated fines generally reduces the elastic modulus due to the lower density of the fines [24], but the effect persists even at modest replacement levels [38,39]. Shrinkage deformations follow a similar trend with increased deformations [38,40]. Low-level substitution can be offset by the densification effect, whereas high-temperature activation or lower water-cement ratios in the precursor material increase particle stiffness and mitigate shrinkage [38,40–42]. Besides, drying shrinkage is affected by the amount of evaporable water, and increases when additional mixing water is used to compensate for the high water demand of activated cement paste [40,41].

Capillary absorption follows the same influencing factors as paste porosity. Higher Portland cement substitution through activated cement paste results in increased absorption, especially when additional mixing water is used for adjusting fresh concrete workability [40]. At a fixed water-binder ratio, the reduction of free water outside of activated cement paste particles lessens capillary absorption [31,40,43]. Compared to ground HCP, thermal activation at up to 1000 °C reduces absorption [33,36,41,42,44]. Water absorption plays an important role in freeze-thaw damage evolution. At similar strength, mortar and concrete containing thermally activated concrete fines exhibit a similar freeze-thaw-resistance as Portland cement reference mixes [45,46]. The diffusion of Cl^- and CO_2 is affected by paste porosity and the binding capacity of hydration products. Subsequently, the aforementioned influences on porosity impact the resistance to carbonation and chloride ingress [28,29,31,43,47,48].

Assessing mechanical and durability properties after partial substitution of Portland cement with thermally activated concrete fines remains challenging, primarily because the substitution also affects compressive strength. This interdependence obscures the isolated effects of the fines themselves. For pure OPC-based HCP, such strength variations may be limited. However, concrete fines sourced from recycling plants contain aggregates of varying amounts and mineralogical compositions, and may incorporate hydration products from alternative binders (e.g., slag, pozzolans). These components alter both reactivity and mechanical performance in ways that are not yet predictable. Although the aggregate fraction of concrete fines is widely recognized as essentially inert and therefore detrimental when used as SCM, the contribution of alternative binder residues remains much less clear [24,43,49–54]. The existing literature regularly uses concrete with fixed water-binder ratios, or increased water contents to compensate for insufficient workability, and therefore does not provide a consistent framework for distinguishing the effects of composition from those of strength change.

In practice, when designing concrete to meet a defined compressive strength, a possible negative impact of SCMs on the latter is usually compensated for by a reduction of the water-binder ratio. Although the procedure can restore compressive strength, it does not uniformly affect other mechanical or durability properties. However, codes and standardized structural design implicitly assume that concretes with the same compressive strength will exhibit comparable deformation behavior and reinforcement corrosion resistance. This assumption has never been validated for systems that incorporate thermally activated concrete fines. No previous study has systematically examined whether restoring compressive strength also recovers mechanical and durability responses altered by the heterogeneous composition of the fines.

2. Experimental program

The experimental program is structured to address this unresolved question directly. The central objective is to determine whether compensating for the strength reduction caused by activated concrete fines also neutralizes their influence on the deformation characteristics and the durability performance. For this means, artificial fines with controlled and varying amounts of inert aggregate and alternative binder residues, and thus varying compressive strength contribution, are employed. By holding compressive strength constant across mixtures, the study isolates the macroscopic effects arising solely from fines composition. This approach provides the first systematic evaluation of whether established empirical relationships linking mechanical and durability behavior to compressive strength remain valid in concretes containing thermally activated fines.

2.1. Materials

Base materials for the experimental procedures were a commercial Portland cement CEM I 42.5 R (“CEM I”), ground granulated blast-furnace slag (“S”) and black coal fly ash (“FA”) as binders, as well as siliceous river sand (0/2 mm, “RS”) and gravel (2/8 mm, “RG”), limestone sand (0/4 mm, “LS”) and greywacke (0/4 mm, “GW”) as aggregates.

Seven different artificial fines were used as representative concrete fines to set up three groups of three (see Table 1). One group altered the binder composition, where, starting with CEM I-paste (“CEM”), 30 wt% of the binder were substituted for fly ash (“FA0”) or slag (“S0”). The second group varied binder content, where RS replaced 50 v% (“RS50”), and 25 v% (“RS75”) of the CEM I-paste (“CEM”). Finally, the third group switched the river sand in RS50 for LS and GW with different aggregate compositions (“LS50” and “GW50”). The artificial fines chosen for the present study resemble possible compositions found in literature. [55] contains a detailed mix design, as well as characterization of the artificial fines performance.

For all artificial fines, three prisms ($(40 \times 40 \times 160)\,mm^3$) were cast, and cured alongside the bulk materials. Bulk materials were stored in sealed buckets with excess water, and demolded after at least nine months to exclude the influence of temporal effects from the subsequent analyses. Samples were dried at 105 °C before grinding in an industrial mill. The temperature of the grinding tube was monitored to not exceed 100 °C.

Table 1
Composition of artificial fines with water-binder ratio $w/b = 0.5$. v_p: paste volume; Agg.: aggregates; FA: fly ash; S: blast-furnace slag; RS: river sand; LS: limestone sand; GW: greywacke.

	Binder	v_p[v%]	Agg.
CEM	100 wt% CEM I	100	–
FA0	70 wt% CEM I + 30 wt% FA	100	–
S0	70 wt% CEM I + 30 wt% S	100	–
RS75	100 wt% CEM I	75	RS
RS50		50	RS
LS50		50	LS
GW50		50	GW

Table 2
Mix design of the reference series CEM I-2.

	Density g/cm^3	Share kg/m^3
River gravel 2/8 mm	2.56	1024
River sand 0/2 mm	2.63	526
CEM I 42.5 R	3.13	488
Water	1.00	244

Afterwards, artificial fines were thermally activated in a static furnace. The target temperature of 600 °C (suffix "−600") was held constant for 6 h. The heating ramp was controlled (5 K/min), while cooling was limited to the passive cooling of the furnace. When reaching 100 °C, samples were stored in sealed containers with a drying agent to prevent moisture ingress. Two types of artificial fines (CEM and RS50) were additionally activated at 400 °C ("−400"), and also used in their ground variant ("−100"). [56] details the thermal activation procedure.

2.2. Experimental procedures

The raw materials were analyzed for their chemical composition through WDXRF measurements (EN 196-2:2013), and their mineralogical composition through XRD. Artificial fines and CEM I were characterized for their chemical composition (wet-chemical analysis and carbon-sulfur analysis, EN 196-2:2013), particle size distribution (laser diffraction), and particle density (pycnometer). Nitrogen absorption/desorption was used to determine both the specific surface areas (BET method) and porosity (BJH method).

Concrete was designed with an aggregate content of 60 v%, split into 20 v% RS (0/2 mm) and 40 v% RG (2/8 mm), which was held constant for all concrete mixes. Sieve analyses yielded $d_{10} \approx 0.12$ mm, $d_{50} \approx 0.34$ mm, and $d_{90} \approx 0.88$ mm for RS, as well as $d_{10} \approx 2.8$ mm, $d_{50} \approx 4.9$ mm, and $d_{90} \approx 7.0$ mm for RG. Limiting the maximum grain size to 8 mm enabled the use of smaller specimen sizes. This subsequently reduced raw material consumption. While this came at the cost of potentially increased scatter, following the size-effect law, it reduced time-intensive thermal activation and allowed for the testing of all material properties from a single batch of concrete per mix. For each binder, two different water-binder ratios (w/b) were adopted: Series 1 used $w/b = 0.5$, without taking artificial fines reactivity into account. Series 2 applied the equivalent concrete performance concept defined in EN 206:2021 and CEN/TR 16639:2014, where $w/c_{eq} = 0.5$ replaces w/b (Eq. (1)).

$$\frac{w}{c_{eq}} = \frac{w}{c + k \cdot a} \quad \text{with } a\text{: SCM-content} \tag{1}$$

The k-value addresses the performance of individual SCMs compared to Portland cement. For $k = 1.0$, the equivalent water-cement ratio equals the water binder ratio, while an alteration of w/b compensates for the effect of Portland cement substitution on concrete performance through SCMs. k-values for individual processed artificial fines were determined in a previous study on compressive strength and subsequently applied in the present work [55]. For each SCM, the water-binder ratio was adjusted to reach the target $w/c_{eq} \approx 0.5$.

Similarly, two reference series without CEM I substitution were defined with $w/b = w/c_{eq} = 0.6$ ("−1") and $w/b = w/c_{eq} = 0.5$ ("−2"). Mixes of CEM I-1 and CEM I-2 were produced twice to enable double determinations of select material properties. For the assessment of activated artificial fines as SCM, a substitution rate of 30 wt% of CEM I was selected. Additionally, CEM-600 and RS50-600 were also used to replace 10 wt% and 50 wt% of CEM I. The mix design for the reference series CEM I-2 is listed in Table 2. Table A.5 in the appendix gives an overview of the different series.

During concrete mixing, workability was adjusted through the addition of superplasticizer. Target consistency was a spread of 17 cm – 19 cm determined by the flow table test in EN 1015-3:2007. After being placed in steel molds, samples were kept humid at 20 °C until demolding at 1 d. Afterwards, specimens were cured depending on the conditioning plan for each concrete property. Unless otherwise stated, all procedures were performed at 20 °C. The subsequent experimental analyses required compromises to enable the determination of various concrete performance indicators from a single batch. The selection of specimen sizes followed the requirement in EN 12390-1:2011 of a minimum size of 28 mm for a maximum aggregate diameter of 8 mm. Fig. A.14 gives an overview of the experimental setups for concrete testing.

Strength development. Strength testing followed the provisions in European standard EN 196-1:2016 and used six prisms ($(40 \times 40 \times 160)\,mm^3$), which were cured underwater. Despite being a test procedure for cement mortar, this choice enabled the determination of two strength parameters on a single specimen. Flexural tests were performed on three prisms at concrete ages of 2 d and 28 d. Compressive tests used three prism halves immediately after flexural tests. The remaining halves were tested at 56 d and 98 d.

Dynamic modulus of elasticity. For the determination of the dynamic modulus of elasticity, three prisms ($(40 \times 40 \times 160)\,mm^3$) were moist cured at 100 % r. h. until the age of 7 d and subsequently stored at 65 % r. h. until the determination of the dynamic moduli through ultrasonic pulse measurements at the concrete age of 28 d.

The dynamic modulus of elasticity E_c was derived from ultrasonic pulse velocity v_u, specimen density ρ_p, and Poisson's ratio ν using Eq. (2). Afterwards, flexural and compressive strength were determined on the same prisms following the provisions in EN 196-1:2016.

$$E_c = v_u^2 \cdot \rho_p \cdot \frac{(1+\nu)(1-2\cdot\nu)}{1-\nu} \tag{2}$$

Shrinkage. Three prisms ($(40 \times 40 \times 160)\,mm^3$) for shrinkage were produced with cast-in pins and stored alongside specimens for dynamic modulus measurements. Deformation and mass loss were determined at a concrete age of 1 d, 7 d (t_0), 14 d, 21 d, 35 d, 63 d, and 98 d, followed by strength tests after the last deformation testing according to EN 196-1:2016.

Shrinkage deformations ε_{cs} were obtained from normalizing the measured absolute length change to the specimen length after demolding.

Chloride diffusion. From each concrete mix, one cylinder ($d = 100\,mm, h = 280\,mm$) was produced and stored underwater after demolding. Water curing was interrupted for cutting the cylinder into 5 slices ($h \approx 45\,mm$) and covering the lateral surfaces of all 5 specimens and one flat surface of three specimens with epoxy resin. At the age of 28 d, these three specimens were taken from the water bath and submerged in a saturated $Ca(OH)_2$-solution for 24 h before being placed in a 16.5 wt%-NaCl-solution for 35 d. While this conditioning follows European standard EN 12390-11:2015, a simplified representative chloride penetration depth was determined using silver nitrate as an indicator on cracked specimens, similar to the rapid chloride migration test in EN 12390-18:2021. The average penetration depth d_c was obtained as the average of nine data points from each cracked surface per specimen.

Capillary absorption. Capillary absorption tests were performed on the two remaining cylindrical specimens, with only the lateral surfaces coated in epoxy resin. After water curing until the age of 28 d, the specimens were stored at 65 % r.h. for at least 6 monthes, until they reached a constant mass. To determine the capillary absorption coefficient $WA_{24\,h}$, the mass change of each specimen after partial submersion of the bottom 5 mm for 24 h was measured and normalized to the surface area.

Carbonation. The determination of the accelerated carbonation coefficient K_{AC} followed the procedure in EN 12390-12:2020. Three prisms ($(40\times40\times160)\,mm^3$) were stored underwater until the age of 28 d with a subsequent dry storage at 65 % r.h. for 14 d. Afterwards, specimens were exposed to 3 v% CO_2 at 57 % r.h. for another 70 d, with intermediate testing ages after 7 d and 28 d exposure. For each determination, a fresh surface from each prism was produced by splitting. After applying a phenolphthalein indicator, the mean carbonation depth $d_{k,t}$ was determined from three measuring points per edge per specimen. K_{AC} was then calculated as the slope of a straight line fitted to the mean carbonation depth over the square root of the duration of the exposure t, using the least squares method on Eq. (3).

$$d_k = K_{AC} \cdot \sqrt{t} \tag{3}$$

Freeze-thaw-cycles. Freeze-thaw tests were based on the cube test in the technical specification CEN/TS 12390-9:2017. Two cubes (100 mm) from mixtures with $w/c_{eq} = 0.5$ were stored underwater until the age of 7 d with a subsequent dry storage at 65 % r.h. for 21 d. Afterwards, both specimens were submerged in a container filled with demineralized water and placed in the freeze-thaw chamber. The first freeze-thaw cycle started after another 24 h, where specimens were left to absorb water. Freezing to −15 °C followed the ramp defined in CEN/TS 12390-9:2017, and for thawing, the chamber was filled with warm water. When the temperature in the specimen container had reached 20 °C, fragments were brushed off and the mass of all fragments was determined through oven-drying. Measurements were taken after 7, 14, and 28 freeze-thaw cycles (FTC), with some test extensions to 56 FTC.

Porosity. For the quantification of porosity through mercury-intrusion, concretes were mirrored through additional paste specimens with the same ratio of CEM I to SCM to water, but without aggregates. Immediately after mixing, samples were left in sealed flasks until demolding and crushing to a particle size of 2 mm – 4 mm at the age of 28 d. Following a solvent exchange through isopropyl, samples were dried at 60 °C before testing.

3. Results and discussion

3.1. Characterization of binders

The physical and chemical characterization of CEM I and the processed artificial fines highlights differences between both groups, as well as between artificial fines of different compositions and activation temperatures (see Tables 3 and 4). For reference, Figs. A.15 and A.16 illustrate the mineralogical composition of the raw materials.

Table 3
Results of the physical analysis of CEM I and activated artificial fines. ρ_p: Particle density (pycnometer), S_{BET}: Specific surface area (BET-Method), p_{BJH}: Pore volume (desorption, BJH-Method) d_{10}, d_{50}, d_{90}: Particle size at 10 v%, 50 v%, and 90 v% cumulatively passing (laser diffraction)

	ρ_p kg/dm^3	S_{BET} m^2/g	p_{BJH} cm^3/kg	d_{10} µm	d_{50} µm	d_{90} µm
CEM I	3.13	1.39	7.08	1.7	12.1	32.9
CEM-100	2.35	18.42	102.15	2.0	14.8	51.8
CEM-400	2.45	14.08	90.98	2.1	16.2	60.8
CEM-600	2.69	14.55	94.56	1.8	14.0	51.1
FA0-600	2.72	11.09	66.35	2.3	23.6	76.7
S0-600	2.77	10.48	63.88	2.1	21.5	76.0
RS75-600	2.77	7.53	47.16	1.7	13.5	51.5
RS50-100	2.54	6.51	36.56	1.9	15.3	50.8
RS50-400	2.59	5.45	33.72	1.9	14.7	49.3
RS50-600	2.59	5.41	33.08	1.9	14.5	49.7
LS50-600	2.73	6.13	35.74	1.6	12.6	74.7
GW50-600	2.72	7.98	42.08	1.7	12.4	51.5

Table 4
Results of the wet-chemical analysis of CEM I and activated artificial fines. Carbon (C), total and reactive (r-)CaO, and total and reactive (r-)SiO_2, all according to EN 196-2:2013, and free f-CaO according to EN 451-1:2017.

	C wt%	CaO wt%	f-CaO wt%	r-CaO wt%	SiO_2 wt%	r-SiO_2 wt%
CEM I	0.5	61.7	0.8	57.7	20.4	19.5
CEM-100	1.0	51.4	12.8	45.4	16.9	16.2
CEM-400	1.2	54.0	11.7	46.9	18.0	17.2
CEM-600	1.3	58.1	7.1	50.7	19.2	18.6
FA0-600	0.9	43.0	0.1	38.0	29.0	26.4
S0-600	0.8	50.1	0.8	45.3	28.0	24.1
RS75-600	1.0	40.8	1.8	35.9	39.6	18.1
RS50-100	1.0	21.1	3.5	17.3	53.3	7.8
RS50-400	1.1	21.8	2.9	17.7	59.1	12.5
RS50-600	1.1	22.0	0.0	18.0	60.1	14.1
LS50-600	7.6	49.4	0.1	13.4	12.0	9.2
GW50-600	0.6	18.2	0.1	16.8	56.1	22.9

Particle density ρ_p, specific surface area S_{BET}, and pore volume p_{BJH} are interdependent: A high density coincides with a low porosity and low specific surface area, exemplified through CEM I. Dried, hydrated cement paste, CEM-100, on the other hand, exhibits the lowest density and highest porosity and specific surface area among the artificial fines. The thermal activation has a densifying effect on the microstructure (compare [18]). Similarly, the effect of hydration products from slag or fly ash yields a denser paste (compare [53,54]). The presence of aggregates results in a reduced paste volume and subsequently increased particle density and reduced specific surface area and porosity (Table 3).

The chemical composition of the processed artificial fines is defined through the composition of the raw materials (see Table A.6). Yet, the wet-chemical analysis allows for a more detailed analysis. For CEM I, the total amount of CaO and SiO_2 matches the results from WDXRF. Table 4 shows that most of these are in a reactive form. When CEM I chemically binds water, the resulting artificial fines CEM-100 have a relatively lower amount of both CaO and SiO_2. During hydration, cement clinker forms calcium hydroxide, which is subsumed in free CaO, and other hydrates, whose calcium content comprises reactive CaO. Due to the loss of chemically bound water during thermal activation, (reactive) CaO and (reactive) SiO_2 increase for CEM-400 and CEM-600. Free CaO decreases, which exists as $Ca(OH)_2$ in CEM-100 and converts to CaO with increasing temperature. However, the offset indicates the formation of additional phases.

Compared to CEM-600, S0-600, and FA0-600, where CEM I was partially replaced by slag or fly ash during artificial fines production, exhibit a significantly higher amount of (reactive) SiO_2, in favor of a reduced amount of reactive and free CaO.

Artificial fines containing quartzitic river sand (RS) as aggregates (RS50 and RS75) have a reduced amount of reactive CaO and SiO_2 compared to CEM. However, the present results suggest an interaction between free CaO and (inert) SiO_2 during thermal activation. Free CaO in RS50-100 is completely consumed, while the amount of reactive SiO_2 almost doubles. RS75-600 shows similar results, which cannot solely be explained when considering these artificial fines as a blend of CEM and inert river sand. The analysis of artificial fines LS50-600 and GW50-600. LS50-600 with calcitic aggregates comprises a low amount of reactive components. GW50-600, on the other hand, contains greywacke with amorphous SiO_2, which increases the amount of reactive SiO_2 in the activated artificial fines.

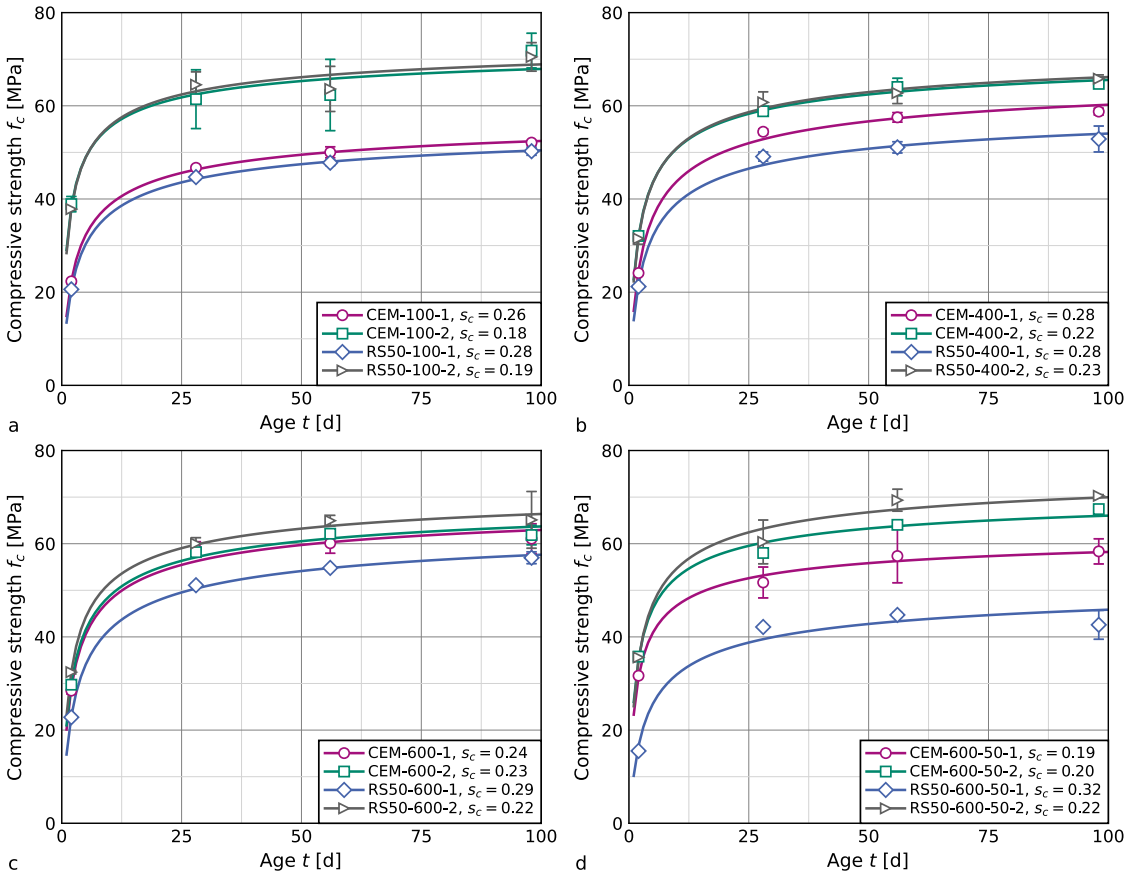

Fig. 1. Temporal compressive strength development of select concrete mixtures with artificial fines "CEM" and "RS50" processed at different temperatures and at different substitution rates. Markers and error bars represent mean values and standard deviations from three prism halves. Lines indicate optimized fit curves for strength development according to Eq. (4).

The results in Table 4 also show that all artificial fines contain carbon (C), which can only partially be explained by the raw material composition. This suggests that despite careful handling of artificial fines, natural carbonation, i.e., during milling, could not completely be avoided. The amount of organic carbon (TOC) was 0.0 wt% for all materials.

3.2. Compressive strength development

Fig. 1 illustrates selected results for concrete mixes containing processed artificial fines "CEM" and "RS50", and data processing of compressive strength tests.

For all concrete mixes, compressive strength results from series 2 are close to each other. Independent of concrete age at testing, concrete containing CEM-100 or RS50-100 exhibits similar compressive strength for each series individually. At all ages, compressive strength for series 2, where the water-binder ratio was reduced based on individual k-values, exceeds results from series 1. Compressive strength of series 1 for both types of artificial fines increases with higher processing temperature, more so for CEM than for RS50, where CEM-600 (with $k = 1.0$) reaches the same strength for both series. This also underlines the overall good reproducibility of the results. Increasing the substitution rate from 30 wt% to 50 wt% results in decreasing concrete strength, with RS50-600-50-1 exhibiting the lowest overall compressive strength of all investigated concrete mixes. Yet, the results for RS50-600-50-2 show that this compressive strength reduction can be compensated for by lowering the water-binder ratio.

The temporal compressive strength development can be further analyzed through two different approaches. Eq. (4) appropriates the model for compressive strength development in *fib* Model Code 2020 [57] for $t_{ref} = 28$ d. The equation was fitted to the experimental data by the least-squares method for each concrete mix. The fit yielded a stabilized reference strength $f_{cm,ref}$ and a strength development parameter s_c. Fig. 1 contains fit results for Eq. (4) for each individual mix. Alternatively, r (Eq. (5)) directly uses the ratio of compressive strength at 2 d and 28 d. However, while r can be more easily determined, this parameter is more sensitive to scatter.

$$f_c(t) = f_{cm,ref} \cdot \exp\left\{ s_c \cdot \left[1 - \left(\frac{t_{\mathrm{ref}}}{t} \right)^{0.5} \right] \right\} \qquad \text{with } t_{ref} = 28\,\mathrm{d} \tag{4}$$

$$r = \frac{f_{c,2\,\mathrm{d}}}{f_{c,28\,\mathrm{d}}} \tag{5}$$

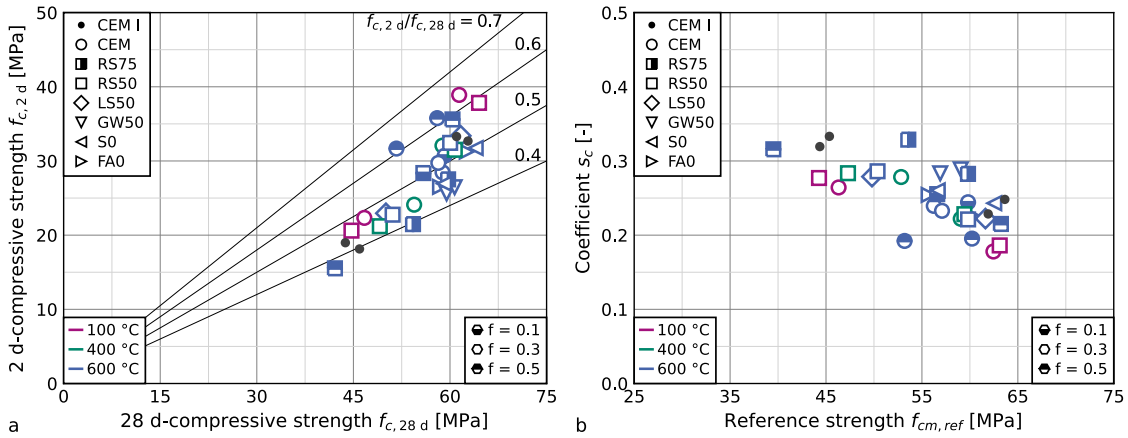

Fig. 2. Temporal compressive strength development of concrete containing processed artificial fines as SCM. Marker shapes indicate different artificial fines, fill styles indicate substitution rates (f), and color indicates processing temperatures.
(a): Compressive strength after 2 d over compressive strength after 28 d. Straight lines indicate strength ratio r (see Eq. (5))
(b): Parameters $f_{cm,ref}$ and s_c as results from fitting Eq. (4) to experimental results after 2 d, 28 d, 56 d and 98 d.

Fig. 2 illustrates the results for both approaches. Increasing $f_{c,28\,d}$ comes with disproportionally increased $f_{c,2\,d}$. Regardless of artificial fines composition (which affects compressive strength differently, as seen by the width of results for compressive strength in general), r ranges from <0.4 for the lowest strength concrete to >0.6 for the highest strength concrete. Similarly, s_c decreases from >0.3 to <0.2.

This behavior is well known. The *fib* Model Code 2020 [57] proposes $s_c = 0.2$ for concrete with CEM I 42.5 R and 35 MPa < f_{ck} < 60 MPa, and $s_c = 0.3$ for $f_{ck} \leq 35$ MPa. Here, f_{ck} denotes the characteristic compressive strength measured on cylinders. For comparison, the present analysis assumes prism compressive strength to exceed characteristic compressive strength by 18 MPa. This simplified offset comprises the difference between characteristic and mean compressive strength (8 MPa) and between cylindrical and cube compressive strength (10 MPa for 35 MPa < f_{ck} < 60 MPa). Therefore, the present results for concrete with varying artificial fines compositions and substitution rates, including the CEM I-reference, agree well with the provisions in *fib* Model Code 2020 [57] for the present compressive strength range.

When assessing the influence of artificial fines composition, most materials exhibit a similar behavior, regardless of binder composition or aggregate composition. Only RS75 and GW50 show a slower strength development, indicated through increased s_c. The latter can be explained by the pozzolanic nature of greywacke [51]. The behavior of RS75 remains inexplicable, as the expected results would lie in the range of RS50 and CEM. The thermal activation of RS50 and CEM at 400 °C or 600 °C results in slower strength development compared to 100 °C. The filler effect is present from the start and does not increase compressive strength at a later age, while rehydration of dehydrated fines is faster than CEM I hydration, but still time-dependent. Consequently, s_c for concrete with processed artificial fines reduces with higher substitution rates.

Despite the good agreement of the experimental data and the empirically fitted empirical approach in Eq. (4), there are some residual deviations. This is exemplified by both series RS50-600-50, where the 28 d-strength of the "−1"-mix exceeds the fitted curve, while the results for the "−2"-series exhibit the contrary behavior. Therefore, for the subsequent assessment of shrinkage and durability, where compressive strength was not directly measured, $f_{cm,ref}$ was used instead of $f_{c,28\,d}$ to reduce the potential impact of scatter.

3.3. Dynamic modulus of elasticity

As the experimental determination of the static modulus of elasticity is a time-consuming process, which could not be integrated into the extensive experimental program, the dynamic modulus of elasticity was measured as an inexpensive substitute. Since the aggregate fraction and content, as well as curing conditions, were held constant for all series, the results derived from ultrasonic pulse measurements allow for the qualitative assessment of the influence of the use of artificial fines as SCM [58,59].

Fig. 3 illustrates results for the dynamic modulus of elasticity and compressive strength at the age of 28 d measured on the same concrete specimens.

Overall, the modulus of elasticity increases with increasing compressive strength, corroborating findings in [39] for varying substitution rates. The results show only small deviations of concrete containing processed artificial fines as SCM from the trend set by the CEM I-references. Only series with thermally activated paste (CEM, S0, and FA0) as well as GW50, which contains an increased amount of reactive silica, exhibit a marginally smaller dynamic modulus of elasticity as compared to other series with similar compressive strength. These findings agree with [38], where reduced ultrasonic pulse velocity was linked to higher particle porosity of dehydrated paste and decreasing cement matrix stiffness.

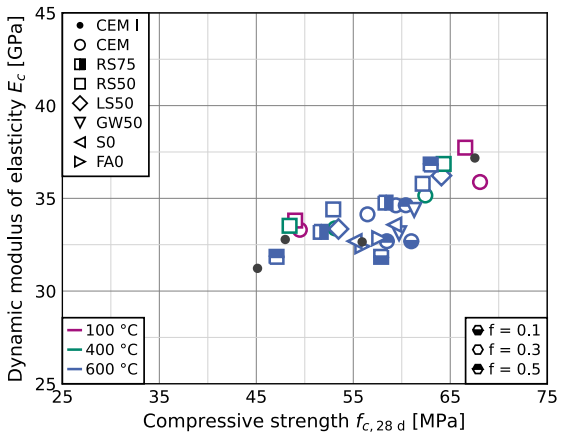

Fig. 3. Dynamic modulus of elasticity and compressive strength at the age of 28 d for different concrete mixes. Marker shapes indicate different artificial fines, fill styles indicate substitution rates (f), and color indicates processing temperatures.

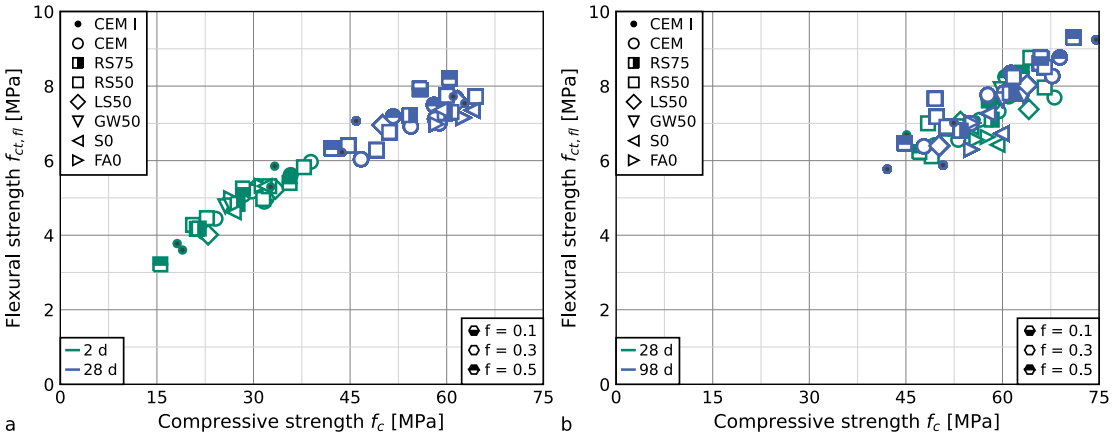

Fig. 4. Flexural and compressive strength at different ages for different concrete mixes. Marker shapes indicate different artificial fines, fill styles indicate substitution rates (f), and color indicates processing temperatures. (a): wet-stored prisms at the ages of 2 d and 28 d, (b): dry-stored prisms at the ages of 28 d and 98 d.

3.4. Flexural strength

The adoption of the test setup from EN 196-1:2016 allows for the determination of flexural and compressive strength on the same concrete specimens and, therefore, the elimination of scatter through unintentional specimen production or handling differences. Flexural strength measurements used wet-stored prisms at the ages of 2 d and 28 d, as well as dry-stored prisms at the ages of 28 d and 98 d. Fig. 4 shows the results of flexural and compressive strength tests.

Strength tests at the ages of 2 d and 28 d yield a nonlinear relationship between flexural and compressive strength (compare [57, 60]). Deviations from this trend are small and independent of concrete composition. This is confirmed for specimens tested at the ages of 28 d and 98 d, however, with an increased scatter. In contrast to early testing ages, strength increase is small, as also illustrated in Fig. 1.

3.5. Shrinkage

Concrete shrinkage comprises different components, with drying shrinkage induced through the loss of evaporable water being its major component [57]. For normal strength concrete, basic shrinkage as a consequence of cement hydration is several magnitudes smaller and therefore negligible [61]. In the present research, specimens were stored at 100 % r.h. until the age of 7 d, to further exclude an influence of basic shrinkage on measured deformations.

Fig. 5 illustrates the temporal development of shrinkage deformations ε_{cs} up to a concrete age of 98 d. As the difference between deformations at a concrete age of 1 d and 7 d is not uniform and also smaller than the standard deviation of three prisms, the assumption to neglect basic shrinkage seems justified. Therefore, the shrinkage development ε_{cs} starting at $t_s = 7$ d corresponds to the drying shrinkage.

The assessment of shrinkage deformations is generally impeded by a high scatter, especially in the present case of discontinuous measurements. [57] gives a coefficient of variation of 30 % for its model, which was partially adopted here to broaden the analytical

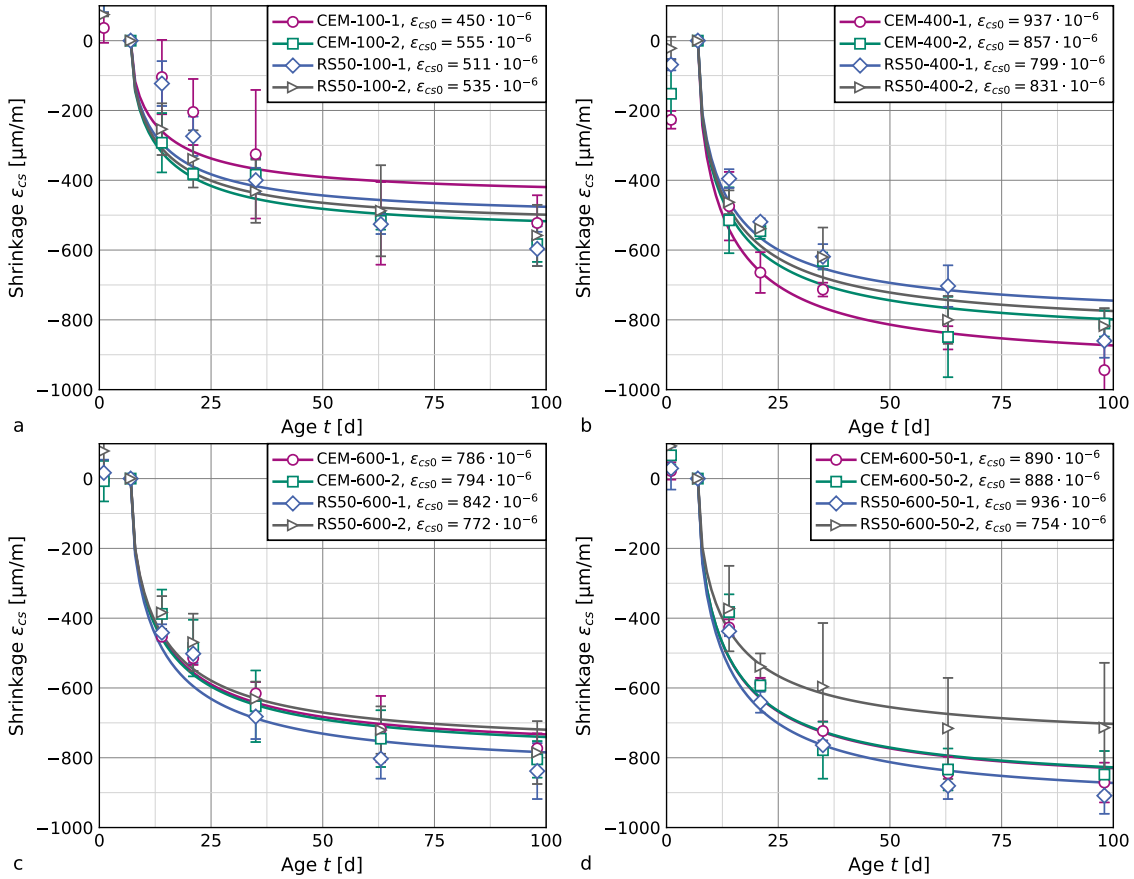

Fig. 5. Shrinkage deformation development for concrete mixes containing artificial fines "CEM" and "RS50", processed at different temperatures and with different substitution rates. Averages and standard deviations from three prisms as well as individual fit curves Eq. (6).

database. Here, drying shrinkage development consists of a drying shrinkage coefficient, a humidity coefficient, and a time function. As humidity is an invariant in the present study, the model is facilitated to comprise the time function $\beta_{ds}(t-t_s)$ and the shrinkage coefficient ε_{cs0}, which denotes the ultimate shrinkage deformation for $t - t_s \to \infty$ (see Eq. (6)).

$$\varepsilon_{cds}(t, t_s) = -\varepsilon_{cs0} \cdot \beta_{ds}(t - t_s) \tag{6}$$

$$\beta_{ds}(t - t_s) = \left(\frac{t - t_s}{0.035 \cdot h^2 + (t - t_s)} \right)^{0.5} \tag{7}$$

Eq. (6) condenses all material-dependent properties into ε_{cs0}, while the time function $\beta_{ds}(t - t_s)$ is only affected by specimen geometry, which was not altered in the present study ($h = 20\,\text{mm}$). Thus, ε_{cs0} obtained from fitting Eq. (6) to the experimental data by means of the least-squares method allows for the assessment of cement substitution through processed artificial fines. As exemplified in Fig. 5, most series show a good fit. Only concrete series with artificial fines "CEM-100" and "RS50-100", which were processed at 100 °C instead of activation at higher temperatures, exhibit a systematically slower shrinkage deformation development. This results in a systematic underestimation of the absolute shrinkage deformations for these series by Eq. (6).

This also shows in Fig. 6, where ε_{cs0} is illustrated over the reference strength $f_{cm,ref}$ and the dynamic modulus of elasticity E_c. Compared to the two reference series without CEM I-substitution, shrinkage increases with the inclusion of thermally activated artificial fines, which is in line with findings in [38,40]. This effect is especially pronounced for paste fines (CEM, S0, FA0) and for GW50 with its high content of reactive silica. In other artificial fines, ground inert aggregates may serve as micro-aggregates, which impede shrinkage deformations due to their high stiffness. The comparison of ε_{cs0} and E_c instead of $f_{cm,ref}$ substantiates this hypothesis.

3.6. Porosity

While mercury intrusion porosimetry measurements were conducted on separately produced paste specimens rather than concrete, the results still allow for assessing the impact of porosity on compressive strength.

Results for the reference series CEM I-1 and CEM I-2 confirm the reduction of total porosity alongside increasing compressive strength due to a reduction of the water-cement ratio (see Fig. 7(a)).

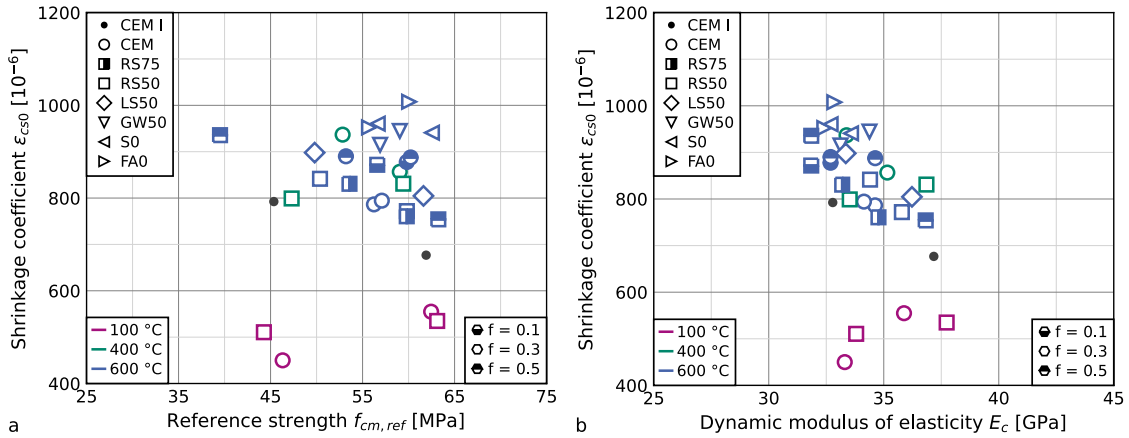

Fig. 6. Shrinkage coefficients ε_{cs0} over reference compressive strength $f_{cm,ref}$ (a), and dynamic moduli of elasticity E_c (b). Marker shapes indicate different artificial fines, fill styles indicate substitution rates (f), and color indicates processing temperatures.

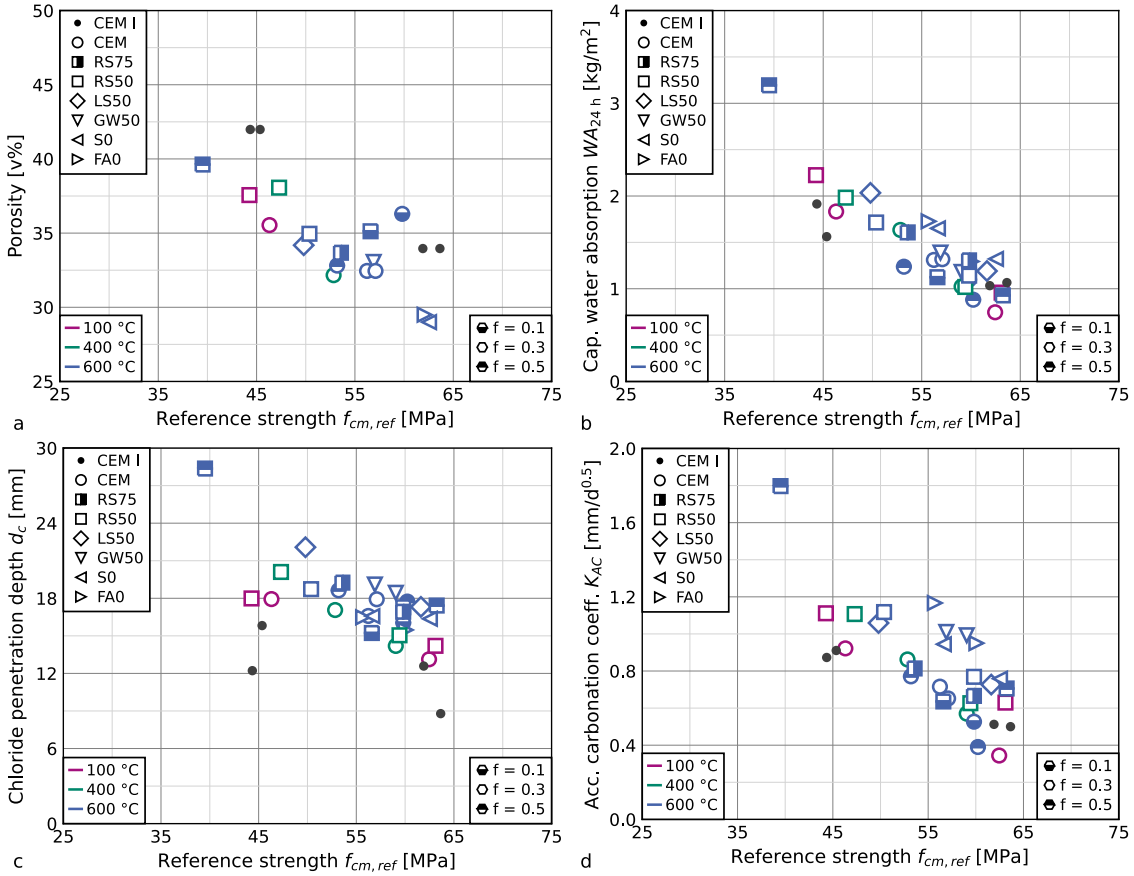

Fig. 7. Compressive strength dependency of different concrete durability parameters: Total porosity on paste specimens (a), capillary water absorption (b), chloride penetration depth (c), and accelerated carbonation coefficient (d). Marker shapes indicate artificial fines type and substitution rate, and marker colors indicate artificial fines activation temperature for different water-binder ratios.

However, except for the two series, where only 10 wt% of CEM I was replaced, all other series exhibit reduced paste porosity in concrete of similar strength, with the offset appearing to be independent of fines composition and activation temperature. While total porosity comprises all measured pores greater than 2 µm, the illustration of pore radius (r_p) distributions in Fig. 8 reveals the effect of CEM I-substitution beyond the increase in the effective water-cement ratio.

The higher water content in CEM I-1 compared to CEM I-2 leads to a significantly increased amount of pores with 100 nm < r_p < 1000 nm and r_p < 20 nm. When partially replacing CEM I through activated concrete fines, the total water-binder ratio remains constant, but the paste microstructure changes for the reduction in cement hydration products and the increase in small inert particles. Subsequently, the porosity of the remaining hydration products is only marginally altered. For artificial fines containing

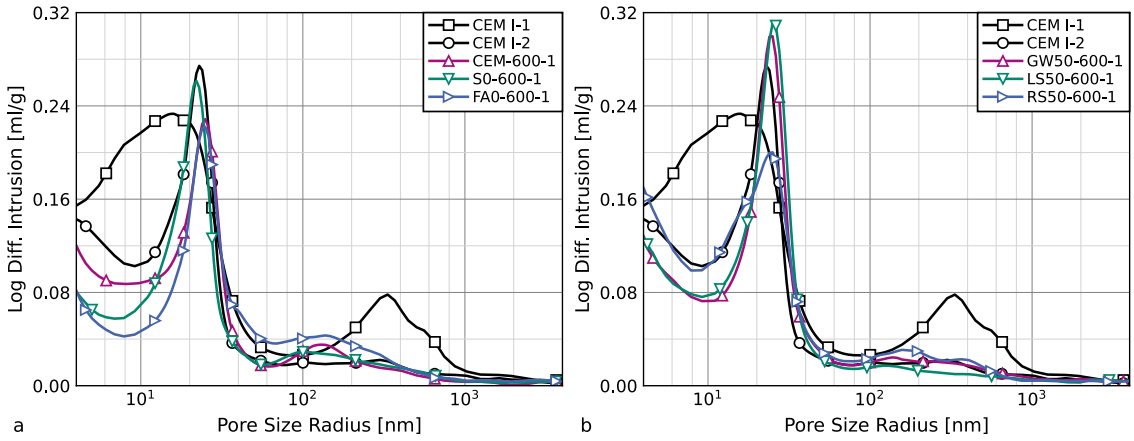

Fig. 8. Differential pore radius distribution (logarithmic) for reference series CEM I-1 and CEM I-2 as well as thermally activated artificial fines from pure paste (a), and artificial fines with different aggregate composition (b).

ground aggregates, this mostly affects pores with $r_p < 25\,\text{nm}$. Paste fines, which yield the highest concrete strength as SCM, have a similar decreasing effect on pores with $r_p < 25\,\text{nm}$, but at a higher magnitude. Conversely, porosity with $40\,\text{nm} < r_p < 200\,\text{nm}$ increases in comparison with artificial fines containing aggregates. This can be attributed to the reduction in w/b in the paste surrounding artificial fines particles due to the absorption, and consumption, of mixing water. This counteracts the higher internal porosity of these particles [25].

3.7. Capillary absorption

The effect of CEM I substitution through thermally activated artificial fines does not go beyond the reduction in compressive strength (Fig. 7(b)). When the reduction of strength is compensated for through reduced water-binder ratios, the water absorption coefficient $WA_{24\,\text{h}}$ also reduces, despite the increased total porosity. However, for low-strength concrete, water absorption is increased compared to the reference CEM I-1.

Capillary absorption interrelates with porosity, and no binding mechanisms can be expected. Fig. 9 illustrates the relationship between pore volume and capillary water absorption. Pore volume can be calculated directly from mercury intrusion measurements. As there is no consensus on a threshold for capillary activity, the definition in [37] was adopted, where harmful pores have a minimum radius (r_p) of 25 nm. Pores with a radius between 10 nm and 25 nm are considered “less harmful”. Capillary suction decreases with increasing pore radius [62]. Therefore, an upper threshold of 1000 nm was chosen. Results in Fig. 8 exhibit nearly identical results for $r_p > 1000\,\text{nm}$. The results in Fig. 9 show that for a lower pore radius of 25 nm, water absorption of concrete mixes containing the artificial fines “CEM”, “FA0”, or “S0”, which consist of pure cement paste with different binder compositions, agrees with interpolated results for the reference mixes CEM I-1 and -2. For the same pore volume, fines containing aggregates (RS75, RS50, and LS50) exhibit increased water absorption. Inert particles are surrounded by an interfacial transition zone (ITZ) with increased porosity, and for high concentrations of the particles, these ITZs may form a continuous network, which affects transport mechanisms beyond global porosity [62]. This hypothesis also explains the deviating behavior of RS50-600-50-1, which is the concrete mix with the highest amount of inert particles.

One notable exception is GW50, where aggregates are partly reactive and therefore might exhibit densified ITZs, resulting in reduced water absorption. Substantiating this hypothesis, however, requires elaborate microscopical analyses, like SEM, which were not part of the present experimental setup.

When including less harmful pores ($10\,\text{nm} < r_p < 25\,\text{nm}$) in the analysis (Fig. 9 b), the relationship between capillary absorption and pore volume is still observable, but disagrees with the reference mix CEM I-1. Therefore, the following analyses use a pore size of $r_p > 25\,\text{nm}$.

3.8. Chloride diffusion

Overall, regardless of compressive strength, chloride penetration depths d_c are increased, compared to the reference series without CEM I substitution. While the results for the artificial fines “CEM”, consisting of pure CEM I-paste, are similar to the repetition of the reference series, which agrees with [43], results for other types of artificial fines exhibit an increased chloride penetration depth. Fig. 7(c) highlights individual magnitudes of this effect in connection with fines composition and processing.

Chloride diffusion is affected by interacting concrete properties, such as the w/b ratio, the degree of hydration, and pore structure [63]. Furthermore, chlorides may be chemically bound by cement hydration products, with aluminous compounds providing the highest binding capacity [62,64]. Fig. 10 illustrates individual mechanisms. In Fig. 10 a, chloride penetration depths of concrete with constant w/b (“−1”) are plotted over paste pore volume. The results show a weak, but noticeable correlation

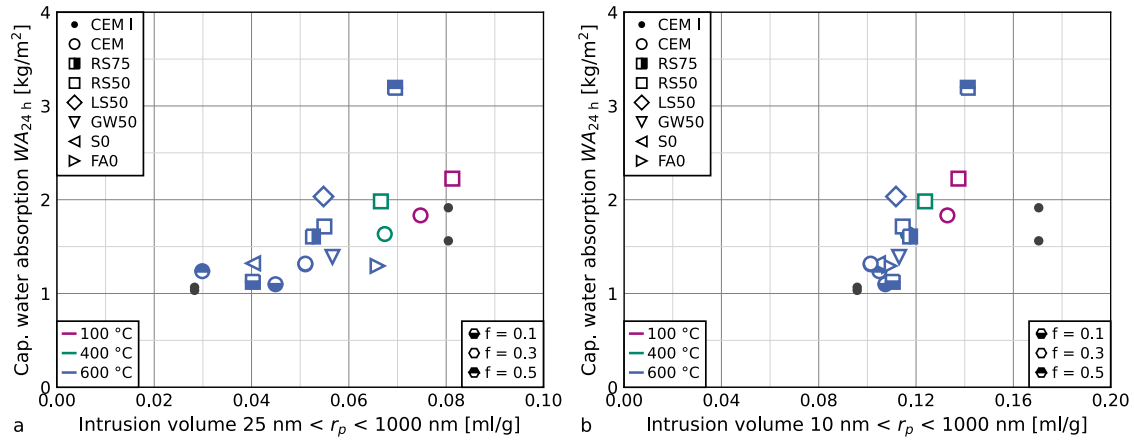

Fig. 9. Influence of pore volume for pore radius $25\,\text{nm} < r_p < 1000\,\text{nm}$ (a) and $5\,\text{nm} < r_p < 1000\,\text{nm}$ (b) of reference mixes and concrete mixes with constant w/b ("−1") on the capillary water absorption coefficient WA_{24}. Marker shapes indicate artificial fines type and substitution rate, and marker colors indicate artificial fines activation temperature for different water-binder ratios.

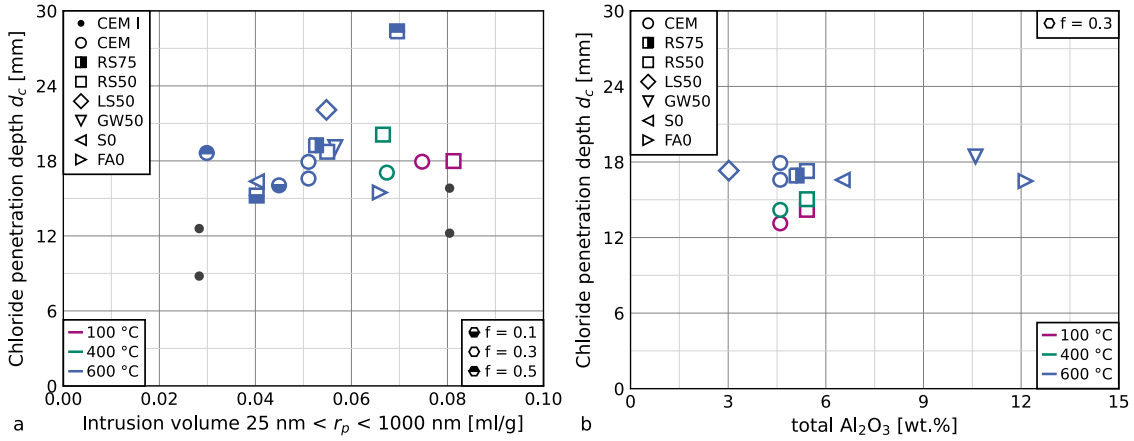

Fig. 10. Influence of pore volume of reference mixes and concrete mixes with constant w/b ("−1") (a) and influence of Al_2O_3-content in processed artificial fines in concrete mixes with constant w/c_{eq} ("−2") (b) on chloride penetration depth d_c. Marker shapes indicate artificial fines type and substitution rate, and marker colors indicate artificial fines activation temperature for different water-binder ratios.

between both parameters (compare [31,48,65]). In [31], the authors report an impact of open porosity between processed fines and OPC-paste, similar to capillary absorption, which further explains the present results.

Similar to capillary absorption, this trend is affected by artificial fines composition, where paste fines ("CEM", "FA0", "S0") exhibit lower penetration depths at similar porosity. Fig. 10 b illustrates the chloride penetration depth of concrete of the same target strength ("-2) over the total amount of Al_2O_3 in artificial fines, obtained from WDXRF-measurements (Table A.6). While fines processed at 600 °C exhibit similar penetration depths, regardless of fines composition, Fig. 10 b highlights the influence of the processing temperature. Artificial fines "CEM" and "RS50" exhibit a reduced penetration depth after processing at 400 °C or 100 °C, which suggests microstructural changes in these fines. [25] reports that sulfo-aluminates, which are a major contributor to chloride binding, carbonate easily. This agrees with findings in [47], where the chloride binding capacity increases when the activation temperature exceeds 800 °C, at which carbonates are essentially disintegrated. Accordingly, the concrete mix "CEM-100-2" exhibits the lowest chloride penetration depth of all mixes containing processed artificial fines. Here, essentially, CEM-100 substitutes CEM I and water, so that the newly formed paste and CEM-100 have a similar composition.

Regardless, these findings should be regarded with caution, as the repetition accuracy of the results must be considered. Presently, the double determination of CEM-600 yields a difference of $\Delta d_c = 1.3\,\text{mm}$ despite being produced on the same day from the same batches of raw materials. Even more, the repetition of CEM I-1 and CEM I-2 exhibits a difference of $\Delta d_c = 3.7\,\text{mm}$. In contrast to CEM-600, these series were produced with a temporal difference of three months. However, all results lie within the precision estimates for repeatability (CEM-600) or reproducibility (CEM I), detailed in EN 12390-11:2015 and EN 12390-18:2018.

3.9. Carbonation

Similar to chloride diffusion, concrete carbonation is enhanced by the partial replacement of CEM I, but also shows the individual impact of different fines composition and processing (see Fig. 7(d)).

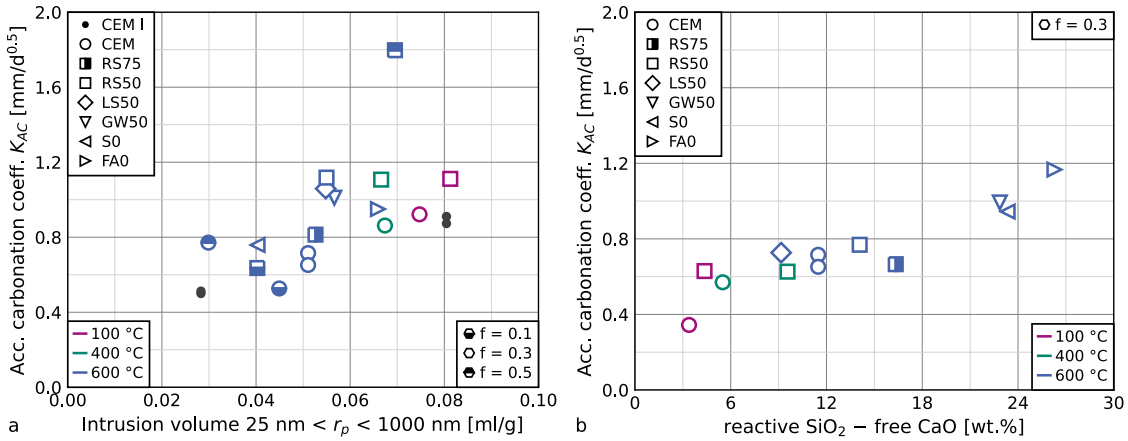

Fig. 11. Influence of pore volume of reference mixes and concrete mixes with constant w/b ("−1") (a) and influence of the chemical composition, represented through the difference in reactive SiO_2 and free CaO, in processed artificial fines in concrete mixes with constant w/c_{eq} ("−2") (b) on the accelerated carbonation coefficient K_{AC}. Marker shapes indicate artificial fines type and substitution rate, and marker colors indicate artificial fines activation temperature for different water-binder ratios.

The partial substitution of CEM I through processed CEM only affects carbonation alongside compressive strength reduction. Regardless of the processing temperature, K_{AC} follows the same relationship as the reference series CEM I-1 and CEM I-2. This may be caused by the binding of CO_2 in $Ca(OH)_2$. CEM-100 is essentially hydrated CEM I and therefore contains the same amount of $Ca(OH)_2$. During thermal activation, the hydration partially reverses, but upon rehydration, new $Ca(OH)_2$ forms. On the other hand, the amount of $Ca(OH)_2$ is reduced by fines with a high content of reactive SiO_2, which consumed the former for a pozzolanic reaction. Fig. 11 b exemplifies this behavior for concrete mixes with similar strength ("−2") by plotting the accelerated carbonation coefficient K_{AC} over the difference between reactive SiO_2 and free CaO. Subsequently, this exemplifies that even after compensating for compressive strength through adapting w/b, the fines composition impacts the carbonation behavior, which substantiates a hypothesis in [31]. Paste pore volume exhibits an additional influence on carbonation, which is similar to that of compressive strength. Fig. 11 a shows an increase of K_{AC} with higher pore volume. Here, concrete mixes without strength compensation ("−1") containing CEM regardless of the processing temperature follow the trend line set up by the reference mixes with pure CEM I. Fines with a reduced CaO- or increased SiO_2-content exhibit higher carbonation coefficients. These observations agree with results reported in [43], where the substitution of CEM I through activated cement paste has no effect on carbonation for substitution rates up to 30 wt%, whereas activated concrete fines containing inert particles increase carbonation depth. In comparison with chloride penetration, carbonation is affected to a larger extent by porosity, which was found to be caused by the semi-dry conditioning, whereas for chloride penetration, specimens are saturated [31].

3.10. Freeze-thaw-cycles

Due to the limited volume of the testing device, the effect of freeze-thaw-cycles on concrete containing processed artificial fines could only be investigated for mixes with $w/c_{eq} \approx 0.5$, so that the influence of diverging compressive strength can be ruled out from the interpretation of the results.

Fig. 12 illustrates the development of the mass loss with increasing number of freeze-thaw-cycles (FCT). For both presented types of artificial fines, "CEM-600" and "RS50-600", the substitution of 10 wt% CEM I has no effect on the mass loss after 56 FTC. For both SCMs, the substitution of 30 wt% CEM I increases the mass loss, while a higher substitution (50 wt%) has the adverse effect. This trend follows the capillary water absorption coefficient $WA_{24\,h}$, which was only evaluated up to 28 FCT (see Fig. 13).

After 28 FTC, the mass loss of the reference CEM I-2 is surpassed by half of the concrete mixes containing processed artificial fines. Generally, mass loss increases with higher water absorption, regardless of CEM I-substitution (compare [66]). As capillary absorption was not measured for series "−2", an influence of the latter cannot be derived from the data, but remains possible, especially since superplasticisers are known to refine porosity, and CEM-600-50 and RS50-600-50 required the highest amounts for a good workability (see Table A.5) [43].

4. Conclusion

For the design of durable concrete structures, compressive strength remains the most important material parameter, on which design codes are based. However, when sustainability requires the substitution of Portland cement (CEM I) through supplementary cementitious materials (SCMs), this may affect concrete compressive strength and other mechanical parameters as well as durability in different magnitudes, so that the applicability of established building codes may be compromised. The present study, therefore, used seven thermally activated artificial fines with different compositions, including binder type, aggregate content, and composition, as SCMs. The assessment of mechanical properties, as well as durability, included the production of two different

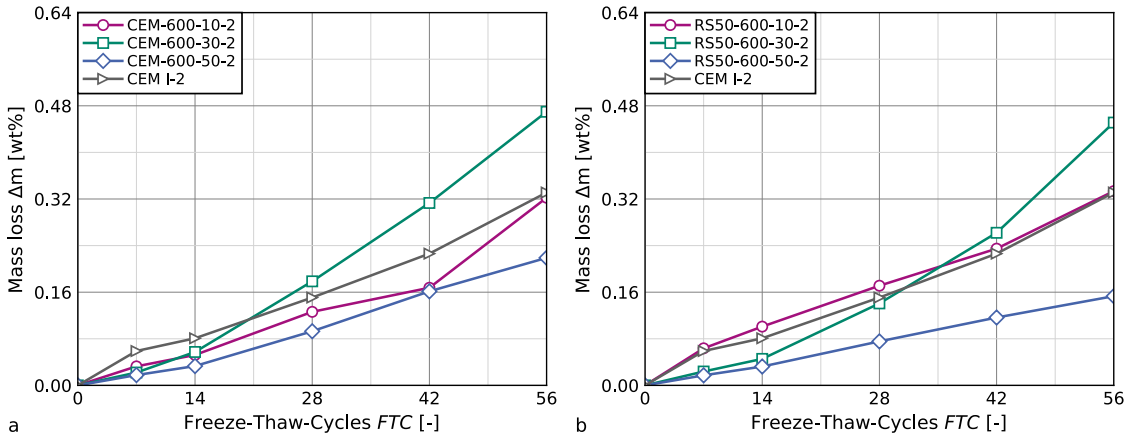

Fig. 12. Development of the cumulative mass loss after increasing freeze-thaw-cycles of concrete mixes containing 0 wt%-50 wt% CEM-600 (a) or RS50-600 (b) as CEM I-substitute.

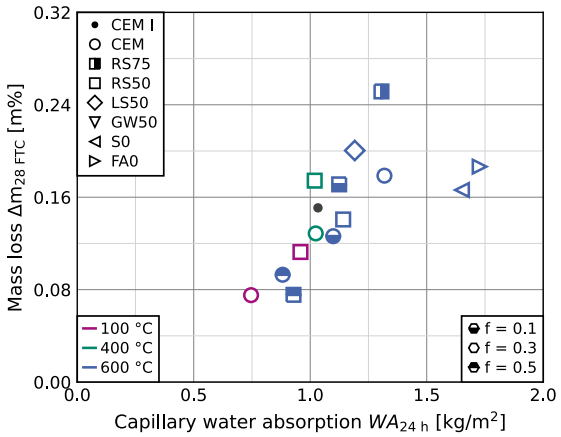

Fig. 13. Cumulative mass loss $\Delta m_{28\ FCT}$ and capillary water absorption coefficient $WA_{24\,h}$ of different concrete mixes with similar strength (series "−2"). Marker shapes indicate artificial fines type and substitution rate, and marker colors indicate artificial fines activation temperature for different water-binder ratios.

concrete mixes for each SCM with different compressive strengths. This enabled the assessment of whether the substitution of CEM I through activated artificial fines compromises concrete properties beyond compressive strength.

- Concrete compressive strength generally reduces when CEM I is partially substituted with processed artificial concrete fines. This can be compensated for by the reduction of the water-binder ratio following the *k*-value concept in EN 206:2021.
- Concrete containing processed fines exhibits a fast compressive strength development, which is similar to or exceeds the strength development of CEM I-concrete.
- Flexural strength of concrete containing processed fines changes alongside compressive strength, and follows the same relationship as CEM I-concrete.
- The dynamic modulus of elasticity and shrinkage are affected by the amount of inert particles contained in activated fines. A higher amount of inert particles reduces concrete deformations.
- While the total porosity of concrete at similar strength reduces with CEM I-replacement, the substitution negatively affects the resistance to chloride penetration and carbonation. This may have been caused by the reduced amount of cement hydration products, which can chemically bind chlorides and CO_2.
- Capillary water absorption of concrete containing processed fines follows the same dependence on compressive strength as CEM I-concrete. The freeze-thaw-resistance increases with higher water absorption.

In conclusion, the present results show that concrete with a CEM I substitution through up to 50 wt% thermally activated artificial fines exhibits a good mechanical behavior. Therefore, existing building standards and their underlying empirical relationships between compressive strength and other mechanical properties are applicable to estimate the long-term behavior of concrete containing activated fines as SCM.

However, especially for the mostly negative influence of activated fines on concrete durability, additional research, e.g., through SEM-EDS is required, where the effect of CEM I substitution on microstructure and the binding capacity of hydration products is

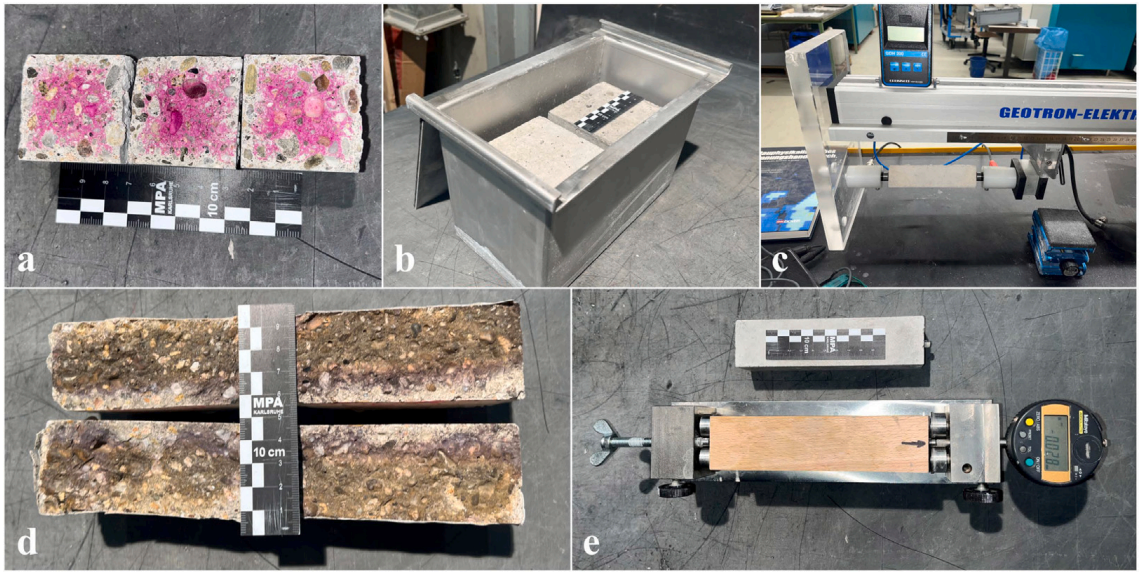

Fig. A.14. Photographic illustration of the test setups. (a): split prisms with phenolphtailein, indicating carbonation depth. (b): cubes in freeze-thaw container. (c): prism in ultrasonic pulse applicator. (d): split cylinders with silver nitrate, indicating chloride penetration. (e): shrinkage strain gauge with calibration rod.

linked to corrosive processes. The results highlight that a more thorough understanding of these processes is necessary, similar to more established SCMs, as presented in [67,68]. Ultimately, additional research needs to translate the present findings to recycled concrete fines from industrial sources and include a broader dataset to statistically secure the findings.

CRediT authorship contribution statement

Jan P. Höffgen: Writing – original draft, Visualization, Methodology, Funding acquisition, Formal analysis, Conceptualization. **Marius Schmitt:** Writing – review & editing, Formal analysis. **Frank Dehn:** Writing – review & editing, Supervision, Project administration, Funding acquisition.

Declaration of Generative AI and AI-assisted technologies in the writing process

During the preparation of this work, the authors used Grammarly and DeepL in order to check for spelling and wording errors. After using these tools/services, the authors reviewed and edited the content as needed and take full responsibility for the content of the published article.

Funding

This work was supported by the Dres. Edith und Klaus Dyckerhoff-Stiftung, grant no. T0218/36374.

Declaration of competing interest

The authors declare that they have no known competing financial interests or personal relationships that could have appeared to influence the work reported in this paper.

Appendix

See Table A.5, Table A.6, Fig. A.14, Fig. A.15 and Fig. A.16.

Data availability

Data will be made available on request.

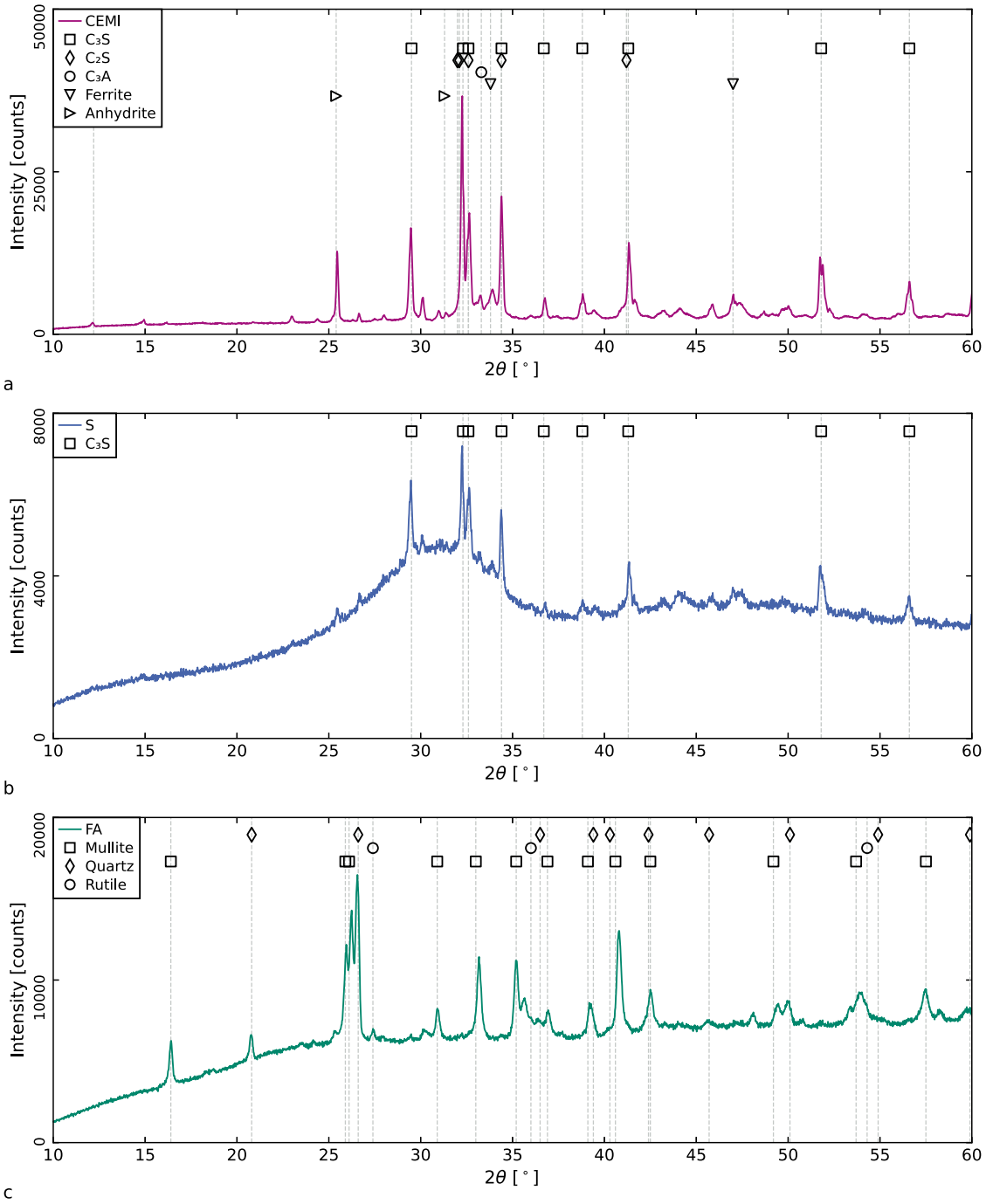

Fig. A.15. Qualitative X-ray Diffraction (XRD) of binders. (a): CEM I, (b): Slag (S), (c): Fly Ash (FA).

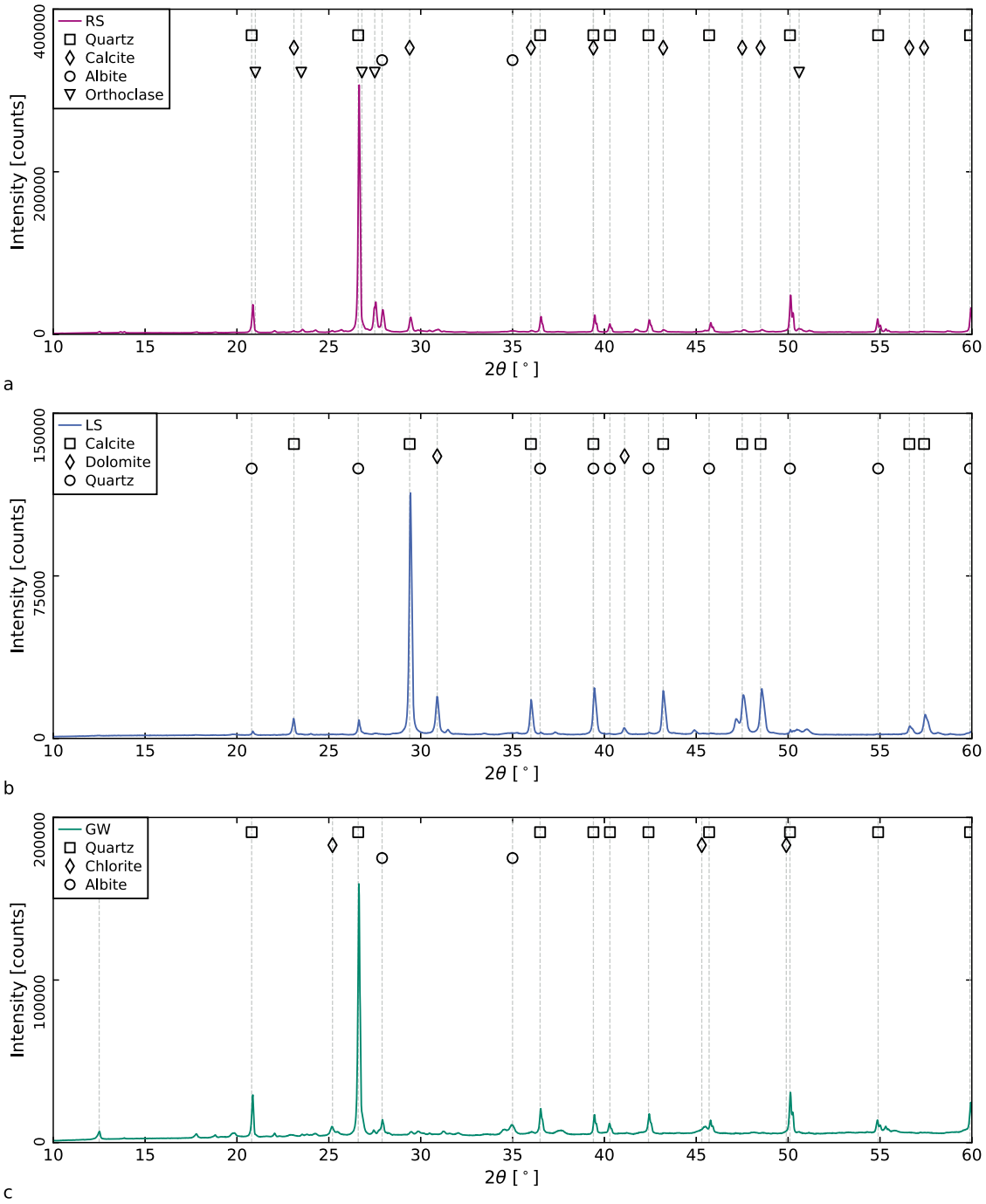

Fig. A.16. Qualitative X-ray Diffraction (XRD) of aggregates. (a): River Sand (RS), (b): Limestone (LS), (c): Greywacke (GW).

Table A.5
Overview of different series. SCM: supplementary cementitious material. f: substitution rate of CEM I through SCM. k: assumed k-value. w/b: selected water-binder ratio. w/c_{eq}: resulting equivalent water-cement ratio. w: water content. c: CEM I content. a: SCM content. SP: superplasticizer dosage for achieving target consistency. Aggregate content for all series: RS: 526 kg/m^3, RG: 1024 kg/m^3.

Series	SCM	f –	k –	w/b –	w/c_{eq} –	w kg/m^3	c kg/m^3	a kg/m^3	SP kg/m^3
CEM I-1	CEM I	0.0		0.60	0.60	261	435		0.0
CEM I-2				0.50	0.50	244	488		0.0
CEM-100-1	CEM-100	0.3	0.20	0.50	0.66	235	329	141	2.3
CEM-100-2				0.38	0.50	208	383	164	8.2
CEM-400-1	CEM-400	0.3	0.66	0.50	0.56	236	331	142	3.5
CEM-400-2				0.45	0.50	226	352	151	4.3
CEM-600-1	CEM-600	0.3	1.00	0.50	0.50	239	335	144	3.2
CEM-600-2				0.50	0.50	239	335	144	3.6
CEM-600-10-2		0.1	1.00	0.50	0.50	243	437	49	0.0
CEM-600-50-1		0.5	0.80	0.50	0.56	237	237	237	7.0
CEM-600-50-2				0.45	0.50	226	251	251	12.7
FA0-600-1	FA0-600	0.3	1.20	0.50	0.47	240	336	144	1.6
FA0-600-2				0.53	0.50	245	324	139	0.8
S0-600-1	S0-600	0.3	1.20	0.50	0.47	240	337	144	1.7
S0-600-2				0.53	0.50	246	325	139	0.6
RS75-600-1	RS75-600	0.3	0.84	0.50	0.53	240	337	144	1.3
RS75-600-2				0.47	0.49	234	349	150	2.1
RS50-100-1	RS50-100	0.3	0.25	0.50	0.65	238	333	143	0.0
RS50-100-2				0.39	0.50	213	383	164	4.0
RS50-400-1	RS50-400	0.3	0.46	0.50	0.60	238	334	143	1.2
RS50-400-2				0.41	0.49	219	374	160	4.7
RS50-600-1	RS50-600	0.3	0.50	0.50	0.59	238	334	143	1.2
RS50-600-2				0.43	0.49	224	364	156	3.4
RS50-600-10-2		0.1	1.00	0.50	0.50	242	436	48	0.0
RS50-600-50-1		0.5	0.40	0.50	0.71	235	235	235	3.5
RS50-600-50-2				0.35	0.50	199	285	285	10.0
LS50-600-1	LS50-600	0.3	0.51	0.50	0.59	240	336	144	1.2
LS50-600-2				0.43	0.50	225	367	157	3.4
GW50-600-1	GW50-600	0.3	0.80	0.50	0.53	240	336	144	1.2
GW50-600-2				0.47	0.50	234	348	149	2.5

Table A.6
Chemical composition of the raw materials for concrete and artificial fines production through Wavelength Dispersive X-ray Fluorescence Spectroscopy (WDXRF) (EN 196-2:2013). LOI: Loss on ignition.

	Na_2O wt%	MgO wt%	Al_2O_3 wt%	SiO_2 wt%	P_2O_5 wt%	K_2O wt%	CaO wt%	TiO_2 wt%	MnO wt%	Fe_2O_3 wt%	LOI wt%
CEM I	0.1	1.9	4.6	19.8	0.2	0.8	60.7	0.2	0.2	3.2	2.4
S	0.2	5.6	11.0	35.7	0.1	0.7	41.6	1.0	0.6	1.3	−1.0
FA	0.4	1.3	29.7	48.1	0.3	1.3	3.1	3.4	0.1	9.2	1.8
RS	1.2	0.6	5.8	80.6	0.1	2.0	4.1	0.1	0.0	1.1	3.8
LS	0.0	3.0	2.3	7.7	0.1	0.8	44.3	0.1	0.0	0.9	38.5
GW	0.8	1.9	13.3	68.8	0.1	3.1	1.1	0.9	0.1	5.4	3.8

References

[1] J.H. Aquino Rocha, R.D. Toledo Filho, The utilization of recycled concrete powder as supplementary cementitious material in cement-based materials: A systematic literature review, J. Build. Eng. 76 (2023) 107319, http://dx.doi.org/10.1016/j.jobe.2023.107319.

[2] A. Carriço, J.A. Bogas, M. Guedes, Thermoactivated cementitious materials – A review, Constr. Build. Mater. 250 (2020) 118873, http://dx.doi.org/10.1016/j.conbuildmat.2020.118873.

[3] Z. He, X. Zhu, J. Wang, M. Mu, Y. Wang, Comparison of CO2 emissions from OPC and recycled cement production, Constr. Build. Mater. 211 (2019) 965–973, http://dx.doi.org/10.1016/j.conbuildmat.2019.03.289.

[4] E.A. Ohemeng, S.O. Ekolu, A review on the reactivation of hardened cement paste and treatment of recycled aggregates, Mag. Concr. Res. 72 (10) (2020) 526–539, http://dx.doi.org/10.1680/jmacr.18.00452.

[5] S. Real, V. Sousa, I. Meireles, J.A. Bogas, A. Carriço, Life Cycle Assessment of Thermoactivated Recycled Cement Production, Mater. (Basel, Switzerland) 15 (19) (2022) http://dx.doi.org/10.3390/ma15196766.

[6] V. Sousa, J.A. Bogas, Comparison of energy consumption and carbon emissions from clinker and recycled cement production, J. Clean. Prod. 306 (2021) 127277, http://dx.doi.org/10.1016/j.jclepro.2021.127277.

[7] V. Sousa, J.A. Bogas, S. Real, I. Meireles, Industrial production of recycled cement: Energy consumption and carbon dioxide emission estimation, Environ. Sci. Pollut. Res. 30 (4) (2022) 8778–8789, http://dx.doi.org/10.1007/s11356-022-20887-7.
[8] V. Sousa, J.A. Bogas, S. Real, I. Meireles, A. Carriço, Recycled cement production energy consumption optimization, Sustain. Chem. Pharm. 32 (2023) 101010, http://dx.doi.org/10.1016/j.scp.2023.101010.
[9] L. Xu, J. Wang, K. Li, S. Lin, M. Li, T. Hao, Z. Ling, D. Xiang, T. Wang, A systematic review of factors affecting properties of thermal-activated recycled cement, Resour. Conserv. Recycl. 185 (2022) 106432, http://dx.doi.org/10.1016/j.resconrec.2022.106432.
[10] S.C. Angulo, M.S. Guilge, V.A. Quarcioni, M.A. Cincotto, T.R. Nobre, H. Pöllmann, The role of calcium silicates and quicklime on the reactivity of rehydrated cements, Constr. Build. Mater. 340 (2022) 127625, http://dx.doi.org/10.1016/j.conbuildmat.2022.127625.
[11] T.F. Baggio, E. Possan, J.J. De Oliveira Andrade, Physical-chemical characterization of construction and demolition waste powder with thermomechanical activation for use as supplementary cementitious material, Constr. Build. Mater. 437 (2024) 136907, http://dx.doi.org/10.1016/j.conbuildmat.2024.136907.
[12] R. Baldusco, T.R.S. Nobre, S.C. Angulo, V.A. Quarcioni, M.A. Cincotto, Dehydration and Rehydration of Blast Furnace Slag Cement, J. Mater. Civ. Eng. 31 (8) (2019) 04019132, http://dx.doi.org/10.1061/(ASCE)MT.1943-5533.0002725.
[13] J.A. Bogas, S. Real, A. Carriço, J. Abrantes, M. Guedes, Hydration and phase development of recycled cement, Cem. Concr. Compos. 127 (2022) 104405, http://dx.doi.org/10.1016/j.cemconcomp.2022.104405.
[14] A. Carriço, S. Real, J.A. Bogas, M.F. Costa Pereira, Mortars with thermo activated recycled cement: Fresh and mechanical characterisation, Constr. Build. Mater. 256 (2020) 119502, http://dx.doi.org/10.1016/j.conbuildmat.2020.119502.
[15] K. Kalinowska-Wichrowska, M. Kosior-Kazberuk, E. Pawluczuk, The Properties of Composites with Recycled Cement Mortar Used as a Supplementary Cementitious Material, Materials 13 (1) (2020) 64, http://dx.doi.org/10.3390/ma13010064.
[16] N. Noel, T. Mielke, G. Semugaza, A.Z. Gierth, S. Helmich, S. Nawrath, D.C. Lupascu, Chemical transformations during the preparation and rehydration of reactivated virgin cements, CEMENT 19 (2025) 100129, http://dx.doi.org/10.1016/j.cement.2025.100129.
[17] S. Real, A. Carriço, J.A. Bogas, M. Guedes, Influence of the Treatment Temperature on the Microstructure and Hydration Behavior of Thermoactivated Recycled Cement, Materials 13 (18) (2020) 3937, http://dx.doi.org/10.3390/ma13183937.
[18] G. Semugaza, T. Mielke, M.E. Castillo, A.Z. Gierth, J.X. Tam, S. Nawrath, D.C. Lupascu, Reactivation of hydrated cement powder by thermal treatment for partial replacement of ordinary portland cement, Mater. Struct. 56 (3) (2023) http://dx.doi.org/10.1617/s11527-023-02133-9.
[19] R. Serpell, M. Lopez, Properties of mortars produced with reactivated cementitious materials, Cem. Concr. Compos. 64 (2015) 16–26, http://dx.doi.org/10.1016/j.cemconcomp.2015.08.003.
[20] R. Serpell, F. Zunino, Recycling of hydrated cement pastes by synthesis of α'H-C2S, Cem. Concr. Res. 100 (2017) 398–412, http://dx.doi.org/10.1016/j.cemconres.2017.08.001.
[21] Y. Sui, C. Ou, S. Liu, J. Zhang, Q. Tian, Study on Properties of Waste Concrete Powder by Thermal Treatment and Application in Mortar, Appl. Sci. 10 (3) (2020) 998, http://dx.doi.org/10.3390/app10030998.
[22] E. Tajuelo Rodriguez, K. Garbev, D. Merz, L. Black, I.G. Richardson, Thermal stability of C-S-H phases and applicability of Richardson and Groves' and Richardson C-(A)-S-H(I) models to synthetic C-S-H, Cem. Concr. Res. 93 (2017) 45–56, http://dx.doi.org/10.1016/j.cemconres.2016.12.005.
[23] J. Zelic, L. Ugrina, D. Jozic, Application of Thermal Methods in the Chemistry of Cement: Kinetic Analysis of Portlandite from Non-Isothermal Thermogravimetric Data, in: The First International Proficiency Testing Conference, n. d., Sinaia, Romania, 2007, pp. 420–429.
[24] J.A. Bogas, A. Carriço, M. Pereira, Mechanical characterization of thermal activated low-carbon recycled cement mortars, J. Clean. Prod. 218 (2019) 377–389, http://dx.doi.org/10.1016/j.jclepro.2019.01.325.
[25] J.A. Bogas, A. Carriço, A.J. Tenza-Abril, Microstructure of thermoactivated recycled cement pastes, Cem. Concr. Res. 138 (2020) 106226, http://dx.doi.org/10.1016/j.cemconres.2020.106226.
[26] Z. Shui, D. Xuan, H. Wan, B. Cao, Rehydration reactivity of recycled mortar from concrete waste experienced to thermal treatment, Constr. Build. Mater. 22 (8) (2008) 1723–1729, http://dx.doi.org/10.1016/j.conbuildmat.2007.05.012.
[27] X. Xi, Y. Zheng, C. Du, P. Zhang, M. Sun, Study on the hydration characteristics, mechanical properties, and microstructure of thermally activated low-carbon recycled cement, Constr. Build. Mater. 447 (2024) 138042, http://dx.doi.org/10.1016/j.conbuildmat.2024.138042.
[28] J. Kim, N. Kim, Exploring the role of thermal activation of cement exposed to the external environment on the improvement of concrete properties, J. Mater. Res. Technol. 24 (2023) 2868–2878, http://dx.doi.org/10.1016/j.jmrt.2023.03.195.
[29] D. Qian, R. Yu, Z. Shui, Y. Sun, C. Jiang, F. Zhou, M. Ding, X. Tong, Y. He, A novel development of green ultra-high performance concrete (UHPC) based on appropriate application of recycled cementitious material, J. Clean. Prod. 261 (2020) 121231, http://dx.doi.org/10.1016/j.jclepro.2020.121231.
[30] Z. Shui, D. Xuan, W. Chen, R. Yu, R. Zhang, Cementitious characteristics of hydrated cement paste subjected to various dehydration temperatures, Constr. Build. Mater. 23 (1) (2009) 531–537, http://dx.doi.org/10.1016/j.conbuildmat.2007.10.016.
[31] J.A. Bogas, A. Carriço, S. Real, Durability of concrete produced with recycled cement from waste concrete, 3rd International Congress on Materials & Structural Stability, Mater. Today: Proc. 58 (2022) 1149–1154, http://dx.doi.org/10.1016/j.matpr.2022.01.280.
[32] V. Letelier, E. Tarela, P. Muñoz, G. Moriconi, Combined effects of recycled hydrated cement and recycled aggregates on the mechanical properties of concrete, Constr. Build. Mater. 132 (2017) 365–375, http://dx.doi.org/10.1016/j.conbuildmat.2016.12.010.
[33] Z. Ma, J. Shen, H. Wu, P. Zhang, Properties and activation modification of eco-friendly cementitious materials incorporating high-volume hydrated cement powder from construction waste, Constr. Build. Mater. 316 (2022) 125788, http://dx.doi.org/10.1016/j.conbuildmat.2021.125788.
[34] A. Tokareva, S. Kaassamani, D. Waldmann, Fine demolition wastes as Supplementary cementitious materials for CO2 reduced cement production, Constr. Build. Mater. 392 (2023) 131991, http://dx.doi.org/10.1016/j.conbuildmat.2023.131991.
[35] P. Vashistha, Y. Oinam, H.-K. Kim, S. Pyo, Effect of thermo-mechanical activation of waste concrete powder (WCP) on the characteristics of cement mixtures, Constr. Build. Mater. 362 (2023) 129713, http://dx.doi.org/10.1016/j.conbuildmat.2022.129713.
[36] H. Wu, C. Liang, Z. Zhang, P. Yao, C. Wang, Z. Ma, Utilizing heat treatment for making low-quality recycled aggregate into enhanced recycled aggregate, recycled cement and their fully recycled concrete, Constr. Build. Mater. 394 (2023) 132126, http://dx.doi.org/10.1016/j.conbuildmat.2023.132126.
[37] M. Wei, L. Chen, N. Lei, H. Li, L. Huang, Mechanical properties and microstructures of thermally activated ultrafine recycled fine powder cementitious materials, Constr. Build. Mater. 475 (2025) 141195, http://dx.doi.org/10.1016/j.conbuildmat.2025.141195.
[38] S. Real, J.A. Bogas, A. Carriço, S. Hu, Mechanical Characterisation and Shrinkage of Thermoactivated Recycled Cement Concrete, Appl. Sci. 11 (6) (2021) 2454, http://dx.doi.org/10.3390/app11062454.
[39] E.M. Getachew, B.W. Yifru, B.T. Habtegebreal, M.D. Yehualaw, Performance evaluation of mortar with ground and thermo-activated recycled concrete cement, Cogent Eng. 11 (1) (2024) 2357726, http://dx.doi.org/10.1080/23311916.2024.2357726.
[40] A. Carriço, J.A. Bogas, S. Real, M.F.C. Pereira, Shrinkage and sorptivity of mortars with thermoactivated recycled cement, Constr. Build. Mater. 333 (2022) 127392, http://dx.doi.org/10.1016/j.conbuildmat.2022.127392.
[41] J. Kim, A. Ubysz, Thermal activation of multi-recycled concrete powder as supplementary cementitious material for repeated and waste-free recycling, J. Build. Eng. 98 (2024) 111169, http://dx.doi.org/10.1016/j.jobe.2024.111169.
[42] A. Tokareva, D. Waldmann, Durability of cement mortars containing fine demolition wastes as supplementary cementitious materials, Constr. Build. Mater. 477 (2025) 141316, http://dx.doi.org/10.1016/j.conbuildmat.2025.141316.
[43] A. Carriço, S. Real, J.A. Bogas, Durability performance of thermoactivated recycled cement concrete, Cem. Concr. Compos. 124 (2021) http://dx.doi.org/10.1016/j.cemconcomp.2021.104270.

[44] H. Wu, D. Yang, Z. Ma, Micro-structure, mechanical and transport properties of cementitious materials with high-volume waste concrete powder and thermal modification, Constr. Build. Mater. 313 (2021) 125477, http://dx.doi.org/10.1016/j.conbuildmat.2021.125477.
[45] N. Algourdin, Q. Nguyen, Z. Mesticou, A. Si Larbi, Durability of recycled fine mortars under freeze–thaw cycles, Constr. Build. Mater. 291 (2021) 123330, http://dx.doi.org/10.1016/j.conbuildmat.2021.123330.
[46] M. Wei, L. Chen, N. Lei, H. Li, L. Huang, Experimental investigation on freeze–thaw resistance of thermally activated recycled fine powder concrete, Constr. Build. Mater. 457 (2024) 139378, http://dx.doi.org/10.1016/j.conbuildmat.2024.139378.
[47] Z. He, R. Hu, Z. Ma, X. Liu, C. Wang, H. Wu, Reusing thermoactivated construction waste spoil as sustainable binder for durable concrete: Microstructure and chloride transport, Constr. Build. Mater. 398 (2023) 132553, http://dx.doi.org/10.1016/j.conbuildmat.2023.132553.
[48] L. Xu, J. Wang, X. Hu, B. Ran, T. Wu, X. Zhou, Y. Xiong, Physical performance, durability, and carbon emissions of recycled cement concrete and fully recycled concrete, Constr. Build. Mater. 447 (2024) 138128, http://dx.doi.org/10.1016/j.conbuildmat.2024.138128.
[49] A. Carriço, J.A. Bogas, S. Hu, S. Real, M.F. Costa Pereira, Novel separation process for obtaining recycled cement and high-quality recycled sand from waste hardened concrete, J. Clean. Prod. 309 (2021) 127375, http://dx.doi.org/10.1016/j.jclepro.2021.127375.
[50] E.W. Klingsch, Explosive Spalling of Concrete in Fire (Ph.D. thesis), ETH Zurich, Zürich, 2014, http://dx.doi.org/10.3929/ethz-a-010243000.
[51] A. Lipowsky, A. Müller, Gesteinsmehl als Zuschlagstoffe in hydraulischen Bindemitteln, Aufbereitungs-Technik/Mineral Process. 58 (12) (2017) 52–64.
[52] R. Serpell, M. Lopez, Reactivated cementitious materials from hydrated cement paste wastes, Cem. Concr. Compos. 39 (2013) 104–114, http://dx.doi.org/10.1016/j.cemconcomp.2013.03.020.
[53] L. Xu, J. Wang, K. Li, M. Li, S. Lin, T. Hao, T. Wang, Y. Guo, Z. Ling, Investigations on the rehydration of recycled blended SCMs cement, Cem. Concr. Res. 163 (2023) 107036, http://dx.doi.org/10.1016/j.cemconres.2022.107036.
[54] L. Xu, J. Wang, K. Li, T. Hao, Z. Li, L. Li, B. Ran, H. Du, New insights on dehydration at elevated temperature and rehydration of GGBS blended cement, Cem. Concr. Compos. 139 (2023) 105068, http://dx.doi.org/10.1016/j.cemconcomp.2023.105068.
[55] J.P. Höffgen, F. Dehn, Influence of thermally activated artificial concrete fines composition on mortar strength development, Dev. the Built Environ. 24 (2025) 100775, http://dx.doi.org/10.1016/j.dibe.2025.100775.
[56] J.P. Höffgen, S. Bruckschlögl, B. Wetz, F. Dehn, Influence of thermally activated industrial concrete fines of different origin on mortar strength development, Case Stud. Constr. Mater. (2025) e05427, http://dx.doi.org/10.1016/j.cscm.2025.e05427.
[57] International Federation for Structural Concrete (Ed.), Fib model code for concrete structures (2020), Version 1, International Federation for Structural Concrete (fib), Lausanne, 2023.
[58] N. Ekin, O. Uyanik, Comparison of Static and Dynamic Elastic Moduli in Concrete: Effects of Compressive Strength, Curing Conditions and Reinforcement, Iran. J. Sci. Technol. Trans. Civ. Eng. 45 (4) (2021) 2327–2343, http://dx.doi.org/10.1007/s40996-020-00513-7.
[59] A.I. Marques, J. Morais, P. Morais, M.D.R. Veiga, C. Santos, P. Candeias, J.G. Ferreira, Modulus of elasticity of mortars: Static and dynamic analyses, Constr. Build. Mater. 232 (2020) 117216, http://dx.doi.org/10.1016/j.conbuildmat.2019.117216.
[60] R. Campos, M.M.M. Larrain, M. Zaman, V. Pozadas, Relationships between compressive and flexural strengths of concrete based on fresh field properties, Int. J. Pavement Res. Technol. 14 (2) (2021) 161–167, http://dx.doi.org/10.1007/s42947-020-1074-0.
[61] H.S. Müller, F. Acosta Urrea, V. Kvitsel, Modelle zur Vorhersage des Schwindens und Kriechens von Beton: Teil 1: Analyse des Schwindmodells in DIN EN 1992-1-1:2011 und neuer Ansatz im Eurocode 2 prEN 1992-1-1:2020, Beton- Und Stahlbetonbau 116 (1) (2021) 2–18, http://dx.doi.org/10.1002/best.202000082.
[62] F.W. Locher, Cement Principles of Production and Use, Verl. Bau und Technik, Düsseldorf, 2006.
[63] N. Ukrainczyk, T. Bernard, A. Babaahmadi, L. Huang, C. Zausinger, A. Soive, S. Bonnet, F. Georget, M. Mrak, S. Dolenec, T. Völker, P. Suraneni, W. Wilson, Test methods for chloride diffusivity of blended cement pastes: A review by RILEM TC 298-EBD, Mater. Struct. 58 (10) (2025) 324, http://dx.doi.org/10.1617/s11527-025-02809-4.
[64] K. De Weerdt, W. Wilson, A. Machner, F. Georget, Chloride profiles – What do they tell us and how should they be used? Cem. Concr. Res. 173 (2023) 107287, http://dx.doi.org/10.1016/j.cemconres.2023.107287.
[65] Y. Yang, R.A. Patel, S.V. Churakov, N.I. Prasianakis, G. Kosakowski, M. Wang, Multiscale modeling of ion diffusion in cement paste: Electrical double layer effects, Cem. Concr. Compos. 96 (2019) 55–65, http://dx.doi.org/10.1016/j.cemconcomp.2018.11.008.
[66] J. Stark, B. Wicht, Dauerhaftigkeit Von Beton, second ed., Springer-Verlag, Berlin, 2013, http://dx.doi.org/10.1077/978-3-642-35278-2.
[67] S. Greve-Dierfeld, B. Lothenbach, A. Vollpracht, B. Wu, B. Huet, C. Andrade, C. Medina, C. Thiel, E. Gruyaert, H. Vanoutrive, I.F. Del Saéz Bosque, I. Ignjatovic, J. Elsen, J.L. Provis, K. Scrivener, K.-C. Thienel, K. Sideris, M. Zajac, N. Alderete, Ö. Cizer, P. van den Heede, R.D. Hooton, S. Kamali-Bernard, S.A. Bernal, Z. Zhao, Z. Shi, N. Belie, Understanding the carbonation of concrete with supplementary cementitious materials: A critical review by RILEM TC 281-CCC, Mater. Struct. 53 (6) (2020) http://dx.doi.org/10.1617/s11527-020-01558-w.
[68] F. Georget, A. Babaahmadi, A. Machner, M. Mrak, S. Dolenec, Q.X. Xiong, J. Shiju, D. Snoeck, P. Suraneni, W. Wilson, Measuring chloride binding in cementitious materials: A review by RILEM TC 298-EBD, Mater. Struct. 58 (10) (2025) 348, http://dx.doi.org/10.1617/s11527-025-02802-x.

Supplementary Data to Paper P3

Tab. A21: Particle size distributions of CEM I and processed artificial fines. d_i: particle size at i % passing [µm].

	d_{10}	d_{30}	d_{50}	d_{70}	d_{90}
CEM I	1.7	5.9	12.1	20.6	32.9
CEM-100	2.0	6.2	14.8	28.5	51.8
CEM-400	2.1	6.6	16.2	32.6	60.8
CEM-600	1.8	5.6	14.0	27.6	51.1
FA0-600	2.3	8.2	23.6	43.2	76.7
S0-600	2.1	6.8	21.5	42.4	76.0
RS75-600	1.7	5.3	13.5	27.6	51.5
RS50-100	1.9	6.0	15.3	29.2	50.8
RS50-400	1.9	5.9	14.7	28.1	49.3
RS50-600	1.9	5.9	14.5	27.9	49.7
LS50-600	1.6	4.6	12.6	36.2	74.7
GW50-600	1.7	4.8	12.4	26.4	51.5

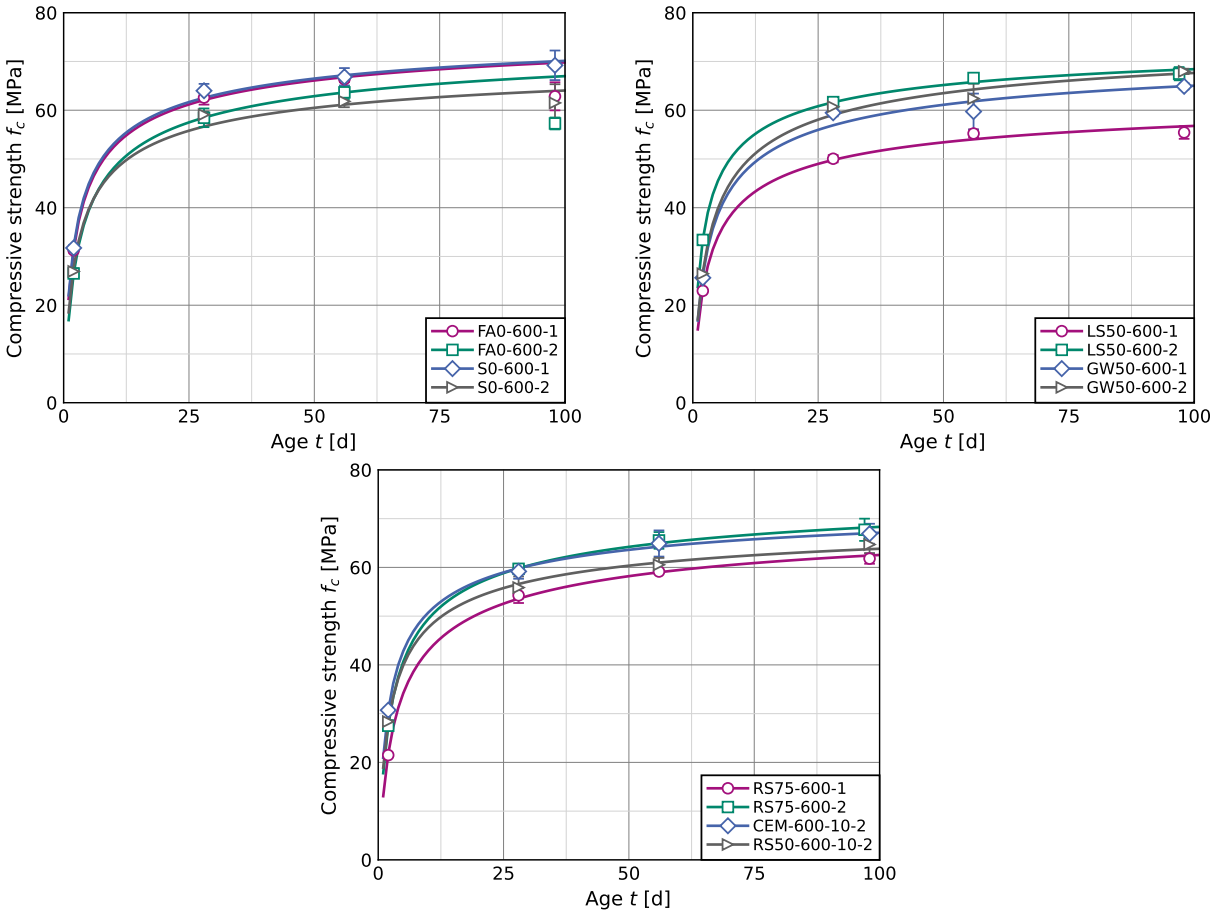

Fig. A4: Temporal compressive strength development of select concrete mixtures with artificial fines FA0-600, S0-600, LS50-600, GW50-600, and RS75-600 at 30 wt% CEM I-substitution, as well as CEM-600 and RS50-600 at 10 wt% substitution (P3, fig. 1)
Results for FA0 at 98 d were not used for the calculation of fit parameters.

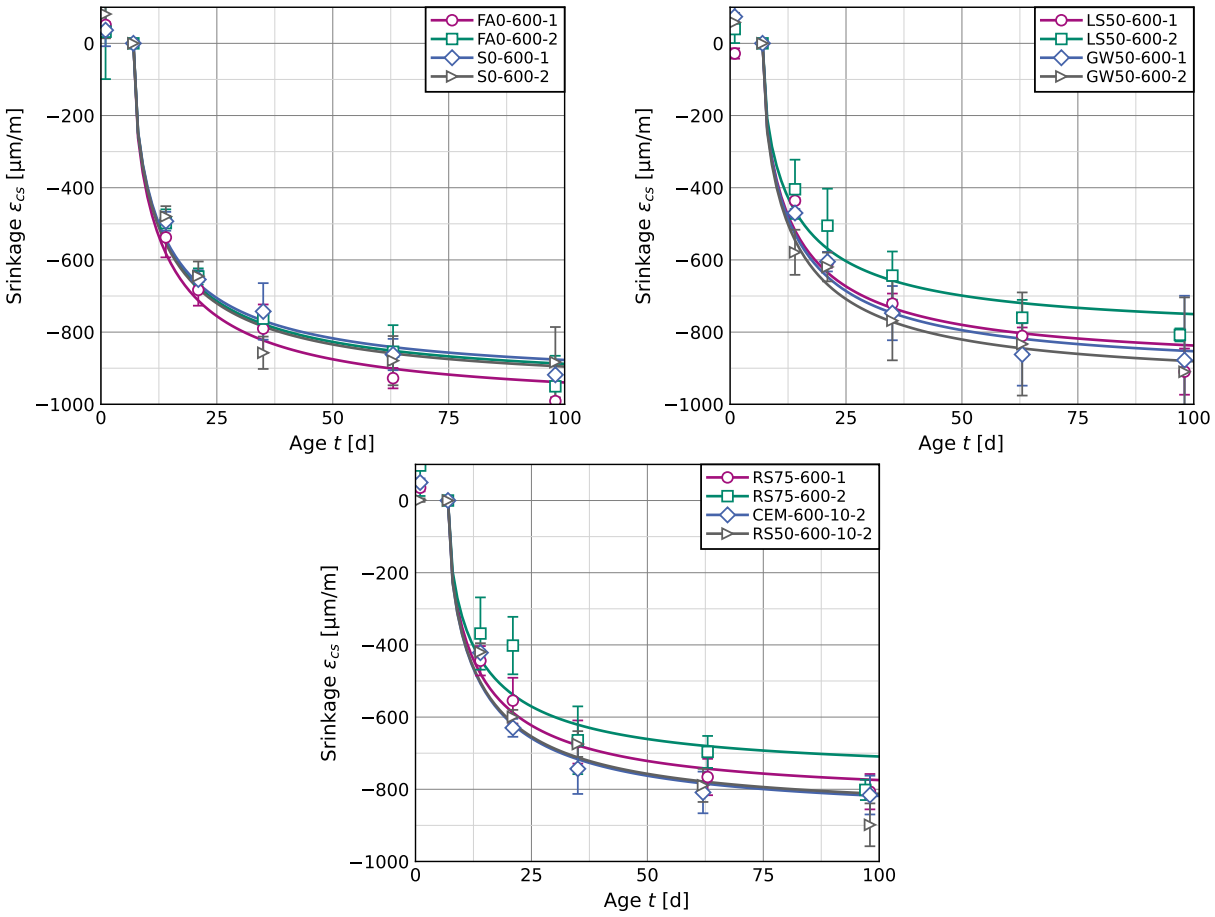

Fig. A5: Shrinkate deformations of concrete containing processed artificial fines FA0-600, S0-600, LS50-600, GW50-600, and RS75-600 at 30 wt% CEM I-substitution as well as CEM-600 and RS50-600 at 10 wt% substitution (P3, fig. 5).

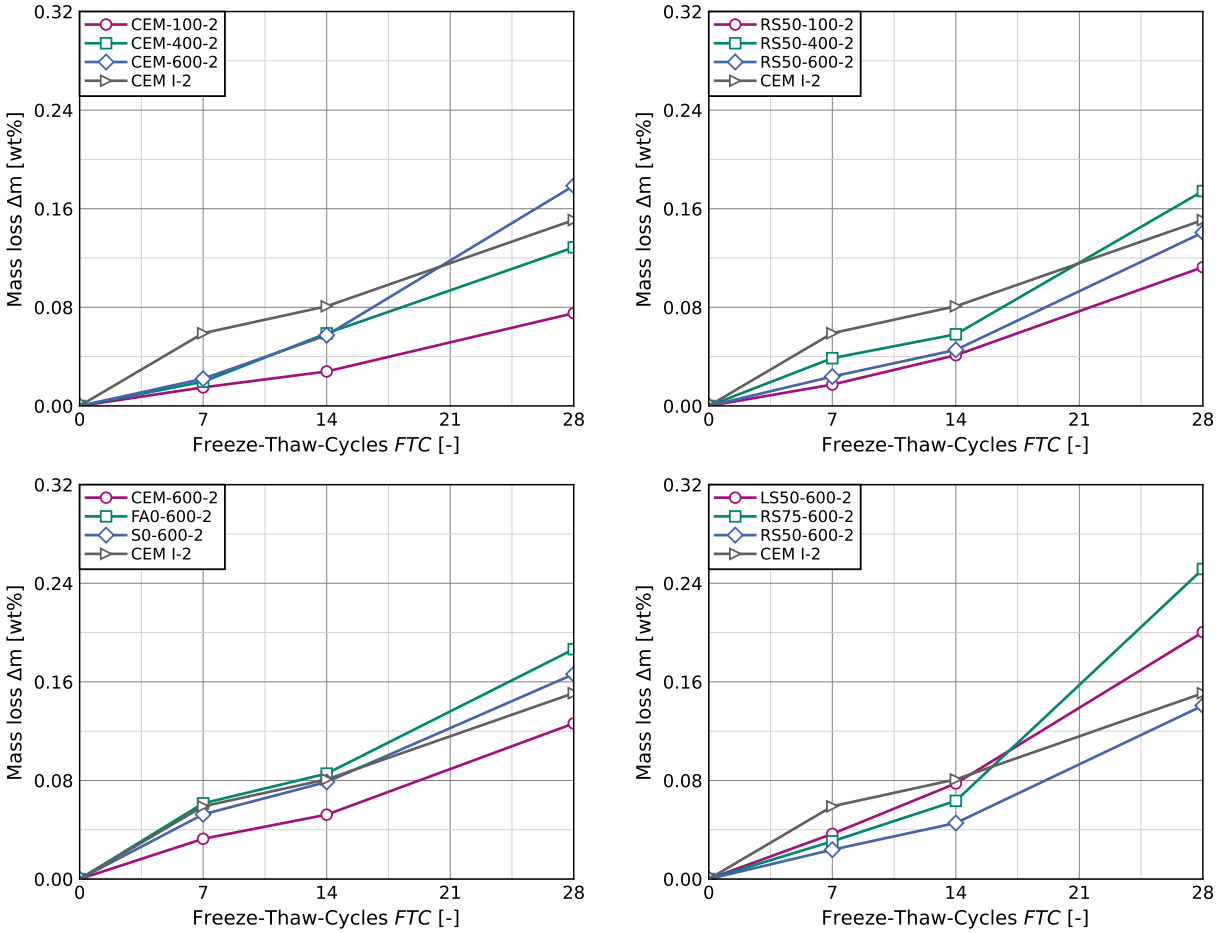

Fig. A6: Cumulative mass loss of selected concrete mixes with different processed artificial fines for increasing freeze-thaw-cycles (P3, fig. 12).

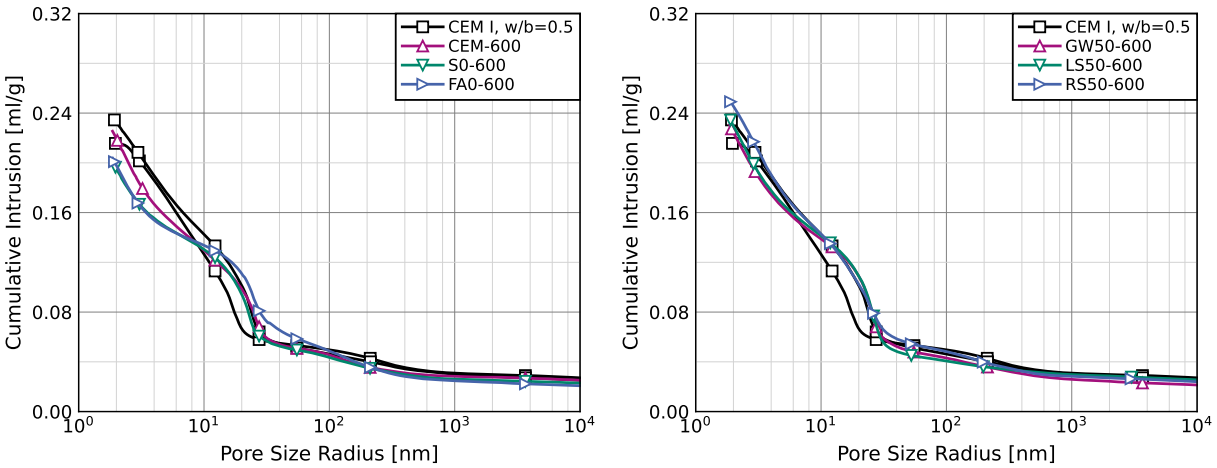

Fig. A7: Cumulative pore radius distribution (logarithmic) for reference series CEM I-1 and CEM I-2 as well as thermally activated artificial fines from pure paste (left), and artificial fines with different aggregate composition (right) (P3, fig. 8).

Tab. A22: Results of strength development in P3.
$f_{ct,fl}$: flexural strength on wet stored prisms, f_c: compressive strength on wet stored prisms, s_c: strength development coefficient.

	$f_{ct,fl,2\,d}$ MPa	$f_{ct,fl,28\,d}$ MPa	$f_{c,2\,d}$ MPa	$f_{c,28\,d}$ MPa	$f_{c,56\,d}$ MPa	$f_{c,98\,d}$ MPa	$f_{cm,ref}$ MPa	s_c -
CEM I-1	3.6(3)	6.2(6)	19.0(5)	43.8(16)	46.6(12)	53.8(3)	44.4	0.32
CEM I-2	5.3(2)	7.5(1)	32.7(11)	62.8(57)	66.6(11)	73.8(31)	63.6	0.25
CEM I-3	3.8(4)	7.1(2)	18.1(2)	45.9(13)	48.9(10)	53.5(4)	45.4	0.33
CEM I-4	5.9(4)	7.7(8)	33.3(4)	61.0(13)	66.5(19)	69.3(15)	61.9	0.23
CEM-100-1	4.1(1)	6.0(1)	22.3(4)	46.7(5)	50.0(12)	52.1(4)	46.3	0.26
CEM-100-2	6.0(6)	7.7(2)	38.9(16)	61.4(63)	62.3(76)	71.8(37)	62.5	0.18
RS50-100-1	4.3(2)	6.4(7)	20.6(2)	44.7(6)	47.8(6)	50.3(9)	44.3	0.28
RS50-100-2	5.8(1)	7.7(4)	37.8(2)	64.5(28)	63.6(48)	70.5(31)	63.1	0.19
CEM-400-1	4.4(0)	6.9(0)	24.1(4)	54.4(6)	57.5(10)	58.8(7)	52.8	0.28
CEM-400-2	5.0(2)	7.4(4)	32.1(2)	58.8(5)	64.0(19)	64.7(3)	59.0	0.22
RS50-400-1	4.2(2)	6.3(4)	21.2(1)	49.1(10)	51.1(12)	52.9(28)	47.3	0.28
RS50-400-2	5.0(2)	7.3(1)	31.5(12)	60.7(23)	62.7(23)	65.8(8)	59.4	0.23
CEM-600-1	5.1(3)	7.0(4)	28.5(7)	58.8(16)	60.1(21)	61.1(32)	56.2	0.24
CEM-600-2	5.2(3)	7.1(4)	29.7(1)	58.2(1)	62.1(10)	61.9(21)	57.1	0.23
RS50-600-1	4.5(3)	6.8(3)	22.8(3)	51.1(5)	54.8(3)	57.0(13)	50.4	0.29
RS50-600-2	5.3(5)	7.7(3)	32.4(4)	60.0(13)	64.9(11)	65.1(61)	59.8	0.22
GW50-600-1	4.8(1)	7.3(4)	25.6(2)	59.5(7)	59.7(37)	64.9(6)	56.9	0.28
GW50-600-2	4.8(3)	7.6(4)	26.5(3)	60.7(10)	62.4(30)	68.0(5)	59.0	0.29
LS50-600-1	4.0(3)	7.0(2)	23.0(4)	50.0(7)	55.2(8)	55.4(13)	49.8	0.28
LS50-600-2	5.2(3)	7.6(2)	33.4	61.7(4)	66.6	67.5(14)	61.6	0.22
RS75-600-1	4.2(2)	7.2(4)	21.5(4)	54.3(16)	59.2(3)	61.8(11)	53.6	0.33
RS75-600-2	4.8(1)	7.3(3)	27.5(5)	59.7(10)	65.5(17)	67.7(23)	59.8	0.28
FA0-600-1	5.3(2)	7.2(6)	31.3(5)	62.6(14)	66.4(6)	62.9(29)	60.1	0.23
FA0-600-2	5.0(4)	7.0(4)	26.5(6)	58.4(19)	63.7(14)	57.3(12)	55.7	0.25
S0-600-1	5.3(2)	7.4(5)	31.7(6)	64.0(14)	66.8(18)	69.2(30)	62.5	0.24
S0-600-2	4.6(3)	7.4(1)	26.9(6)	59.1(6)	61.8(12)	61.5(38)	56.7	0.26
CEM-600-10-2	5.3(1)	7.2(3)	30.7(5)	59.2(15)	64.9(27)	66.9(20)	59.8	0.24
CEM-600-50-1	4.9(0)	7.2(6)	31.7(3)	51.7(33)	57.4(57)	58.4(27)	53.2	0.19
CEM-600-50-2	5.6(4)	7.5(1)	35.8(2)	58.0(7)	64.1(3)	67.4(7)	60.2	0.20
RS50-600-10-2	5.3(3)	7.9(1)	28.4(3)	55.9(23)	60.5(14)	64.7(18)	56.6	0.26
RS50-600-50-1	3.2(3)	6.3(4)	15.5(2)	42.1(3)	44.7(5)	42.6(31)	39.5	0.32
RS50-600-50-2	5.4(3)	8.2(2)	35.6(7)	60.4(47)	69.3(24)	70.3(3)	63.2	0.22

Tab. A23: Results of strength, deformation and durability tests in P3.
$f_{ct,fl}$: flexural strength on dry stored prisms, f_c: compressive strength on dry stored prisms, $E_{c,dyn}$: dynamic modulus of elasticity, ε_{cs0}: shrinkage coefficient, K_{AC}: carbonation coefficient, d_c: chloride penetration depth, Δm_{28}: mass loss after 28 freeze-thaw cycles

	$f_{ct,fl,28\,d}$ MPa	$f_{ct,fl,98\,d}$ MPa	$f_{c,28\,d}$ MPa	$f_{c,98\,d}$ MPa	$E_{c,dyn,28\,d}$ GPa	ε_{cs0} µm/m	K_{AC} mm/d^{0,5}	d_c mm	Δm_{28} wt%
CEM I-1	6.7(5)	5.8(2)	45.1(14)	42.1(5)	31.2(5)	447	0.87	12.2	
CEM I-2	7.1(7)	5.9(5)	55.9(15)	50.8(21)	32.7(7)	422	0.50	8.8	
CEM I-3	6.4(3)	7.0(4)	48.0(3)	52.4(18)	32.8(3)	792	0.91	15.8	
CEM I-4	8.3(2)	9.2(8)	67.5(23)	74.5(15)	37.2(3)	677	0.51	12.6	0.15
CEM-100-1	6.4(4)	6.4(1)	49.5(10)	47.8(9)	33.3(10)	450	0.92	17.9	
CEM-100-2	7.7(4)	8.3(5)	68.1(5)	67.7(16)	35.9(3)	555	0.34	13.1	0.08
RS50-100-1	6.1(10)	7.2(2)	49.0(4)	49.8(10)	33.8(2)	511	1.11	18.0	
RS50-100-2	8.0(4)	8.6(3)	66.5(2)	65.8(9)	37.7(3)	535	0.63	14.2	0.11
CEM-400-1	6.6(6)	7.0(6)	53.1(12)	55.1(7)	33.4(2)	937	0.86	17.1	
CEM-400-2	8.0(4)	7.8(3)	62.4(6)	60.2(24)	35.2(6)	857	0.57	14.2	0.13
RS50-400-1	7.0(5)	6.9(7)	48.4(6)	51.3(2)	33.5(4)	799	1.11	20.1	
RS50-400-2	8.8(4)	8.5(3)	64.3(29)	66.6(6)	36.9(4)	831	0.63	15.0	0.17
CEM-600-1	7.3(2)	7.8(7)	59.4(13)	57.7(17)	34.6(2)	786	0.72	16.6	
CEM-600-2	7.1(4)	8.0(2)	56.5(11)	63.5(16)	34.1(3)	794	0.65	17.9	0.18
RS50-600-1	6.9(5)	7.7(1)	52.9(6)	49.5(39)	34.4(1)	842	1.12	18.7	
RS50-600-2	8.2(11)	8.2(3)	62.2(21)	61.7(34)	35.8(4)	772	0.77	17.3	0.14
GW50-600-1	7.9(3)	7.6(6)	59.7(2)	60.0(16)	33.1(4)	915	1.01	19.1	
GW50-600-2	7.9(5)	7.7(8)	61.3(5)	63.3(21)	34.4(3)	945	0.99	18.4	
LS50-600-1	7.0(6)	6.4(3)	53.5(4)	50.1(3)	33.3(3)	898	1.06	22.1	
LS50-600-2	7.4(3)	8.0(2)	64.1(6)	63.8(19)	36.2(5)	805	0.73	17.3	0.20
RS75-600-1	6.9(3)	6.8(3)	51.6(21)	53.5(15)	33.2(3)	831	0.81	19.3	
RS75-600-2	7.1(10)	7.8(8)	58.3(10)	61.1(8)	34.8(4)	761	0.67	16.9	0.25
FA0-600-1	6.6(9)	7.0(4)	57.7(9)	55.3(13)	32.8(4)	1008	0.95	15.5	
FA0-600-2	6.6(2)	6.3(6)	55.9(6)	55.1(16)	32.4(2)	952	1.17	16.5	0.19
S0-600-1	6.4(4)	6.7(2)	59.2(3)	59.9(16)	33.6(2)	941	0.76	16.4	
S0-600-2	6.9(3)	7.3(7)	55.1(4)	57.8(16)	32.7(0)	960	0.94	16.6	0.17
CEM-600-10-2	7.7(8)	7.8(8)	61.0(3)	62.9(12)	34.6(4)	878	0.53	16.0	0.13
CEM-600-50-1	7.5(4)	8.4(6)	58.5(29)	61.3(12)	32.7(2)	890	0.77	18.6	
CEM-600-50-2	8.2(7)	8.8(10)	60.4(31)	68.9(7)	34.6(2)	888	0.39	17.7	0.09
RS50-600-10-2	7.6(3)	8.8(4)	57.9(7)	66.0(15)	35.2(2)	872	0.64	15.2	0.17
RS50-600-50-1	6.2(3)	6.5(4)	47.1(3)	44.8(2)	31.8(5)	936	1.80	28.4	
RS50-600-50-2	8.4(6)	9.3(7)	63.0(28)	71.0(11)	36.8(4)	754	0.71	17.4	0.08

Paper P4

Influence of Thermally Activated Industrial Concrete Fines of Different Origin on Concrete Long-Term Behavior

Jan P. Höffgen
Lukas Reichert
Bernd Susset
Annegret Walz
Peter Grathwohl
Frank Dehn

Developments in the Built Environment 26

April 2026, 100948

DOI: 10.1016/j.dibe.2026.100948

Publisher's version

Developments in the Built Environment 26 (2026) 100948

Contents lists available at ScienceDirect

Developments in the Built Environment

journal homepage: www.sciencedirect.com/journal/developments-in-the-built-environment

Influence of thermally activated industrial concrete fines of different origin on concrete long-term behavior

Jan P. Höffgen [a,*], Lukas Reichert [a], Bernd Susset [b], Annegret Walz [b], Peter Grathwohl [b], Frank Dehn [a]

[a] Karlsruhe Institute of Technology (KIT), Institute for Concrete Structures and Building Materials (IMB), Gotthard-Franz-Str. 3, Karlsruhe, 76131, Germany
[b] University of Tübingen, Department of Geosciences, Schnarrenbergstraße 94-96, Tübingen, 72076, Germany

ARTICLE INFO

Keywords:
Concrete
Cement
Mineral waste
Recycling
Thermal activation
Supplementary cementitious material

ABSTRACT

The use of thermally activated concrete fines as a supplementary cementitious material (SCM) offers a promising approach to construction-waste recycling. However, due to the lower reactivity of activated concrete fines compared to Portland cement, the substitution affects concrete performance, similar to established SCMs such as fly ash. While the composition of activated concrete fines varies, the effect on concrete compressive strength is similarly variable. The present study successfully adopts a previously developed model to compensate for compressive strength loss, which allows for the assessment of a wide range of concrete performance parameters for six different concrete fines. Results show that mechanical performance changes alongside compressive strength. The substitution of Portland cement negatively affects the resistance to carbonation, which is in-line with established SCMs. Chloride ingress lacks the positive effects of fly ash or slag. While concrete fines may contain harmful substances, elution results indicate parameter dependent effects of thermal activation.

1. Introduction

The use of inorganic wastes as supplementary cementitious materials (SCMs) offers an established approach to both resource efficiency and the reduction of CO_2-intensive Portland cement use.

When, during the concrete mixing process, Portland cement is partially substituted with SCMs, adjustments to the water-binder ratio are made to compensate for changes in compressive strength (Coffetti et al., 2022; Gao et al., 2013; Knight et al., 2023; Barthel et al., 2016). SCMs can be classified by their reactivity. Unlike Portland cement, most SCMs are non-hydraulic and rely on calcium hydroxide produced by Portland cement hydration to form calcium-silicate-hydrates. High-silicium SCMs, so-called pozzolans with calcium oxide to silicon dioxide molar ratios (C/S) lower than 0.5, consume calcium hydroxide (Barthel et al., 2016; Herrmann et al., 2018; Orozco et al., 2024). Latent-hydraulic SCMs with $0.5 < C/S < 1.5$ require calcium hydroxide as a catalyst for their hydration (Amran et al., 2021; Koenders et al., 2025). Both types of SCMs may provide additional reaction products, based on their individual chemical compositions (Snellings et al., 2023). In contrast, inert SCMs are nonreactive and serve as nuclei for cement hydration or as fillers that densify the cement paste (Scrivener et al., 2015; Panesar and Zhang, 2020).

However, the substitution also affects concrete long-term behavior, which is equally significant for the design of durable structures. Building standards rely on established empirical relationships to predict mechanical properties, long-term deformations, or corrosion resistance based on concrete compressive strength (International Federation for Structural Concrete, 2023). Cement substitution through pozzolanic or latent-hydraulic SCMs results in a reduction of early strength with a higher strength gain after 28 d (Nath and Sarker, 2011; Lübeck et al., 2012; Sakthivel et al., 2019). While the modulus of elasticity exhibits a similar behavior, total shrinkage is reduced, but increases for high substitution rates (Nath and Sarker, 2011; Darquennes et al., 2012; Sakthivel et al., 2019; Wang et al., 2022). Due to the reduced amount of $Ca(OH)_2$, the substitution of Portland cements leads to increased carbonation rates (Younsi et al., 2011; Gruyaert et al., 2013a,b). Chloride ingress is reduced due to the higher binding capacity of hydration products and a refinement of the pore system (Güneyisi and Gesoğlu, 2008; Nath and Sarker, 2011; Gruyaert et al., 2013a). The effect of inert SCMs strongly depends on their content, as the filler effect is only present for a low substitution rate. With increasing substitution, the dilution effect predominates, resulting in overall reduced concrete performance. However, for low substitution rates, the effect on strength and deformations is negligible (Wang et al., 2018).

* Corresponding author.
E-mail address: jan.hoeffgen@kit.edu (J.P. Höffgen).

https://doi.org/10.1016/j.dibe.2026.100948
Received 13 March 2026; Received in revised form 26 April 2026; Accepted 17 May 2026
Available online 25 May 2026

The search for additional SCMs has identified ground concrete fines as a promising precursor for Portland cement substitution (Aquino Rocha and Toledo Filho, 2023; Carriço et al., 2020a; Friol Guedes de Paiva et al., 2021; Kaliyavaradhan et al., 2020; Mao et al., 2024; Ohemeng and Ekolu, 2020; Pavlů, 2018; Rakhimova and Shi, 2024; Xu et al., 2022; Zheng et al., 2024). Those wastes consist of natural aggregates and hardened cement paste. Aggregates are mostly inert, but may exhibit a pozzolanic reactivity if they contain amorphous silicates (Lipowsky and Müller, 2017). Hardened cement paste can be thermally activated. At processing temperatures up to 700 °C, the different cement hydration products decompose and regain hydraulic reactivity (Angulo et al., 2022; Baggio et al., 2024; Baldusco et al., 2019; Baquerizo et al., 2016; Florea, 2014; Horváth et al., 1977; Klingsch, 2014; Schneider, 1982; Wang et al., 2019; Zelic et al., 2007; Zhou and Glasser, 2001; Zhou et al., 2004). Subsequently, mortar or concrete, where Portland cement is partially substituted by thermally activated concrete fines, exhibits the highest compressive strength in a range between 500 °C and 700 °C, with great variations between different publications (Bogas et al., 2019, 2022a; Chen et al., 2024; Kalinowska-Wichrowska et al., 2020; Sui et al., 2020; Tokareva et al., 2023; Wei et al., 2024; Wu et al., 2021; Xi et al., 2024; Zhang et al., 2022). Higher processing temperatures result in phase changes of dehydrated phases in addition to calcination of carbonatic phases (Klingsch, 2014; Noel et al., 2025; Real et al., 2020; Serpell and Lopez, 2015; Xu et al., 2023). Both processes are disadvantageous to producing high-strength cementitious materials (Noel et al., 2025; Real et al., 2020; Semugaza et al., 2023; Serpell and Lopez, 2015; Xu et al., 2023; Vyšvařil et al., 2014).

Similar to established SCMs, the Portland cement substitution using thermally activated concrete fines affects not only compressive strength but also short- and long-term mechanical and durability behavior. The aggregate fraction of concrete fines behaves as an inert SCM (Bogas et al., 2019; Carriço et al., 2021a,b). Dehydrated cement paste is porous, and during rehydration, these pores are filled by internal hydration products, mirroring the original porosity of the precursor (Bogas et al., 2020; Real et al., 2020; Semugaza et al., 2023; Vashistha et al., 2023; Wu et al., 2023; Xu et al., 2023; Xi et al., 2024). Cohesion between particles mainly stems from hydration products of primary cement, where the water consumption of cement paste locally reduces the water-binder ratio (Bogas et al., 2020; Serpell and Lopez, 2015; Baldusco et al., 2019).

Since the rehydration of dehydrated cement paste is a fast process, mortars containing thermally activated cement paste exhibit an accelerated strength development within the first days after mixing (Bogas et al., 2020; Real et al., 2020). Consequently, the compressive strength gain after 28 d is low (Bogas et al., 2020; Real et al., 2020; Kim and Kim, 2023; Semugaza et al., 2023). Overall, flexural strength development mirrors compressive strength (Bogas et al., 2020; Kim and Ubysz, 2024; Ma et al., 2022).

As activated concrete fines have a lower particle density compared to Portland cement, the partial substitution results in lower moduli of elasticity, even for low substitution rates, which do not affect compressive strength (Bogas et al., 2019; Real et al., 2021; Getachew et al., 2024).

The reduced particle stiffness also increases shrinkage deformations (Carriço et al., 2022; Real et al., 2021). Overall, increasing activation temperatures or concrete fines with low porosity result in decreasing shrinkage (Kim and Ubysz, 2024; Carriço et al., 2022; Tokareva and Waldmann, 2025). While the addition of activated concrete fines reduces basic shrinkage (Qian et al., 2020), drying shrinkage is sensitive to the amount of evaporable water, which results in increased deformations when high water-binder ratios are used for improving concrete workability (Kim and Ubysz, 2024; Carriço et al., 2022).

Capillary absorption strongly depends on porosity and pore structure, where increased water–cement ratios increase water uptake (Carriço et al., 2022). This trend is mitigated when water–cement ratios are held constant, allowing for a microstructural densification following water intake in activated cement paste particles (Bogas et al., 2022a; Carriço et al., 2022, 2021b). Increasing activation temperatures up to 1000 °C have a decreasing effect on capillary absorption (Kim and Ubysz, 2024; Ma et al., 2022; Wu et al., 2021, 2023; Tokareva and Waldmann, 2025). These observations also hold for freeze-thaw-damage (Algourdin et al., 2021; Wei et al., 2024).

As resistance to carbonation and chloride diffusion depends on porosity and the binding capacity of cement hydration products, increasing substitution rates have a negative impact (Bogas et al., 2022b; Carriço et al., 2021b; Xu et al., 2024). Chloride ingress reduces with increasing activation temperature and particle fineness (He et al., 2023; Kim and Kim, 2023; Qian et al., 2020).

These findings, with few exceptions (Algourdin et al., 2021; He et al., 2023; Wu et al., 2023; Tokareva and Waldmann, 2025), are based on artificial hardened paste or concrete as a precursor. However, industrial concrete fines from recycling plants never consist of pure paste, but contain varying amounts of aggregates with individual compositions. Besides, in contrast to artificial fines, industrial fines may contain harmful substances, such as organic components or heavy metals (Gao et al., 2015; Weimann, 2009; Wang et al., 2023; Van Praagh et al., 2015; Andrade et al., 2025). In the case of recycled concrete aggregates, heavy metals are mostly immobilized by cement hydration products and are, therefore, unsusceptible to leaching (Engelsen et al., 2010; Kurda et al., 2018; Lu et al., 2019). When cement hydration products are decomposed during an activation process, heavy metals regain solubility, but may be reabsorbed during a later reaction process (Park et al., 2025).

When using thermally activated concrete fines for substituting Portland cement in concrete applications, the overall influence on concrete strength, as well as deformations and long-term behavior, need to be accounted for. However, the available findings on concrete performance lack a broad dataset comprising fines of different compositions. With the application of established SCMs, negative effects on durability are usually mitigated by a reduction of the water-binder ratio alongside the compensation for strength reduction. This serves the goal of producing a concrete with a target strength, which follows the empirical relationships for relevant design properties. A novel model for assessing the impact of activated concrete fines on compressive strength was proposed by the authors of this study (Höffgen et al., 2025; Höffgen and Dehn, 2025). This allows for the design of concrete containing thermally activated fines with a target compressive strength. However, the effects on other concrete properties, beyond compressive strength, including the presence of harmful substances in concrete fines whose behavior may be altered by thermal activation, require additional consideration.

2. Experimental program

The experimental program, therefore, aims to assess the macroscopic properties of concrete incorporating thermally activated concrete fines from six different sources as supplementary cementitious material (SCM). These properties are compared with reference mixes incorporating established SCMs (granulated blast-furnace slag, coal fly ash, and limestone powder). Because compressive strength is the most important concrete property in structural design, the analysis is based on two different mixes from each SCM, each with a different strength. While one half of the mixes uses SCMs without accounting for their impact on compressive strength, the second half uses a model, previously published in Höffgen et al. (2025), to achieve a target compressive strength.

The experimental program follows the procedures of a previously published study by the authors, which focused on the effect of thermally activated artificial concrete fines with known compositions on concrete properties (Höffgen et al., 2026).

2.1. Materials

Six different concrete fines from five different recycling plants, labeled R1–R6, were selected based on preliminary analyses by the authors to account for a wide variation of material properties.

- R1: Fine fraction (<2 mm) from a recycled concrete aggregates production plant. The sample corresponds to A2-0/2 in Höffgen et al. (2025).
- R2: Fine fraction (<2 mm) from a recycled concrete aggregates production plant. The precursor contained grains with a diameter up to 8 mm, which were removed through manual sieving (F-0/2 in Höffgen et al. (2025)).
- R3: Ultrafine fraction (<250 μm) obtained by manually sieving R1 (A2-0/0.25 in Höffgen et al. (2025)).
- R4: Ultrafine fraction (<250 μm) similar to R3, but from a different recycling plant (B1-0/0.25 in Höffgen et al. (2025)).
- R5: Filter cake from a fresh concrete recycling plant (D–F in Höffgen et al. (2025)).
- R6: Filter cake from a crushed concrete recycling plant, which used a wet-separation process to remove hardened cement paste from recycled aggregates (G–F in Höffgen et al. (2025)).

During preprocessing, all materials were dried at 105 °C. The thermal activation used crucibles with a volume of 2.5 l, which were placed in a static furnace. Temperature was increased at a rate of 5 K/min until reaching the target temperature of 600 °C, which was held constant for 6 h. Passive cooling was performed in a container containing silica gel to maintain low relative humidity. Afterwards, activated concrete fines were stored in sealed buckets, except for the mechanical processing, where all concrete fines were milled until passing through a 125 μm-mesh. The activation procedure was adopted from previous investigations by the authors (Höffgen et al., 2025; Höffgen and Dehn, 2025).

Besides these six different activated concrete fines, concrete production used commercial Portland cement CEM I 42.5 R (according to EN 197-1:2011, labeled "CEM I") as base material, as well as ground granulated blast-furnace slag (EN 15167-1:2006, "S"), black coal fly ash (EN 450-1:2012, "FA"), and limestone powder (EN 12620:2008, "L") as reference SCMs with different reactivity. As aggregates, quartzitic river sand (0–2 mm) and fine gravel (2–8 mm) from the same source were used.

2.2. Experimental procedures

As the first step of the analyses, Portland cement (CEM I) and processed concrete fines were analyzed for their physical properties and chemical composition. Physical properties included particle size distribution (laser diffraction) and particle density (pycnometer). Nitrogen adsorption/desorption was used to determine both specific surface area (BET method) and porosity (BJH method). The chemical composition (in accordance with EN 196-2:2013) was determined by measuring the oxide phases of the main elements using wavelength-dispersive X-ray fluorescence (WDXRF) and the trace elements using energy-dispersive X-ray fluorescence (EDXRF) before activation. The analysis of reference SCMs (S, FA, L) comprised a reduced set of parameters. Additionally, activated concrete fines and CEM I were analyzed for their total and reactive CaO and SiO_2, as well as free CaO, the latter according to EN 451-1:2017. The chemical analyses were completed by the determination of sulfate (SO_3), carbon (C), and total organic carbon (TOC) through CSA (carbon–sulfur-analysis). CSA was also repeated on concrete fines prior to activation, with the additional determination of chloride content (Cl).

For *porosimetry* measurements, CEM I, reference SCMs, and activated concrete fines were used as binders to produce paste specimens with a water-binder ratio of $w/b = 0.5$. The share of SCMs of the total binder content was set to $f = 0.3$. Pastes with pure CEM I included $w/b = 0.6$ and $w/b = 0.5$, labeled CEM I-1 and CEM I-2. Pastes were mixed in a slurry mixer, filled in sealed plastic bottles, and placed in a specimen shaker to avoid segregation, before storage at 20 °C. At the age of 28 d, paste specimens were crushed with a chisel and sieved to a particle size between 2 mm and 4 mm for mercury intrusion porosimetry (MIP).

The concrete mix for the following analysis was designed with a paste content of $v_p = 40$ v%, a fine aggregates content of $v_s = 20$ v%, and a coarse aggregates content of $v_g = 40$ v%. For assessing the different kinds of SCMs, a fixed binder substitution rate of $f = 0.3$ by mass was chosen for all series. The water-binder ratio was set to $w/b = 0.5$ for the first series of mixtures. As all SCMs in this study were known to reduce compressive strength, a second series used a reduced water-binder ratio to produce concrete with similar compressive strength despite the substitution of CEM I. w/b was calculated for each SCM individually, based on estimated reactivity. This procedure relies on the k-value concept detailed in EN:206-2017 for reactive SCMs (see also Höffgen et al. (2025)). Table A.2 in the Appendix details the individual concrete mix designs, including estimates for k, and the resulting water-binder ratios and equivalent water–cement ratios. All series with a water-binder ratio of $w/b = 0.5$ were labeled with the suffix "−1", and series with an equivalent water–cement ratio of $w/c_{eq} = 0.5$ were labeled with the suffix "−2". Concrete without SCMs followed used a different naming scheme, where the mixture with $w/b = w/c_{eq} = 0.5$ used the suffix "−2". To allow for the assessment of varying strength, another concrete mix, CEM I-1 with an increased water-binder ratio of $w/b = w/c_{eq} = 0.6$ was produced.[1] Besides, CEM I-1 and CEM I-2 were partially repeated during the analysis to broaden the dataset. During mixing, PCE-based superplasticizer was added to ensure comparable workability.

For the experimental investigation of hardened concrete properties, from each mix 15 prisms ($(40 \times 40 \times 160)\,mm^3$) and one cylinder ($d = 100$ mm, $h = 280$ mm) were cast. Following demolding after 1 d, all specimens were stored at 20 °C under water, unless otherwise required by the testing procedures. Overall, for allowing the experimental investigation of various concrete properties with overlapping test schedules, simplified procedures were applied.

Strength testing used a total of six prisms, with the determination of the *flexural strength* ($f_{ct,fl}$) on three prisms each at the ages of 2 d and 28 d. These were immediately followed by *compressive strength* (f_c) measurements, but only on three prism halves each. The other halves were resubmerged in water for testing compressive strength at 56 d and 98 d. Testing followed the procedures in EN 196-1:2016.

Six prisms for the determination of the shrinkage development and the dynamic modulus of elasticity were stored in closed containers at 100 % r.h. rather than in water after demolding. Three prisms for *shrinkage* had cast-in measuring pins to measure specimen length with a dial gauge. Deformation measurements and specimen mass were recorded immediately after demolding and at the age of 7 d (t_0). Afterwards, the specimens were stored in a climate chamber at 65 % r.h. Subsequent measurements were performed at the age of 14 d, 21 d, 35 d, 63 d, and 98 d. Resulting deformations were normalized to the prism length, yielding the shrinkage strain over time ($\varepsilon_{cs}(t)$). Prisms for the *dynamic modulus of elasticity* (E_c) were stored alongside shrinkage specimens until ultrasonic pulse measurements at the age of 28 d. Afterwards, these prisms were tested for their flexural and compressive strength at the ages of 28 d and 98 d, respectively.

The three remaining prisms were removed from the water storage at the age of 28 d and placed in a climate chamber at 65 % r.h. for 14 d. Afterwards, specimens were moved to a *carbonation* chamber with

[1] CEM I-1 and CEM I-2 are identical to reference mixes in a previous study by the authors (Höffgen et al., 2026). All other concrete mixes, and subsequent results, are unique to this study.

Table 1
Results of the physical and wet-chemical analysis of CEM I, reference SCMs (S, FA, L) and concrete fines (R1–R6) before activation ("−100") and after activation at 600 °C ("−600").
ρ_p: particle density, S_{BET}: specific surface area, p_{BJH}: pore volume, d_{10}, d_{50}, d_{90}: particle size at 10 v%, 50 v%, and 90 v% cumulatively passing, C: Carbon, TOC: total organic carbon, Cl: chloride, S: sulfur, SO_3: sulfate, (f/r-)CaO: total, free, and reactive calcium oxide, (r-)SiO_2: total and reactive silicon dioxide.

	ρ_p $\frac{kg}{dm^3}$	S_{BET} $\frac{m^2}{g}$	p_{BJH} $\frac{cm^3}{kg}$	d_{10} µm	d_{50} µm	d_{90} µm	C wt%	TOC wt%	Cl wt%	S wt%	SO_3 wt%	CaO wt%	f-CaO wt%	r-CaO wt%	SiO_2 wt%	r-SiO_2 wt%
CEM I	3.13	1.4	7.1	1.7	12.1	32.9	0.5	0.01	0.07	1.22	3.0	61.7	0.77	57.7	20.4	19.5
S	2.92	0.9	3.9	2.1	12.3	30.0										
FA	2.25	7.6	14.0	2.9	21.6	83.4										
L	2.70	5.7	14.4	1.9	12.5	44.4										
R1-600	2.65	4.8	28.2	1.9	17.9	88.4	3.2	0.03		0.28	0.7	22.1	0.04	8.1	54.3	8.8
R2-600	2.64	3.3	21.9	2.3	25.9	99.1	1.5	0.02		0.17	0.4	12.2	0.04	8.2	71.2	8.4
R3-600	2.64	5.9	34.0	1.8	14.1	81.0	3.2	0.03		0.35	0.9	22.8	0.06	8.8	52.2	10.1
R4-600	2.60	6.8	41.1	2.0	18.4	97.6	2.5	0.02		0.45	1.1	21.4	0.10	10.8	54.5	13.3
R5-600	2.64	13.6	87.3	2.0	18.8	96.2	1.5	0.03		0.44	1.0	23.8	0.17	17.2	56.6	13.7
R6-600	2.66	12.8	72.3	1.8	11.6	40.5	3.0	0.07		0.37	0.9	19.8	0.05	7.7	47.0	14.5
R1-100							3.5	0.15	0.04	0.27						
R2-100							1.7	0.12	0.01	0.19						
R3-100							3.7	0.24	0.04	0.39						
R4-100							3.0	0.35	0.01	0.45						
R5-100							2.1	0.18	0.04	0.50						
R6-100							4.1	0.99	0.04	0.37						

57 % r.h. and 3 v% CO_2. After exposure for 7 d, 28 d, and 70 d, the prisms were temporarily removed from the carbonation chamber and split, to produce a fresh surface for measuring the carbonation depth with the phenolphtalein indicator test on three measuring points per edge. The accelerated carbonation coefficient (K_{AC}) was then calculated as the slope of the development of the mean carbonation depth over the square root of exposure duration according to EN 12390-12:2020.

Water storage of the cylinder was shortly interrupted when the specimen was cut into five smaller slices with a height of approximately 45 mm. These were then sealed with an epoxy resin, baring both flat surfaces of two cylinder slices and one flat surface of each of the three remaining slices. All specimens then reentered water storage until the age of 28 d. The specimens with one unsealed flat surface were conditioned in a saturated $Ca(OH)_2$-solution for 24 h before storage in a 16.5 wt%-NaCl-solution. After 35 d, specimens were split, and the *chloride* penetration depth (d_c) was determined using the silver nitrate indicator test as an average of nine datapoints per specimen half. While this procedure is usually applied for evaluating the rapid chloride migration test (i.e., EN 12390-18:2021), the time-consuming determination of chloride profiles, which allows for the calculation of the chloride diffusion coefficient (D_{nss}) according to EN 12390-11:2015, was only performed for two additional specimens of the concrete mix CEM I-2.1.

The remaining two cylinder slices with sealed lateral surfaces were stored at 65 % r.h. for at least 6 months until reaching constant weight. The *capillary absorption* coefficient $WA_{24\,h}$ was determined by normalizing the mass change after partially (5 mm) submerging the cylinders in water for 24 h, to the surface area.

The *leaching* behavior of concrete fines was investigated in a three-step approach, using the percolation method specified in German standard DIN 19528:2023-07. The first and second steps used concrete fines before and after thermal activation, without grinding. For the third step, concrete prisms for strength testing from the "−1" series were dried at 105 °C and crushed to a maximum particle size of 4 mm. The materials were compacted in columns, with steps 1 and 3 using a target volume of $v_c \approx 500$ ml and step 2, for material availability reasons, limited to $v_c \approx 90$ ml. The water-solid ratio was set to $w/s = 2$ for all tests. The eluates were evaluated for their anion (ion chromatography), metal (inductively coupled plasma mass spectrometry), and PAH (Polycyclic Aromatic Hydrocarbons, gas chromatography-mass spectroscopy) fractions.

3. Results and discussion

3.1. Characterization of binders

Table 1 details the physical and chemical characterization of CEM I, reference SCMs (slag, fly ash, and limestone powder), as well as processed concrete fines.

The physical properties of slag are similar to CEM I. Limestone powder exhibits a slightly higher maximum particle size with higher specific surface area and pore volume. Among the reference SCMs in this study, fly ash exhibits the coarsest particle-size distribution, the lowest density, and the highest specific surface area and pore volume.

On average, activated concrete fines exhibit a similar specific surface area and particle size distribution as fly ash, albeit at a higher particle density and higher pore volume. Individually, specific surface area and pore volume depend on the preprocessing procedure, with smaller particles prior to activation yielding higher values. This is not reflected in the particle size distribution. R1-600 and R3-600, from the same processing plant, have higher concentrations of fine particles than the other samples. The only exception is R6-600, which has a significantly lower d_{90}, suggesting a smaller filter size than R5-600. Since particle size and specific surface area are independent, a remaining explanation is the hypothesized concentration of hardened cement paste particles with reduced precursor particle size (Juan and Gutiérrez, 2009). This also corroborates the observed increase in specific surface area and porosity with smaller precursor particle size, since dehydrated cement paste exhibits a loose microstructure with high porosity (Baldusco et al., 2019; Bogas et al., 2019; Carriço et al., 2020b; Kim et al., 2021).

Table A.3 in the Appendix section details the chemical composition of CEM I, reference binders, and concrete fines before activation. CEM I consists of CaO, SiO_2 and, to a lesser amount, Al_2O_3 and Fe_2O_3, which corresponds to a typical Portland cement composition (Andrade Neto et al., 2025). Slag and fly ash exhibit an increased share of both SiO_2 and Al_2O_3, while CaO decreases. Limestone powder, on the other hand, almost exclusively consists of CaO (in the form of $CaCO_3$, as indicated by the high loss on ignition). The chemical composition of concrete fines varies, with generally high amounts of SiO_2 and CaO. In general, the comparison of results across the three preprocessing groups reveals that the smaller precursor particle size of R3/R4 is associated with a higher CaO to SiO_2 ratio, and this trend becomes even more pronounced for R5/R6. However, because both CaO and SiO_2 are

present in aggregates and in hydrated cement paste, WDXRF results are not suitable for assessing the reactivity of concrete fines. Table 1 details results of the wet-chemical analyses for CEM I and activated concrete fines. The increase of CaO and SiO_2, compared to WDXRF, can be explained through the mass loss during activation. In contrast to WDXRF, the wet-chemical analysis enables the determination of reactive CaO and SiO_2. In CEM I, most of CaO and SiO_2 are reactive, with only minor inert components, presently in the form of carbonates or sulfates. In activated concrete fines SiO_2 and, to a lesser extent, CaO are mostly inert. Reactive SiO_2 increases with higher precursor fineness. Reactive CaO shows a similar trend, except for R6. Consequently, the reactive CaO/SiO_2 molar ratio ranges between 0.6 for R6 and 1.3 for R5. The amount of free CaO, which includes $Ca(OH)_2$, is particularly low for all activated concrete fines, which suggests an extended carbonation of all precursors.

3.2. Porosity

The partial substitution of CEM I through SCMs affects the pore radius distribution (see Fig. 1). For all SCMs tested at a constant water-binder ratio, this is reflected in a shift in gel porosity with pores smaller than 50 nm. In contrast, an increased water–cement ratio also increases capillary porosity in the range of 100 nm–1000 nm.

Limestone powder (L) has the most significant effect on porosity, while slag (S) only marginally affects the pore size distribution, compared to CEM I at the same water-binder ratio. The impact of activated concrete fines is similar to fly ash (FA), which shows a minor shift of the gel porosity and a slight increase of capillary porosity (compare Vashistha et al., 2023; Wu et al., 2021; Wei et al., 2025). Overall, the activated fines exhibit a similar pore-radius distribution regardless of preprocessing.

3.3. Compressive strength development

The results from compressive strength measurements, as shown in Fig. 2, exhibit the hypothesized behavior. Compressive strength at 28 d of concrete mixes with a constant (equivalent) water–cement ratio of 0.5 ("−2") is similar for all series, while mixes with a constant water-binder ratio, and subsequently increased (equivalent) water–cement ratios ("−1") have a reduced compressive strength.

For concrete containing activated fines, compressive strength increases with reduced precursor particle size. This confirms the applied k-values for the individual SCMs and activated fines, except for R5-600, where the increased compressive strength of both mixes suggests a higher k-value. The high strength for R5-600 aligns with the highest share of reactive CaO and SiO_2 (see Table 1 and Fig. 3). A similar effect of reactive CaO is also apparent, but less pronounced. Furthermore, R5-600 paste exhibits the lowest porosity of all pastes measured. However, the general relationship between porosity and compressive strength is relatively weak compared with CEM I and reference SCMs (see Fig. 3), thereby corroborating the results in Xi et al. (2024).

The illustration of porosity and compressive strength in Fig. 3 uses the reference strength $f_{c,ref}$, which results from the assessment of the temporal strength development. Here, the empirical model from *fib* Model Code 2020 (International Federation for Structural Concrete, 2023) in Eq. (1) was fitted to the experimental data from each concrete series by applying the least squares method. Subsequently, $f_{cm,ref}$ denotes the compressive strength at the reference age (t_{ref} = 28 d). $f_{cm,ref}$ was obtained as a result from the fit, rather than used as an input parameter, to obtain a stabilized reference strength for later comparisons. For most series, $f_{cm,ref}$ is similar to $f_{c,28\,d}$, but some series show larger deviations, which may be subject to random influences during storage and testing. Most noteworthy is FA-2, for which the double determination yields substantial differences at the testing ages 56 d and 98 d. The other repeated series (CEM I-1 and -2 as well as FA-1) show a good reproducibility.

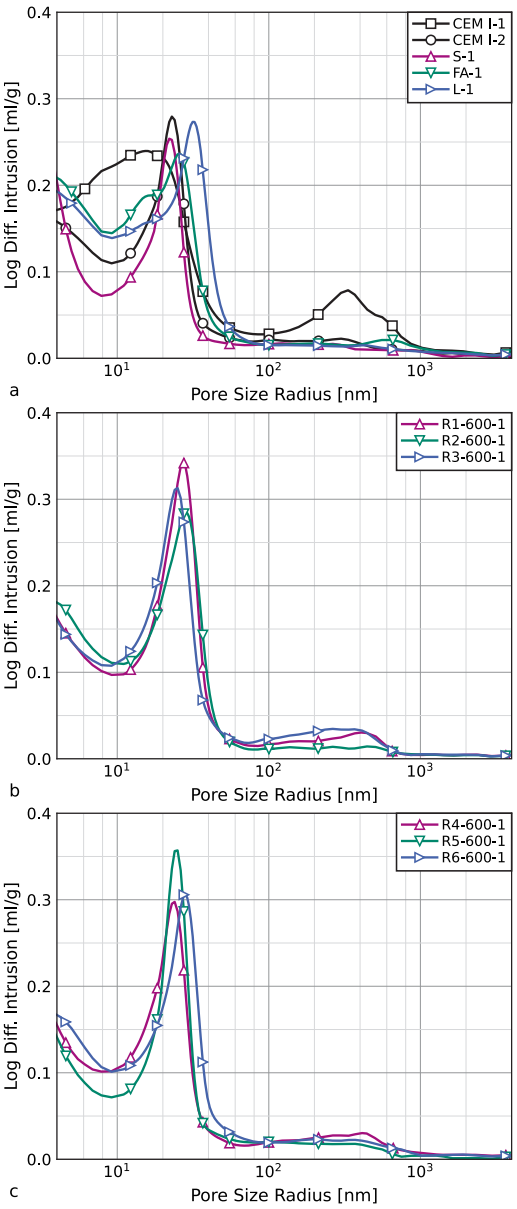

Fig. 1. Differential pore radius distribution (logarithmic) for reference series CEM I-1 and CEM I-2 and established SCMs S, FA, and L (a), as well as thermally activated concrete fines from (b and c).

$$f_c(t) = f_{cm,ref} \cdot \exp\left\{ s_c \cdot \left[1 - \left(\frac{t_{ref}}{t} \right)^{0.5} \right] \right\} \quad (1)$$

The second parameter in Eq. (1), s_c, describes the velocity of the strength development, with lower values indicating high early strength, and high values signifying increased strength gain after the reference age t_{ref}. In *fib* Model Code 2020 (International Federation for Structural Concrete, 2023), s_c ranges between 0.2 for concrete with cement strength class CR and 35 MPa < f_{ck} < 60 MPa, and 0.3 for $f_{ck} \leq$ 35 MPa.[2] For strength class CN, these values increase to 0.4 and 0.5, respectively. Presently, concrete mixes "CEM I" can be classified as

[2] *fib* Model Code 2020 (International Federation for Structural Concrete, 2023) defines f_{ck} as the characteristic cylinder compressive strength. To enable a comparison with present data, $f_{cm,ref} \approx f_{ck}$ + 18 MPa can be assumed. The offset comprises the difference between the mean and characteristic

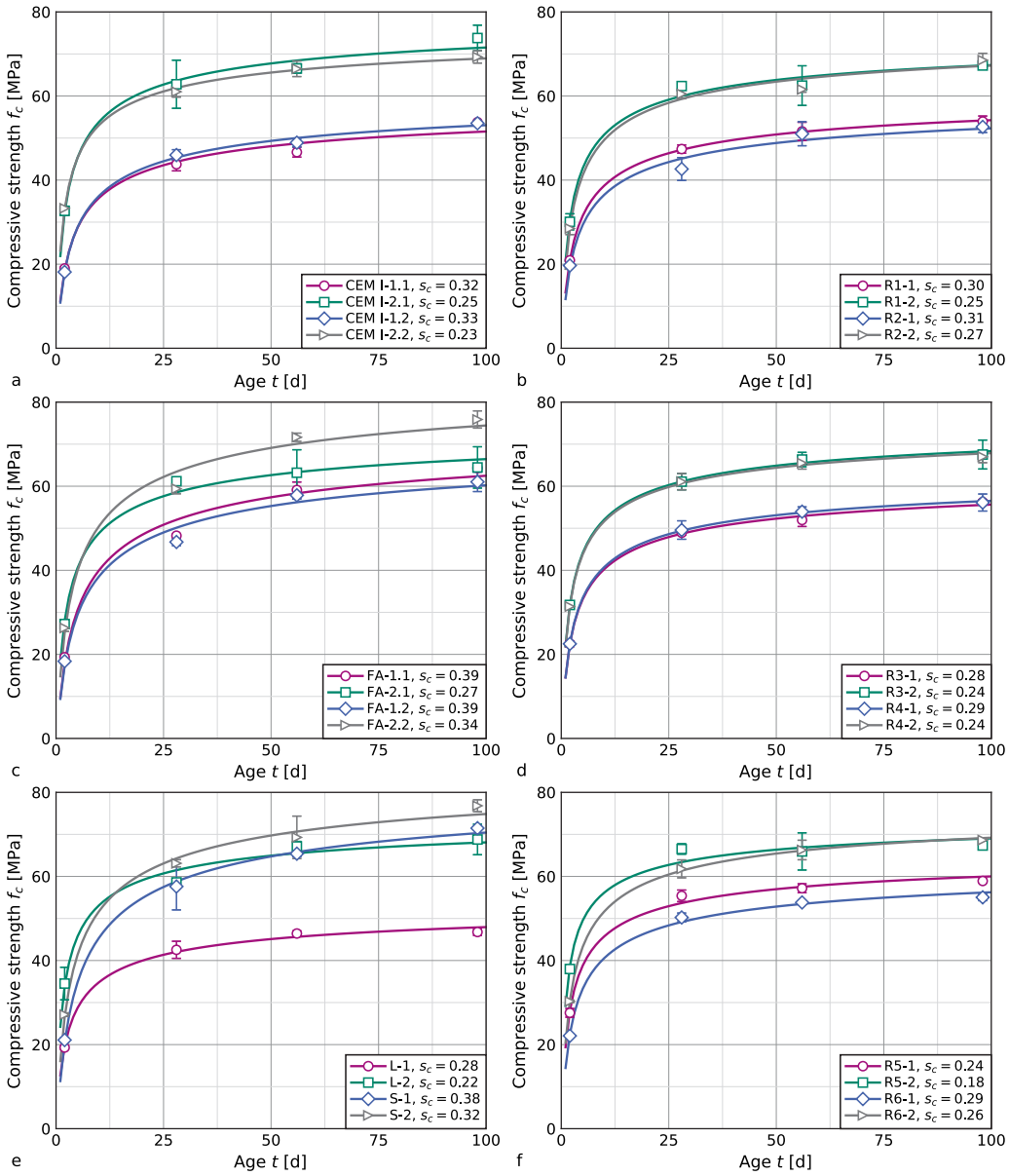

Fig. 2. Temporal development of compressive strength for reference mixes (a, c, d), and concrete containing activated fines (b, d, f). Diagrams for CEM I and FA show results from repeated concrete mixes. Markers indicate the measured averages and standard deviations from three prisms; lines represent the corresponding fit curves used to determine $f_{cm,ref}$ and s_c (Eq. (1)).

strength class CR, and concrete mixes "FA" match the description of strength class CN. Present results for CEM I fit these provisions, as illustrated in Fig. 4. s_c for the four series "FA" tend to fall below the provisions in International Federation for Structural Concrete (2023), indicating a faster-than-expected strength development. Findings for concrete incorporating slag are similar to those for fly ash, whereas limestone powder has a marginally accelerating effect on the temporal development of strength. All concrete series with activated concrete fines exhibit s_c in the range of CEM I for the entire compressive strength range, which signifies a fast compressive strength development similar to CEM I.

An alternative, simplified method for assessing compressive strength development is the quotient r in Eq. (2), which is, however, limited to strength results at 2 d and 28 d.

$$r = \frac{f_{c,2\,\mathrm{d}}}{f_{c,28\,\mathrm{d}}} \tag{2}$$

Fig. 4 shows the results for both evaluation methods. Except for FA-2, all concrete mixes with slag or fly ash yield the highest values of s_c and the lowest values of r. Concrete mixes with activated concrete fines exhibit similar results as the CEM I base mixes or the reference series, where limestone powder partially replaces CEM I (compare Bogas et al., 2020; Real et al., 2020; Kim and Kim, 2023; Semugaza et al., 2023).

3.4. Flexural strength

A benefit of using prisms for strength testing, according to EN 196-1:2016, is the ability to measure flexural strength alongside compressive strength on the identical specimens. In the present study, flexural strength was determined on three water-cured specimens at the ages of 2 d and 28 d and on dry-cured specimens at the ages of 28 d and 98 d.

compressive strength of 8 MPa and the difference between the cubic and cylindrical compressive strength of 10 MPa.

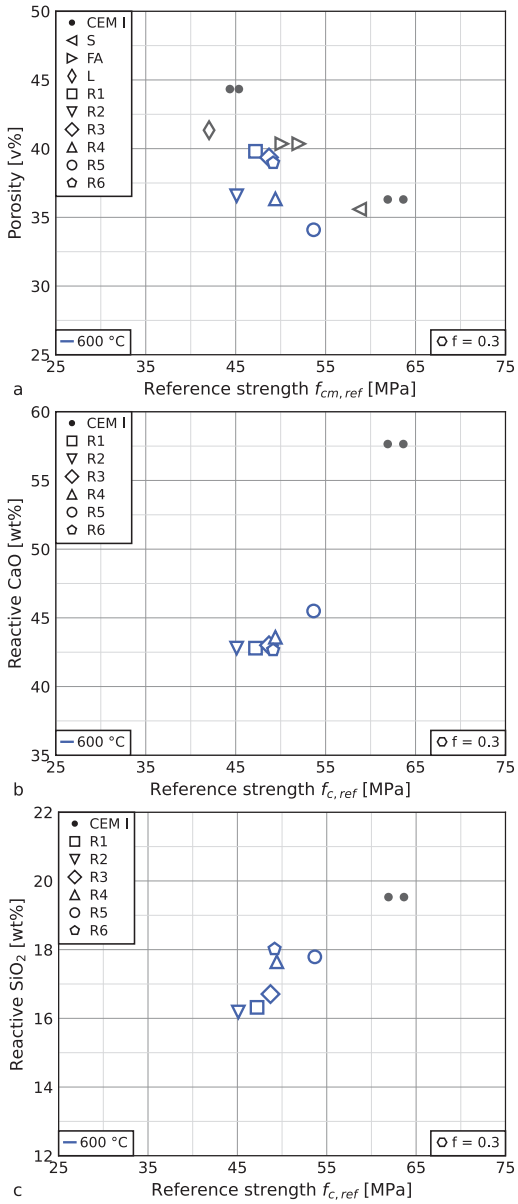

Fig. 3. Relationship between concrete compressive strength $f_{cm,ref}$ and total paste porosity (a), total reactive CaO (b) and total reactive SiO_2, both as the weighted sum of CEM I and R1-R6.

Fig. 5 illustrates the results of flexural and compressive strength tests of water-cured prisms.

The relationship between flexural and compressive strength follows a nonlinear trend (compare Campos et al., 2021; Liu et al., 2023; International Federation for Structural Concrete, 2023), with overall minor deviations. Furthermore, these deviations are independent of testing age and cement substitution with SCMs or activated concrete fines. Overall, the only influencing factor on flexural strength appears to be compressive strength, suggesting good transferability of design specifications for established SCMs to thermally activated concrete fines.

3.5. Dynamic modulus of elasticity

The dynamic modulus of elasticity was determined in this study as an inexpensive and rapid alternative to measuring the static modulus of elasticity. Nonetheless, the results obtained from ultrasonic pulse measurements allow for the qualitative assessment of the impact of activated concrete fines on the modulus of elasticity, because the overall concrete composition and the curing conditions were not varied throughout the test series (Ekin and Uyanik, 2021; Marques et al., 2020).

Fig. 6 compares results of the experimental determination of the dynamic modulus of elasticity to the prism compressive strength, which were determined on the identical specimens at the age of 28 d.

In addition to the increase in the dynamic modulus of elasticity with increasing concrete compressive strength, which corroborates findings in Getachew et al. (2024), the results indicate an effect of cement substitution with SCMs. While slag and limestone powder exhibit results similar to those of the base mixes with CEM I, the substitution with fly ash tends to increase the dynamic modulus of elasticity. Although compressive strength remains the most significant factor affecting the dynamic modulus, the present results show a decrease in the dynamic modulus with increasing reactivity of activated concrete fines, regardless of compressive strength. R1-600 and R2-600, which exhibit the lowest reactivity, have higher dynamic moduli than the base and reference mixes. The lowest dynamic moduli are achieved by R5-600, which shows the highest reactivity among all concrete mixes.

The reason for this may lie within the high porosity of dehydrated cement paste, and, subsequently, of thermally activated concrete fines with increasing paste content (compare Table 1). In contrast to established reactive SCMs like fly ash or slag, hydration products in activated concrete fines tend to form inside the porous particles, so that rehydrated fines exhibit a similar porosity as the respective precursors and no overall paste densification (Bogas et al., 2019; Real et al., 2021). On the other hand, a high content of inert aggregate particles within activated fines acts similarly to limestone powder and increases material stiffness (compare Wang et al., 2018).

3.6. Shrinkage

Concrete shrinkage comprises various components, with drying shrinkage being the primary factor. This type of shrinkage results from the loss of evaporable water (International Federation for Structural Concrete, 2023). In the case of normal-strength concrete, shrinkage caused by cement hydration is relatively minor and can be overlooked (Müller et al., 2021). To eliminate the impact of this type of shrinkage on the measured deformations, the specimens were kept at 100 % r.h. until they were 7 d old.

The development of shrinkage deformations over time, up to 98 d of concrete age, is illustrated in Fig. 7. Given that the difference in deformations between 1 d and 7 d of age is inconsistent and smaller than the standard deviation of the measurements, it is logical to disregard basic shrinkage. As a result, the shrinkage deformation ε_{cs} observed from 7 d of age onward is attributable solely to drying shrinkage.

Evaluating shrinkage deformations can be challenging due to high data variability, particularly when measurements are taken intermittently. To address this, the material model proposed in International Federation for Structural Concrete (2023) was employed to enhance the analytical framework. This model incorporates a drying shrinkage coefficient, a humidity coefficient, and a time function. Since humidity remains constant in this study, Eq. (3) simplifies this approach to include only the time function and the shrinkage coefficient ε_{cs0}, representing the ultimate shrinkage deformation.

$$\varepsilon_{cds}(t,t_s) = -\varepsilon_{cs0} \cdot \left(\frac{t - t_s}{0.035 \cdot h^2 + (t - t_s)} \right)^{0.5} \tag{3}$$

For all concrete mixes, Eq. (3) was fitted to the evolution of the mean shrinkage deformations over time. As the parameter h in Eq. (1) represents specimen geometry, which was identical for all specimens, the parameter ε_{cs0}, resulting from the least-squares method, describes the summarized influence of the cement substitution through SCMs and activated concrete fines.

While International Federation for Structural Concrete (2023) includes an increase in shrinkage deformation with decreasing compressive strength, this effect only shows for the individual types of SCMs

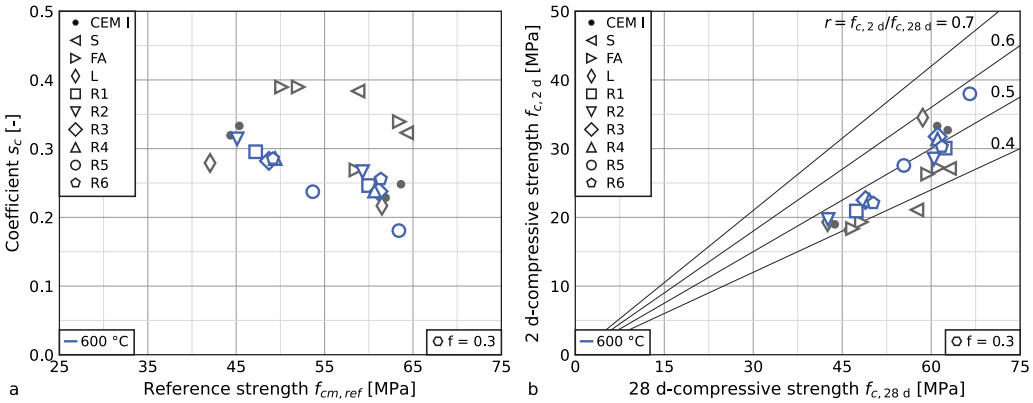

Fig. 4. Temporal development of compressive strength. Relationship between parameters $f_{cm,ref}$ and s_c from fitting Eq. (1) to experimental results after 2 d, 28 d, 56 d and 98 d (a) and relationship between experimental compressive strength at 2 d and 28 d (b).

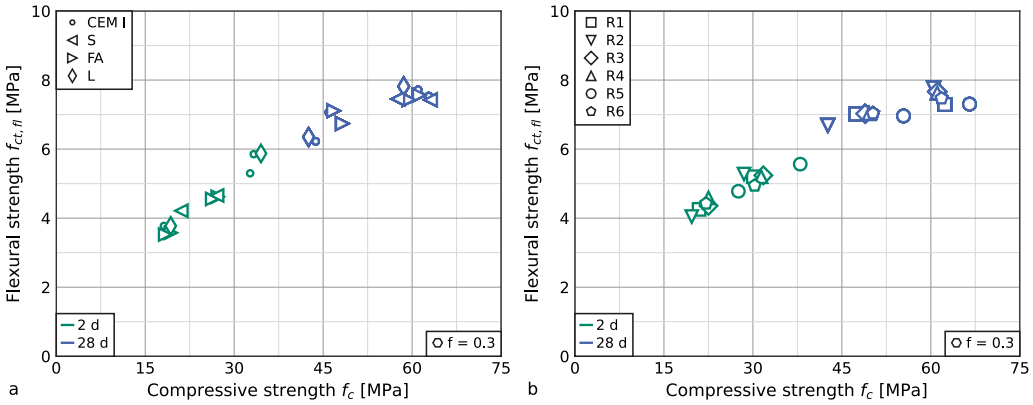

Fig. 5. Relationship between flexural and compressive strength at 2 d and 28 d after water-storage. Reference mixes with CEM I, S, FA, and L (a), and concrete mixes containing activated concrete fines (b).

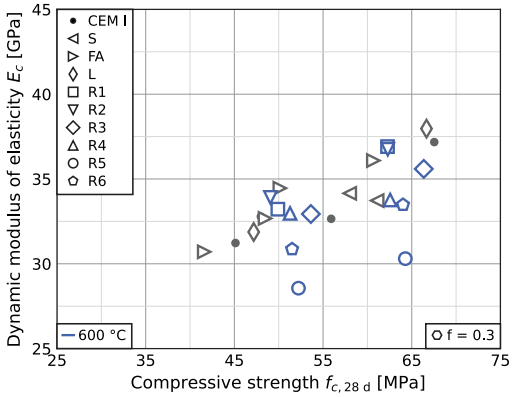

Fig. 6. Relationship between compressive strength and dynamic modulus of elasticity at the age of 28 d.

and activated concrete fines: For all mixes within this study, the "−1"-series with lower strength exhibits higher shrinkage deformations (see Fig. 8). However, the variation among these series is significantly greater than the effect of compressive strength. Nonetheless, it is evident that activated concrete fines, as well as slag, increase shrinkage, whereas fly ash and limestone powder have a decreasing effect (Nath and Sarker, 2011; Sakthivel et al., 2019; Darquennes et al., 2012; Wang et al., 2022). The scatter reduces when, instead of $f_{cm,ref}$, the dynamic modulus of elasticity is used as the base parameter. This suggests similar influencing factors, such as the mitigating effect of a high amount of inert particles, which hinder shrinkage due to their high stiffness. At the same time, a high amount of reactive phases, such as those present in R5-600, allows for higher deformation, as shrinkage only occurs in the cement paste.

3.7. Capillary absorption

The capillary water absorption coefficient $WA_{24\,h}$ for concrete containing thermally activated concrete fines increases with decreasing strength with minor deviations from the trendline. An identical pattern is observed for concrete containing limestone powder, with series L-1 exhibiting the lowest compressive strength and the highest water absorption among all series in this study. However, while the compensation of compressive strength loss due to partial cement replacement through the effective water–cement ratio also negates any measurable effects on water absorption, series CEM I-1 exhibits a reduced water absorption coefficient at a compressive strength similar to R1-600 and R2-600. This effect can, to a lesser extent, be observed for the cement substitution through slag or fly ash. Fig. 9(a) illustrates these findings.

These observations do not align with the results for total porosity, in contrast to the findings in Wu et al. (2023) on the influence of the substitution rate. However, the influence of compressive strength confirms previous findings on activated artificial cement paste (Bogas et al., 2022a; Carriço et al., 2022, 2021b). The overall increase in water absorption alongside a decrease in compressive strength is consistent with previous findings in Kim and Ubysz (2024), Bogas et al. (2022b) and Wu et al. (2023).

3.8. Chloride diffusion

The determination of the chloride profiles from profile grinding of series CEM I-2.1 yielded a diffusion coefficient of D_{nss} = 296 mm²/a =

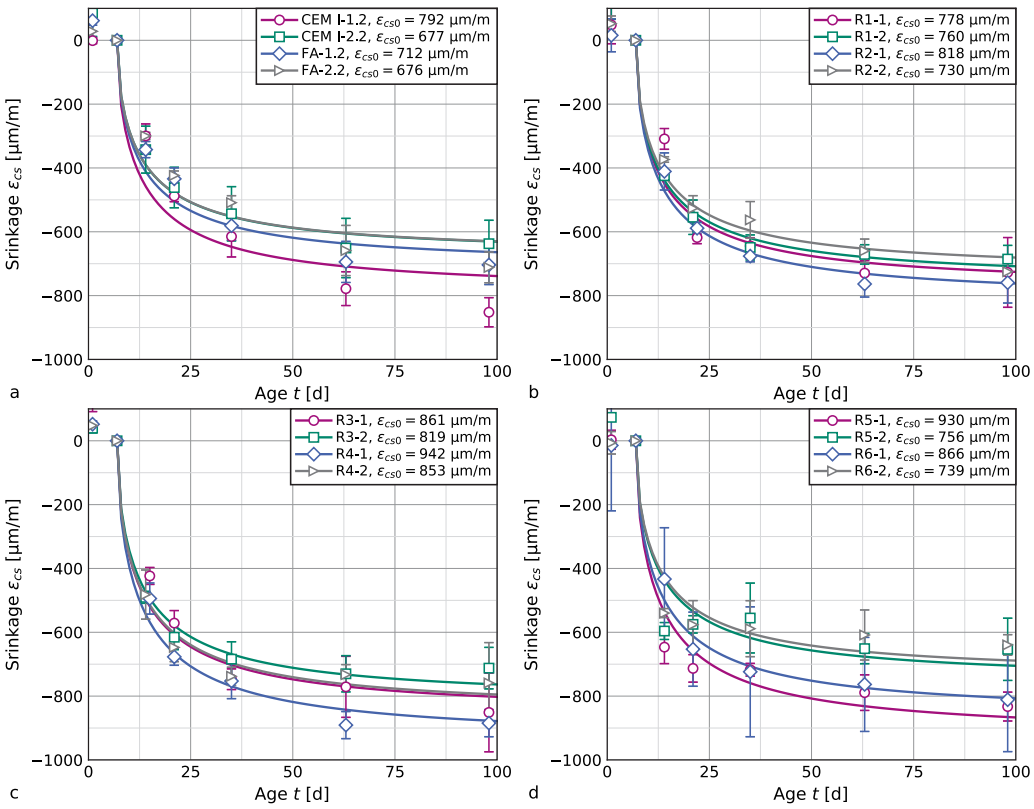

Fig. 7. Temporal development of shrinkage deformation for reference mixes (CEM I-1.2, CEM I-2.2, FA-1.2, FA-2.2, a), and concrete containing activated fines (b–d). Markers indicate the measured averages and standard deviations from three prisms; lines represent the corresponding fit curves used to determine ε_{cs0} (Eq. (3)).

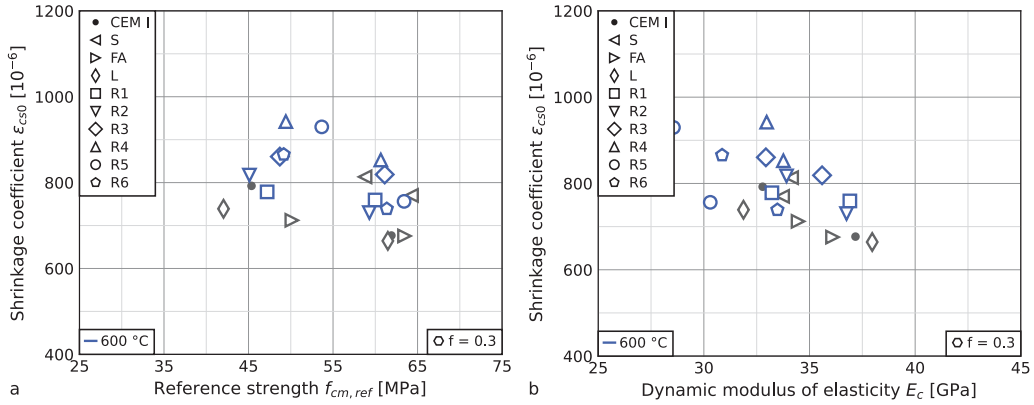

Fig. 8. Relationship between shrinkage coefficients ε_{cs0} and reference compressive strength $f_{cm,ref}$ (a), or dynamic moduli of elasticity E_c (b).

9.4×10^{-12} m^2/s and a superficial chloride content of C_s = 1.14 wt% with an initial chloride content of C_i = 0.02 wt%, both relative to the mass of concrete. The average chloride penetration depth of d_c = 8.8 mm, obtained from the silver nitrate indicator test on specimens from the same series, corresponds to a chloride content of C = 0.28 wt% normalized to the mass of concrete.

The silver nitrate indicator test on specimens from the repetition of this series yielded a penetration depth of d_c = 12.6 mm. The repeated series CEM I-1, FA-1, and FA-2 show a similar offset between the measurements (compare Fig. 9b). As the respective specimens were produced at the beginning and at the end of the study, which spanned several months, an inhomogeneity in the chloride content of the raw materials cannot be ruled out by the interpretation. However, the results show increased chloride penetration depth in concrete mixes containing activated concrete fines compared with the reference series containing pure CEM I, slag, or fly ash. An increased chloride content of concrete fines can be ruled out as a cause due to the results presented in Table 1. An alternative explanation is the chloride-binding capacity of hydration products from CEM I, slag, and fly ash, which is apparently absent in activated concrete fines (compare Liu et al., 2023). This agrees with previous findings, which identified a temperature dependence of the chloride-binding capacity of thermally activated concrete fines (He et al., 2023; Carriço et al., 2021b).

3.9. Carbonation

The results in Fig. 9(c) show a similar behavior of concrete containing activated fines on carbonation as on chloride ingress. However, activated concrete fines have a lower carbonation coefficient K_{AC} than

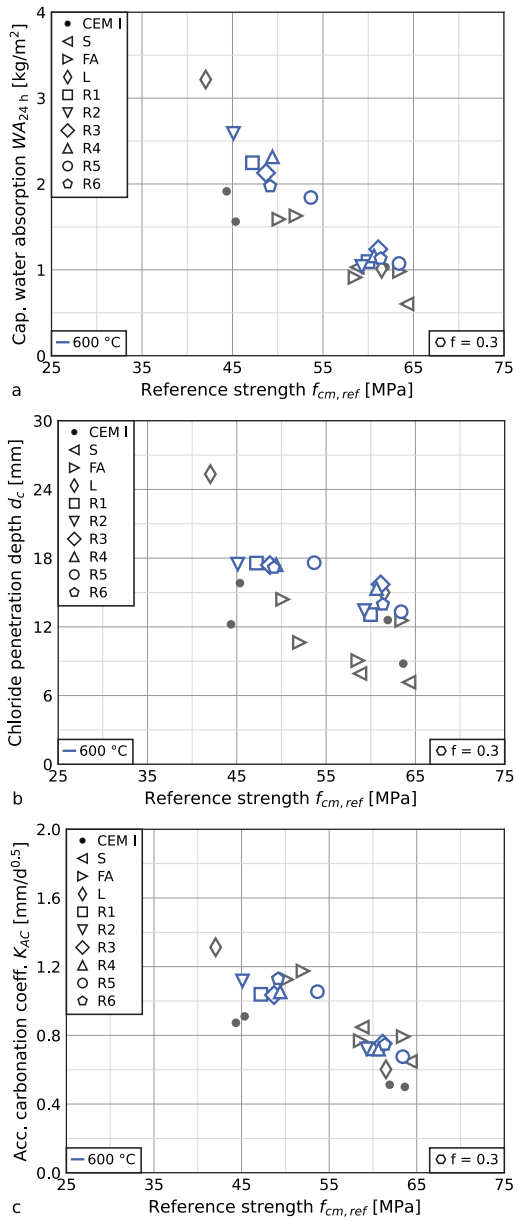

Fig. 9. Influence of compressive strength on concrete durability: Capillary water absorption (a), chloride penetration depth (b), and accelerated carbonation coefficient (c).

mixtures containing fly ash, and are similar to limestone powder and slag. A reason for this behavior may lie in the reduced alkalinity of the pore solution, which stems from $Ca(OH)_2$ forms during the hydration of CEM I. While limestone powder or slag reduces the $Ca(OH)_2$-content through the reduction of CEM I, the pozzolanic reaction of fly ash consumes $Ca(OH)_2$ and subsequently lowers the binding capacity of CO_2. The renewed formation of calcium-silicate-hydrates from dehydrated paste does not require additional $Ca(OH)_2$. Simultaneously, results in Table 1 show a negligible amount of free CaO, which implies a similarity to the reaction of slag. These findings confirm and expand on previously published results (Carriço et al., 2021b; Bogas et al., 2022b).

3.10. Leaching

Fig. 10 illustrates findings for select trace metal contents and organic compounds determined through both EDXRF and selected percolation tests. Tabulated results are depicted in Tables A.3, A.4, A.5, and A.6 in the Appendix.

Metal content in concrete fines varies widely. While EDXRF yields concentrations near or below the detection limit, some metals, exemplified in Fig. 10a, exhibit elevated concentrations, albeit with substantial differences among them. Overall, but not universally, metal concentrations increase with higher precursor fineness. Among the established SCMs, slag and limestone exhibit metal concentrations lower than those of most RCFs, whereas fly ash shows the highest concentrations of all materials. Results agree with findings listed in Park et al. (2025).

Percolation tests were performed to determine which of these metals are prone to leaching by water and therefore pose a potential risk of environmental contamination. Due to the high labor- and time intensiveness of this method, percolation for a water/solid ratio of $w/s = 2$ was limited to unaltered concrete fines, thermally activated fines, and concrete mixes containing activated fines with a constant water-binder ratio of $w/b = 0.5$. Results in Fig. 10b indicate a distinct variation between different metals, with Cr and Cu showing a higher elution compared to the other metals. On average, the eluates contain 0.34(30) % of the total Cu and 0.16(12) % of the total Cr content. For Ni, the ratio is 0.08(6) %, and 0.03 % or lower for other metals.

Yet, the behavior is strongly affected by the thermal activation (Fig. 10c). The eluble content of As, Cu, Ni, and Pb reduces, while Zn remains unaffected. A possible explanation for this behavior might lie in the immobilization of metals in dehydrated cement paste particles. Cr, however, behaves contrarily, with a significantly increased elution for thermally activated concrete fines. This may be triggered by the oxidation of Cr(III) to Cr(IV) at temperatures higher than 200 °C (Wang et al., 2025). While it is established that Cr, like other metals, can be immobilized in cement hydrates, this immobilization apparently fails upon decomposing the hydrates. This corroborates findings in Ma et al. (2023), where the leaching of Cr in acidic solutions increases with processing temperatures up to 800 °C. However, in contrast to the present study, this effect is also reported for other metals Ni, Cu or Pb, while Zn exhibits a decreasing behavior, albeit with a strong influence of the leaching solution (Ma et al., 2023).

Regardless, the elution of crushed concrete containing activated fines (Fig. 10d) exhibits a very similar behavior, and especially in the case of Cr, an apparent renewed immobilization in cement hydrate phases (compare Park et al., 2025).

The analysis of anions yields a similar behavior with variations between different concrete fines. After thermal activation, nitrite, nitrate, and sulfate content in the eluate decrease, while chloride and bromide are unaffected. The eluates from concrete contain lower amounts of anions, except for sulfate, which increases alongside the increased sulfate content in CEM I (compare Table 1).

Measurements of the total organic carbon (TOC) in unprocessed and processed concrete fines show an almost complete decomposition during thermal activation (Table 1). The same effect is apparent in the eluates, where the content of polycyclic aromatic hydrocarbons (PAH16) significantly reduces after thermal activation.

Ultimately, these results show that chrome, copper and sulfate are of special concern with regards to individual use cases. The exceedance of threshold concentrations (as defined through national regulations such as ErsatzbaustoffV (2021)) may preclude certain applications.

4. Conclusion

The substitution of Portland cement with waste materials impacts concrete compressive strength alongside other mechanical parameters and durability. This study compares the impact of granulated blast-furnace slag, fly ash, or limestone powder to six concrete fines of different origin and composition. For each supplementary cementitious material, the analysis uses a dual approach with the mitigation of compressive strength loss in contrast to an unaccounted substitution. This allows for the assessment of concrete performance at a constant compressive strength level.

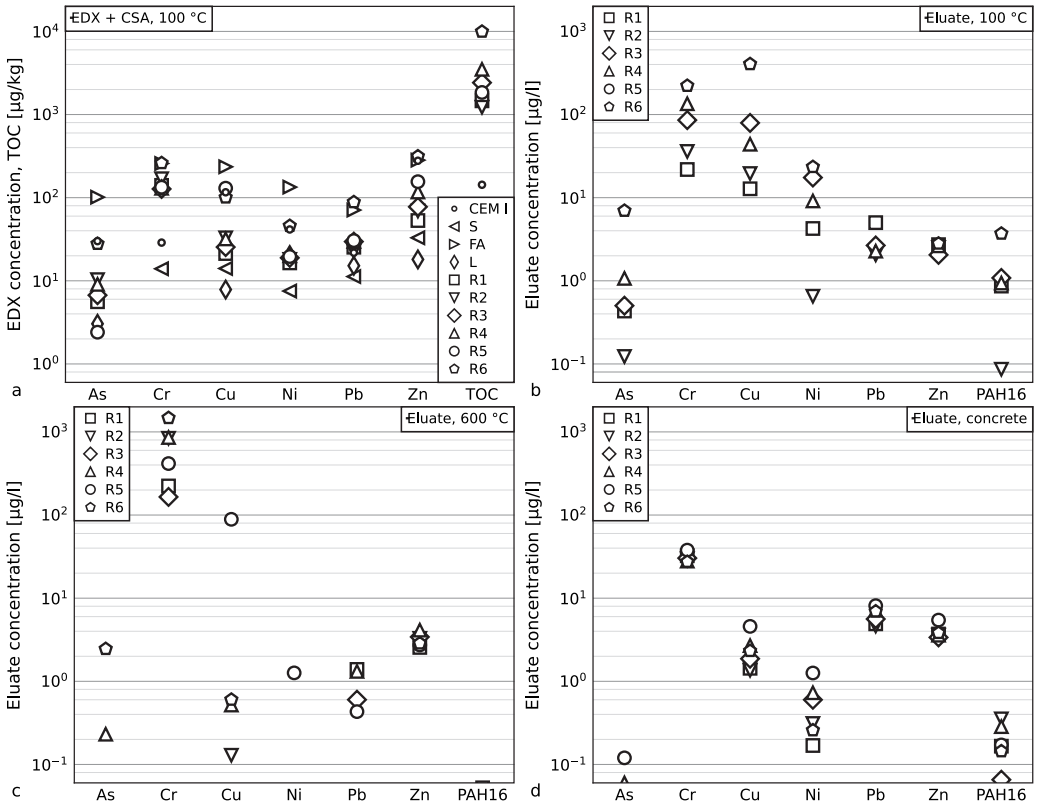

Fig. 10. Results of metal concentrations and total organic carbon content (TOC) and PAH16 concentrations. a: precursors through EDX and CSA, b: elutates from precursors ("100 °C"), c: thermally activated, unmilled concrete fines ("600 °C"), d: concrete mixes "–1" containing activated, milled concrete fines.

- Concrete containing thermally activated concrete fines or limestone powder exhibits a fast strength development, while fly ash or slag show a higher strength increase with later ages.
- Overall, flexural strength, the dynamic modulus of elasticity, and capillary water absorption are not affected beyond compressive strength reduction. A mitigation of strength loss also largely negates deviations in these concrete performance parameters.
- Concrete containing activated concrete fines exhibits higher shrinkage deformations compared to concrete with established SCMs.
- Chloride ingress and carbonation are increased for concrete containing activated fines compared to a CEM I-reference, but perform similarly to established SCMs. The only exception is the chloride binding capacity of hydration products from slag or fly ash, which is missing in activated fines.
- Concrete fines may contain harmful substances. The elution of those mostly reduces following thermal activation, with the notable exception of chrome.

In conclusion, the present results show a sufficient agreement of concrete with established SCMs and concrete containing thermally activated concrete fines of different origins. Therefore, a cement substitution of 30 wt% is feasible to obtain concrete mixtures, which agree with existing building standards and the underlying empirical relationships between compressive strength, mechanical properties, and durability. However, the simplifications chosen for enabling the qualitative comparison of a broad set of concrete properties require additional research. These procedures require a closer alignment with standardized experimental setups. Furthermore, the present results underline the need for investigating binding mechanisms of (re) activated cement hydrates and harmful substances, such as CO_2, chlorides, or heavy metals. A scaled-up industrial application of thermally activated concrete fines requires the quantitative assessment of harmful substance contents in the eluates with regard to threshold values defined for individual use cases.

CRediT authorship contribution statement

Jan P. Höffgen: Writing – original draft, Visualization, Methodology, Funding acquisition, Formal analysis, Conceptualization. **Lukas Reichert:** Writing – review & editing, Formal analysis. **Bernd Susset:** Writing – review & editing, Conceptualization. **Annegret Walz:** Writing – review & editing, Methodology, Formal analysis. **Peter Grathwohl:** Validation, Resources. **Frank Dehn:** Writing – review & editing, Supervision, Project administration, Funding acquisition.

Declaration of Generative AI and AI-assisted technologies in the writing process

During the preparation of this work, the authors used Grammarly and DeepL in order to check for spelling and wording errors. After using these tools/services, the authors reviewed and edited the content as needed and take full responsibility for the content of the published article.

Funding

This work was supported by the Dres. Edith und Klaus Dyckerhoff-Stiftung, grant no. T0218/36374.

Declaration of competing interest

The authors declare that they have no known competing financial interests or personal relationships that could have appeared to influence the work reported in this paper.

Appendix

See Tables A.2–A.6.

Data availability

Data will be made available on request.

Table A.2
Overview of different series. SCM: supplementary cementitious material. f: substitution rate of CEM I through SCM. k: assumed k-value. w/b: selected water-binder ratio. w/c_{eq}: resulting equivalent water–cement ratio. w: water content. c: CEM I content. a: SCM content. SP: superplasticizer dosage for achieving target consistency. Aggregate content for all series: RS: 526 kg/m^3, RG: 1024 kg/m^3.

Series	SCM	f –	k –	w/b –	w/c_{eq} –	w kg/m^3	c kg/m^3	a kg/m^3	SP kg/m^3
CEM I-1	CEM I	0.0		0.60	0.60	261	435		0.0
CEM I-2				0.50	0.50	244	488		0.0
S-1	S	0.3	0.8	0.50	0.53	242	339	145	0.0
S-2				0.46	0.49	234	356	153	0.0
FA-1	FA	0.3	0.5	0.50	0.61	233	327	140	0.0
FA-2				0.43	0.51	219	356	152	2.7
L-1	L	0.3	0.1	0.50	0.68	240	335	144	0.0
L-2				0.36	0.49	207	403	173	5.8
R1-1	R1-600	0.3	0.4	0.50	0.61	239	335	143	0.0
R1-2				0.40	0.49	217	380	163	5.6
R2-1	R2-600	0.3	0.4	0.50	0.61	239	334	143	0.0
R2-2				0.40	0.49	217	380	163	5.4
R3-1	R3-600	0.3	0.5	0.50	0.59	239	334	143	0.0
R3-2				0.42	0.49	222	370	158	4.0
R4-1	R4-600	0.3	0.5	0.50	0.59	238	334	143	0.0
R4-2				0.42	0.49	221	369	158	3.3
R5-1	R5-600	0.3	0.6	0.50	0.57	239	334	143	3.6
R5-2				0.43	0.49	224	365	156	6.7
R6-1	R6-600	0.3	0.6	0.50	0.57	239	335	143	1.6
R6-2				0.43	0.49	224	365	157	5.2

Table A.3
Chemical composition of CEM I, reference SCMs (S, FA, L) and concrete fines (R1–R6) before activation. Oxide phases of main elements through WDXRF, trace elements through EDXRF. Empty entries indicate results below the analytical limit of determination.

	CEM I	S	FA	L	R1	R2	R3	R4	R5	R6
WDXRF [wt%]										
LOI	2.7	−0.9	1.7	39.3	15.3	8.9	21.2	15.0	18.8	17.1
Na_2O	0.0	0.2	0.4		0.4	0.6	0.4	0.6	0.4	1.0
MgO	1.9	5.5	1.2	1.1	1.4	0.8	1.7	1.6	2.0	2.4
Al_2O_3	4.8	11.0	29.2	2.5	4.4	4.8	5.1	5.8	6.0	8.5
SiO_2	20.0	34.9	47.6	6.1	51.3	66.8	43.1	49.7	40.0	44.4
P_2O_5	0.2	0.0	0.3	0.0	0.1	0.1	0.1	0.1	0.1	0.2
K_2O	0.8	0.7	1.3	0.7	1.2	1.5	1.2	1.5	0.6	1.8
CaO	61.7	41.6	3.1	47.2	21.5	12.6	23.4	21.6	27.6	18.6
TiO_2	0.2	1.0	3.4	0.1	0.2	0.2	0.2	0.2	0.3	0.4
MnO	0.2	0.6	0.1	0.0	0.0	0.0	0.0	0.1	0.1	0.1
Fe_2O_3	3.1	1.2	9.0	0.9	1.7	1.6	2.1	2.4	1.7	4.2
EDXRF [mg/kg]										
As	30		101	3	6	10	7	9	2	28
Ba	520	1823	1097	99	310	289	530	322	347	377
Cd	0	0	1	0	1	1		1		
Cr	29	14	258		141	169	127	130	134	261
Cs	13	7	32	9	9		3	5		
Cu	116	14	235	8	21	33	25	32	130	101
Ga	11	8	47	10	11	11	11	11	10	14
Mo	4		9	1	3	5	4	4	3	7
Nb	6	4	126	4	7	6	7	7	7	13
Ni	41	8	134	20	16	18	19	20	20	46
Pb	22	11	71	15	25	23	30	30	30	88
Rb	35	23	117	26	49	63	47	56	25	93
Sb	21	12	6	4						
Sn	49	40	32	22	3	9	5	6	5	5
Sr	703	664	571	986	341	307	355	342	371	526
Th		10	27						3	3
U	1	10	11	5	0	1	1	1	2	1
V	60	62	393	49	45	41	45	50	57	66
Y	20	51	52	4	10	10	13	17	19	22
Zn	278	33	283	18	53	69	78	117	156	315
Zr	67	200	411	45	68	70	94	99	109	136

Table A.4
Results from the eluate analysis on unprocessed concrete fines ("–100"). n.d.: not determined, <l.o.d.: below the limit of detection. Note that, for R5-100, the automatic deactivation failed, resulting in an increase in W/S.

		R1-100	R2-100	R3-100	R4-100	R5-100	R6-100
Sample (dry)	g	669	740	545	465	247	394
Eluate	g	1339	1481	1085	914	1538	771
W/S	–	2.00	2.00	1.99	1.97	6.22	1.96
pH	–	12.50	12.15	12.25	12.15	12.38	10.03
Elect. conduct.	mS/cm	6.55	2.90	3.84	3.73	3.80	2.24
Fluoride	mg/l	n.d.	n.d.	n.d.	n.d.	n.d.	n.d.
Chloride	mg/l	82.59	10.36	118.44	26.69	18.64	118.05
Nitrite	mg/l	1.37	0.41	2.29	2.22	0.54	2.86
Bromide	mg/l	0.18	0.20	0.23	0.23	0.52	0.82
Nitrate	mg/l	10.82	1.67	9.35	9.58	1.01	23.20
Phosphate	mg/l	<l.o.d.	<l.o.d.	<l.o.d.	<l.o.d.	<l.o.d.	<l.o.d.
Sulfate	mg/l	33.86	15.61	26.57	391.31	35.44	1233.92
As	µg/l	0.43	0.12	0.50	1.07	0.03	6.97
Cd	µg/l	<l.o.d.	<l.o.d.	<l.o.d.	<l.o.d.	<l.o.d.	<l.o.d.
Cr	µg/l	21.82	35.98	85.67	134.84	77.88	221.85
Co	µg/l	0.43	5.54	10.91	1.92	0.76	18.66
Cu	µg/l	12.79	19.52	79.29	43.91	23.26	404.80
Ni	µg/l	4.26	0.65	17.46	9.13	1.63	23.44
Pb	µg/l	5.01	2.05	2.66	2.27	2.04	<l.o.d.
Th	µg/l	<l.o.d.	<l.o.d.	<l.o.d.	<l.o.d.	0.16	<l.o.d.
Zn	µg/l	2.72	2.52	2.05	2.63	3.54	2.81
PAH16	µg/l	0.86	0.09	1.08	0.94	0.35	3.70

Table A.5
Results from the eluate analysis on thermally activated concrete fines ("–600"). n.d.: not determined, <l.o.d.: below the limit of detection.

		R1-600	R2-600	R3-600	R4-600	R5-600	R6-600
Sample (dry)	g	132	136	97	90	131	70
Eluate	g	263	265	197	182	0	163
W/S	–	1.99	1.95	2.03	2.02	0.00	2.32
pH	–	12.26	12.16	12.15	12.23	12.09	10.57
Elect. conduct.	mS/cm	3.45	1.85	2.97	3.30	2.39	2.66
Fluoride	mg/l	0.88	0.65	0.94	1.28	0.67	n.d.
Chloride	mg/l	73.14	13.92	116.11	26.14	22.76	n.d.
Nitrite	mg/l	<l.o.d.	<l.o.d.	<l.o.d.	<l.o.d.	<l.o.d.	n.d.
Bromide	mg/l	0.24	0.24	0.31	0.30	0.15	n.d.
Nitrate	mg/l	<l.o.d.	<l.o.d.	<l.o.d.	<l.o.d.	<l.o.d.	n.d.
Phosphate	mg/l	<l.o.d.	<l.o.d.	<l.o.d.	<l.o.d.	<l.o.d.	n.d.
Sulfate	mg/l	7.60	21.66	8.65	25.48	25.99	n.d.
As	µg/l	<l.o.d.	<l.o.d.	<l.o.d.	0.23	<l.o.d.	2.45
Cd	µg/l	<l.o.d.	<l.o.d.	<l.o.d.	<l.o.d.	<l.o.d.	<l.o.d.
Cr	µg/l	223.80	838.77	165.17	856.13	416.18	1471.60
Co	µg/l	<l.o.d.	<l.o.d.	<l.o.d.	<l.o.d.	<l.o.d.	<l.o.d.
Cu	µg/l	<l.o.d.	0.13	<l.o.d.	0.52	88.87	0.60
Ni	µg/l	<l.o.d.	<l.o.d.	<l.o.d.	<l.o.d.	1.26	<l.o.d.
Pb	µg/l	1.39	<l.o.d.	0.60	1.32	0.43	<l.o.d.
Th	µg/l	<l.o.d.	<l.o.d.	<l.o.d.	<l.o.d.	<l.o.d.	0.03
Zn	µg/l	2.56	3.29	3.42	4.13	2.74	2.86
PAH16	µg/l	0.05	0.01	0.00	0.00	0.02	0.02

Table A.6
Results from the eluate analysis on concrete containing activated fines ("–1"). n.d.: not determined, <l.o.d.: below the limit of detection.

		R1-1	R2-1	R3-1	R4-1	R5-1	R6-1
Sample (dry)	g	656	683	657	650	636	700
Eluate	g	1313	1369	1329	1300	1278	1371
W/S	–	2.00	2.00	2.02	2.00	2.01	1.96
pH	–	12.60	12.60	12.69	12.63	12.77	12.70
Elect. conduct.	mS/cm	7.77	7.82	7.45	8.18	8.28	7.82

(*continued on next page*)

Table A.6 (*continued*).

		R1-1	R2-1	R3-1	R4-1	R5-1	R6-1
Fluoride	mg/l	n.d.	n.d.	n.d.	n.d.	n.d.	n.d.
Chloride	mg/l	45.35	28.74	38.87	32.91	38.03	29.77
Nitrite	mg/l	<l.o.d.	<l.o.d.	<l.o.d.	<l.o.d.	0.50	0.43
Bromide	mg/l	0.51	0.38	0.50	<l.o.d.	<l.o.d.	<l.o.d.
Nitrate	mg/l	1.71	1.66	1.60	1.95	8.77	3.93
Phosphate	mg/l	<l.o.d.	<l.o.d.	<l.o.d.	<l.o.d.	<l.o.d.	<l.o.d.
Sulfate	mg/l	71.55	53.07	74.29	48.63	74.73	47.54
As	µg/l	<l.o.d.	0.02	<l.o.d.	0.06	0.12	0.04
Cd	µg/l	<l.o.d.	<l.o.d.	<l.o.d.	<l.o.d.	<l.o.d.	<l.o.d.
Cr	µg/l	32.37	29.82	30.32	27.92	37.83	27.40
Co	µg/l	36.02	37.40	37.99	48.98	53.74	46.25
Cu	µg/l	1.44	1.36	1.87	2.69	4.58	2.32
Ni	µg/l	0.17	0.31	0.60	0.73	1.26	0.26
Pb	µg/l	4.91	4.63	5.62	7.16	8.13	6.95
Th	µg/l	<l.o.d.	<l.o.d.	<l.o.d.	<l.o.d.	0.00	<l.o.d.
Zn	µg/l	3.71	3.59	3.37	3.59	5.45	3.82
PAH16	µg/l	0.17	0.35	0.07	0.28	0.17	0.14

References

Algourdin, N., Nguyen, Q., Mesticou, Z., Si Larbi, A., 2021. Durability of recycled fine mortars under freeze–thaw cycles. Constr. Build. Mater. 291, 123330. http://dx.doi.org/10.1016/j.conbuildmat.2021.123330.

Amran, M., Murali, G., Khalid, N.H.A., Fediuk, R., Ozbakkaloglu, T., Lee, Y.H., Haruna, S., Lee, Y.Y., 2021. Slag uses in making an ecofriendly and sustainable concrete: A review. Constr. Build. Mater. 272, 121942. http://dx.doi.org/10.1016/j.conbuildmat.2020.121942.

Andrade, J.F.C., Córdoba, R.E., Schalch, V., 2025. Effect of presence of paint in recycled aggregates on the leaching of pollutants. Constr. Build. Mater. 485, 141904. http://dx.doi.org/10.1016/j.conbuildmat.2025.141904.

Andrade Neto, J., Carvalho, I., Monteiro, P., De Matos, P., Kirchheim, A., 2025. Unveiling the key factors for clinker reactivity and cement performance: A physic-chemical and performance investigation of 40 industrial clinkers. Cem. Concr. Res. 187, 107717. http://dx.doi.org/10.1016/j.cemconres.2024.107717.

Angulo, S.C., Guilge, M.S., Quarcioni, V.A., Cincotto, M.A., Nobre, T.R., Pöllmann, H., 2022. The role of calcium silicates and quicklime on the reactivity of rehydrated cements. Constr. Build. Mater. 340, 127625. http://dx.doi.org/10.1016/j.conbuildmat.2022.127625.

Aquino Rocha, J.H., Toledo Filho, R.D., 2023. The utilization of recycled concrete powder as supplementary cementitious material in cement-based materials: A systematic literature review. J. Build. Eng. 76, 107319. http://dx.doi.org/10.1016/j.jobe.2023.107319.

Baggio, T.F., Possan, E., De Oliveira Andrade, J.J., 2024. Physical-chemical characterization of construction and demolition waste powder with thermomechanical activation for use as supplementary cementitious material. Constr. Build. Mater. 437, 136907. http://dx.doi.org/10.1016/j.conbuildmat.2024.136907.

Baldusco, R., Nobre, T.R.S., Angulo, S.C., Quarcioni, V.A., Cincotto, M.A., 2019. Dehydration and rehydration of blast furnace slag cement. J. Mater. Civ. Eng. 31 (8), 04019132. http://dx.doi.org/10.1061/(ASCE)MT.1943-5533.0002725.

Baquerizo, L.G., Matschei, T., Scrivener, K.L., 2016. Impact of water activity on the stability of ettringite. Cem. Concr. Res. 79, 31–44. http://dx.doi.org/10.1016/j.cemconres.2015.07.008.

Barthel, M., Rübner, K., Kühne, H.-C., Rogge, A., Dehn, F., 2016. From waste materials to products for use in the cement industry. Adv. Cem. Res. 28 (7), 458–468. http://dx.doi.org/10.1680/jadcr.15.00149.

Bogas, J.A., Carriço, A., Pereira, M., 2019. Mechanical characterization of thermal activated low-carbon recycled cement mortars. J. Clean. Prod. 218, 377–389. http://dx.doi.org/10.1016/j.jclepro.2019.01.325.

Bogas, J.A., Carriço, A., Real, S., 2022a. Durability of concrete produced with recycled cement from waste concrete. Mater. Today: Proc. 58, 1149–1154. http://dx.doi.org/10.1016/j.matpr.2022.01.280.

Bogas, J.A., Carriço, A., Tenza-Abril, A.J., 2020. Microstructure of thermoactivated recycled cement pastes. Cem. Concr. Res. 138, 106226. http://dx.doi.org/10.1016/j.cemconres.2020.106226.

Bogas, J.A., Real, S., Carriço, A., Abrantes, J., Guedes, M., 2022b. Hydration and phase development of recycled cement. Cem. Concr. Compos. 127, 104405. http://dx.doi.org/10.1016/j.cemconcomp.2022.104405.

Campos, R., Larrain, M.M.M., Zaman, M., Pozadas, V., 2021. Relationships between compressive and flexural strengths of concrete based on fresh field properties. Int. J. Pavement Res. Technol. 14 (2), 161–167. http://dx.doi.org/10.1007/s42947-020-1074-0.

Carriço, A., Bogas, J.A., Guedes, M., 2020a. Thermoactivated cementitious materials – A review. Constr. Build. Mater. 250, 118873. http://dx.doi.org/10.1016/j.conbuildmat.2020.118873.

Carriço, A., Bogas, J.A., Hu, S., Real, S., Costa Pereira, M.F., 2021a. Novel separation process for obtaining recycled cement and high-quality recycled sand from waste hardened concrete. J. Clean. Prod. 309, 127375. http://dx.doi.org/10.1016/j.jclepro.2021.127375.

Carriço, A., Bogas, J.A., Real, S., Pereira, M.F.C., 2022. Shrinkage and sorptivity of mortars with thermoactivated recycled cement. Constr. Build. Mater. 333, 127392. http://dx.doi.org/10.1016/j.conbuildmat.2022.127392.

Carriço, A., Real, S., Bogas, J.A., 2021b. Durability performance of thermoactivated recycled cement concrete. Cem. Concr. Compos. 124, http://dx.doi.org/10.1016/j.cemconcomp.2021.104270.

Carriço, A., Real, S., Bogas, J.A., Costa Pereira, M.F., 2020b. Mortars with thermo activated recycled cement: Fresh and mechanical characterisation. Constr. Build. Mater. 256, 119502. http://dx.doi.org/10.1016/j.conbuildmat.2020.119502.

Chen, L., Wei, M., Lei, N., Li, H., 2024. Effect of chemical–thermal activation on the properties of recycled fine powder cementitious materials. Case Stud. Constr. Mater. 20, e02956. http://dx.doi.org/10.1016/j.cscm.2024.e02956.

Coffetti, D., Crotti, E., Gazzaniga, G., Carrara, M., Pastore, T., Coppola, L., 2022. Pathways towards sustainable concrete. Cem. Concr. Res. 154, 106718. http://dx.doi.org/10.1016/j.cemconres.2022.106718.

Darquennes, A., Rozière, E., Khokhar, M.I.A., Turcry, Ph., Loukili, A., Grondin, F., 2012. Long-term deformations and cracking risk of concrete with high content of mineral additions. Mater. Struct. 45 (11), 1705–1716. http://dx.doi.org/10.1617/s11527-012-9867-5.

Ekin, N., Uyanik, O., 2021. Comparison of static and dynamic elastic moduli in concrete: Effects of compressive strength, curing conditions and reinforcement. Iran. J. Sci. Technol. Trans. Civ. Eng. 45 (4), 2327–2343. http://dx.doi.org/10.1007/s40996-020-00513-7.

Engelsen, C.J., Van Der Sloot, H.A., Wibetoe, G., Justnes, H., Lund, W., Stoltenberg-Hansson, E., 2010. Leaching characterisation and geochemical modelling of minor and trace elements released from recycled concrete aggregates. Cem. Concr. Res. 40 (12), 1639–1649. http://dx.doi.org/10.1016/j.cemconres.2010.08.001.

ErsatzbaustoffV, 2021. Verordnung zur Einführung einer Ersatzbaustoffverordnung, zur Neufassung der Bundes-Bodenschutz- und Altlastenverordnung und zur Änderung der Deponieverordnung und der Gewerbeabfallverordnung: ErsatzbaustoffV.

Florea, M.V.A., 2014. Secondary Materials Applied in Cement-Based Products : Treatment, Modelling and Environmental Interaction (Ph.D. thesis). Technische Universiteit Eindhoven, http://dx.doi.org/10.6100/IR772902.

Friol Guedes de Paiva, F., Tamashiro, J.R., Pereira Silva, L.H., Kinoshita, A., 2021. Utilization of inorganic solid wastes in cementitious materials – A systematic literature review. Constr. Build. Mater. 285, 122833. http://dx.doi.org/10.1016/j.conbuildmat.2021.122833.

Gao, X., Gu, Y., Xie, T., Zhen, G., Huang, S., Zhao, Y., 2015. Characterization and environmental risk assessment of heavy metals in construction and demolition wastes from five sources (chemical, metallurgical and light industries, and residential and recycled aggregates). Environ. Sci. Pollut. Res. 22 (12), 9332–9344. http://dx.doi.org/10.1007/s11356-014-4058-2.

Gao, Y., Schutter, G., Ye, G., Yu, Z., Tan, Z., Wu, K., 2013. A microscopic study on ternary blended cement based composites. Constr. Build. Mater. 46, 28–38. http://dx.doi.org/10.1016/j.conbuildmat.2013.04.021.

Getachew, E.M., Yifru, B.W., Habtegebreal, B.T., Yehualaw, M.D., 2024. Performance evaluation of mortar with ground and thermo-activated recycled concrete cement. Cogent Eng. 11 (1), 2357726. http://dx.doi.org/10.1080/23311916.2024.2357726.

Gruyaert, E., Maes, M., De Belie, N., 2013a. Performance of BFS concrete: K-Value concept versus equivalent performance concept. Constr. Build. Mater. 47, 441–455. http://dx.doi.org/10.1016/j.conbuildmat.2013.05.006.

Gruyaert, E., Van Den Heede, P., De Belie, N., 2013b. Carbonation of slag concrete: Effect of the cement replacement level and curing on the carbonation coefficient – Effect of carbonation on the pore structure. Cem. Concr. Compos. 35 (1), 39–48. http://dx.doi.org/10.1016/j.cemconcomp.2012.08.024.

Güneyisi, E., Gesoğlu, M., 2008. A study on durability properties of high-performance concretes incorporating high replacement levels of slag. Mater. Struct. 41 (3), 479–493. http://dx.doi.org/10.1617/s11527-007-9260-y.
He, Z., Hu, R., Ma, Z., Liu, X., Wang, C., Wu, H., 2023. Reusing thermoactivated construction waste spoil as sustainable binder for durable concrete: Microstructure and chloride transport. Constr. Build. Mater. 398, 132553. http://dx.doi.org/10.1016/j.conbuildmat.2023.132553.
Herrmann, A., Koenig, A., Dehn, F., 2018. Structural concrete based on alkali-activated binders: Terminology, reaction mechanisms, mix designs and performance. Struct. Concr. 19 (3), 918–929. http://dx.doi.org/10.1002/suco.201700016.
Höffgen, J.P., Bruckschlögl, S., Wetz, B., Dehn, F., 2025. Influence of thermally activated industrial concrete fines of different origin on mortar strength development. Case Stud. Constr. Mater. e05427. http://dx.doi.org/10.1016/j.cscm.2025.e05427.
Höffgen, J.P., Dehn, F., 2025. Influence of thermally activated artificial concrete fines composition on mortar strength development. Dev. the Built Environ. 24, 100775. http://dx.doi.org/10.1016/j.dibe.2025.100775.
Höffgen, J.P., Schmitt, M., Dehn, F., 2026. Influence of thermally activated artificial concrete fines composition on concrete long-term behavior. J. Build. Eng. 112, 115767. http://dx.doi.org/10.1016/j.jobe.2026.115767.
Horváth, I., Proks, I., Nerád, I., 1977. Activation energies of the thermal decompositions of C3AH6 AND C3AD6 by the isothermal TG method. J. Therm. Anal. 12 (1), 105–110. http://dx.doi.org/10.1007/BF01909862.
International Federation for Structural Concrete (Ed.), 2023. Fib Model Code for Concrete Structures (2020), Version 1 International Federation for Structural Concrete (fib), Lausanne.
Juan, M.S., Gutiérrez, P.A., 2009. Study on the influence of attached mortar content on the properties of recycled concrete aggregate. Constr. Build. Mater. 23 (2), 872–877. http://dx.doi.org/10.1016/j.conbuildmat.2008.04.012.
Kalinowska-Wichrowska, K., Kosior-Kazberuk, M., Pawluczuk, E., 2020. The properties of composites with recycled cement mortar used as a supplementary cementitious material. Materials 13 (1), 64. http://dx.doi.org/10.3390/ma13010064.
Kaliyavaradhan, S.K., Ling, T.-C., Mo, K.H., 2020. Valorization of waste powders from cement-concrete life cycle: A pathway to circular future. J. Clean. Prod. 268, 122358. http://dx.doi.org/10.1016/j.jclepro.2020.122358.
Kim, J., Kim, N., 2023. Exploring the role of thermal activation of cement exposed to the external environment on the improvement of concrete properties. J. Mater. Res. Technol. 24, 2868–2878. http://dx.doi.org/10.1016/j.jmrt.2023.03.195.
Kim, J.-H., Seo, E.-A., Kim, D.-G., Chung, C.-W., 2021. Utilization of recycled cement powder as a solidifying agent for radioactive waste immobilization. Constr. Build. Mater. 289, 123126. http://dx.doi.org/10.1016/j.conbuildmat.2021.123126.
Kim, J., Ubysz, A., 2024. Thermal activation of multi-recycled concrete powder as supplementary cementitious material for repeated and waste-free recycling. J. Build. Eng. 98, 111169. http://dx.doi.org/10.1016/j.jobe.2024.111169.
Klingsch, E.W., 2014. Explosive Spalling of Concrete in Fire (Ph.D. thesis). ETH Zurich, Zürich, http://dx.doi.org/10.3929/ethz-a-010243000.
Knight, K.A., Cunningham, P.R., Miller, S.A., 2023. Optimizing supplementary cementitious material replacement to minimize the environmental impacts of concrete. Cem. Concr. Compos. 139, 105049. http://dx.doi.org/10.1016/j.cemconcomp.2023.105049.
Koenders, E., Weise, K., Mayer, M., Morina, N., 2025. Werkstoffe im Bauwesen: Einführung für Bauingenieure und Architekten. Springer Fachmedien Wiesbaden, Wiesbaden, http://dx.doi.org/10.1007/978-3-658-49382-0.
Kurda, R., Silvestre, J.D., De Brito, J., 2018. Toxicity and environmental and economic performance of fly ash and recycled concrete aggregates use in concrete: A review. Heliyon 4 (4), e00611. http://dx.doi.org/10.1016/j.heliyon.2018.e00611.
Lipowsky, A., Müller, A., 2017. Gesteinsmehl als Zuschlagstoffe in hydraulischen Bindemitteln. Aufbereitungs-Technik/Mineral Process. 58 (12), 52–64.
Liu, J.-C., Hossain, U., Xuan, D., Asad Ali, H., Ng, S.T., Ye, H., 2023. Mechanical and durability performance of sustainable concretes containing conventional and emerging supplementary cementitious materials. Dev. the Built Environ. 15, 100197. http://dx.doi.org/10.1016/j.dibe.2023.100197.
Lu, C.-C., Hsu, M.H., Lin, Y.-P., 2019. Evaluation of heavy metal leachability of incinerating recycled aggregate and solidification/stabilization products for construction reuse using TCLP, multi-final pH and EDTA-mediated TCLP leaching tests. J. Hazard. Mater. 368, 336–344. http://dx.doi.org/10.1016/j.jhazmat.2019.01.066.
Lübeck, A., Gastaldini, A., Barin, D., Siqueira, H., 2012. Compressive strength and electrical properties of concrete with white Portland cement and blast-furnace slag. Cem. Concr. Compos. 34 (3), 392–399. http://dx.doi.org/10.1016/j.cemconcomp.2011.11.017.
Ma, X., He, T., Da, Y., Lin, Y., Feng, Y., Zhang, W., 2023. Evaluation of the ability of cement prepared with incineration fly ash to solidify heavy metals at high temperatures. J. Build. Eng. 78, 107559. http://dx.doi.org/10.1016/j.jobe.2023.107559.
Ma, Z., Shen, J., Wu, H., Zhang, P., 2022. Properties and activation modification of eco-friendly cementitious materials incorporating high-volume hydrated cement powder from construction waste. Constr. Build. Mater. 316, 125788. http://dx.doi.org/10.1016/j.conbuildmat.2021.125788.
Mao, Y., Hu, X., Alengaram, U.J., Chen, W., Shi, C., 2024. Use of carbonated recycled cement paste powder as a new supplementary cementitious material: A critical review. Cem. Concr. Compos. 154, 105783. http://dx.doi.org/10.1016/j.cemconcomp.2024.105783.
Marques, A.I., Morais, J., Morais, P., Veiga, M.D.R., Santos, C., Candeias, P., Ferreira, J.G., 2020. Modulus of elasticity of mortars: Static and dynamic analyses. Constr. Build. Mater. 232, 117216. http://dx.doi.org/10.1016/j.conbuildmat.2019.117216.
Müller, H.S., Acosta Urrea, F., Kvitsel, V., 2021. Modelle zur Vorhersage des Schwindens und Kriechens von Beton: Teil 1: Analyse des Schwindmodells in DIN EN 1992-1-1:2011 und neuer Ansatz im Eurocode 2 prEN 1992-1-1:2020. Beton- Und Stahlbetonbau 116 (1), 2–18. http://dx.doi.org/10.1002/best.202000082.
Nath, P., Sarker, P., 2011. Effect of fly ash on the durability properties of high strength concrete. Procedia Eng. 14, 1149–1156. http://dx.doi.org/10.1016/j.proeng.2011.07.144.
Noel, N., Mielke, T., Semugaza, G., Gierth, A.Z., Helmich, S., Nawrath, S., Lupascu, D.C., 2025. Chemical transformations during the preparation and rehydration of reactivated virgin cements. Cement 19, 100129. http://dx.doi.org/10.1016/j.cement.2025.100129.
Ohemeng, E.A., Ekolu, S.O., 2020. A review on the reactivation of hardened cement paste and treatment of recycled aggregates. Mag. Concr. Res. 72 (10), 526–539. http://dx.doi.org/10.1680/jmacr.18.00452.
Orozco, C., Babel, S., Tangtermsirikul, S., Sugiyama, T., 2024. Comparison of environmental impacts of fly ash and slag as cement replacement materials for mass concrete and the impact of transportation. Sustain. Mater. Technol. 39, e00796. http://dx.doi.org/10.1016/j.susmat.2023.e00796.
Panesar, D.K., Zhang, R., 2020. Performance comparison of cement replacing materials in concrete: Limestone fillers and supplementary cementing materials – A review. Constr. Build. Mater. 251, 118866. http://dx.doi.org/10.1016/j.conbuildmat.2020.118866.
Park, K.S., Zajac, M., Matschei, T., Vollpracht, A., 2025. The fate of heavy metals in recycled concrete paste upon enforced carbonation: A review. Resour. Conserv. Recycl. Adv. 28, 200289. http://dx.doi.org/10.1016/j.rcradv.2025.200289.
Pavlů, T., 2018. The utilization of recycled materials for concrete and cement production- A review. IOP Conf. Ser.: Mater. Sci. Eng. 442 (1), 012014. http://dx.doi.org/10.1088/1757-899X/442/1/012014.
Qian, D., Yu, R., Shui, Z., Sun, Y., Jiang, C., Zhou, F., Ding, M., Tong, X., He, Y., 2020. A novel development of green ultra-high performance concrete (UHPC) based on appropriate application of recycled cementitious material. J. Clean. Prod. 261, 121231. http://dx.doi.org/10.1016/j.jclepro.2020.121231.
Rakhimova, N., Shi, C., 2024. Upcycling of concrete wastes as precursors in alkali-activated materials: A review. Constr. Build. Mater. 436, 136978. http://dx.doi.org/10.1016/j.conbuildmat.2024.136978.
Real, S., Bogas, J.A., Carriço, A., Hu, S., 2021. Mechanical characterisation and shrinkage of thermoactivated recycled cement concrete. Appl. Sci. 11 (6), 2454. http://dx.doi.org/10.3390/app11062454.
Real, S., Carriço, A., Bogas, J.A., Guedes, M., 2020. Influence of the treatment temperature on the microstructure and hydration behavior of thermoactivated recycled cement. Materials 13 (18), 3937. http://dx.doi.org/10.3390/ma13183937.
Sakthivel, T., Gettu, R., Pillai, R.G., 2019. Compressive strength and elastic modulus of concretes with fly ash and slag. J. Inst. Eng. (India): Ser. A 100 (4), 575–584. http://dx.doi.org/10.1007/s40030-019-00376-w.
Schneider, U., 1982. Verhalten von Beton Bei Hohen Temperaturen. DAfStb-Heft, vol. 337, Wilhelm Ernst und Sohn, Berlin.
Scrivener, K.L., Juilland, P., Monteiro, P.J., 2015. Advances in understanding hydration of Portland cement. Cem. Concr. Res. 78, 38–56. http://dx.doi.org/10.1016/j.cemconres.2015.05.025.
Semugaza, G., Mielke, T., Castillo, M.E., Gierth, A.Z., Tam, J.X., Nawrath, S., Lupascu, D.C., 2023. Reactivation of hydrated cement powder by thermal treatment for partial replacement of ordinary portland cement. Mater. Struct. 56 (3), http://dx.doi.org/10.1617/s11527-023-02133-9.
Serpell, R., Lopez, M., 2015. Properties of mortars produced with reactivated cementitious materials. Cem. Concr. Compos. 64, 16–26. http://dx.doi.org/10.1016/j.cemconcomp.2015.08.003.
Snellings, R., Suraneni, P., Skibsted, J., 2023. Future and emerging supplementary cementitious materials. Cem. Concr. Res. 171, 107199. http://dx.doi.org/10.1016/j.cemconres.2023.107199.
Sui, Y., Ou, C., Liu, S., Zhang, J., Tian, Q., 2020. Study on properties of waste concrete powder by thermal treatment and application in mortar. Appl. Sci. 10 (3), 998. http://dx.doi.org/10.3390/app10030998.
Tokareva, A., Kaassamani, S., Waldmann, D., 2023. Fine demolition wastes as Supplementary cementitious materials for CO2 reduced cement production. Constr. Build. Mater. 392, 131991. http://dx.doi.org/10.1016/j.conbuildmat.2023.131991.
Tokareva, A., Waldmann, D., 2025. Durability of cement mortars containing fine demolition wastes as supplementary cementitious materials. Constr. Build. Mater. 477, 141316. http://dx.doi.org/10.1016/j.conbuildmat.2025.141316.
Van Praagh, M., Modin, H., Trygg, J., 2015. Organic compounds in concrete from demolition works. Waste Manage. 45, 186–193. http://dx.doi.org/10.1016/j.wasman.2015.06.037.
Vashistha, P., Oinam, Y., Kim, H.-K., Pyo, S., 2023. Effect of thermo-mechanical activation of waste concrete powder (WCP) on the characteristics of cement mixtures. Constr. Build. Mater. 362, 129713. http://dx.doi.org/10.1016/j.conbuildmat.2022.129713.

Vyšvařil, M., Bayer, P., Chromá, M., Rovnaníková, P., 2014. Physico-mechanical and microstructural properties of rehydrated blended cement pastes. Constr. Build. Mater. 54, 413–420. http://dx.doi.org/10.1016/j.conbuildmat.2013.12.021.

Wang, C.-q., Cheng, L.-x., Huang, Q.-c., Shui, Z.-h., Liu, Y.-y., Zhao, H., Zhang, Z.-j., 2023. Basic performance, heavy metal leaching mechanism and risk assessment analysis of waste concrete. Arch. Civ. Mech. Eng. 23 (2), 122. http://dx.doi.org/10.1007/s43452-023-00666-y.

Wang, J., Lacarrière, L., Sellier, A., 2019. Multicomponent modelling of cement paste dehydration under different heating rates. Mater. Struct. 52 (1), 6. http://dx.doi.org/10.1617/s11527-018-1306-9.

Wang, D., Shi, C., Farzadnia, N., Shi, Z., Jia, H., 2018. A review on effects of limestone powder on the properties of concrete. Constr. Build. Mater. 192, 153–166. http://dx.doi.org/10.1016/j.conbuildmat.2018.10.119.

Wang, S., Yu, H., Liu, S., Yaras, A., Hu, L., Zhang, W., Peng, M., Enkhchimeg, B., Mao, L., 2025. New insights into the environmental safety of incorporating Cr(III) into cement matrix: Cr(VI) formation driven by low-intensity fire. Constr. Build. Mater. 489, 140694. http://dx.doi.org/10.1016/j.conbuildmat.2025.140694.

Wang, L., Yu, Z., Liu, B., Zhao, F., Tang, S., Jin, M., 2022. Effects of fly ash dosage on shrinkage, crack resistance and fractal characteristics of face slab concrete. Fractal Fract. 6 (6), 335. http://dx.doi.org/10.3390/fractalfract6060335.

Wei, M., Chen, L., Lei, N., Li, H., Huang, L., 2024. Experimental investigation on freeze–thaw resistance of thermally activated recycled fine powder concrete. Constr. Build. Mater. 457, 139378. http://dx.doi.org/10.1016/j.conbuildmat.2024.139378.

Wei, M., Chen, L., Lei, N., Li, H., Huang, L., 2025. Mechanical properties and microstructures of thermally activated ultrafine recycled fine powder cementitious materials. Constr. Build. Mater. 475, 141195. http://dx.doi.org/10.1016/j.conbuildmat.2025.141195.

Weimann, K., 2009. Untersuchungen zur Nassaufbereitung von Betonbrechsand unter Verwendung der Setzmaschinentechnik. BAM-Dissertationsreihe, Bundesanstalt für Materialforschung und -prüfung (BAM), Berlin, no. 51.

Wu, H., Liang, C., Zhang, Z., Yao, P., Wang, C., Ma, Z., 2023. Utilizing heat treatment for making low-quality recycled aggregate into enhanced recycled aggregate, recycled cement and their fully recycled concrete. Constr. Build. Mater. 394, 132126. http://dx.doi.org/10.1016/j.conbuildmat.2023.132126.

Wu, H., Yang, D., Ma, Z., 2021. Micro-structure, mechanical and transport properties of cementitious materials with high-volume waste concrete powder and thermal modification. Constr. Build. Mater. 313, 125477. http://dx.doi.org/10.1016/j.conbuildmat.2021.125477.

Xi, X., Zheng, Y., Du, C., Zhang, P., Sun, M., 2024. Study on the hydration characteristics, mechanical properties, and microstructure of thermally activated low-carbon recycled cement. Constr. Build. Mater. 447, 138042. http://dx.doi.org/10.1016/j.conbuildmat.2024.138042.

Xu, L., Wang, J., Hu, X., Ran, B., Wu, T., Zhou, X., Xiong, Y., 2024. Physical performance, durability, and carbon emissions of recycled cement concrete and fully recycled concrete. Constr. Build. Mater. 447, 138128. http://dx.doi.org/10.1016/j.conbuildmat.2024.138128.

Xu, L., Wang, J., Li, K., Hao, T., Li, Z., Li, L., Ran, B., Du, H., 2023. New insights on dehydration at elevated temperature and rehydration of GGBS blended cement. Cem. Concr. Compos. 139, 105068. http://dx.doi.org/10.1016/j.cemconcomp.2023.105068.

Xu, L., Wang, J., Li, K., Lin, S., Li, M., Hao, T., Ling, Z., Xiang, D., Wang, T., 2022. A systematic review of factors affecting properties of thermal-activated recycled cement. Resour. Conserv. Recycl. 185, 106432. http://dx.doi.org/10.1016/j.resconrec.2022.106432.

Younsi, A., Turcry, P., Rozière, E., Aït-Mokhtar, A., Loukili, A., 2011. Performance-based design and carbonation of concrete with high fly ash content. Cem. Concr. Compos. 33 (10), 993–1000. http://dx.doi.org/10.1016/j.cemconcomp.2011.07.005.

Zelic, J., Ugrina, L., Jozic, D., 2007. Application of thermal methods in the chemistry of cement: Kinetic analysis of portlandite from non-isothermal thermogravimetric data. In: The First International Proficiency Testing Conference. n. d., Sinaia, Romania, pp. 420–429.

Zhang, D., Zhang, S., Huang, B., Yang, Q., Li, J., 2022. Comparison of mechanical, chemical, and thermal activation methods on the utilisation of recycled concrete powder from construction and demolition waste. J. Build. Eng. 61, 105295. http://dx.doi.org/10.1016/j.jobe.2022.105295.

Zheng, Y., Xi, X., Liu, H., Du, C., Lu, H., 2024. A review: Enhanced performance of recycled cement and CO2 emission reduction effects through thermal activation and nanosilica incorporation. Constr. Build. Mater. 422, 135763. http://dx.doi.org/10.1016/j.conbuildmat.2024.135763.

Zhou, Q., Glasser, F.P., 2001. Thermal stability and decomposition mechanisms of ettringite at <120°C. Cem. Concr. Res. 31 (9), 1333–1339. http://dx.doi.org/10.1016/S0008-8846(01)00558-0.

Zhou, Q., Lachowski, E.E., Glasser, F.P., 2004. Metaettringite, a decomposition product of ettringite. Cem. Concr. Res. 34 (4), 703–710. http://dx.doi.org/10.1016/j.cemconres.2003.10.027.

Supplementary Data to Paper P4

Tab. A24: Particle size distributions of reference binders and processed concrete fines. d_i: particle size at i % passing [µm].

	d_{10}	d_{30}	d_{50}	d_{70}	d_{90}
CEM I	1.7	5.9	12.1	20.6	32.9
S	2.1	6.6	12.3	19.5	30.0
FA	2.9	9.9	21.6	43.3	83.4
L	1.9	6.8	12.5	20.7	44.4
R1-600	1.9	6.4	17.9	44.2	88.4
R2-600	2.3	9.3	25.9	54.3	99.1
R3-600	1.8	5.1	14.1	39.5	81.0
R4-600	2.0	6.6	18.4	48.4	97.6
R5-600	2.0	6.7	18.8	48.0	96.2
R6-600	1.8	5.3	11.6	22.3	40.5

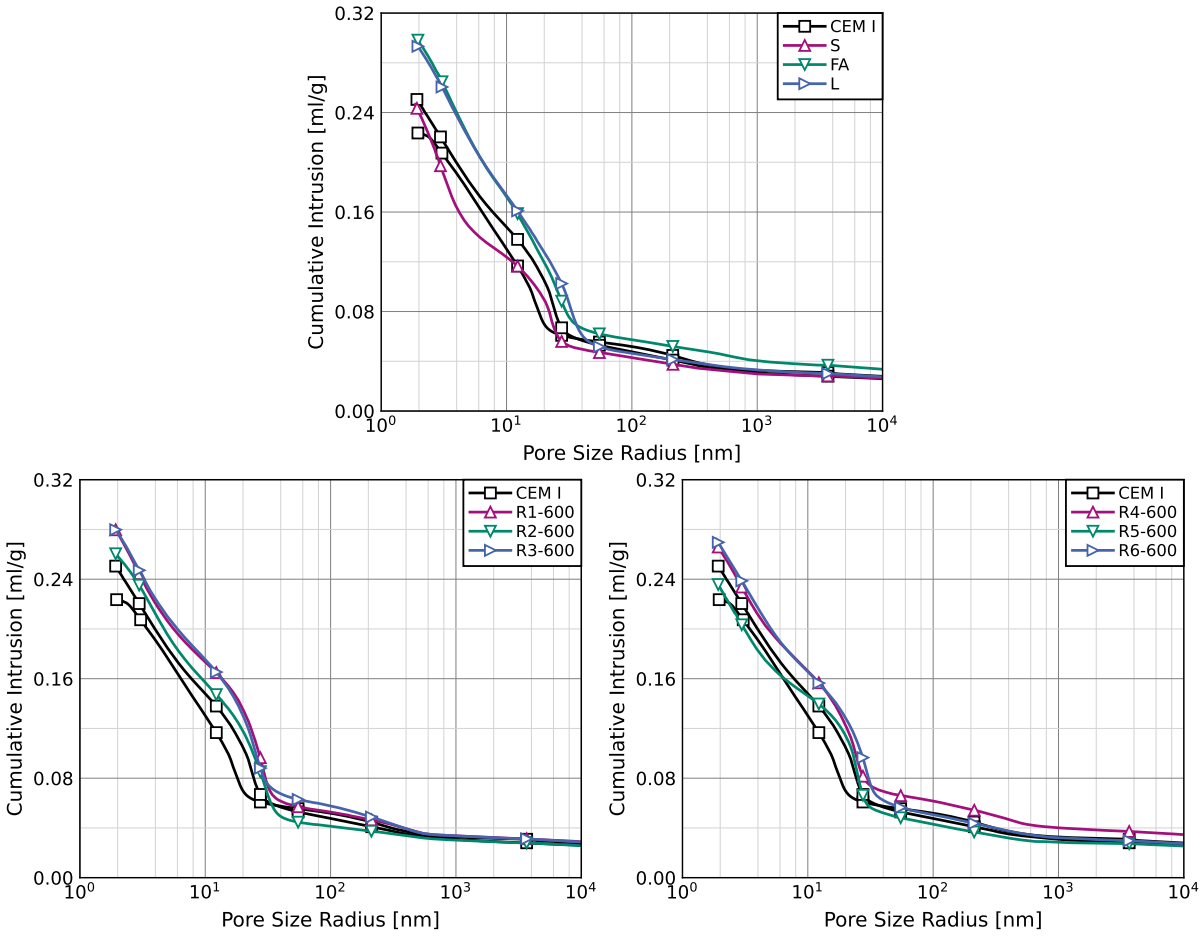

Fig. A8: Cumulative pore radius distribution (logarithmic) for reference series CEM I-1 and CEM I-2 and established SCMs S, FA, and L, as well as thermally activated concrete fines (P4, fig. 1).

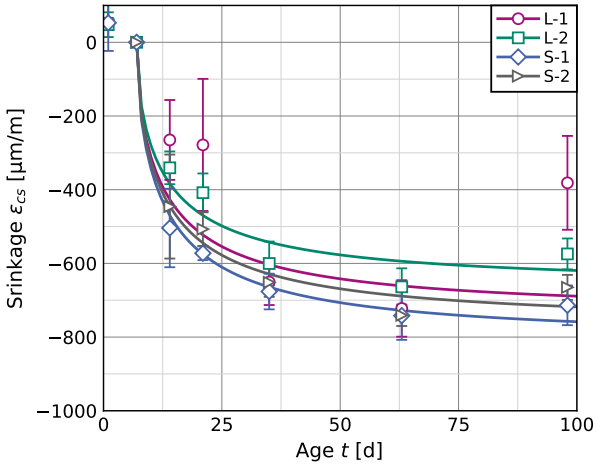

Fig. A9: Temporal development of shrinkage deformation for reference mixes S and L. Markers indicate measured averages and standard deviations from three prisms, lines represent corresponding fit curves for the determination of ε_{cs0} (P4, fig. 7).

Tab. A25: Results of strength development in P4.
$f_{ct,fl}$: flexural strength on wet stored prisms, f_c: compressive strength on wet stored prisms, s_c: strength development coefficient.

	$f_{ct,fl,2\,d}$ MPa	$f_{ct,fl,28\,d}$ MPa	$f_{c,2\,d}$ MPa	$f_{c,28\,d}$ MPa	$f_{c,56\,d}$ MPa	$f_{c,98\,d}$ MPa	$f_{cm,ref}$ MPa	s_c -
CEM I-1	3.6(3)	6.2(6)	19.0(5)	43.8(16)	46.6(12)	53.8(3)	44.4	0.32
CEM I-2	5.3(2)	7.5(1)	32.7(11)	62.8(57)	66.6(11)	73.8(31)	63.6	0.25
CEM I-3	3.8(4)	7.1(2)	18.1(2)	45.9(13)	48.9(10)	53.5(4)	45.4	0.33
CEM I-4	5.9(4)	7.7(8)	33.3(4)	61.0(13)	66.5(19)	69.3(15)	61.9	0.23
FA-1	3.6(2)	6.7(6)	19.3(3)	48.2(4)	59.1(19)	64.3(6)	52.0	0.39
FA-2	4.6(4)	7.6(3)	27.2(2)	61.2(5)	63.2(55)	64.5(49)	58.5	0.27
FA-3	3.5(2)	7.1(2)	18.4(6)	46.7(9)	57.8(9)	61.0(23)	50.1	0.39
FA-4	4.6(4)	7.4(5)	26.3(8)	59.4(12)	71.7(10)	75.9(20)	63.5	0.34
S-1	4.2(2)	7.5(4)	21.1(6)	57.6(56)	65.4(7)	71.5(2)	58.8	0.38
S-2	4.7(5)	7.4(8)	27.1(4)	63.1(9)	69.3(51)	76.8(14)	64.3	0.32
L-1	3.8(2)	6.4(3)	19.3(5)	42.5(20)	46.4(6)	46.8(8)	42.0	0.28
L-2	5.9(1)	7.8(3)	34.5(39)	58.6(9)	67.1(12)	68.8(36)	61.5	0.22
R1-1	4.3(2)	7.0(2)	20.9(1)	47.4(10)	51.6(22)	53.9(13)	47.2	0.30
R1-2	5.2(1)	7.3(2)	30.1(19)	62.4(7)	62.5(47)	67.3(5)	60.0	0.25
R2-1	4.0(3)	6.7(2)	19.7(2)	42.6(27)	51.0(29)	52.6(13)	45.1	0.31
R2-2	5.3(5)	7.8(6)	28.5(15)	60.5(11)	61.6(7)	68.5(16)	59.3	0.27
R3-1	4.4(4)	7.0(2)	22.5(7)	48.9(6)	52.0(15)	56.2(6)	48.7	0.28
R3-2	5.2(5)	7.7(2)	31.8(6)	61.1(19)	66.3(17)	67.5(34)	61.1	0.24
R4-1	4.6(1)	7.0(5)	22.5(4)	49.6(22)	53.9(11)	56.1(20)	49.4	0.29
R4-2	5.2(4)	7.6(4)	31.4(1)	61.1(20)	65.5(14)	67.0(14)	60.7	0.24
R5-1	4.8(1)	7.0(2)	27.6(10)	55.4(14)	57.2(11)	58.9(4)	53.7	0.24
R5-2	5.6(3)	7.3(1)	38.0(3)	66.5(12)	65.9(44)	67.4(4)	63.4	0.18
R6-1	4.4(2)	7.0(5)	22.1(3)	50.2(10)	53.8(4)	55.0(8)	49.2	0.29
R6-2	4.9(6)	7.5(6)	30.3(3)	61.8(21)	66.3(23)	68.6(1)	61.4	0.26

Tab. A26: Results of strength, deformation and durability tests in P4.
$f_{ct,fl}$: flexural strength on dry stored prisms, f_c: compressive strength on dry stored prisms, $E_{c,dyn}$: dynamic modulus of elasticity, ε_{cs0}: shrinkage coefficient, K_{AC}: carbonation coefficient, d_c: chloride penetration depth, Δm_{28}: mass loss after 28 freeze-thaw cycles.

	$f_{ct,fl,28\,\mathrm{d}}$ MPa	$f_{ct,fl,98\,\mathrm{d}}$ MPa	$f_{c,28\,\mathrm{d}}$ MPa	$f_{c,98\,\mathrm{d}}$ MPa	$E_{c,dyn,28\,\mathrm{d}}$ GPa	ε_{cs0} µm/m	K_{AC} mm/d^{0,5}	d_c mm	Δm_{28} wt%
CEM I-1	6.7(5)	5.8(2)	45.1(14)	42.1(5)	31.2(5)	447	0.87	12.2	
CEM I-2	7.1(7)	5.9(5)	55.9(15)	50.8(21)	32.7(7)	422	0.50	8.8	
CEM I-3	6.4(3)	7.0(4)	48.0(3)	52.4(18)	32.8(3)	792	0.91	15.8	
CEM I-4	8.3(2)	9.2(8)	67.5(23)	74.5(15)	37.2(3)	677	0.51	12.6	0.15
FA-1	6.1(4)	5.7(5)	41.6(31)	48.5(14)	30.7(11)	306	1.17	10.6	
FA-2	6.6(6)	6.0(1)	48.5(13)	48.9(16)	32.7(2)	417	0.77	9.1	
FA-3	7.3(1)	6.4(2)	50.1(10)	55.0(10)	34.5(2)	712	1.13	14.4	
FA-4	8.2(4)	7.6(6)	60.7(12)	65.4(22)	36.1(4)	676	0.79	12.6	0.19
S-1	7.2(3)	7.3(5)	58.0(3)	57.3(5)	34.2(7)	813	0.85	7.9	
S-2	7.8(3)	8.5(8)	61.1(7)	65.2(6)	33.7(5)	770	0.65	7.2	
L-1	7.1(10)	6.5(6)	47.2(4)	47.6(10)	31.9(4)	739	1.31	25.3	
L-2	8.6(1)	8.8(2)	66.7(31)	70.3(14)	38.0(1)	664	0.60	15.0	
R1-1	7.0(3)	7.4(2)	49.9(10)	54.5(4)	33.2(4)	778	1.04	17.6	
R1-2	7.4(4)	7.4(6)	62.3(17)	61.7(17)	36.9(4)	760	0.72	13.1	
R2-1	7.3(2)	7.6(0)	49.1(7)	53.2(3)	33.9(1)	818	1.12	17.5	
R2-2	7.7(4)	7.9(8)	62.3(2)	61.9(7)	36.8(6)	730	0.72	13.4	
R3-1	7.1(4)	7.0(11)	53.6(7)	53.2(8)	32.9(5)	861	1.03	17.4	
R3-2	7.1(13)	7.6(8)	66.4(17)	61.3(15)	35.6(8)	819	0.75	15.7	
R4-1	7.1(2)	7.3(6)	51.3(28)	50.0(9)	33.0(2)	942	1.05	17.4	
R4-2	7.0(4)	7.4(8)	62.6(23)	60.4(9)	33.8(5)	853	0.72	15.3	
R5-1	6.7(2)	6.3(5)	52.2(12)	50.5(2)	28.6(1)	930	1.05	17.6	
R5-2	7.8(2)	7.5(3)	64.3(7)	61.6(21)	30.3(2)	756	0.68	13.3	0.11
R6-1	7.1(0)	6.2(7)	51.5(15)	48.8(10)	30.9(2)	866	1.13	17.2	
R6-2	8.2(9)	8.0(5)	64.0(18)	65.7(7)	33.5(6)	739	0.75	14.0	0.23